Freeze Drying from Small Containers: Heat and Mass Transfer and Implications on Process Design

Gefriertrocknung in kleinen Behältern:
Wärme- und Massenübergänge und Bedeutung für das Prozessdesign

Der Naturwissenschaftlichen Fakultät
der Friedrich-Alexander-Universtät Erlangen-Nürnberg
zur
Erlangung des Doktorgrades Dr. rer. nat

vorgelegt von
Silja von Graberg
aus Hamburg

Contents

List of Publications **11**

List of Abbreviations **13**

Motivation for this Work **15**

1 Fundamentals of Freeze Drying **17**
1.1 Stages of the Freeze Drying Process . . . 17
1.1.1 Freezing . . . 17
1.1.2 Primary Drying . . . 18
1.1.3 Secondary Drying . . . 20
1.2 Basics of Formulation Design . . . 22
1.2.1 Lyoprotectants: Stabilising Excipients . . . 22
1.2.2 Determination of the Critical Formulation Temperature . . . 22
1.2.3 Crystallising Excipients as Bulking Agents . . . 25
1.3 Mathematical Models of the Freeze Drying Process . . . 27
1.3.1 Model Based on Pseudo-Steady State . . . 27
1.3.2 Dynamic Model . . . 28
1.4 Influence of Container on the Freeze Drying Process . . . 30
1.4.1 Resistances to Water Vapour Flow . . . 30
1.4.2 Heat Transfer into the Product . . . 31
1.4.3 Heat Input by Radiation . . . 33
1.4.4 Heat Input by Conduction . . . 35
1.4.5 Heat Input by Conduction through the Gas . . . 35
1.5 Experimental Determination of K_{cont} . . . 37
1.5.1 Gravimetric Procedure for Determination of Mass Flow . . . 37
1.5.2 Online Determination of Water Vapour Mass Flow . . . 37
1.6 Tools for Enhancement of Heat Transfer to Product . . . 38
1.6.1 Aluminium as a Material with High Thermal Conductivity . . . 38
1.6.2 Influence of Vial Type on Drying Heterogeneity . . . 38

2 Materials and Methods **39**
2.1 Materials . . . 39
2.1.1 Primary Packaging Material . . . 39
2.1.2 Formulation . . . 41
2.1.3 Freeze Drying Equipment . . . 41
2.2 Sublimation Tests and Product Runs . . . 44
2.2.1 Experimental Design: 96-Well PCR-Plates . . . 44
2.2.2 Experimental Design: VirTis Freeze Drying System™ . . . 48
2.2.3 Experimental Design: *2R* Glass Vials . . . 51
2.2.4 Cycle Design: Case Study With a Cytokine . . . 52
2.2.5 Analytical Equipment and Procedures . . . 55

3 Results and Discussion **59**
3.1 96-Well PCR-Plates: Sublimation Tests . . . 59
3.1.1 Determination of Effective Contact Area . . . 59
3.1.2 Theoretical Discussions on Heat Input into Well Plates . . . 60
3.1.3 Sublimation Tests for Well Plates Without Al-Blocks . . . 63
3.1.4 Suspended Well Plates Test . . . 64
3.1.5 Sublimation Tests of Well-Plates With Al-Blocks . . . 65
3.1.6 Sublimation Tests with Heat Sink Grease . . . 69
3.1.7 Summary: Heat Transfer into Well Plates . . . 70
3.2 96-well PCR-Plates: Product Runs . . . 72
3.2.1 Applicability of Heat Transfer Coefficients . . . 72
3.2.2 Calculation of Primary Drying Time from Initial Temperature Differences 72
3.2.3 Estimation of Average Mass Flow from Product Run Results . . . 76
3.2.4 Online Determination of Mass Flow by TDLAS . . . 83
3.2.5 Auto MTM with 96-Well PCR-Plates . . . 85
3.2.6 Heat Transfer Coefficients Calculated from Excipient-Runs . . . 86
3.2.7 Product Temperature Profiles . . . 91
3.2.8 Product Analysis . . . 94
3.2.9 Considerations for Cycle Design in 96-Well PCR-Plates . . . 109
3.2.10 Testing the SMART™ Software with 96-Well PCR-Plates . . . 112
3.3 96-Well Freeze Drying System™ (VirTis) . . . 117
3.3.1 Contact Area to Flat Surface and to Al-Block Cavities . . . 117
3.3.2 Results of Sublimation Tests . . . 118
3.4 2 R Serum Tubing Vials . . . 124
3.4.1 Contact Area to Shelf Surface . . . 124
3.4.2 Results of Sublimation Tests . . . 124
3.4.3 Verification of K_{2R} Data for Product Runs . . . 127
3.5 Formulation Design for Small Volumes to be Freeze Dried: A Case Study with a Cytokine . . . 131
3.5.1 General Introduction . . . 131
3.5.2 Optimisation of Amorphous Formulations . . . 131
3.5.3 General Product Characteristics . . . 136
3.5.4 DSC Scans of Lyophilised Product . . . 138
3.5.5 Gel Electrophoresis and Activity Tests . . . 141
3.5.6 Conclusions from Cytokine Formulation Experiments . . . 146
3.6 Case Study with a Cytokine: Testing of "First Guess" Freeze Drying Cycles for FDS and Well Plates . . . 147

4 Summary and Conclusion **153**

5 German Summary (Deutsche Zusammenfassung) **155**

References **166**

Curriculum Vitae **167**

Attachments **169**

List of Publications

This thesis has been published in parts:

- S. v. Graberg and H. Gieseler. Freeze Drying in Non-Vial Container Systems: Evaluation of Heat Transfer Coefficients of PCR-Plates and Correlation to Freeze-Drying Cycle Design. *Proc. CPPR Freeze-Drying of Pharmaceuticals and Biologicals*, Garmisch-Partenkirchen, Germany, October 3-6, 2006.

- S. v. Graberg and H. Gieseler. Freeze Drying from 96-Well PCR-Plates: Transferability of Heat Transfer Coefficients Obtained from Sublimation Tests to Product Runs and Considerations for Cycle Design. *Proc. AAPS Annual Meeting and Exposition*, San Diegeo (CA), USA, November 11-15, 2007.

- S. v. Graberg, W. Hyla, and H. Gieseler. Freeze Drying from Small Product Containers and its Implication on Freeze Drying Process Design: Evaluation of Heat Transfer Coefficients of a New 96-Well Freeze Drying System in Comparison to 2R Tubing Vials and Polypropylene 96-Well PCR-Plates. *Proc. CPPR Freeze-Drying of Pharmaceuticals and Biologicals*, Breckenridge (CO), USA, August 6-9, 2008.

- S. v. Graberg, H. Gieseler, S. Edelburg, S. Kock and V. Nölle. Amorphous and Partially Crystalline Formulation Strategies for a Human Cytokine: A Case Study. *Proc. CPPR Freeze-Drying of Pharmaceuticals and Biologicals*, Breckenridge (CO), USA, August 6-9, 2008.

List of Abbreviations

In the following, a tabular overview of abbreviations and symbols used in this work and an explanation of their meaning is presented.

Symbol	Unit	Meaning
	$°C$	degrees Celsius, commonly used unit of temperature
a_c	$-$	energy accommodation coefficient (dimensionless)
A_{cont}	cm^2	outer surface area of container through which heat enters into the product
A_{FDS}	cm^2	outer surface area of a single tube of the glass tube array through which heat enters into the product
A_P	cm^2	inner cross-sectional area of container
A_{PCR}	cm^2	outer surface area of a single well through which heat enters into the product
API	$-$	active pharmaceutical ingredient
A_v	cm^2	outer cross-sectional area of a vial
C_p	$J\ g^{-1}K^{-1}$	(specific) heat capacity of a material (in units of energy per mass)
d	m	molecular diameter
DSC	$-$	differential scanning calorimetry
$\bar{e}$	$-$	effective emissivity (dimensionless)
	g	gram, unit of mass
h	J/cal	enthalpy, "heat", SI unit is J
K	$cal\ s^{-1}cm^{-2}K^{-1}$	heat transfer coefficient
	K	Kelvin, unit of the absolute temperature and unit for temperature differences
K_{2R}	$cal\ s^{-1}cm^{-2}K^{-1}$	heat transfer coefficient of $2R$ vials
K_c	$cal\ s^{-1}cm^{-2}K^{-1}$	contribution to heat transfer by direct conduction
K_g	$cal\ s^{-1}cm^{-2}K^{-1}$	contribution to heat transfer by conduction through the gas
K_{FDS}	$cal\ s^{-1}cm^{-2}K^{-1}$	heat transfer coefficient of 96 small glass tubes in an array inserted into black painted aluminium blocks
K_K	$cal\ s^{-1}cm^{-2}K^{-1}$	contribution to heat transfer by non-pressure dependent mechanisms (direct conduction, radiation)
K_P	$cal\ s^{-1}cm^{-2}Torr{-}1$	fitting parameter for heat transfer into vials depending on the heat conductivity of the gas Value of K_K used throughout this work (References: [1], [2]) $33.2 * 10^{-4}$ cal $s^{-1}cm^{-2}K^{-1}$
K_{PCR}	$cal\ s^{-1}cm^{-2}K^{-1}$	heat transfer coefficient of a 96 well PCR-plate
K_r	$cal\ s^{-1}cm^{-2}K^{-1}$	contribution to heat transfer by radiation
K_v	$cal\ s^{-1}cm^{-2}K^{-1}$	heat transfer coefficient of vials
l	cm	separation distance between freeze dryer shelf and container bottom
l_{dry}	cm	thickness of the primary dried product layer
l_{MFP}	m	length of the mean free path
L	cm	fill depth of product solution in the container
m	g	mass

table continued on next page

Symbol	Unit	Meaning
N_A	mol^{-1}	Avogadro number, $6.022 \cdot 10^{23}$ mol^{-1}, [3]
P	$Torr$ or Pa or bar	pressure (SI unit is Pascal, Pa) throughout this work, $Torr$ is used.
P_c	$Torr$	chamber pressure
PCR	–	polymerase chain reaction
P_{ice}	$Torr$	vapour pressure of ice
$q_{s,ice}$	$cal\ g^{-1}$	specific heat of sublimation of ice (SI unit is $J\ g^{-1}$) value used throughout this work: 670 cal g^{-1}
Q	cal or J	heat (SI unit is J)
r	cm	inner radius of a vial or container
R	$J\ K^{-1}mol^{-1}$	universal gas constant, 1.986 cal K^{-1}mol^{-1}, [3]
R_x	$Torr\ h\ g^{-1}$	resistance to water vapour flow x indicates origin of resistance
R_P	$Torr\ h\ g^{-1}$	product resistance
R_s	$Torr\ h\ g^{-1}$	stopper resistance
$\hat{R}_P$	$cm^2\ Torr\ h\ g^{-1}$	area normalised product resistance
t	s or min or h	time in seconds (s), minutes (min), or hours (h)
T	K (or $°C$)	temperature (in Kelvin K or $°C$)
T_b	$°C$	temperature at the bottom of the conainer
T_c	$°C$	collapse temperature, critical formulation temperature of amorphous products
T_{eu}	$°C$	eutectic melting temperature
T_g	$°C$	glass transition temperature
T_g'	$°C$	glass transition temperature of the maximally freeze concentrated solution
T_p	$°C$	product temperature at the sublimation interface
T_s	$°C$	temperature at the shelf surface
	W	Watt, unit of power
TC	–	abbreviation used for thermocouple
α	–	function of energy accommodation coefficient and absolute temperature (dimensionless)
δ	m	thickness of container wall
Δ	–	difference, i.e. in temperature
ε	–	effective emissivity of a surface (dimensionless)
λ	$W\ m^{-1}K^{-1}$	heat conductivity of a material
λ_{Al}		237 W m^{-1}K^{-1} heat conductivity of Aluminium [4]
$\lambda_{AISI316}$		16.2 W m^{-1}K^{-1} heat conductivity of stainless steel [5]
$\lambda_{styrofoam}$		$20 - 35$ W m^{-1}K^{-1} heat conductivity of styrofoam [6]
λ_0	$cal\ s^{-1}cm^{-1}K^{-1}$	heat conductivity of the gas at ambient pressure value used throughout this work: $4.29 \cdot 10^{-5}$ cal s^{-1}cm^{-1}K^{-1}, [1], [7]
Λ_0	$cal\ s^{-1}cm^{-2}K^{-1}Torr^{-1}$	free molecular heat conductivity of the gas at 0 °C value used throughout this work: $6.34 \cdot 10^{-3}$ cal s^{-1}cm^{-2}K^{-1}Torr^{-1}, [1], [7]
σ	$W\ m^{-2}K^{-4}$	Stefan-Boltzmann constant, $5.67 \cdot 10^{-8}$ W m^{-2}K^{-4} [8]

Motivation for this Work

Relevance of Freeze Drying in Atypical Container Systems

Based on the growing number of recombinant protein drugs [9] over the past two decades freeze drying, or lyophilization, has become an important technology to achieve short and long term storage stability for such delicate pharmaceuticals. This drying procedure is the method of choice for all active pharmaceutical ingredients (APIs) which are prone to degradation or inactivation in solution or at temperatures higher than ambient. The freeze drying process, however, consumes a high amount of energy, and is time consuming in comparison to other drying processes such as spray drying. Moreover, investment and maintenance costs are high and the batch size is limited. Commercial freeze dryers have a load capacity in the order of $50,000$ vials per batch, and a typical freeze drying run takes several days from beginning to end [10]. In order to design an optimised freeze drying process it is not only necessary to develop a suitable formulation but also to thoroughly characterise heat and mass transfer conditions of the chosen container system and the freeze dryer.

The continually increaseing number of recombinant protein drugs that have to be administered parenterally generates a growing need for easy, safe, and pain free administration. Apart from experiments performed to test mucosal application of proteins, peptides, and vaccines [11], easy-to-handle pre-filled syringes and injectors are found increasingly more often on the market [12]. Other approaches to generate robust, stable protein formulations are also tested. Hirschberg et al. developed biodegradable hollow miniature implants filled with vaccine [13]. These vaccines do not need refrigeration to maintain their activity, which is a valuable advantage over liquid vaccination injections. In some cases like mucoadhesive application of non-protein drugs development of freeze dried formulations is a possible alternative to compressed tablets [14]. These examples show that non-vial container systems, especially small containers, are becoming more interesting for freeze drying of pharmaceuticals.

Scope of this Thesis

In this work heat and mass transfer studies were performed for the first time with polypropylene plates commonly used for polymerase chain reaction (96-well PCR-plates), $2R$ (2 mL) glass vials, and an array of 96 0.5 mL glass tubes inserted into an aluminium base plate. These studies were followed by investigations to show the applicability of the determined heat transfer coefficients to freeze drying cycle development for the tested container systems. Finally, a guideline was developed which describes rational freeze drying process design with genuine product when using such atypical container systems.

Chapter 1

Fundamentals of Freeze Drying

1.1 Stages of the Freeze Drying Process

1.1.1 Freezing

Lyophilisation means removal of the solvent medium by sublimiation. Sublimation is the term for the transition from solid (frozen) state to gaseous state [3]. The entire freeze drying process is divided into three phases: freezing, primary drying, and secondary drying [15]. In general, the (aqueous) product solution is first filled into the primary packaging containers and loaded onto the shelves of a freeze dryer (see Figure 1.1). The heat transfer fluid pumped through channels within the shelves of the freeze dryer is gradually cooled down, and heat is removed from the product until all water has turned to ice and all components are completely solidified.

At the beginning of the cooling period, the solution supercools to temperatures below the eutectic melting temperature (T_{eu}) of the crystallising components of the product solution (water and possibly other components such as mannitol or glycine) [3]. In this stage, formation of ice

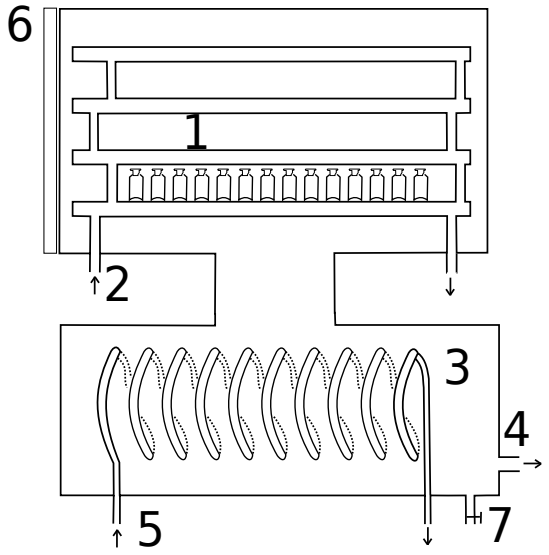

Figure 1.1: Schematic set-up of a freeze dryer. 1: Drying chamber with product (vials) loaded onto one of the three shelves; 2: inlet for heat transfer fluid; 3: condenser with coils; 4: connection to vacuum pump; 5: inlet for condenser cooling fluid; 6: freeze dryer door; 7: drain for water from condenser.

nuclei is a stochastic process. Under normal conditions, the temperature of nuclei formation will differ slightly from vial to vial. If no clean-room environment is present, ice nucleation in a freeze dryer typically starts at −10 to −20 °C [16,17]. After formation of the nuclei, ice crystals grow, as well as other crystals of the eutectic mixture. All non-crystallising components in the remaining liquid phase are further concentrated.

As the temperature of the ice - solution mixture gradually decreases, the viscosity of the remaining liquid phase continuously increases until it reaches the glass transition temperature of the maximally freeze concentrated solution, T'_g [18]. At this temperature or temperature range, the viscosity in the remaining fluid denoted as being in the "rubber state" becomes so high that molecular mobility is decreased to a level comparable to that of molecular mobility in solids: the liquid phase has formed a glass. As opposed to the crystalline phase or phases, the glassy phase is amorphous with no clearly defined short-range molecular order.

The process protocol of the freezing stage can itself be divided into several individual steps with different assigned shelf temperatures, according to the requirements of the product solution. Crystallising excipients often require a thermal treatment called "tempering" or "annealing" in the freezing phase that is different from the treatment of non-crystallising, amorphous excipients [19,16]. The annealing phase is used to enhance the formation or growth of large (ice) crystals.

1.1.2 Primary Drying

Principle of Ice Removal by Sublimation

At the beginning of primary drying, the condenser of the freeze dryer unit is cooled down to a temperature typically in the order of −60 to −80 °C [20], [21]. Then, the vacuum pump is switched on and the chamber pressure is lowered to a setting typically within the range of 6 to 26 Pa for freeze drying of pharmaceuticals. (Note that in this publication, most pressure information will be given in *mTorr* although Pascal (*Pa*) is the SI unit for pressure. For freeze drying, millimetres of mercury (*Torr*) is the most common pressure unit in the United States, and *bar* is most widely used in Europe. The reader is reminded that 1 Pa is defined as a pressure of 1 N/m^2; and that 1 bar equals 10^5 Pa. *Torr* can be converted to either of the two other units by simple multiplication operations. 1 Torr is approximately 1.333 mbar, or 133.3 Pa. Thus, the pressure range given above approximates to the range of 45 to 200 mTorr.)

After evacuation of the chamber, the shelf temperature is elevated to a predefined set point. Under these conditions (water frozen to ice, very low pressure) a direct change of state from the solid phase (ice) to the vapour phase takes place (cf. Figure 1.2). The water vapour generated by this sublimation process flows from the drying chamber to the condenser. Due to the cold condenser fluid, the temperature of the condenser coils is much lower than the ice temperature in the product. This temperature drop causes a substantial decrease in water vapour saturation pressure and thus the water vapour is turned to ice again on the cold condenser coils.

Sustaining Water Vapour Mass Flow

The continuous removal of water vapour is necessary for the progress of product drying. Mass flow would reach a dynamic equilibrium as soon as the chamber pressure attained the saturation vapour pressure of water vapour at the product temperature [7], [23]. To put it in other words, the driving force for continuous sublimation is the difference in water vapour saturation pressure between ice in the product and ice on the cold condenser coils. This difference in water vapour saturation pressure originates in the temperature difference between the product temperature at the ice sublimation interface and the temperature of the condenser coils or plates.

A high product temperature yields a high difference in water vapour saturation pressure and a high sublimation rate, leading to a comparatively short primary drying phase. If the product temperature is very low, the difference in water vapour saturation pressure between product and condenser will decrease and the duration of the primary drying phase is considerably increased. For example, the water vapour saturation pressure at approximately −20 °C is over 100 Pa and the water vapour saturation pressure at −40 °C is only approximately 10 Pa (Water vapour

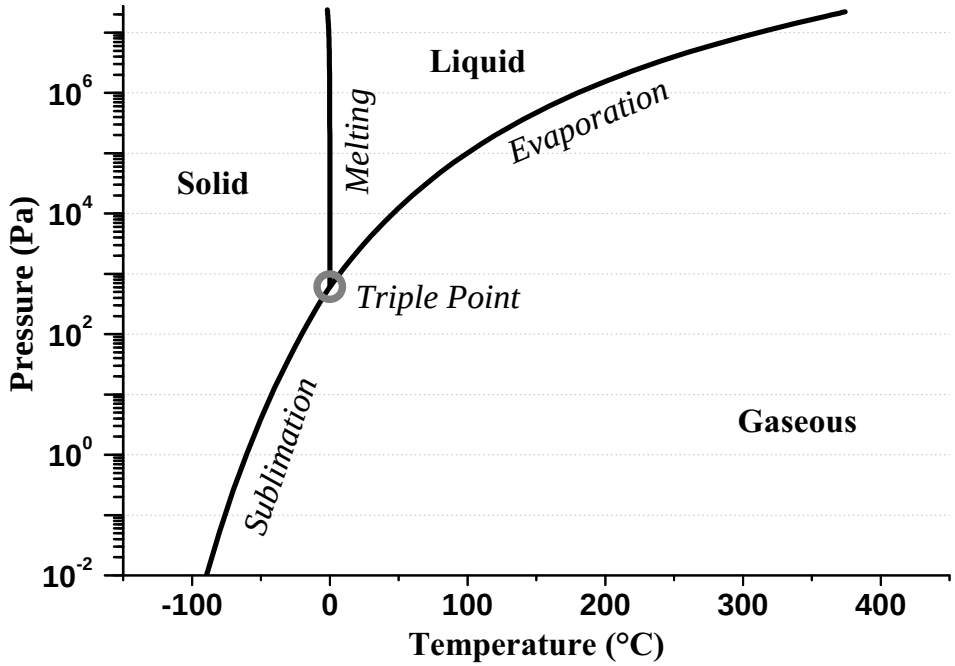

Figure 1.2: Phase diagram of water. Phase transition of solid to vapour phase is sublimation, the important phase change for freeze drying. Water vapour saturation pressure is shown on the logarithmic y-axis. The order of magnitude of vapour saturation pressure increases with temperature (x-axis), this is especially pronounced for sublimation. Water shows an anomaly in the melting curve: the melting point decreases slightly with increasing pressure because liquid water of 4 °C has a higher density than ice at 0 °C. The Figure is based on literature data [22].

saturation pressure at typical condenser temperatures is less than 1 Pa) [22]. For this reason, the product temperature should be kept above approximately −40 °C whenever possible.

Primary Drying Endpoint Detection

Primary drying is finished when all ice has been removed from the frozen product. There are several methods for primary drying endpoint detection. Often temperature sensors placed in product containers are used. As long as sublimation continues the product remains colder than the shelf surface temperature as the sublimation process consumes energy in the form of heat [24]. When all ice is removed from the product container, the product temperature measured by the temperature probe rises until it reaches the shelf temperature. This method for primary drying endpoint detection is accurate if the temperature sensor is placed at the position in the container where the ice sublimes last. Placed in a different position, the temperature rise detected by the sensor would occur as soon as the sensor had lost contact with the remaining ice in the product, before the sublimation process in the observed product container had completely finished [24].

For vials placed on a freeze dryer shelf the correct position for the temperature probe is at the bottom of the vial in the centre [25]. However, the temperature sensor placed in the vial makes this particular vial different from the regular product vials without a temperature probe [1]. This difference could cause a different nucleation behaviour in this vial during freezing which in turn may influence the primary drying rate. If the temperature probe needs a wire for data recording, there might be additional transfer of energy (in the form of heat) via conduction through the wire. Temperature probes can only be applied to a small number of vials, they do not supply information about primary drying progress for non-probed vials. The position of the

probe vials on the shelf is also critical for correct endpoint determination. Vials at edge or corner positions of the array on the shelf receive an extra amount of radiative heat from the sides [26]. Their product temperature is higher and primary drying time is shorter than for vials in the centre of the array, surrounded by other vials filled with product. Bearing all this in mind, when temperature probe readings show that the primary drying endpoint is reached, a safety margin ought to be added to account for possibly slower primary drying rates in non-probed vials.

A method for primary drying endpoint detection of the whole batch in the freeze dryer is comparative pressure measurement [27]. Here, two different pressure sensors are used for determination of the end of the sublimation phase. One sensor is the pirani gauge. The measuring principle of the pirani gauge is based on decreasing thermal conductivity of the gas with decreasing pressure (less heat removal by conduction through the gas). The heat conductivity of the considered gas also depends on its composition, i.e. air, nitrogen, and / or water vapour. The heat conductivity of pure water vapour is approximately 1.6-fold higher than that of nitrogen [28], [29]. The pirani gauge installed in the freeze dryer unit used in this study is calibrated for nitrogen.

The measuring principle of the other pressure sensor, the capacitance manometer, is independent of gas composition. The readings of pirani gauge and capacitance manometer are therefore in good agreement as long as air or pure nitrogen are in the drying chamber. During primary drying, the atmosphere in the chamber consists almost completely of water vapour. Under these conditions the pirani gauge reads a 1.6-fold higher pressure than the capacitance manometer. Towards the end of primary drying, all ice has been removed from the product and the water vapour atmosphere is gradually replaced by nitrogen through a controlled air leak that maintains chamber pressure at the designated value. Due to this change in gas composition, the reading of the pirani gauge changes until it shows again the same pressure as the capacitance manometer. At this point, there will be no more ice in any of the product containers and the primary drying phase is concluded [27].

Maintaining the Product Temperature

Since sublimation is an endothermic process, energy must also be provided to maintain the sublimation rate [22]. Energy is taken out of the product in the form of heat. Omission of heat supply would inevitably lead to constant cooling of the product until it reaches the same temperature as the condenser. Heat is supplied by the heat transfer fluid flowing in channels or coils within the shelves. A well-designed freeze drying process must balance the amount of heat removed by sublimation and the amount of heat supplied by the shelves. If the shelf temperature is too high, an amorphous product might be warmed up until it reaches or passes a product-dependent critical formulation temperature, the so-called collapse temperature, T_c. At or above this temperature, the amorphous, glassy phase undergoes irreversible change, losing its rigidity (product collapse) [30]. A crystalline product will melt if it is warmed up to the eutectic melting temperature T_{eu}. If, however, the shelf temperature set point is selected far from optimum (i.e very low), the process will take much longer than necessary [20]. This is particularly important for the primary drying phase because it generally is the longest stage of the entire freeze drying process. Primary drying time for a typical process in vials often ranges anywhere in between 10 h and several days [31].

1.1.3 Secondary Drying

When all ice has been removed from the product, primary drying is completed. Yet there still remains an amount of "unfrozen water" dispersed within the product matrix. In a frozen amorphous product the total amount of this dispersed water can be as high as 10 to 20 % of the original water in the solution [32]. However, desorption of this "unfrozen" water starts locally in the product as soon as all ice has been removed by sublimation from that particular region. Sublimation may still continue in a more recessed region in the same product container [33].

In this work, a process design perspective is adopted in defining the starting point of secondary drying as the time point when all ice has sublimed. In an amorphous product, the content of "unfrozen" water at this time point was found to be less than 10 %, in the range of 4 to

8 % [33]. Note that water acts as a plasticiser in an amorphous solid and lowers its glass transition temperature T_g [34]. As soon as all ice has sublimed, there exists no freeze-concentrated solution any more so the temperature at which the product softens and changes to the rubbery state is correctly denominated as a glass transition.

Increasing the product temperature enhances diffusion of sorbed water from the interior of the product matrix towards the surface where desorption of sorbed water from the surface takes place [33]. If the product temperature T_p surpasses T_g (or T_c) during primary or secondary drying, softening of the lyophilisate matrix occurs. If this happens the cake will often undergo a volume contraction and then appears to be "shrunk" [35]. It is important to heat an amorphous product slowly during the initial ramping phase at the start of secondary drying so that the product temperature always remains below the momentary glass transition temperature. With continuous loss of water, T_g rises so that the final temperature set point for secondary drying is usually above ambient temperature and often as high as 40 °C [36, 37, 38]. The product is maintained at this temperature for several hours and residual moisture at the end of freeze drying is typically less than 1 % [39, 40]. The final product, the lyophilisate, is a solid structure with many very small pores. These pores enlarge the total surface area of the lyophilisates (e.g. approximately to 1 m^2/g in freeze dried sucrose [35]) and fast reconstitution of a solution upon addition of water is enhanced. This property of easy and fast rehydration is described by the term "lyophilic" meaning "liking the solvent".

1.2 Basics of Formulation Design

1.2.1 Lyoprotectants: Stabilising Excipients

The goal of the freeze drying process is to obtain a solid product containing a fully active drug. The active component may undergo structural changes or decompositon during freezing or drying due to chemical or physical instabilities. These instabilities can be caused by the dehydration effect of ice formation, freeze concentration, and other freezing- or heat-induced stresses. For example, it was reported that during freezing an increase in ionic strength of the remaining solution as well as pH shifts may lead to protein aggregation and/or unfolding [41, 42].

Stabilising excipients are often needed to protect the API. These stabilisers, or lyoprotectants, are interacting with the active ingredient, so that degradation reactions or, in the case of proteins, loss of the native globular structure are hindered [43]. These necessary interactions can only take place if the excipients and the active ingredient remain in the amorphous phase during freezing. The disaccharides sucrose and trehalose are well known to form amorphous matrices during freezing and their good stabilising abilities in freeze dried formulations have been shown many times before [38,36,44]. Raffinose is a non-reducing trisaccharide consisting of galactose, glucose, and fructose [45]. The advantages and disadvantages of raffinose as a stabiliser in freeze dried formulations have been discussed [46], [47].

It has been reported that a high molar ratio (360 : 1) of amorphous excipient to protein (monoclonal antibody) may be required for sufficient stabilisation [48]. Formulations containing only amorphous components form glasses during freezing. As has been said (section 1.1.2), amorphous formulations have the disadvantage of losing structural integrity during primary drying if the product temperature surpasses the collapse temperature of the formulation, T_c. If this happens, the porous structure formed after sublimation of ice crystals is lost. The product matrix loses its desired properties, such as elegant appearance of the smooth "cake" structure, fast and complete reconstitution, and possibly stabilisation of the active ingredient [49, 30].

The critical formulation temperature should not be any lower than the "target product temperature". This target product temperature denominates the temperature intended for the sublimation front of the frozen product solution during primary drying. This temperature is often a compromise between optimisation of primary drying time (the higher the product temperature, the shorter the primary drying phase) and achievement of a smooth, rugged lyophilisate (a product temperature during primary drying below the critical formulation temperature usually leads to desirable appearance of the lyophilisate [20]). Even a 1 °C increase in product temperature can shorten primary drying time by a significant amount [20]. Usually, product temperatures as low as approximately −40 °C are still considered as manageable [49], [38], [21].

If the solid content in the formulation is low (i.e. less than 10 mg/mL), the pores within the lyophilisate take up most of the space and the solid structure itself is fine and brittle. During primary drying, there is a strong flow of water vapour which is able to tear off small particles from the solid fraction and carry them with it [15]. This phenomenon is called product fly-out. In order to prevent it, a minimum content of solids of at least 20 mg/mL in the formulation should be attained. This can be achieved by adding a surplus of the stabilising excipient or by using a bulking agent. These are usually crystallising excipients, and interactions between these and the active substance are not intended. A high content of solids (i.e. more than 100 mg/mL, [21]) in the formulation leads to formation of a lyophilisate which is rather dense with only small pores. The water vapour flow during primary drying is slower through these small pores, due to an increase in the product resistance of the dried layer, and the primary drying time is increased [50], [20].

1.2.2 Determination of the Critical Formulation Temperature

Freeze Dry Microscopy

As a result of the above said, the product temperature of an amorphous product may not exceed T_c at any point during the sublimation phase. This process-governing critical formulation temperature can only be determined by freeze dry microscopy [51]. For this analysis, a microscope

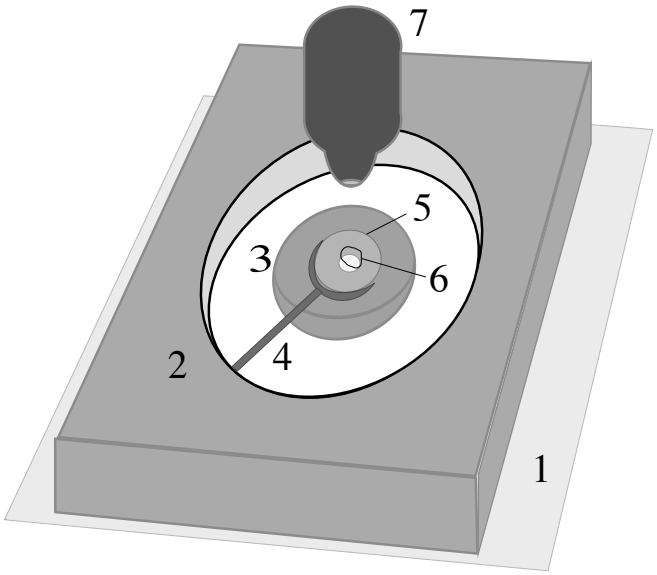

Figure 1.3: Schematic of the set-up of the stage of a freeze dry microscope. The corpus of the freeze drying stage (2) rests on the microscope's regular stage (1). The freeze drying chamber contains the silver-block oven (3) with a hole for transmittance of light. The circular object slide (5) is mounted to the silver-block oven by a microscope slide fastener (4) which enables small movements of the object slide during the measurement. The sample droplet (6, approximately 2 μL) is applied to the middle of the object glass. The sample is covered with a small cover glass (not shown) and the freeze drying chamber is closed with a lid (also not shown). The sample is frozen and the chamber is evacuated. Then the sample is heated with a controlled heating rate. Direct observation of the sublimation front is possible through the chamber lid with the objective of the microscope (7).

with a freeze drying stage is needed.

The stage consists of a vacuum tight chamber that encloses the sample holder, and a heat source, see Figure 1.3. Heat is usually supplied by direct contact of the object slide to a silver-block oven. The chamber allows observation of the sample on the microscope slide during the entire experiment through glass openings in bottom and lid of the chamber. A small droplet (2 to 10 μL, [52]) of the solution to be analysed is placed on the slide and covered with a small cover glass. This array is then fastened in the chamber and the chamber lid is screwed on. The temperature of the silver-block oven is lowered until the droplet is completely frozen. Then the chamber is evacuated and the temperature of the silver-block oven is gradually raised with a controlled heating rate.

Sublimation of ice starts at the edge of the frozen droplet, the sublimation front gradually moves towards the sample centre. The beginning of collapse can be determined as the temperature at which formation of "holes" in the freeze dried matrix just behind the sublimation front occurs. The observed holes are indicators for mobility in the primary dried structure that leads to collapse of the small pores left behind after sublimation of ice crystals. The collapsing pores tear the fragile primary-dried matrix apart and thus gaps appear in the matrix [52].

Differential Scanning Calorimetry

For formulation screening, the glass transition temperature of the maximally freeze concentrated solution, T_g' can be used instead of T_c. A glass transition occurs when an amorphous material changes from the brittle, glassy state to the rubbery, viscous state or vice versa. This second order phase transition can be determined by differential scanning calorimetry, DSC. This is a

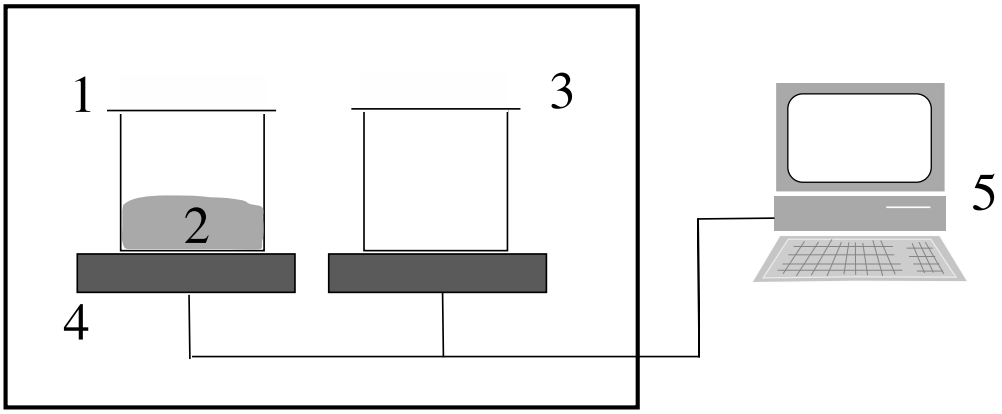

Figure 1.4: Schematic of the set-up of a DSC unit. 1: sample pan, 2: sample inside pan, 3: empty reference pan, 4: heater, 5: computer to monitor and control temperature at contact area of heaters with respective pan.

method to determine thermal events in a material by comparison of heat capacity of the sample to a reference.

The functional unit of a power-compensated differential scanning calorimeter consists of a closed chamber containing two heaters which are operated and controlled by computer software, see Figure 1.4. On the heaters, two pans of approximately the same weight and identical material and geometry are placed [53]. The most common material for DSC pans or crucibles is aluminium. One of these pans is empty and serves as the reference. The other contains a sample (5 to 40 μL for liquids, mass of solid samples depends on density of material) of the substance to be analysed. The pans are warmed up (scanned) with a constant heating rate (i.e. 10 K/min). The software controls that the heating rate in sample and reference pan are exactly the same. Heat is needed to heat up the pans themselves; the amount of heat needed for this should be almost identical for both pans and depends on the weight and material of the pans.

Additional heat is needed to keep up the heating rate in the sample pan as the sample itself must be heated as well. The difference Δh in units of energy or power (J or W) or energy per unit mass (J/g) between heat flow to reference pan and heat flow to sample pan is plotted against temperature (in units of K or $^\circ C$) in the DSC-curve [54]. A schematic of a DSC-curve is given in Figure 1.5. The amount of heat needed to warm up a material by one Kelvin is the material's heat capacity C_p [3]. As long as no thermal events occur, the DSC-curve shows just a straight line, the heat capacity of the material in the sample pan. If the glass transition of a (partially) amorphous material is reached, a step change ΔC_p occurs in the thermogrgam.

Below the glass transition, molecules in the amorphous material are immobilised. Above the glass transition temperature, molecules have gathered enough energy to undergo a higher amount of segmental motion. This means that the heat capacity of the material has changed (risen). Contrary to crystallisation and melting events, no latent heat is given off (crystallisation) or absorbed (melting) in this phase change. This absence of latent heat during the conversion is the reason why a glass transition is called a second order phase transition. Thermal events involving latent heat are visible as peaks or dips in the thermogram and they are called first order phase transitions [55].

A glass transition occurs over a temperature range, not at a clearly defined temperature. Usually the temperature in the middle between beginning and end of the step change (midpoint) is denominated as the glass transition temperature, T_g. There is no universal convention for determination of T_g, other methods are also used (i.e. onset of step change, inflection point of slope [56], [55]). The glass transition temperature also depends on the measuring conditions, namely the heating rate, and the thermal history of the sample. In freeze drying literature, the expression T_g' has been adopted to denominate a glass transition of a frozen (aqueous), maximally freeze-concentrated solution of amorphous material [49], [37].

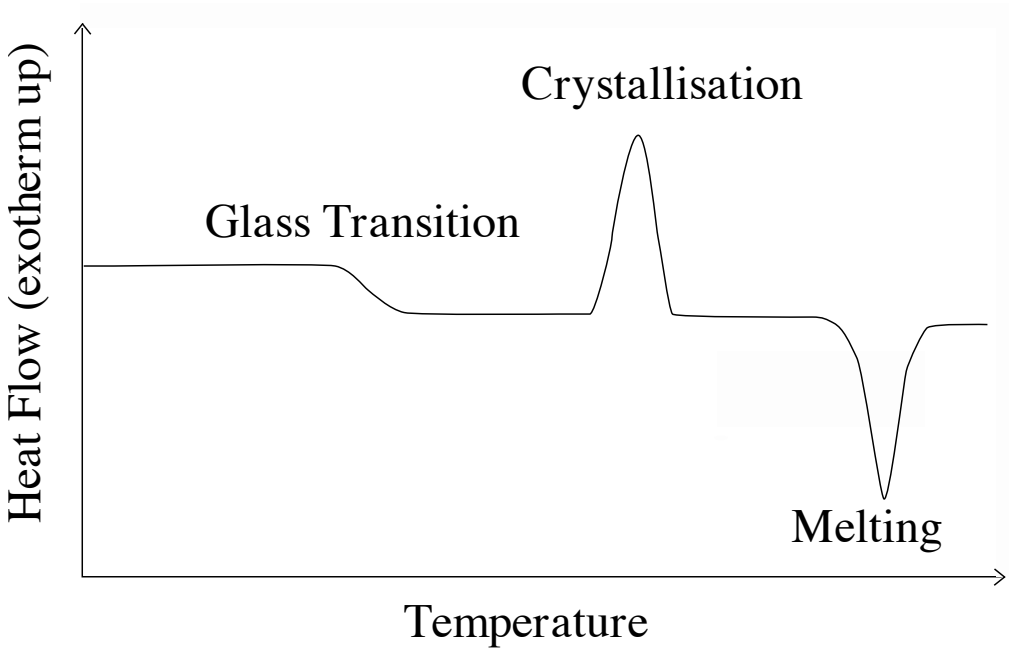

Figure 1.5: Schematic of a DSC thermogram showing glass transition, crystallisation, and melting events. Exothermic heat flow is shown in upwards direction.

Special care must be taken during sample preparation. For example, if the glass transition temperature of a lyophilisate shall be determined, it is important to assure that the residual moisture content in the sample does not change during sample preparation. Additionally adsorbed moisture acts as a plasticiser, lowering the glass transition temperature of the sample.

During DSC experiments with solutions containing crystallising excipients such as mannitol, precautions should be taken to maximise crystallisation of these excipients: for mannitol, the freezing rate should be reduced to 0.5 °C/min until a temperature of −20 °C has been reached. An additional annealing step at −20 °C for 20 min should also be included in the DSC temperature program.

Typically T_c measured by freeze dry microscopy and T_g' determined by differential scanning calorimetry are not equal but lie close to each other. The collapse temperature is usually a few Kelvin (2 to 5 K) higher than the glass transition temperature of the maximally freeze concentrated solution [37]. Typical collapse temperatures for amorphous stabilisers of low molecular weight can be found at approximately −30 °C (sucrose: −32 °C, trehalose: −28 °C) [21].

1.2.3 Crystallising Excipients as Bulking Agents

Some commonly used excipients such as mannitol or glycine are added as a bulking agent to a formulation because they reliably form mechanically rugged, smooth cakes [57]. To achieve complete crystallisation, formulations containing a bulking agent usually require an annealing step in the freezing phase. This thermal treatment is carried out after the solution is completely frozen. The temperature of the frozen product is raised to a temperature in between T_g' of the remaining non-crystaline, amorphous fraction of the product and the eutectic melting temperature T_{eu} of crystalline parts. This temperature is held for several hours. The additional energy provided by this higher temperature leads to crystal growth and reduces the fraction of amorphous bulking agent [58]. Incomplete crystallisation may lead to vial breakage [59].

In addition to formation of elegant cakes, many crystallising excipients have the advantage of possessing higher critical formulation temperatures than stabilisers of small molecular weight: since they are crystalline, their solutions will not collapse during primary drying but melt at the eutectic temperature. As an example, T_{eu} for mannitol solution is −1.5 °C [60, 61]. These

temperatures are considerably higher than collapse temperatures of many amorphous stabilisers and consequently primary drying for a crystalline formulation can often be carried out at a much higher product temperature. For a formulation with such a high critical formulation temperature, the limitation for further shortening of primary drying time could lie in sub-optimal design of the freeze dryer, and not in the formulation [62].

During the past years, formulations containing crystallising components as well as a smaller amount of amorphous stabiliser have been tested. These partially crystalline formulations are often primary dried at product temperatures exceeding T_c of the amorphous formulation constituent [60]. Then "micro-collapse" will occur within the matrix: the amorphous component collapses yet the crystallising bulking agent builds up the main body of the cake and supports the structure even if the amorphous fraction loses its rigidity. Thus, micro-collapse is tolerable as it has no negative effect on the macroscopic cake appearance. In many cases the active ingredient will not suffer unduly while undergoing this treatment [49]. There are other cases in which the API did lose activity after freeze drying at a product temperature exceeding T_g' [63]. If the loss of activity is restricted to an acceptably small amount, these partially crystalline formulations combine the advantages of fast reconstitution times, good appearance of the lyophilisate cake, and short freeze drying cycles with good stabilisation of the active ingredient.

Presence of (crystallising) buffer components can cause problems. Large pH shifts upon freezing have been reported, namely for phosphate buffer [64]. As a general rule, the concentration of buffer components should be kept to a minimum.

1.3 Mathematical Models of the Freeze Drying Process

1.3.1 Model Based on Pseudo-Steady State

During the primary drying phase, the process of ice sublimation or mass flow of water vapour must be maintained by supply of energy in the form of heat. The optimum shelf temperature corresponding to the target product temperature is still often determined by trial and error. If heat and mass transfer characteristics of the freeze dryer, the container, and the product are known, the optimum shelf temperature can be estimated based on calculations describing coupled heat and mass transfer [1]. Several mathematical models have been developed to describe the progress of primary and secondary drying for pharmaceuticals in vials [65], [66], [67], [50]. There are no models dealing with other containers or a different container geometry.

Pikal applies a model for freeze drying in vials which is based on pseudo-steady state conditions and a moving planar boundary during primary drying [50]. A pseudo-steady state exists as long as the amount of heat entering into the product is balanced by the amount of heat removed through sublimation of ice. Under these conditions the product temperature does not change significantly. Pikal argues that even after a change in shelf temperature, these pseudo-steady state conditions will be attained within 30 min and so can be found during most of primary drying. Contrary to experimental findings he assumes a planar sublimation interface moving from the surface of the frozen solution towards the bottom of the vial, ignoring effects of radiative heat input through vial walls [50]. Although simplified, Pikal's model yields results for prediction of sublimation rates and primary drying times which are in good agreement with experimental data [50].

Integral part of Pikal's model is a software algorithm, the SMART™ Freeze Dryer software (SP Scientific, Stone Ridge, NY, USA). This algorithm is used to analyse pressure rise data which are collected during the freeze drying run carried out in an especially equipped freeze dryer. In order to use this technology, a valve between drying chamber and condenser is closed very quickly (closing time <1 s) at intervals of 30 or 60 min during primary drying [31]. After completion of the freezing step, the shelf temperature is ramped to the desired primary drying setpoint. After approaching this point the first set of pressure rise data is collected with a 60 min delay to avoid a bias caused by non-steady state conditions at the initial phase of primary drying.

The valve remains closed for 25 s. During this short period of time, the pressure in the chamber increases. Data points of chamber pressure rise over time are collected (usually 4 data points per second during the measuring interval of 25 s, [31], [68]). A mathematical model equation (MTM equation, cf. [50], [31], [68]) is fitted to these pressure rise data. Parameters determined by the data fit include vapour pressure of ice (P_{ice}) at the point of measurement as well as the area normalised product and stopper resistance ($R_P + R_s$). All of these parameters are printed into a table.

If P_{ice} is known, the product temperature (T_p) can directly be calculated. This procedure is denoted Manometric Temperature Measurement (MTM), which uses a proprietary algorithm (the MTM equation) to determine these two parameters. For accurate determination of P_{ice}, a sufficiently large area of the total sublimation interface is needed. The minimum area of the sublimation interface for valid MTM results was determined to be 300 cm^2 [25]. This means the number of containers still in the state of sublimation must be high enough for an accurate measurement of the ice vapour pressure.

The pressure rise curve recorded during the MTM measurement is a combination of three mechanisms. First, sublimation of ice at constant temperature of the product leads to an increase in chamber pressure while the connection to the condenser is closed. Increase in chamber pressure leads to a decrease in the sublimation rate, as the difference between chamber pressure and sublimation pressure decreases. Heat flow from the shelf is not reduced so that as a result of lessened heat consumption by sublimation, the product temperature increases. Sublimation pressure increases with the increase in product temperature, contributing to the pressure rise. Then there is a linear pressure increase attributed to the (very low) leak rate of the chamber [50]. Each of these three mechanisms contributing to pressure increase in the chamber is represented by a term in the MTM-equation [69].

The SMART™ software uses P_{ice} and $\hat{R}_P$ data in combination with additional heat and mass transfer equations to calculate additional important parameters which facilitate process optimisation [31]. These parameters include mass flow and vial heat transfer coefficients. Based on these results, automatic adjustments in the freeze drying recipe are performed by the software.

Within the SMART™ feature, MTM data can be collected when predefining a cycle recipe, omitting the cycle optimisation algorithm. This sub-feature is called Auto-MTM. In this way, information on P_{ice} and the sum of product resistance and stopper resistance, $R_P + R_s$, can be gained while performing a freeze drying cycle, based on a user predefined cycle recipe. While these measurements are based on the same algorithm as the SMART™ software they are only performed to collect data without automatic adjustments in the settings for shelf temperature or chamber pressure. For each MTM-measurement, the directly determined parameter P_{ice} and the parameters calculated from the fit results, i.e. T_P and R_P, are printed into a table.

Later, this model was extended to non-steady state conditions and applied to secondary drying as well [2]. For a rational cycle development, this model requires information about the nature of the formulation (i.e. crystalline or amorphous, type of API) and its critical temperature, as well as knowledge of the heat transfer coefficient and geometry (product area) of the designated container. Using these parameters as input data in the calculations, an estimation for optimum shelf temperature for primary drying can be made [25].

Other models have since been developed which are based on a similar strategy: determination of the average temperature at the sublimation interface of a whole batch of vials in a freeze dryer by performing a pressure rise test and subsequent data analysis [70]. The results are then directly implemented for a freeze drying cycle optimisation.

1.3.2 Dynamic Model

Another model for vials was developed by Sheehan and Liapis [67]. The authors designed a dynamic model which includes the change of shape of the receding boundary between frozen solution and primary dried product. The main scope of the authors is to create a predictive theoretical model to decrease process development time. To achieve this, the model should be able to predict and describe position, shape, velocity, and temperature distribution of the moving boundary between frozen solution and primary dried structure. The model also includes a simulation of progress of secondary drying. It describes the temperature distribution in the matrix at different times from beginning of secondary drying and the distribution for the concentration of bound water in the matrix.

Contrary to Pikal's method described above, the focus in this method is laid on the description of progress for primary and secondary drying in an individual vial. The geometry of the vial is described by the parameters of the fill depth L, the inner radius r, and the thickness of the glass wall δ. No attention is given to the shape of the vial bottom and the separation distance l of the vial bottom to a flat surface. Calculations for the model are based on heat input from three directions: top, bottom, and sides. Heat input from sides and top is considered to originate exclusively from radiation. For heat input from the bottom, radiative heat transfer is neglected. To fully describe primary drying a set of 32 equations is used. Special consideration is given to the ability to describe curvature of the sublimation interface in dependence of amount of heat input from the sides. Another set of 21 equations is applied for description of secondary drying.

In the research paper, this model is applied to freeze drying of skim milk under different processing conditions. The authors differentiate between three cases. In all cases, an individual vial in an array of vials on a tray was considered. The arrangement of the vials was considered to be a square pattern, not a hexagonal pattern. The latter, however, is the most economical and most widely used packing pattern for vials in a freeze dryer because it yields the highest number of vials per batch. The authors describe the use of a tray to place the vials in the freeze dryer. This tray adds an additional barrier to heat transfer. This barrier is not discussed in the paper. Removal of the bottom of the tray is a simple measure to enhance heat transfer to the product and shorten drying times [71], [1].

In the first case the model was applied to a vial placed on the edge of the array of vials on the tray. For the modelling of the primary drying stage, the shelf temperature was set to the

highest possible value that resulted in a product temperature still below the critical formulation temperature. For the second case, the position of the vial in the array was not altered but the shelf temperature set point during primary drying was kept very low. In the third case, a vial placed in the centre of the array was considered. The temperature regime was similar to the shelf temperature profile of the first case.

The model succeeded in prediction of nearly identical primary drying times for cases I and III and a significantly longer primary drying time for case II. It also predicted a curvature of the sublimation front for the vials placed on the edge of the array. It calculated hardly any curvature of the sublimation interface for the vial in case III placed in the centre of the array. For secondary drying, the model predicts a similar distribution of product temperature and residual moisture for the edge vials of cases I and II. The secondary drying results for the vial in the centre (case III) describe a more homogeneous distribution of both temperature and residual moisture in the product matrix.

In order to produce these results, numerical values for over 30 parameters had to be used for solving the set of equations. These parameters included, for example, heat capacity of water vapour, heat capacity of ice, concentration of bound (unfrozen) water in the frozen sample, geometrical view factors of upper and lower shelf of the freeze dryer as well as of freeze dryer wall for the vial under consideration, heat conductivity of glass, partial pressure of water vapour and inert gas, and many others. Some of these, i.e. concentration of unfrozen water in the frozen sample, are different for each formulation under consideration and difficult to determine by measurement. The equations could not be solved by simple calculations but had to be implemented in a computer programme.

If all these parameters have to be determined anew for each formulation to be tested, this model is very complicated to use. No data is presented to show validity of the prediction of distribution of product temperature and residual moisture to a freeze drying cycle. Optimisation of a freeze drying cycle has to take into account the whole batch of vials in the freeze dryer, not only a single vial in a prominent or atypical position. If this model is used, it should be applied to those vials that need the longest time interval to complete primary and secondary drying. Usually, these are the vials in the centre of the array [1]. The inconvenience of implementation of this more sophisticated mathematical model is not balanced by the gain of additional information for a "standard" process optimisation problem.

1.4 Influence of Container on the Freeze Drying Process

1.4.1 Resistances to Water Vapour Flow

In most freeze drying processes for pharmaceuticals, glass vials are used as containers for the product solution. For these vials, Pikal, Roy, and Shah stated [1] that water vapour flow from subliming ice in the frozen product towards the condenser has to overcome three barriers or resistances. It is easier to use the term of resistance to water vapour flow than permeability for water vapour flow (which is the reciprocal to resistance) because several resistances in series simply add up to the total resistance [50].

The largest resistance for water vapour flow is the layer of already dried product. The layer thickness increases with progress of primary drying [69]. Pikal et al. determined the dried product resistances R_P using a microbalance [72]. According to these studies, mass flow of water vapour is restricted due to the small size of channels and pores left behind after sublimation of ice crystals as a passage way for water vapour from deeper within the product. The smaller the ice crystals are, the smaller will be the resulting pores and the higher the product resistance.

The freezing step has great impact on product resistance because it determines the ice crystal size [16]. When a formulation is cooled, ice crystals will not form as soon as the temperature of the solution has fallen below its eutectic melting temperature. The phenomenon that a solution remainins in the liquid phase below the melting temperature until crystallisation sets in is termed supercooling [73]. Ice crystal growth is induced by formation of ice nuclei. Creation of these nuclei is a stochastic process. The probability of nuclei formation increases with increasing degree of supercooling [73]. A high degree of supercooling leads to formation of a large number of nuclei which form a large number of small crystals. At a slow freezing rate, probability of nucleation at a small degree of supercooling is higher than at a fast freezing rate. If nucleation sets in at a higher temperature, fewer nuclei are formed and the resulting ice crystals are larger.

Irrespective of the freezing protocol ice crystals and resulting pores will be of a size that water vapour flow within the dried product is free molecular or Knudsen flow and pressure-independent [1]. Free molecular flow takes place if the mean free path of a gas molecule is in the same order of magnitude or larger than the dimensions of the channel through which the gas is flowing. The mean free path is the average distance that a gas molecule may travel before it collides with another gas molecule. The order of magnitude of the mean free path depends on the number of gas molecules per unit volume, that is, it depends on pressure [7].

The dried product resistance R_P not only depends on the thickness of the dried product layer, but also on the area of the ice-vapour interface which in turn is affected by vial size and type [1]. Moreover, the shape and size of the ice-vapour interface change during primary drying as the sublimation front curves downward at the vial sides. This deviation from planar progression of the sublimation interface is caused by radiative heat input into vial walls [2, 26]. Using manometric temperature measurement technology, the product resistance can be determined during a regular freeze drying cycle at intervals during primary drying [69]. There are different measurement techniques and associated software tools available today for determination of R_P of formulations in vials [69], [70].

The next barrier for water vapour flow arises from the stopper inserted into the vial neck. The stopper design allows placement in such a way that one or several channels are left open ("semi-stoppered" position). Water vapour generated by sublimation can pass through these channels and leave the interior of the vial. The openings of stoppers in semi-stoppered position are a few millimetres wide, even in stoppers for small (i.e. 2R) vials [74]. In comparison to the dimensions of these openings, the mean free path of a water molecule is small. Water vapour flow through the openings of the stoppers is therefore governed by viscous flow mechanisms [1].

The resistance caused by the stoppers on vials is denoted as R_s. There are several other, smaller resistances for a water vapour molecule on the way to the condenser coils where it is turned to ice again (resistance of the pipe connecting freeze drying chamber and condenser, resistance in the condenser itself). There may be an additional resistance to water vapour flow if the vials are placed in a tray with a lid [50]. Water vapour flow within the chamber is also dominated by viscous flow and is pressure dependent. All of these described resistances contribute to the total resistance to water vapour flow:

$$\frac{\mathrm{d}m}{\mathrm{d}t} = \frac{\Delta P}{R_p + R_s + R_x}. \tag{1.1}$$

The driving force for mass flow $\frac{\mathrm{d}m}{\mathrm{d}t}$ (in units of g/h per vial) is the pressure difference ΔP (pressure in $Torr$) between sublimation pressure P_{ice} at the ice sublimation interface and chamber pressure P_c. The resistance of the dried product layer R_P (in units of $Torr\ h\ g^{-1}$) usually accounts for approximately 90 % of the total resistance to mass transport [1]. For reasons of comparability of formulations freeze dried in different types of vials, the area normalised product resistance $\hat{R}_P$ is calculated using the internal cross-sectional area of the vial, A_P. Units of $\hat{R}_P$ are $cm^2\ Torr\ h\ g^{-1}$. R_s in Equation 1.1 is the resistance of the stopper, R_x stands for the sum of all other resistances to water vapour flow.

As a summary it can be stated that the dried product causes the main resistance to water vapour flow and the container itself has little importance on the restrictions to mass flow. This will be true for non-vial containers also as long as obstructions in the water vapour flow path leave openings dimensionally comparable to those in semi-stoppered vials.

1.4.2 Heat Transfer into the Product

Whether T_c or T_{eu} is the critical temperature for the product, a "target product temperature" for primary drying must be defined. This target product temperature should be slightly lower than the critical formulation temperature to include a temperature safety margin in process design. This safety margin is needed to take into account uncertainties in temperature measurement and variability in product temperature in between vials (or other containers) placed in different positions on the freeze dryer shelf. There are economic reasons to optimise the freeze drying process and keep process costs and total duration of the cycle low. To minimise primary drying time, the temperature safety margin should be low and the target product temperature should be kept as close to the critical formulation temperature as possible. Pikal stated [50] that an increase of product temperature by 1 °C decreases primary drying time by approximately 13 %.

For very long primary drying phases (i.e. longer than 48 h), the product temperature should be kept 1 to 2 K below the critical formulation temperature. For short primary drying times (i.e. less than 12 h) this safety margin can be increased to as much as 5 K [31].

Heat transfer from the shelf surface to the product in vials has been studied extensively [1, 75, 68, 50]. Other containers are also used in freeze drying, such as ampoules and dual chamber syringes [76, 77]. There is an increasing demand for easy-to-handle pre-filled syringes and injectors [12]. Other approaches and product conceptions including novel containers are also tested to generate robust, stable protein formulations (i.e. biodegradable, hollow miniature implants filled with vaccine [13]). Optimising absorption of an API and achievement of better patient compliance are also important objectives to test freeze dried formulations as an alternative (i.e. mucoadhesive application of non-protein drugs as freeze dried formulations is a possible alternative to swallowing compressed tablets [14]).

As a consequence for process design, heat and mass transfer characteristics of the non-vial containers suited for these novel dosage forms need to be studied. Apart from experiments performed within the scope of this thesis [78, 79, 80], there is very little literature about heat transfer mechanisms for any other non-vial containers. Hottot and al. have studied freezing as well as heat and mass transfer behaviour of pre-filled syringes [81], [82]. In their studies, they determined both resistance of the product to water vapour flow (R_P) and heat transfer coefficients using a pressure rise analysis mehtod.

In order to correctly determine heat transfer coefficients, theoretical considerations concerning heat transfer into the product have to be made. Heat can enter into the product from three directions [2, 67]:

1. from the radiation surface (bottom side of upper shelf)

$$\mathrm{d}Q_1 = K_1(T - T_{up}) \tag{1.2}$$

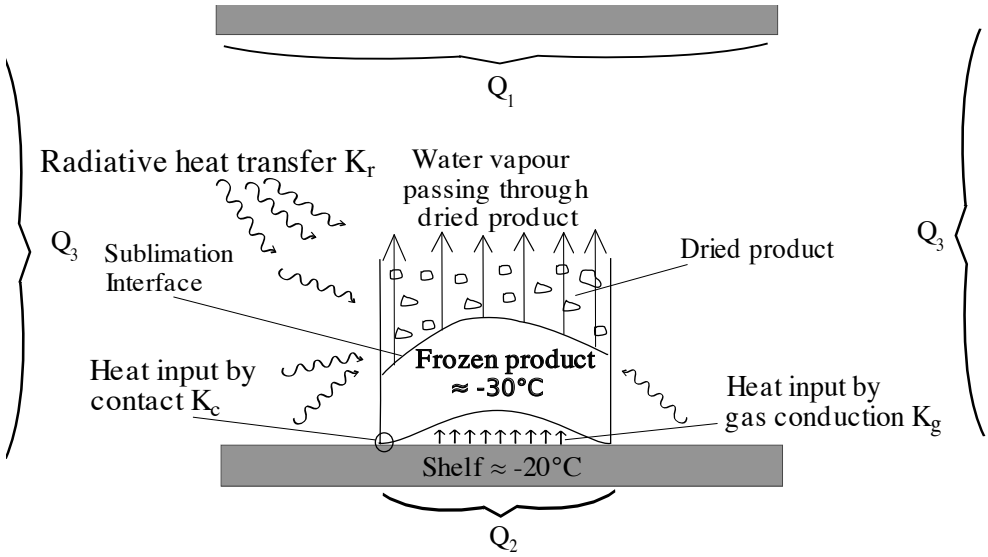

Figure 1.6: Schematic of heat transfer into a vial placed on a freeze dryer shelf. Heat can enter into the vial from top (Q_1), bottom (Q_2), and sides (Q_3). Heat is transferred by three mechanisms: radiation (corresponding to radiation contribution to heat transfer, K_r), conduction (K_c), and conduction through the gas in places where the separation distance between heat source (shelf) and container (vial bottom) is small (K_g).

2. from the surface on which the containers are placed

$$\mathrm{d}Q_2 = K_2(T - T_s) \tag{1.3}$$

3. from the sides (freeze dryer wall or door)

$$\mathrm{d}Q_3 = K_3(T - T_w) \tag{1.4}$$

with heat fluxes, $\mathrm{d}Q_i$, in power per area (kW/m^2) and heat transfer coefficients, K_i, in power per area per Kelvin ($kW\ m^{-2}K^{-1}$). A schematic of the heat and mass transfer mechanisms contributing to the primary drying phase in a vial is given in Figure 1.6. For pharmaceuticals in vials, the main portion of primary drying is carried out under conditions that can be described as a pseudo-steady state or dynamic equilibrium. During this phase, the energy needed to sublime a certain mass of ice in a given time is equalled by the energy provided by the shelf:

Heat input into product by shelf fluid = heat removed by sublimation.

A brief overview of mechanisms of heat transfer for vials is given below. During steady state conditions, all heat supplied by the shelf is used for sublimation of ice and the product temperature does not change. If these conditions apply, the following equation is valid [1]:

$$\frac{\mathrm{d}Q}{\mathrm{d}t} = \frac{\mathrm{d}m \cdot q_{s,ice}}{\mathrm{d}t} = A_v \cdot K_v \cdot (T_s - T_b). \tag{1.5}$$

Equation 1.5 shows the direct proportionality of heat flow $\frac{\mathrm{d}Q}{\mathrm{d}t}$ (time t in s) to mass flow $\frac{\mathrm{d}m}{\mathrm{d}t}$ (g/s). Unfortunately, in freeze drying literature the unit calory (cal) for heat flow $\mathrm{d}Q$ and calculation of heat transfer coefficients is still commonly found. The factor of proportionality $q_{s,ice}$ is the heat of sublimation (sublimation enthalpy) of ice. The value of $q_{s,ice}$ is slightly temperature-dependent [22]. The lower the temperature of ice, the higher the sublimation enthalpy. In freeze drying literature different values for $q_{s,ice}$ can be found: 660 cal/g, [50], [72], [1], [83], 667 cal/g [31], 676 cal/g [62], 680 cal/g [2], [84], [67]. Recent measurements and calculations [22]

determined a value for $q_{s,ice}$ of approximately 2840 kJ/kg for the temperature range relevant during the primary drying phase of a freeze drying process (product temperatures approximately from −35 °C to −10 °C, shelf temperatures approximately from −30 °C to 20 °C). Conversion to the older unit yields 679 cal/g. Throughout the calculations performed in this work, 670 cal/g is used as an average of the above cited values for $q_{s,ice}$. This value was chosen to achieve comparability of heat transfer coefficients calculated in these studies to heat transfer coefficient data in the literature. The error introduced into calculations by this deviation in values for heat of sublimation is less than 2 %.

The difference $T_s - T_b$ in equation 1.5 equals the difference of shelf surface temperature beneath the container (T_s) to product temperature at the bottom of the container, at a point close to the shelf surface (T_b). For all considerations of heat transfer, temperature differences are employed and the result of the calculation will be the same whether temperatures are used as degrees Centigrade ($°C$) or as Kelvin (K). The SI unit of temperature is Kelvin, and in literature dealing with container heat transfer coefficients, the temperature unit employed is also Kelvin. This unit is used throughout this study for all temperature differences.

The efficiency of heat transfer from the shelf surface to the product in a vial can be expressed by the vial heat transfer coefficient, K_v ($cal\ s^{-1}cm^{-2}K^{-1}$). This parameter depends on the geometry and material of the vial (or other container used, as is the case in this work), and on the chamber pressure. A_v (cm^2) is the outer cross-sectional area of the vial bottom. With regard to other container geometries, the area of contact / direct view between heat source and container wall must be applied to determine A_{cont}, the area through which heat is transferred into the product.

K_v itself is the sum of three contributions to heat transfer: heat transfer by radiation, K_r, heat transfer through direct contact (heat conduction, K_c), and heat transfer by conduction through the gas, K_g [1]

$$K_v = K_r + K_c + K_g. \tag{1.6}$$

Figure 1.6 on the facing page is a schematic illustrating the contribution to total heat flow into a vial by the three individual mechanisms of heat transfer. The pressure dependence of the vial heat transfer coefficient K_v can be expressed as [83]

$$K_v = K_K + \frac{K_P \cdot P}{1 + l(K_P/\lambda_0) \cdot P}. \tag{1.7}$$

K_K ($cal\ s^{-1}cm^{-2}K^{-1}$) in equation 1.7 is a constant representing the sum of the contribution to heat transfer by direct contact and by radiation. Heat transfer into the product by radiation may take place from all three directions, top, bottom, and sides. Vial heat transfer coefficients are usually determined for vials placed in the centre of a closely packed array on the shelf. These centre vials receive no net radiative heat input from the sides, because the neighbouring vials have the same temperature. Therefore, (see equation 1.4) $K_3 = 0$ and consequently $Q_3 = 0$. The contribution to heat transfer by radiation from the top shelf corresponds to heat flow Q_1 in equation 1.2. Contribution to heat transfer by radiation from the bottom shelf makes up part of Q_2. Heat transfer by direct contact occurs through the container bottom and corresponds to another part of heat flow Q_2 in equation 1.3. At 0 mTorr, total heat transfer into the product is equal to K_K.

The value of K_P appears to be the same for all vials. It has been determined as $33.2 \cdot 10^{-4}$ cal $s^{-1}cm^{-2}Torr^{-1}$ [2, 1]. Containers other than vials must not necessarily have the same value for K_P. l (cm) is the separation distance between the bottom of the vial and the bottom shelf [2]. λ_0 ($cal\ s^{-1}cm^{-1}K^{-1}$) is the heat conductivity of the gas at ambient pressure.

1.4.3 Heat Input by Radiation

The magnitude of the radiative contribution to heat transfer varies with the geometry and material of the freeze dryer [26]. Heat input by radiation is highly dependent on the emissivity of the emitting surface. Emissivity ε is the ratio of the radiation intensity of a nonblack body to the radiation intensity of a blackbody at the same temperature [3]. Radiation hitting a real body is partially reflected (e.g. on a polished surface), partially transmits the body, and is partially

absorbed. If this body is in thermodynamic equilibrium (its temperature does not change) then the amount of emitted radiation will be equal to the amount of radiation that has been absorbed (Kirchhoff's Law [23]).

The emissivity of a surface can be determined using an infrared thermometer. Determination of a surface's temperature by infrared technology requires knowledge of the emissivity of the surface in the temperature range under consideration. If the temperature of the surface is known (i.e. through measurement with a thermocouple), then it can be used to determine the surface's emissivity [3].

A polished stainless steel freeze dryer door or wall has an emissivity less than 0.5 [28] whereas the Plexiglas door of a laboratory scale freeze dryer will have an emissivity that is almost unity (0.9, [85]). This means that a plexiglas door has characteristics close to a full radiator: practically all radiation hitting the surface is absorbed and practically all the absorbed radiation is emitted again. Only a very small amount of the radiation hitting this surface is reflected from the surface or transmits the body without absorption.

As mentioned before (see 1.4.2) heat input by radiation into vials or other containers in a freeze dryer mainly occurs from the shelves while atypical radiation arises from freeze dryer walls and door. At least for vial freeze drying, this undesired contribution to heat transfer leads to differences in product temperature and primary drying time between edge- and centre-placed vials. It is most pronounced under conditions of very low pressure (little contribution to total heat transfer by conduction through the gas) and very low shelf temperature [26]. Low shelf temperatures increase the temperature difference between non-temperature controlled emitting surface (freeze dryer wall and door) and receiving surface (product container in line of view of emitting surface). The increase in temperature difference between heat source and heat sink elevates the radiative heat flow (see Equation 1.9). Rambhatla and Pikal [26] determined sublimation rates of pure water for edge and centre vials for different shelf temperatures. The ratio of heat transfer rate of edge vials to centre vials decreases from approximately 1.3 at a shelf temperature of -25 °C to approximately 1.1 at a shelf temperature of 0 °C. Studies performed by Hottot et al. [86] led to similar results.

Apart from this atypical radiation input, radiative heat transfer can be divided into the two contributions of top shelf and bottom shelf radiation. The difference between the fourth powers of the absolute temperatures of the two surfaces impacts radiative heat flow $\frac{\mathrm{d}Q_r}{\mathrm{d}t}$ [26, 1]:

$$K_r \propto \frac{\mathrm{d}Q_{r,top}}{\mathrm{d}t} + \frac{\mathrm{d}Q_{r,bottom}}{\mathrm{d}t} \tag{1.8}$$

and

$$\frac{\mathrm{d}Q_r}{\mathrm{d}t} = A_v \cdot \bar{e} \cdot \sigma \cdot (T_2^4 - T_1^4) \tag{1.9}$$

where σ ($5.67 \cdot 10^{-8}$ W m^{-2}K^{-4}, [87]) is the Stefan-Boltzmann constant, and $\bar{e}$ (dimensionless) is the "effective" emissivitiy for the heat exchange. The latter depends on the relative area of the emitting to the receiving surface, emissivities of the two surfaces and a geometrical view factor. For vials, the view factor for bottom radiation (radiation from shelf surface to the bottom of the vial) is approximately 1. The emissivity of glass is also nearly 1, so the effective emissivity for bottom radiation, $\bar{e}_{v,bot}$ is roughly equal to the emissivity of the shelf surface (ε_s) [1]. These considerations might not be true for containers made of other materials than glass and with geometries different from vials.

Effective emissivity $\bar{e}_{v,top}$ for top radiation for vials can best be determined experimentally. Pikal, Roy, and Shah [1] argued that the effective emissivity for top radiation should be essentially independent of the emissivity of the shelf, as the shelf area view factor of the vial top is much greater than the vial area. They determined $\bar{e}_{v,top}$ in heat transfer experiments with single vials of different types and sizes. The vials were altered to be able to measure the pressure inside the vial. These alterations and the additional equipment may introduce a significant difference in heat transfer behaviour in these vials compared to regular vials in a closely packed array on the shelf. Results of these experiments showed no significant influence of vial type, size, or dry product layer on the value of $\bar{e}_{v,top}$. The mean value of $\bar{e}_{v,top}$ was determined as 0.84.

The cooler temperature T_1 in equation 1.9 is essentially the same as the product temperature measured at the centre bottom of the vial or other container, T_b. The higher temperature T_2 is the same as the temperature of the shelf surface, T_s.

An estimation of total radiative heat transfer can be achieved by an experimental set-up with containers suspended several centimetres above the shelf [26]. With this set-up however, the relative area of emitting and receiving surfaces as well as the geometrical view factor for bottom radiation change and therefore $\bar{e}_{v,bot}$ will differ slightly from containers placed directly on the shelf.

1.4.4 Heat Input by Conduction

The magnitude of heat input by conduction is directly dependent on the area of direct contact between the container and the shelf or the heat source. This contact area is almost never equal to A_v or A_{cont}. The contact area may be estimated with print tests [1]. Another way of determining the contact area of, i.e., a vial to the shelf surface is a detailed analysis of the geometry of the vial bottom. Pikal et al. [2] divided the vial bottom into 12 segments and assigned different separation distances l to these segments. Two of the segments were in contact with the shelf ($l =$ 0 cm). Theoretically, if the area of contact, $A_{contact}$, the thermal conductivity of the container material, λ_{cont} ($W\ m^{-1}K^{-1}$), and the thickness of the container bottom, δ_{cont} (m) at the points of contact are known, heat transfer by conduction could be estimated:

$$\frac{\mathrm{d}Q}{\mathrm{d}t} = \frac{\lambda_{cont}}{\delta_{cont}} \cdot A_{contact} \cdot (T_s - T_b). \tag{1.10}$$

In practice this influence of heat transfer by contact to total heat transfer during the sublimation phase cannot be calculated because the temperature difference between shelf surface (T_s) and product at the container bottom (T_b) results from all three contributions to heat transfer (radiation, conduction and conduction through the gas).

1.4.5 Heat Input by Conduction through the Gas

Heat input into a container during a freeze drying cycle by gas conduction can be described as follows: a gas molecule with a certain kinetic energy hits a surface. It might rest on this surface for a brief period of time and then fly off again. During this very short stay, some energy might be transferred from the surface to the molecule or vice versa. How much energy is transferred during the collision depends on the characteristics of the surface and of the gas. During the primary drying stage of freeze drying, the gas in the chamber of the freeze dryer is mostly water vapour [1]. The ability of a material to change (kinetic) energy of gas molecules during a collision is expressed in the energy accommodation coefficient, a_c. The value of a_c ranges from 0 to 1. If $a_c = 0$ no energy is exchanged. Recent research [1] has determined an average a_c for 10 ml and 20 ml tubing vials (both sizes procured from Kimble Glass Co. as well as from Wheaton Glass Co.) of 0.67. It can be speculated that a_c is similar for all glass vials, as the energy accomodation coefficient depends on the material of the surfaces under consideration [1]. a_c may be different for materials other than glass.

$$K_g = \frac{\alpha \cdot \Lambda_0 \cdot P}{1 + l(\frac{\alpha \cdot \Lambda_0}{\lambda_0})P}. \tag{1.11}$$

In Equation 1.11, α is a function of the accommodation coefficient a_c and the absolute temperature T [1]:

$$\alpha = \frac{a_c}{2 - a_c} \cdot \sqrt{\frac{273.2}{T}}. \tag{1.12}$$

Λ_0 ($cal\ s^{-1}cm^{-2}K^{-1}Torr^{-1}$) is the free molecular heat conductivity of the gas at 0 °C, λ_0 ($cal\ s^{-1}cm^{-1}K^{-1}$) is the heat conductivity of the gas at ambient pressure [7]. In the case of the freeze drying process, the gas can be considered - at least in primary drying - as 100 % water vapour [1]. For water vapour, the value of Λ_0 is $6.34 \cdot 10^{-3}$ cal $\mathrm{s^{-1}cm^{-2}K^{-1}Torr^{-1}}$ and

λ_0 is $4.29 \cdot 10^{-5}$ cal $s^{-1}cm^{-1}K^{-1}$ [1]. K_g varies with pressure P $(Torr)$ and also depends on the separation distance l (cm) between heat source (shelf surface) and container wall. The larger the distance between heat source and heat sink, the more likely is a collision of the molecule to which energy has been transferred with another gas molecule. During this collision, energy is interchanged between the two molecules and the direction of flight of both molecules might be changed. The mean free path l_{MFP} (m) between collisions of gas molecules can be estimated using the kinetic theory of gases [88],

$$l_{MFP} = \frac{R \cdot T}{\sqrt{2} \cdot \pi \cdot d^2 \cdot N_A \cdot P} \tag{1.13}$$

with d (m) as the diameter of the molecules of the gas, R as the universal gas constant (8.314 J $K^{-1}mol^{-1}$ or 1.986 cal $K^{-1}mol^{-1}$) and N_A as the Avogadro-number, $6.022 \cdot 10^{23}$ mol^{-1}. If water molecules are considered as hard spheres, the diameter can be taken as $4.18 \cdot 10^{-10}$ m [3]. The result of equation 1.13 is only an average. About 37 % of the molecules will not have collided after they travelled the length of l_{MFP} [88]. At the pressures and temperatures used in freeze drying, l_{MFP} is in the order of 1 mm or less (cf. Table 1.1).

Table 1.1: Length of the mean free path (l_{MFP}) of a water molecule at −30 °C and pressure settings relevant for freeze drying of pharmaceuticals.

Pressure $(mTorr)$	Pressure (Pa)	l_{MFP} (mm)
30	4.00	1.08
50	6.67	0.65
100	13.33	0.32
150	20.00	0.22
200	26.66	0.16
500	66.66	0.06

1.5 Experimental Determination of K_{cont}

Equation 1.5 on page 32 is used for the experimental determination of heat transfer coefficients. Data needed for calculation of the vial heat transfer coefficient K_v or the container heat transfer coefficient K_{cont} include mass flow dm/dt, area for heat input A_{cont}, and the temperature difference between the shelf surface (T_s) and the inside wall of the container close to the shelf surface, T_b. A_v (or A_{cont}) can be determined from the dimensions of the container. The temperature difference can be measured during the pseudo-steady state phase of sublimation with thermocouples. Mass flow may be determined gravimetrically or online.

1.5.1 Gravimetric Procedure for Determination of Mass Flow

Sublimation tests with pure water are performed to determine the amount of heat needed for sublimation of a certain amount of ice in the container system under consideration. The water is filled into the containers, these are weighed and then placed in the freeze dryer. The water is frozen to ice. The pressure in the freeze drying chamber is reduced to a pre-defined set point, and the shelf temperature is increased to yield a moderate to high sublimation rate. Temperature data are collected throughout this phase. When approximately 30 % of the ice has sublimed, the sublimation process is stopped (i.e. by rapidly raising the chamber pressure to ambient pressure). The containers are taken out of the freeze dryer and reweighed. The difference in mass and the duration of the sublimation phase are used to calculate mass flow.

This procedure is repeated at different chamber pressure set points to evaluate heat transfer characteristics of the container system throughout the pressure range typically used for freeze drying.

1.5.2 Online Determination of Water Vapour Mass Flow

Instead of determining the average water vapour mass flow during primary drying by weighing, the mass flow can also be measured online using a spectroscopic method, Tunable Diode Laser Absorption Spectroscopy (TDLAS). This technology allows instantaneous measurement of the water vapour concentration and the gas flow velocity in the duct connecting the freeze drying chamber with the condenser [83]. Either one or two near infrared laser beams pass through coated windows and optically measure the water vapour concentration and the velocity in the spool piece [89].

Assuming that the geometrical data of the container (A_v / A_{cont}) are known, and that the relevant temperatures (T_s, T_P / T_b) are also determined throughout the experiment, then the heat transfer coefficient can be directly calculated while sublimation is still on-going. The use of this technology has the advantage that mass flow rates at different chamber pressure set points can be determined within a single freeze drying run. From this set of mass flow data, the heat transfer coefficient for several different chamber pressure set points can also be determined within a single freeze drying run [83].

1.6 Tools for Enhancement of Heat Transfer to Product

1.6.1 Aluminium as a Material with High Thermal Conductivity

Literature reports that studies were performed with auxiliary material to improve conductive heat transfer. Patel et al. tested a device made of aluminium to achieve better heat transfer into vials [90]. Aluminium has a high thermal conductivity ($\lambda_{Al} = 237$ $Wm^{-1}K^{-1}$ at room temperature, [4]), many times the value of stainless steel ($\lambda_{AISI316} = 16.2$ $Wm^{-1}K^{-1}$ at 100 °C, [5]). This characteristic of the light metal is only of significant value for freeze drying if a reasonable amount of direct contact can be achieved between the heat source (i.e. shelf surface) and the aluminium device as well as between the device and the product container. If there still are small gaps between the metal surfaces and between the Al-surface and the container wall, heat transfer will again occur by conduction through the gas and by radiation.

To increase the contact area between the heat transfer enhancing tool and vials, Yalkowski et al. designed a fluid filled cushion of about 1 mm thickness [91]. The soft bag was fabricated from two sheets of aluminium foil lined with polyethylene which were welded by heat. Before the final seal was placed, the bag was filled with glycerine and degassed. This cushion was placed on the freeze dryer shelf and the vials were set on top of it. Since the cushion was flexible the vials "sank in" with the rim of the bottom, the usual line of direct contact. The fluid cushion deformed to fit to the contour of the vial bottom. To maximise contact, Yalkowski and his co-workers applied additional force in the form of an aluminium plate with holes. The holes were placed over the vials' necks. This perforated plate was held in place with clamps fastened to an additional plate fixed underneath the shelf. Using this device, a decrease in primary drying time by over 30 % and an increase (approximately 10 °C) in product temperature for molded vials were observed.

1.6.2 Influence of Vial Type on Drying Heterogeneity

The data presented by Yalkowski et al. (see section 1.6.1) was gained during freeze drying of mannitol solution at 20 mTorr which is a very low pressure setting for freeze drying of pharmaceuticals, namely a crystalline product with a high critical product temperature [20]. Typically, pressure is set to a value in between 50 mTorr and 200 mTorr. Another run at a setting of 200 mTorr but without the device also yielded a decrease in primary drying time of roughly 25 %, demonstrating the increase of heat transfer attainable by enhancement of gas conduction. However, the inter-vial variance of product temperatures was also decreased if the cushion was applied. It is stated in the paper that the advantages of the fluid cushion are largest for molded vials. Yet it is also stated that tubing vials show less drying heterogeneity in primary drying as their bases are more uniform and much flatter and, in freeze drying, these are considered superior to molded vials. The application of the perforated aluminium plate and the additional plate underneath each shelf to maintain the perforated plate in its place make handling of this fluid cushion device impractical for production cycles. Moreover, heat transfer by radiation from the top shelf will most probably be decreased due to the additional, non-heated plate. This decrease in radiative heat transfer may compensate some of the benefits of the increased heat transfer by direct conduction through the cushion.

In the present thesis, heat transfer characteristics of three container systems are evaluated. One of the container systems tested in these studies consists of commercial, flat-bottomed $2R$ (2 mL) serum tubing glass vials. The other two container systems are atypical containers (96-well PCR-plates, an array of 96 small glass tubes) using aluminium blocks (Al-blocks) for enhancement of heat transfer. The non-vial containers are inserted into cavities in the Al-blocks which are designed for a close fit to the dedicated container bottom. Sublimation tests are performed to determine heat transfer coefficients for each of the container systems over the pressure range of 30 to 500 mTorr. Contribution to total heat transfer by radiation, by conduction, and by conduction through the gas are discussed for each of the tested container systems. Differences, benefits and limitations of the three systems are compared. Applicability of the determined heat transfer coefficients to cycle design is tested with a sample formulation. The results of these studies are implemented into a guideline describing steps for freeze drying cycle design for a new, untested container system.

Chapter 2

Materials and Methods

2.1 Materials

2.1.1 Primary Packaging Material

96-Well PCR-Plates

96-well PCR-plates used in this thesis were obtained from Brand GmbH & Co. KG, Wertheim (Germany). The plates were made of polypropylene, were colourless, and had no rim (Brand catalogue number 781350, see Figure 2.1). Each individual well consisted of a conic section at the bottom joined to an almost cylindrical section directly underneath the well opening in the rectangular polypropylene plate. The average weight of an empty well plate was determined to be 17.7 g. Maximal nominal fill volume was 200 μL per well. Easy rehydration of freeze dried product demands that the wells must not be filled to the maximum filling level. 100 μL was considered as the maximum fill for practical handling. Two different assemblies were tested for freeze drying: well plates alone and well plates inserted into custom made aluminium blocks (Al-blocks).

Figure 2.1: 96-well PCR-plate used in this study.

Aluminium Blocks (Al-Blocks) for Well Plates

Al-blocks used with 96-well PCR-plates matched well plates in size (length 123 mm, width 82 mm, height 20 mm). They were custom made at Erlangen University with 96 identical, tapered bores adjusted for a tight fit of the conic-shaped section of the wells within the blocks (see Figure 2.2). The submersed portion of the well roughly corresponded to the 100 μL filling line. The nearly cylindrical part of the wells was not submersed in the Al-block bore holes. The Al-blocks were designed for use in a freeze drying process with actual product. An additional drilling step in

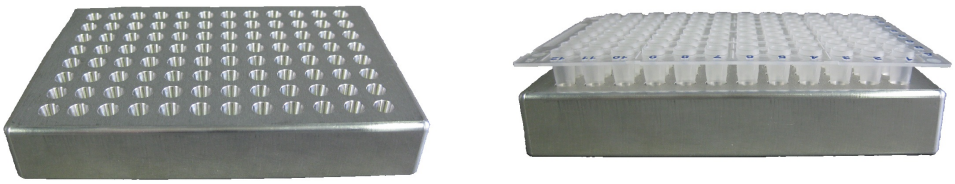

Figure 2.2: Aluminium block used with well plates and well plate inserted into Al-block.

the production process of the Al-blocks would have been necessary for complete submersion of a well including the upper, cylindrical portion. Also, the height of the Al-blocks would have had to be increased. The bore holes in the Al-blocks were deeper than the height of the submersed portion of the well plates. The distance between the underside of the Al-blocks and the deepest point of a drill hole was approximately 2 mm. The entire surface of the Al-blocks was polished. Some of the surfaces' shine was lost during the experiments due to oxidation. Even the slightly oxidised surface had an emissivity of no more than 0.3.

VirTis Freeze Drying System™ (FDS)

Sublimation tests were performed with a container system which consisted of 0.5 mL glass tubes in an array of 96 (VirTis, an SP Scietific brand in Gardiner, NY, USA). The tubes had a fill volume of 0.5 mL, a tube-like shape, and a flat bottom. The tubes were inserted into black-painted aluminium blocks which had precision drillings adjusted to the shape and size of the glass tubes (see Figure 2.3). The blocks consisted of a base plate (area of 127 mm x 85 mm, height of approx. 6 mm) and an inner, higher section which contained the bore holes. The measurements of this inner section were 120 mm x 79 mm with a height (without the base plate) of 13 mm. The bore holes had a depth of 15 mm, so that the thickness of the aluminium at the bottom of a drill hole corresponded to approximately 4 mm.

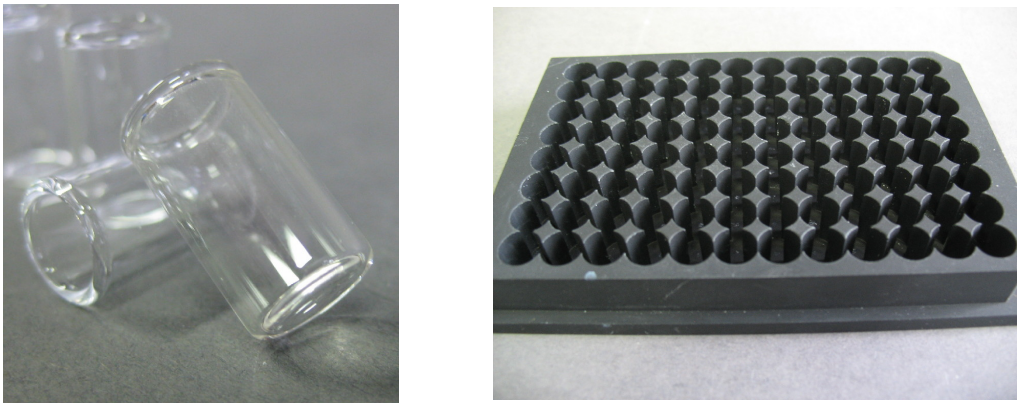

Figure 2.3: Vials of the VirTis Freeze Drying System™ and black painted aluminium block used as heat transfer enhancer and for facilitation of handling for FDS-vials. The base-plate section and the inner, higher section of Al-block are discernible.

There are rubber mats of 96 stoppers intended for use with this array. The rubber stoppers were inserted in a thick but flexible plastic foil. Once the stoppers were placed on the tube-array and correctly inserted by pressing them down into the openings of the individual tubes, the

plastic foil could be removed so that the 96 tubes stoppered with one of the mats could all be handled individually. These stoppers were not part of the set-up for the present sublimation tests.

2R Serum Tubing Vials

$2R$ (2 mL) glass vials and stoppers were also tested as a container system. Vials were non-siliconised serum tubing vials (Figure 2.4) produced by Thüringer Pharmaglas GmbH & Co. KG, Neuhaus am Rennweg, Germany. All vials belonged to the same batch (No. 25210/1). Stoppers were siliconised bromobutyl stoppers produced by Helvoet Pharma (Alken, Belgium).

Figure 2.4: $2R$ vials and stoppers used in these studies.

2.1.2 Formulation

For all formulations, double distilled water from an in-house distillation unit was used. Analytical grade excipients included D-mannitol, D-trehalose dihydrate, sucrose (D-saccharose), and D-raffinose pentahydrate (Sigma-Aldrich, Steinheim, Germany). All excipients were used as received. Buffering agents included citric acid monohydrate, potassium dihydrogen phosphate (Merck KGaA, Darmstadt, Germany), disodium hydrogen phosphate, and Trizma®base (Fluka Chemie AG, Basel, Switzerland). A recombinant human cytokine (Miltenyi Biotec GmbH, molecular weight of approximately 17,000 Da) was used as a model protein. The bulk cytokine was already purified ($> 97\%$ as determined by gel filtration and chip-based gel electrophoresis) and contained only low amounts of endotoxins and host cell DNA. The concentration of the bulk cytokine was 50 μg/mL.

2.1.3 Freeze Drying Equipment

All experiments were performed on a Lyostar II laboratory scale freeze dryer (SP Scientific, Stone Ridge, NY, USA). It has a shelf area of 0.5 m^2. The leak rate was less than 20 mTorr/h for all tests. The emissivity of the freeze dryer shelves was tested with an infrared thermometer (cf. section 2.2.5) and determined to be (in average) 0.6 for all shelves. The unit is equipped with a pirani gauge (calibrated for nitrogen) as well as a calibrated capacitance manometer in the drying chamber and an additional capacitance manometer in the condenser. The capacitance manometer installed in the drying chamber was used to control chamber pressure. Comparative pressure measurement was used as endpoint indicator for primary drying for runs with product.

Thermocouples (TC, Omega Newport Electronics GmbH, 0.08 mm wire diameter, copper / constantan) were used to measure ice and product temperatures as well as the shelf surface temperature beneath the containers. The thermocouples are calibrated at the factory. A mixture of distilled water containing ice is used to confirm the accuracy of the TC ports in the freeze dryer and the software offset. Adhesive thermocouples (Omega Newort Electronics GmbH, copper / constantan, standard wire diameter) were used to measure the temperature of the radiation surface.

Freeze Drying Using SMART™

The freeze dryer was also equipped with the SMART™ Freeze Dryer software (SP Scientific, Stone Ridge, NY, USA). Transferability of the SMART™ software and freeze drying cycle optimisation algorithm to 96-well plates as containers was tested using 100 μL per well of trehalose solution at a concentration of 5 % (w/w) or 50 mg/g. Table 2.1 gives an overview of data related to the formulation and to the container system which were used with the SMART™ software for these tests.

Table 2.1: Summary of formulation related and container related input data used for testing SMART™ Freeze Dryer software with 96-well PCR-plates.

Parameter	Trehalose Solution
Physical Form	Amorphous
Nature of Drug Product	Small Molecule
Type of Bulking Agent	Amorphous
Type of Vials	Molded
Number of Vials	36
Inner Area of Vials	19.02 cm^2
Fill Volume	9.60 mL
Fill Depth	0.50 cm
Fill Weight	9.57 g
Collapse Temperature	−30 °C
Concentration of Solution	50 mg/g

Auto-MTM

Auto-MTM data was only collected for a few selected full load product runs with mannitol and trehalose solution, both at a concentration of 50 mg/g. Note that some information on formulation (i.e. fill volume and mass per container) and on the primary packing material (such as number of containers, geometry of container bottom) still has to be provided by the user, cf. Table 2.2.

TDLAS

Few selected experiments in this work were performed using Tunable Diode Laser Absorption Spectroscopy (TDLAS, cf. section 1.5.2), a spectroscopic method for instantaneous determination of water vapour concentration, gas flow velocity, and mass flow rate [83] (IMA Edwards, LyoFlux 100, Physical Sciences Inc., Andover, MA). In the experimental set-up used in these studies, a single laser beam has been used. Data obtained by TDLAS was compared to mass flow data calculated from water loss during primary drying. Mass flow data were gained for 96-well PCR-plates using TDLAS for a single full load run with mannitol solution and a single full load run with trehalose solution, both at a concentration of 50 mg/g.

Table 2.2: Summary of input data used for Auto-MTM freeze drying runs with 96-well PCR-plates.

Parameter	Mannitol	Trehalose
Number of Vials	36	36
Inner Area of Vials	19.0 cm^2	19.0 cm^2
Fill Volume	9.60 mL	9.60 mL
Fill Depth	0.50 cm	0.50 cm
Fill Weight	9.60 g	9.60 g
Concentration of Solution	50 mg/g	50 mg/g

2.2 Sublimation Tests and Product Runs

2.2.1 Experimental Design: 96-Well PCR-Plates

Determining Geometry and Contact Area of Well Plates

A calliper rule was used to measure length and outer diameter at different heights of approximately 40 wells. The mean inner cross-sectional diameter of a well at the 200 μL filling mark was determined. The mean outer surface area was determined for 20, 100, and 200 μL fill. To calculate outer surface areas, the geometric shape of the wells was determined as two adjacent cone segments (upper portion of a well from about 100 μL to 200 μL filling level as one cone section, lower part of a well up to 100 μL filling level as second cone section with a different angle of aperture). The tips of the wells were not pointed but rounded off. Information on the wall thickness of the wells was kindly provided by Brand GmbH & Co. KG. The inner diameters of the wells could be calculated using the wall thickness and the outer diameter.

The effective contact area of well plates to an even surface and to aluminium blocks was determined from simple print tests. For determination of the contact area to a surface, well plates were pressed on an ink pad and subsequently placed on a sheet of paper which was placed on a flat and even surface. Imprints of empty plates and plates filled completely with water were compared. The effective contact area to a flat surface was roughly estimated from these prints (cf. section 3.1.1).

The side contact area of well plates to the walls of the bore holes in the Al-blocks was determined as follows: Viscous water-based, organic solvent free emulsion paint (OBI classic Voll- und Abtönfarbe, Obi-Baumarkt Erlangen) was applied with a small brush to all bores of one aluminium block. The paint was viscous enough to stay on the inside wall of the bores for at least 15 min before creeping down the sides of the bores and gathering in the bottom of the bore holes. This was time enough to apply the paint in a thin layer on all 96 drill holes of the block. A well plate was then tightly inserted into the painted block and removed directly afterwards. The well plate was capsized and a photograph was taken of the capsized well plate so that wells were shown at an angle in between approximately 70 ° and approximately 30 ° from the vertical position. A grid of horizontal and vertical lines was drawn onto the photograph with a distance of approximately 2 mm in between the lines. Grid squares covering a well were counted. Coverage of these squares with paint spots was estimated on a percentage basis. The amount of coverage of grid squares was added up for a whole well. This procedure was repeated for all wells on the photograph. The area of contact was estimated from the ratio of paint-covered to non-stained outer surface of the photograph of the wells for a whole plate. Errors in determination of effective contact area arise from inevitable differences in thickness of paint layer applied to the bore walls, manual drawing of the grid lines resulting in squares with slightly different sizes, and visual estimation of amount of coverage with paint. This test was repeated five times with different well plates.

Sublimation Tests with Pure Water

Sublimaiton tests with pure water were conducted to determine heat transfer coefficients of the tested containers. For 96-well plates the procedure was as follows: 12 empty well plates were weighed one by one, subsequently filled with 200 μL of water per well and reweighed with the same laboratory balance (Sartorius type LA 620S, Sartorius AG, Göttingen, Germany). The well plates were either placed directly onto one shelf of the freeze dryer (Figure 2.5) or first inserted into Al-blocks and then placed on the freeze dryer shelf (Figure 2.6).

Thermocouples were inserted into a total of six wells distributed in two well plates. The TC tips were placed in bottom centre position (T_b). Two of the TCs were placed in edge wells of the two plates placed in the centre of the array. All other TCs were put in centre wells. Two more thermocouples were taped to the shelf surface beneath the well plates equipped with thermocouples or beneath the corresponding Al-blocks (T_s). The commercially available self-adhesive tape used to fix these TC tips on the shelf surface was a thin adhesive aluminium foil usually used for heat reflection / insulation on plastic tubing. The temperature of the upper shelf surface (radiation surface) was measured with an adhesive thermocouple throughout the

process. These temperature data were not used for calculations, they merely served as a reference or comparison to shelf surface temperatures measured beneath product containers.

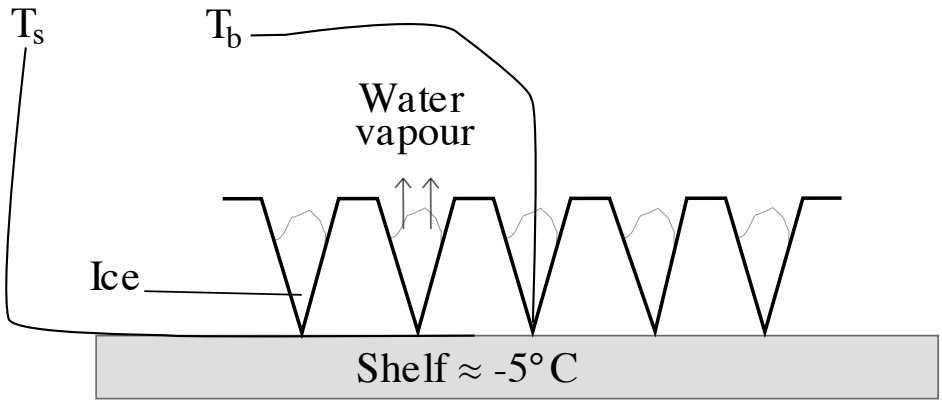

Figure 2.5: Schematic set-up for sublimation tests with well plates without Al-blocks.

After loading and placement of temperature probes, aluminium foil was placed in between the shelves and the freeze dryer front door. The stiff foil was arranged in order to fill out the whole opening and to reduce radiative heat flow arising from the Plexiglas door of the freeze dryer, which is known to have a high emissivity [85]. The shelf temperature was lowered to 5 °C and held for 15 min, then the temperature was further decreased to −5 °C and again held for 15 min. These "holding"-steps were included to ensure a homogeneous temperature distribution in all wells in the batch. 15 min was considered to be sufficiently long for equilibration of the temperature within a volume of 200 μL. After these two "holding" steps, the temperature was lowered to −40 °C and held for 45 min. Table 2.3 shows a summary of the freezing protocol. Product thermocouples were checked to read −38 °C or lower before the end of the freezing step.

Then the chamber was evacuated to the designated pressure set point for the experiment and the shelf temperature was subsequently raised to −5 °C to supply energy for a moderate sublimation rate. All ramping steps were executed with a ramp rate of 1 °C/min.

The sublimation process was stopped after approximately three to four hours, so that not more than approximately 50 % of the ice had sublimed. The plates were taken out of the freeze dryer (in most cases without thawing the ice prior to unloading) and reweighed. The sublimation tests were carried out at chamber pressures of $30, 50, 100, 200$, and 500 mTorr. At least two tests

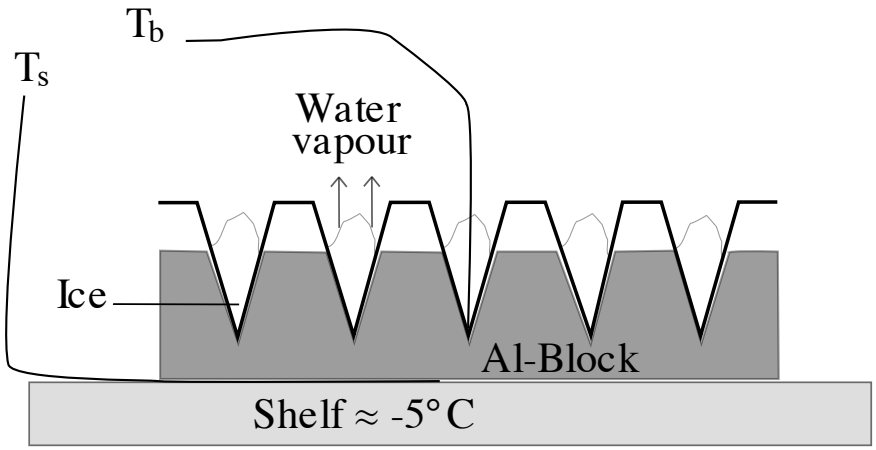

Figure 2.6: Schematic set-up for sublimation tests with well plates including Al-blocks.

Table 2.3: Summary of the freezing programme used for the sublimation tests with pure water in 96-well PCR-plates.

Starting Temp. ($°C$)	End Temp. ($°C$)	Step Duration (min)
≈ 20	5	≈ 15
5	5	15
5	-5	10
-5	-5	15
-5	-40	35
-40	-40	45

were performed for each set-up per pressure setting.

Offset runs were conducted at 30, 100, and 500 mTorr; once with and once without Al-blocks. For these runs, the freezing phase was carried out as described above, but the chamber pressure was quickly raised to break off sublimation as soon as the target shelf temperature for the sublimation phase (-5 °C) was reached. The results of these offset runs were used to calculate the mass loss during the initial ramping phase of the sublimation tests from -40 °C to -5 °C, and during unloading.

Calculation of Heat Transfer Coefficients

For all sublimation tests performed with well plates, heat transfer coefficients of well plates K_{PCR} were calculated from Equation 1.5 on page 32 for each individual well plate. Mass loss (dm) was calculated from weight of the filled well plate before the run and weight of the well plate directly after venting the freeze dryer to stop sublimation. From this value the mass loss during the initial ramping phase in primary drying determined in an offset run was subtracted.

The corrected mass loss in grams was multiplied with the heat of sublimation of ice, $q_{s,ice}$ (670 cal/g, cf. section 1.4.2) to calculate the amount of heat needed for sublimation of the ice during the experiment. The time interval dt was taken as the duration of the "steady state phase" of the experiment, the interval during which the shelf temperature was equal to -5 °C. T_P was calculated as the average of all TC readings of TCs placed in tips of centre wells during the "steady state phase". T_s was calculated as the average of all TC readings during the "steady state phase" of TCs placed beneath well plates on the shelf surface. The area relevant for heat input, A_{PCR}, was determined from the geometrical dimensions of the wells and theoretical considerations. The calculated heat transfer coefficients were fitted to equation 1.7 using Origin 8 software (OriginLab Corporation, Northampton, MA (USA), version 8G SR1). Table 2.4 gives an overview of the constants used for calculations and for the fitting equation during this study.

Table 2.4: List of constants used in this work.

Symbol	Value	Unit	Reference
K_K	$33.2 * 10^{-4}$	$cal\ s^{-1}cm^{-2}K^{-1}$	[1], [2]
N_A	$6.022 * 10^{23}$	mol^{-1}	[3]
R	1.986	$calK^{-1}mol^{-1}$	[3]
λ_0	$4.29 * 10^{-5}$	$cals^{-1}cm^{-1}K^{-1}$	[1], [7]
Λ_0	$6.34 * 10^{-3}$	$cal\ s^{-1}cm^{-2}K^{-1}Torr^{-1}$	[1], [7]

Well Plates on Plexiglas Holders

Additional sublimation tests were conducted using a slightly modified experimental design. In order to study heat transfer by radiation, well plates were placed on holders made from Plexiglas so that the well plates were suspended above the shelf. The contact surface between holders and well plates was additionally insulated with foamed polystyrene, which is a poor thermal conductor (λ for styrofoam ranges from 20 to 35 mW $m^{-1}K^{-1}$, [6]).

The holders were designed to suspend the well plates in the middle between two shelves, leaving a gap of approximately 5 cm in between shelf / radiation surface and well plate. A total of five well plates was prepared, filled with 200 μL of water per well, and weighed. These plates were evenly distributed on one shelf of the freeze dryer. Thermocouples (cf. section 2.1.3) were placed in nine wells (three wells per plate in three well plates, same edge and centre differentiation as described for set-up with well plates on shelf / in Al-blocks). The same freezing protocol was used as for the standard sublimation tests described above.

Tests with suspended well plates were conducted at a pressure setting of 100 mTorr. This pressure setting was chosen since it represents a typical pressure setting for a pharmaceutical product with an intermediate critical formulation temperature. After sublimation of approximately 50 % of the ice, the sublimation process was stopped, remaining ice in the well plates was thawed, and the plates were reweighed. A single offset run was performed for this set-up to further reduce the weighing error and be able to compare this data to data gained during sublimation tests without thawing of the ice prior to unloading.

Well Plates Lined with Heat Sink Grease

A fourth experimental set-up was designed to compare the impact of heat input by gas conduction to heat input by direct contact between Al-block and well plate. For these experiments, the drillings in two of the twelve Al-blocks used in the standard set-up with Al-blocks were lined with a thin layer of heat sink grease (main constituents are zinc oxide and a mixture of aliphatic carbohydrates) to achieve conditions of full or nearly full contact between well plate and Al-block.

The rest of the procedure was maintained as described above (see section 2.2.1). One of the two well plates inserted into Al-blocks with heat sink grease was equipped with three thermocouples and another TC was placed on the shelf surface underneath the block. This experiment was performed at three different pressure settings (30, 100, and 500 mTorr).

Lag Time for Temperature Equilibration in Al-Blocks

The "lag time" for temperature adjustment between shelf surface and inner surface of Al-block bore holes was also determined. Twelve Al-blocks were placed on one shelf of the freeze dryer. Thermocouples (0.08 mm wire diameter) were taped on the bore hole wall of six drillings in two of the Al-blocks (three TCs per block). Two additional TCs were taped on the shelf surface beneath the Al-blocks equipped with thermocouples in bore holes. For this experiment no well plates were used.

The shelf temperature was ramped down to -40 °C following the freezing protocol used in well plate experiments (cf. Table 2.3). Then the chamber was evacuated to the pressure set point of 100 mTorr. The shelf temperature was raised to -20 °C and held until thermocouple readings in bore holes and beneath Al-blocks were equilibrated. Then the shelf temperature was again set to -40 °C and held until temperature equilibration. This procedure was repeated with shelf temperature settings of -10 and 0 °C. All ramping rates, except for the last, were 1 °C/min. The ramp rate from -40 to 0 °C was 0.2 °C/min. Results of this test are discussed in sections 3.1.5 and 3.2.9.

Product Runs

The applicability of heat transfer coefficients for well plates determined by sublimation tests with pure water was verified with product runs using mannitol and trehalose solutions, representing a crystalline and an amorphous product, respectively. The concentration of excipients was 50 mg/g throughout this work. Empty and filled well plates were weighed prior to loading the freeze dryer.

Product runs were performed with 20 and 100 μL fill volume and with well plates alone as well as with well plates inserted into aluminium blocks. The freezing protocol was the same as for the sublimation tests.

For mannitol, no extra annealing step was included in the process. This decision was made after considering that one main advantage of using small product volumes is a significant decrease in primary drying time. This would have been balanced at least in part by a long annealing process. As the well plates are made of Plexiglas, there was no risk of container breakage at the end of the freezing step.

All product runs were carried out at a chamber pressure of 100 mTorr during primary drying. Three different settings for the shelf temperature during primary drying were used (-20 °C, -10 °C, and 0 °C) to compare the degree of collapse in the amorphous product. At these shelf temperature settings, no signs of melting were expected for crystalline product. Observation of the state of mannitol (crystalline, or at least partially amorphous) after freeze drying without an annealing step was part of these investigations. For all of these experiments a single shelf of the freeze dryer was completely loaded with a total of twelve well plates. Some of these runs were repeated as full load experiments with all three shelves completely loaded.

The primary drying endpoint was determined by comparative pressure measurement (see 2.1.3). When primary drying was completed, the shelf temperature was lowered to -40 °C and the chamber was vented using dry nitrogen. Three sample well plates were taken out of the chamber, one of which had been placed in the corner, and one had been placed in the centre of the well plate array on the shelf. The position of the third sampling well-plate was from the edge, but not from a corner position. The sampled well plates were immediately transferred into a glove box with a relative humidity of less than 5 % determined by a due-point sensor.

Then the chamber door was closed, and secondary drying was started for the remaining well plates. The final shelf temperature set point for secondary drying was 40 °C, the ramp rate (from -40 to 40 °C) was set to 0.5 °C/min. The product was held at 40 °C for 6 h, the chamber pressure remained at 100 mTorr throughout secondary drying as well.

The samples taken out after primary drying were used for Karl Fischer analysis of the residual moisture content in the product after primary drying. In this way, the average mass flow of water vapour during primary drying of the product runs could be calculated from the initial mass of water in the solution and the remaining moisture at the end of primary drying. These average mass flow data were then used to ascertain heat transfer coefficients determined by sublimation tests.

Testing after completion of secondary drying of well plates which were not removed from the freeze-dryer after primary drying included determination of the degree of crystallinity of mannitol samples using X-ray powder diffractometry, SEM, and, for a selected number of well plates, Karl Fischer analysis of the residual moisture content. Observation and comparison of signs of collapse and swellback was executed on (secondary dried) samples of product runs which were examined with SEM.

Mass flow data were also determined by using TDLAS for a single full load run with mannitol and a single full load run with trehalose solution. Data obtained by TDLAS were compared to mass flow data calculated from water loss during primary drying. Additional information (i.e. product resistance data) could be gained using MTM measurements during primary drying. MTM data were only collected for a few selected full load product runs. Transferability of the SMART™ software and freeze drying cycle optimisation algorithm to 96-well plates as containers was tested using sucrose solution at a concentration of 50 mg/g.

2.2.2 Experimental Design: VirTis Freeze Drying System™

Determining Geometry and Contact Area

As opposed to the custom made Al-blocks for the well plates, the VirTis Freeze Drying System™ (FDS) is a commercially available product consisting of 96 small glass tubes inserted into Al-blocks. The contact area of the tubes to the inside of the block cavities was examined in a similar way as for the well plates and their Al-blocks. A thin layer of white water soluble paint (water-based dispersion used for coating of tablets, containing sucrose, calcium carbonate, titanium

Figure 2.7: Set-up for sublimation tests with the Freeze Drying System. Tubes with white rim are tubes selected for weighing before and after each run. One half of the tubes selected for weighing was placed in edge positions, the other half was placed in centre positions. Positions of selected tubes differed from one block to the next. Vials in block V are not correctly placed in the picture.

dioxide, talcum, polyvinyl pyrrolidone, glycerol, and an anti-foaming agent) was applied to the cavity walls. The paint was viscous enough to stay on the inside wall of the bores for at least 15 min before the material started creeping down towards the bottom of the bores. This allowed to apply the paint in a thin layer on all 96 drill holes of the block. Tubes were inserted into the prepared cavities and then removed again. The ratio of paint-covered to unstained areas of tube walls and bottom was approximated (see section 2.2.1).

Performance of Sublimation Tests

For determination of the heat transfer coefficients, an array of six Al-blocks with tubes was used (cf. Figure 2.7). Twelve tubes per block were chosen for weighing, six of them were centre-placed tubes and six of them were edge- and corner-placed tubes. A tube was considered to be in a centre position from the third row on inwards. The weights of these empty tubes were determined. All tubes were filled with 400 μL of distilled water. The selected tubes were then reweighed.

Thin-wire thermocouples (see section 2.1.3 on page 41) were placed in three of the blocks, one of which was placed on the corner of the array of six blocks. Three TCs per block were placed in bottom centre positions of the tubes. Thermocouple-equipped tubes were not selected for weighing, as the thermocouple wires often are still frozen in remaining bits of ice at the end of a sublimation test and might be easily damaged upon removal. However, the temperature measured in the TC-tubes was assumed to be representative of the temperature in adjacent tubes.

Since no stoppers were used for the freeze drying array, a thermocouple holder was designed. It consisted of a steel mesh fastened with rubber bands to the blocks. The TC-wires were threaded in the mesh so that the protruding tip (the point of measurement) was fixed in the right length to be in contact with the tube bottom. Thermocouple ends were arranged in tube centre bottom positions. The thermocouple ends protruding from the tube and inserted into the mesh were run in a short, stiff piece of cable cover which served as a strut to prevent slipping out of place of the thermocouple tips (cf. Figure 2.8).

The blocks were placed on one half of a shelf in the freeze dryer. Aluminium foil was used as a radiation shield. The freeze drying protocol was as follows: decrease of the shelf temperature to 5 °C, holding at 5 °C for 15 min, further decrease of the shelf temperature to −5 °C, again holding

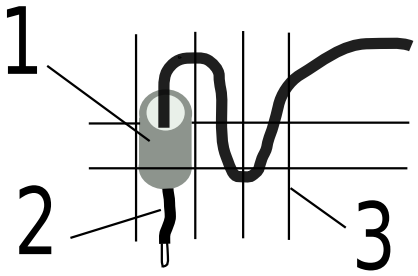

Figure 2.8: The thermocouple holder for the Freeze Drying System™ consisted of a wire mesh (3) in which short pieces of cable cover (1) were placed as reinforcements for TC-wires (2). The TC-wires were threaded through openings in the mesh and then run through the cable covers which assured the position of the measuring tip in bottom centre position of an FDS tube (not shown in schematic).

Table 2.5: Summary of the freezing programme used for the sublimation tests with pure water in the VirTis Freeze Drying System™.

Starting Temp. ($°C$)	End Temp. ($°C$)	Step Duration (min)
≈ 20	5	≈ 15
5	5	15
5	-5	10
-5	-5	15
-5	-40	35
-40	-40	60

it for 15 min, then decrease of the shelf temperature to the final set point of -40 °C for a holding time of 60 min (cf. Table 2.5). The chamber pressure was lowered to the designated set point and the shelf temperature was then raised to -5 °C. The vacuum was broken after approximately two hours, the remaining ice was thawed and the blocks were taken out to reweigh the selected tubes. Pressure set points were at $30, 50, 100, 200$, and 500 mTorr, the same as for well plates. Runs were performed in duplicate for each pressure setting. Offset runs were conducted for $30, 100$, and 500 mTorr.

For all sublimation tests performed with the Freeze Drying System™, heat transfer coefficients K_{FDS} were calculated from Equation 1.5 on page 32 for each of the individually weighed tubes. Mass loss ($\mathrm{d}m$) was calculated from the weight of the filled tube before the run and the weight of the tube directly after disruption of the sublimation phase. Off this value the mass loss during the initial ramping phase in primary drying determined in an offset run was subtracted. Corrected mass loss in grams was multiplied with the heat of sublimation of ice, $q_{s,ice}$ (670 cal/g) to calculate the amount of heat needed for sublimation of the ice during the experiment.

The time interval $\mathrm{d}t$ was the duration of the "steady state phase" of the experiment, the interval during which the shelf temperature was equal to -5 °C. T_P was calculated as the average of all TC readings during the "steady state phase" of TCs placed in centre bottom positions of the tubes. T_s was calculated as the average of all TC readings during the "steady state phase" of TCs placed beneath black Al-blocks on the shelf surface. The area relevant for heat input A_{FDS} was determined from geometrical dimensions of the tubes in combination with theoretical considerations and experimetal findings which are explained in detail in section 3.3.2. The calculated heat transfer coefficients were fitted to equation 1.7 using Origin 8 software (OriginLab Corporation, Northampton, MA (USA), version 8G SR1)

2.2.3 Experimental Design: *2R* Glass Vials

Geometry and Contact Area of *2R* Vials

The outer diameter at the bottom of 20 randomly selected vials was measured with a calliper rule. A sample of five vials was carefully cut vertically in order to measure the wall thickness at the vial bottom and at the cylindrical section of the vial. Print tests were conducted with a different set of 20 vials. For these tests, each vial was pressed on an ink pad and then carefully placed on a sheet of paper. The imprints on the sheet of paper were used to estimate the mean ratio of bottom contact area to bottom cross sectional area.

Conduction of Sublimation Tests

For sublimation tests, a tray with removable bottom was loaded with 594 vials. The array consisted of 101 edge vials and 400 centre vials counting the third row of vials inwards as the first row of centre vials (cf. Figure 2.9).

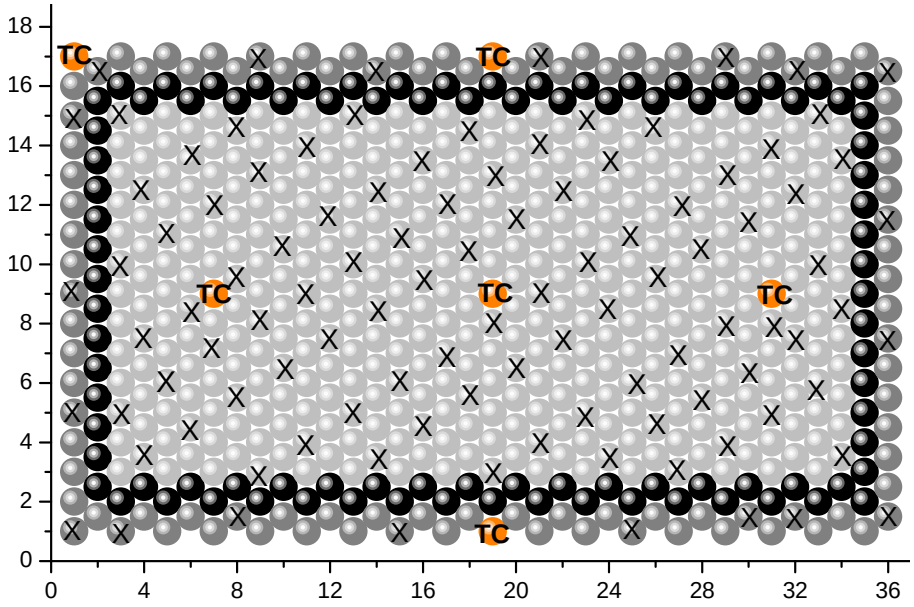

Figure 2.9: Schematic of the set-up for sublimation tests with 2R vials. Edge vials are symbolised by dark grey circles, centre vials by light grey circles. Circles with "X" correspond to vials that were weighed before and after each run. TC-positions are labelled "TC". The second row of vials counting inwards are marked in black.

The second row of vials counted from outward to inward was not considered as completely "typical" as all of these vials had neighbouring vials which were clearly non-typical edge vials. It has been shown that edge vials show a strong tendency to higher sublimation rates during primary drying [26]. These higher sublimation rates are attributed to an extra amount of radiative heat input through vial sides which are not shielded by neighbouring, cold product vials. A vial situated next to a non-typical edge vial might also receive a small amount of extra heat flow from this neighbouring, warmer vial. For this reason, no "second row" vials were included in the study.

Tara weights of vials selected for weighing in the experiment were evaluated. All vials were filled with 1.5 mL of distilled water. Stoppers were then placed on all vials in the semi-stoppered position. A total of 20 edge vials and 84 centre vials were weighed without the stopper. Thermocouples (cf. section 2.1.3 on page 41) were placed in three centre vials (front of the array, centre, and back) as well as in one of the front corner vials and in the middle of the two edge rows on the sides of the tray.

Two adhesive thermocouples were placed on the shelf surface directly above shelf fluid inlet and outlet. Another TC was fixed in the centre of the radiation surface. In order to avoid any disturbances in the vial array, no TC was placed on the shelf surface underneath the vials. After the tray had been placed on the shelf of the freeze dryer, the bottom was removed and the vials were directly placed on the freeze dryer shelf. The stainless steel guardrail of the tray held the vials in their position and also served as a radiation shield towards the front door. Using this set-up means that atypical radiation to the sides of the edge vials originates from the frame of the tray which in turn receives radiation from freeze dryer walls and door.

Stiff aluminium foil was placed between the shelves and the door of the freeze dryer before the freeze dryer door was closed. This procedure was used to minimise radiative heat input from the Plexiglas door. The shelf temperature was first lowered to −5 °C and held for 15 min, then it was decreased to −40 °C and held for 45 min. The chamber was evacuated to the designated pressure set point and the shelf temperature was ramped up to −5 °C. All ramp rates were 1 °C/min.

After sublimation of approximately 30 to 40 % of the ice the process was interrupted and the vials were closed using the stoppering feature of the freeze dryer. The vacuum was broken and the remaining ice was thawed (all thermocouple readings in vials larger than 0 °C, yet still approximately 10 to 15 °C below room temperature), then the bottom of the tray was reinserted and the whole array was removed from the freeze dryer for re-weighing of the selected vials. Pressure settings for the sublimation tests included $50, 100, 150, 200$ and 400 mTorr. Offset runs were conducted at 50 and 400 mTorr to estimate the amount of ice sublimed during ramping.

For all sublimation tests performed with $2R$ vals, heat transfer coefficients K_{2R} were calculated from Equation 1.5 on page 32 for each of the individually weighed vials. Mass loss ($\mathrm{d}m$) was calculated from the weight of the filled vial before the run and the weight of the vial directly after disruption of the sublimation phase. This value was corrected for mass loss during the initial ramping phase in primary drying which had been determined in an offset run. Corrected mass loss in grams was multiplied with heat of sublimation of ice, $q_{s,ice}$ (670 cal/g) to calculate the amount of heat needed for sublimation of the ice during the experiment.

The time interval $\mathrm{d}t$ was the duration of the "steady state phase" of the experiment, the interval during which the shelf temperature was equal to −5 °C. T_P was calculated as the average of all TC readings during the "steady state phase" of TCs placed in centre bottom position of vials. T_s was calculated as the average of all TC readings during the "steady state phase" of TCs placed on the shelf surface (not including the data of the TC placed on the radiation surface).

The area relevant for heat input A_{2R} was the cross sectional area of the vial bottom calculated from the outer vial diameter. This is in accordance with calculations of heat transfer coefficients from vial sublimation tests in previous studies published in the literature [1], [68], [83]. The calculated heat transfer coefficients were fitted to equation 1.7 using Origin 8 software (OriginLab Corporation, Northampton, MA (USA), version 8G SR1).

Runs with Placebo Product

50 mg/g trehalose solution was used as an amorphous model product in freeze drying runs. Two runs were performed using the SMART™ Freeze Dryer software. The fill volume was 0.28 mL in one of these runs and 0.7 mL in the other, corresponding to fill depths of 0.2 cm and 0.5 cm, respectively. As a comparison, MTM runs were performed using the same product and fill volumes and shelf temperature settings of −10 °C for primary drying. For all of these runs, the product vials were surrounded by a row of empty "dummy vials" serving as additional radiation shield, and only a single shelf of the freeze dryer was filled.

2.2.4 Cycle Design: Case Study With a Cytokine

Developing "Standard" Formulations With the Cytokine

The applicability of heat transfer coefficients determined for the different product containers to a product solution containing an active pharmaceutical ingredient and rules or suggestions for

Table 2.6: All tested formulations contained 20 % of cytokine stock solution. Partially crystalline and crystalline formulations also contained mannitol.

Category	Stabilizer	Bulking Agent	Buffering Agent
Amorphous	Sucrose	-	Tris
	Sucrose	-	Phosphate
	Sucrose	-	Citrate
	Trehalose	-	Tris
	Trehalose	-	Phosphate
	Trehalose	-	Citrate
	Raffinose	-	Tris
	Raffinose	-	Phosphate
	Raffinose	-	Citrate
Partially Crystalline	Sucrose	Mannitol	Tris
	Sucrose	Mannitol	Phosphate
	Trehalose	Mannitol	Tris
Crystalline	–	Mannitol	Tris

cycle design derived from heat transfer experiments were tested. The active ingredient chosen for these tests was the human recombinant cytokine (cf. section 2.1.2). The three scenarios of cycle development for a crystalline formulation, partially crystalline formulations, and several fully amorphous formulations with different lyoprotectants were examined. Prior to this study, no formulation for this API existed.

As the total amount of API was limited and it is a substance with high biologic potency, the concentration of cytokine in the formulation was set to 10 μg/mL. The concentration of the purified bulk cytokine was 50 μg/mL. The designated fill volume for $2R$ glass vials was 0.5 mL. It was suggested to include a buffering agent in all formulations to improve the stability of the cytokine in solution prior to freezing. Three buffer systems were chosen for initial testing: sodium / potassium phosphate buffer (pH 7.5), Tris buffer (pH 8.0), and citrate buffer (pH 4.0). Two different ranges for the pH value (neutral to slightly basic and slightly acidic) were selected. Reconstitution after lyophilisation was carried out with 1 mL of water.

Lyoprotectants were chosen to protect the protein during freeze drying and during storage. Sucrose, trehalose, and raffinose were tested in combination with the three buffering agents. A molar ratio of lyoprotectant to protein of at least 360 : 1 as discussed in section 1.2 on page 22 has been used for development of the cytokine formulations.

For all test formulations, the calculated mass of lyoprotectant was in the range of 35 to 60 μg per vial, based on the 360 : 1 rule mentioned above. For purely amorphous formulations a surplus of lyoprotectant was added to attain a target minimum concentration of solids of 20 mg/mL. This was done in order to prevent product "fly-out" during primary drying.

For the partially crystalline test formulations, mannitol was added as a bulking agent intended for crystallisation. Only trehalose and sucrose were used as amorphous excipients in partially crystalline formulations. Additionally, one formulation was tested with cytokine, mannitol and buffer alone, omitting any stabilising excipient. This formulation was used as a comparison to the stabiliser containing formulations. A qualitative overview of formulation compositions is given in Table 2.6.

For Tris and citrate buffer, the concentration upon reconstitution was chosen to be 25 μmol/mL. The concentration of phosphate buffer was set to 1-fold upon reconstitution, which equals 9.5 μmol of phosphate per millilitre.

Small aliquots of the formulations were assembled and analysed by DSC. T_g' values and crystallisation events (if any) were determined for all formulations.

A "target product temperature" was determined for primary drying. As the primary drying phase would otherwise have been very long, the lowest acceptable target product temperature for primary drying for this study was defined as −36 °C. In order to determine the target product temperature of each formulation, a temperature safety margin of at least 2 °C was added to the glass transition temperature (cf. section 1.4.2). Part of this study was formulation optimisation and a "manageable" formulation with a very low attributed target product temperature was not considered as optimised. If T_g' values of the tested formulations were found to be lower than −35 °C the formulations concerned were modified to meet this requirement.

Freeze Drying Cycles for Cytokine Formulations

As a first test for the formulations, two freeze drying runs were performed. Run No. 1 contained only amorphous formulations. A small volume of each formulation was prepared and filled into 7 vials. All vials were placed in a hexagonal array in the centre of a tray with removable bottom. Stoppers were applied in the semi-stoppered position. The remaining space in the tray was filled with several rows of empty vials. The empty vials were considered as radiation shields from freeze dryer walls, guard rail of the tray, and freeze dryer door. In addition, filling the tray and subsequently the shelf with the empty vials assured that the product vials were held in their positions and remained in the closely packed array on the shelf. One thermocouple per formulation was placed in he centre bottom position of one vial and fixed with tape on the outside of the vial.

The tray was then placed on the middle shelf of the freeze dryer and the bottom was removed. Again, aluminium foil was placed in between the shelves and the freeze drying chamber door to reduce radiation effects. The solutions were frozen in several steps to −50 °C and held at this temperature for 120 min. The chamber pressure was lowered to 55 mTorr and the shelf temperature was raised to the product target temperature of the formulation with the lowest T_g'. After all temperature probes had reached a plateau, the product temperature of the most critical formulations were checked. If product temperatures of these formulations were still more than 1 °C below the designated target product temperatures, the shelf temperature was raised by 2 to 5 °C, depending on the magnitude of the current temperature safety margin. This procedure was repeated until the formulation with the lowest critical temperature had reached its target product temperature.

Comparative pressure measurement was used as the primary drying endpoint detection method. Thermocouple readings served as an additional control. The shelf temperature set point for secondary drying was 40 °C. This temperature was attained using a ramp rate of 0.2 °C/min and the product was held at this temperature for a total of 4 h. The chamber pressure was kept at 55 mTorr throughout secondary drying.

Run No. 2 contained all formulations with mannitol as bulking agent intended for crystallisation during freezing. 8 vials were filled per formulation and placed in the centre of one freeze drying tray. Stoppers were placed in the semi-stoppered position. The remaining space on the tray was again filled with empty vials to shield off radiation and fix the vials in their position on the shelf and in the array. One thermocouple per formulation was placed in the centre bottom position of one vial and fixed with tape on the outside of the vial.

The tray was placed on one shelf of the freeze dryer; the bottom of the tray was removed. Aluminium foil was applied as radiation shield in between the array of shelves and the Plexiglas door. The solutions were frozen in several steps to −50 °C. After a short holding step, the shelf temperature was raised again to −22 °C and held for 6 h [57]. The temperature for this annealing step was selected between the T_g' of the non-crystallised mannitol solution (reported as approximately −30 °C, [92]) and T_{eu} of the mannitol-water solution (−1.5 °C, [92]) which crystallises during freezing. After this annealing step, the shelf temperature was again lowered to −45 °C and held for another hour to completely freeze (i.e. solidify) the product. Then the chamber was evacuated to the set point of 100 mTorr. The shelf temperature was raised in intervals until a target product temperature of −30 to −32 °C was reached within the formulations. Parameters for secondary drying were equal to those of the first run.

2.2.5 Analytical Equipment and Procedures

Emissivity Measurements

A hand-held Omega Newport OS532E infrared thermometer with a thermocouple port was used for determination of emissivity (Newport Electronics GmbH, 75392 Deckenpfronn, Germany). The emissivity factor of the infrared thermometer used for the tests was adjustable in increments of 0.01. The temperature of the surface was determined with a calibrated chromel-alumel (type K, also Newport Electronics GmbH) thermocouple inserted into the TC port of the infrared thermometer. At the same time, the surface temperature was determined with the infrared beam. The emissivity setting of the thermometer was adjusted until the temperature readings were identical for both determination methods. This approach for determining the emissivity of a surface has been described in the literature [1].

Karl-Fischer Titration

A Mitsubishi CA-06 titration unit combined with a VA-06 oven was used for Karl-Fischer titration. Reagents for titration were Hydranal®-Coulomat CG catholyte and Hydranal®-Coulomat AG Oven anolyte for Karl-Fischer titration in cells with diaphragm (Fluka chemicals, SIGMA-ALDRICH Laborchemikalien GmbH Seelze, Germany). Prior to each examination, the titration unit and the oven were desiccated until the idle current was below 0.1 μg H_2O/s. The unit was calibrated with a water standard prior to each measuring campaign, or when it had not been used for several weeks.

Samples were filled into custom made sample holders made of glass in a glove box at a maximum relative humidity of 5 %. The samples were then transferred into a small glass vessel inside the oven unit via a ground connection. The small glass vessel was heated to 140 °C prior to each measurement for 3 min to extract water adsorbed to the vessel. This was done by using an automated, pre-programmed procedure. Then the small sample vessel inside the titration unit was allowed to cool off for at least 7 min before the sample was inserted. After transfer of the sample from the sample holder into the small glass vessel, the vessel was moved into the oven and heated to 140 °C to extract all water from the sample. The water vapour removed from the sample was carried with a flow of dry nitrogen into the titration cell. The measurement was repeated with fresh samples ($n = 3$).

Scanning Electron Microscopy

The product morphology of freeze dried samples was analyzed using Scanning Electron Microscopy (SEM). Samples were prepared by first fixing them on aluminium stubs (G301, Plano) with self-adhesive films and gold sputtering at 20 mA / 5 kV for 1.5 min (Hummer JR Technics; Mubich, Germany). The SEM-unit (Amray 1810 T; Amray, Bedford, USA) was set to 20 kV.

X-Ray Powder Diffraction (XRD)

The crystallinity of mannitol-containing products was analysed using a Phillips model X'pert wide angle powder X-ray diffractometer. $°2\theta$ ranged from 0.5 ° to 40 °. Cu $K\alpha$ radiation was used at 40 kV and 40 mA. The percentage of the crystalline phase in the samples was determined according to European Pharmacopoeia [93], chapter 2.9.33., entitled "Characterisation of crystalline solids by XRPD". The quantitative phase analysis was based on the full diffraction pattern. The degree of crystallinity was estimated by measuring three areas of the diffractogram: background area (C), total area of the peaks arising from the crystalline phase (A), and area below A representing the amorphous fraction of the sample (B). The degree of crystallinity was roughly estimated using Equation 2.1.

$$\%crystallinity = 100\frac{A}{A+B-C} \tag{2.1}$$

The background area was determined using an empty sample holder. Microcal Origin software 7.5G SR 3 (OriginLab Corporation, Northampton, MA, USA) was used to calculate integrals.

Table 2.7: Description of standard methods for determination of T_g' and T_g.

Temperature $°C$	Ramp (R) or Hold (H) Step	Ramp Rate / Holding Time $°C/min$ or min
-5	R	-20
-20	R	-1
-20	H	15
-80	R	-20
-80	H	3
$+5$	R	$+3$
-10	R	-20
-10	H	3
$+180$	R	$+3$

Accurate and precise results require homogeneity of all particle phases and a suitable particle size distribution in all phases. Due to the low quantities of material available for the measurements, freeze dried samples were broken apart but not ground prior to the analysis. The homogeneity of the samples was assumed to be sufficient for the measurement. In many cases, the samples consisted of a single substance (mannitol). In cases where additional substances were contained in the lyophilisate, the reproducibility of the results was tested by replicate runs with fresh material originating from the same sample or a different sample processed under the same conditions. The particle size in these samples was small, leading to diffractograms with comparably low intensities.

Differential Scanning Calorimetry

Differential Scanning Calorimetry (DSC) measurements were carried out on a Mettler-Toledo DSC 822e unit (Mettler-Toledo GmbH, Analyical, Schwerzenbach, Switzerland). The calibration of the unit was performed with Indium on a regular basis. 40 μL aluminium crucibles were used and hermetically sealed by compression prior to measurement. The sample size was 30 μL for liquid samples and 2 to 20 mg for freeze dried samples. The STAR^e software 9.01 was used for evaluation of thermal events. Glass transition temperatures were always determined from heating curves and are given as midpoints ($\frac{1}{2}\Delta C_p$) of events under consideration. The scanning rate for determination of glass transition temperatures and other thermal events was 3 °C. Table 2.7 gives an overview of standard DSC-methods used in this study.

For determination of glass transition temperatures of maximally freeze concentrated solutions containing buffering agents, an annealing step was included in the freezing step of the sample. These samples were first cooled to -20 °C with 20 °C/min and then held at -20 °C for 15 min. After that, frozen samples were cooled to -80 °C before reheating. In order to locate possible glass transitions in freeze dried solids at relatively low temperatures, scans with freeze dried solid started at -10 °C.

Additional Analysis of Cytokine Formulations

The stability, aggregation, and degradation of the cytokine was analysed with SDS-PAGE analysis under reducing (dithiothreitol, DTT, Cleland's reagent) and non-reducing conditions. The gel was a 10 well, 4 to 20 % Tris-glycerin gel (Anamed Elektrophorese GmbH). The analysis was performed in a XCell SureLock Mini-Cell (Invitrogen GmbH, Darmstadt, Germany). The conditions for the analysis were 30 mA and 5 W. The run-time was 75 min. The protein was visualised by silver staining (SilverXpress Silver Staining Kit, Invitrogen). The silver staining is more sensitive than the standard Coumassie blue staining technique and allows the detection of subnanogram levels of protein. Each gel electrophoresis was performed using two markers:

Mark12™ Unstained Standard (Invitrogen, Catalog No. LC5677), and a prestained marker (PageRuler™, Fermentas GmbH, St. Leon-Rot, Germany, Catalog No. SM0672).

Purity, multimer formation and aggregation was further analysed by size exclusion chromatography (SEC) using a Bio-Silect SEC 125-5 column (Bio-Rad). This column is suitable for the separation of molecules with molecular masses in between 5,000 Da and 150,000 Da. The eluent was phosphate buffered saline, pH 6.8. The analysis was performed using a Shimadzu HPLC unit (Shimadzu Deutschland GmbH, Duisburg). Viamin B12 (Sigma-Aldrich) was used as an internal standard.

For the cytokine used in this study, a cell proliferation assay using a cytokine-specific cell line was performed. A bioassay test determines the activity of a substance by comparison of the substance's effect on an organism to the effect of a standard preparation of this substance [94]. To determine the activity of the freeze dried cytokine samples, various concentrations of the cytokine sample solution were incubated, each with the same number of cells per well.

The number of viable cells per well was determined with a colorimetric method using a tetrazolium compound (MTS, 3-(4,5-dimethylthiazol-2-yl)-5-(3-carboxymethoxyphenyl)-2-(4-sulfophenyl)-2H-tetrazolium, inner salt, promega GmbH, Mannheim, Germany), and an electron coupling reagent (phenazine ethosulfate). The MTS-tetrazolium compound (Owen's reagent) is converted (reduced, i.e. by NADH in metabolically active cells) to a brown formazan product by mitochondria. The coloured product can be detected and quantified spectroscopically at 490 nm [95]. The amount of formazan formed and therefore the extinction is the greater the higher the number of viable cells. The results of the tests with the freeze dried cytokine samples were compared to the results of a test performed in identical manner using a cytokine WHO-standard.

A certain, low amount of background absorbance may be caused by the assay medium used during the bioassay. This background absorption is determined using a control during the preparation of the tests (preparation of wells without cells) and is subtracted from the results. The successful performance of the bioassay strongly depends on the reliability and sensitivity of the indicator cell line. Overall sensitivities of cell lines maintained in continuous cell culture may be highly variable [95].

A general procedure for performing a cell inhibition assay is described in the following. The inhibition assay was calibrated against the international WHO Standard provided by the NIBSC (National Institute for Biological Standards and Control).

1. Maintain indicator cell line in stock culture (here: cytokine-specific cell line).

2. In a 96-well plate suitable for tissue culture, add i.e. 50 μL per well of the cytokine containing sample or a cytokine standard (in this case: WHO-standard), diluted in the assay medium. The medium may not contain the cytokine that is analysed during the test.

3. The sample solution / the standard is titrated across the well plate in a serial dilution. A serial dilution is a stepwise dilution of a substance in solution, usually using a constant dilution factor at each step. With this procedure, the concentration progresses geometrically in a logarithmic fashion.

4. Three wells per plate should be used for the negative control (cells in addition to cell culture assay medium, no cytokine sample / standard added). In addition to that, approximately three wells are filled only with the cell culture assay medium for control and determination of the background absorption.

5. Equilibrate the prepared well plate (i.e. at 37 °C in humid, 5% CO_2 enriched environment) prior to addition of the cells.

6. Prepare the cells for the test (i.e. washing and centrifugation step of 10 min at 200 xg in the assay medium used for the test).

7. Determine the cell number and viability with Erythrosin B exclusion (Erythrosin B: Sigma-Aldrich, dye content 90 %, catalog No. 198269). Resuspend the cells to an appropriate concentration for the test in the assay medium used for the test.

8. Distribute an appropriate volume / number of cells (i.e. 50 μL / 5,000 cells) into all wells of the well plate which have been prepared with the sample solution / the standard during the serial dilution, including the negative control. Do not add cells to the wells intended for the background absorption control of the assay medium.

9. Incubate the cells for an appropriate period of time in suitable atmosphere.

10. Add a small aliquot (20 μL) of the MTS-tetrazolium reagent solution to all of the wells which have been prepared with assay medium, the sample solution / the standard (including negative control and background absorption control), and the cells. Incubate for 1 to 4 hours.

11. Using a 96-well plate reader, record the absorbance at 490 nm.

From the results, the dose-response curve is determined. Using a data fit, the baseline and maximum responses as well as the ED_{50} of the cytokine are determined. ED_{50} is the concentration of the cytokine that provokes a response half way in between the baseline and the maximum response. Using the results obtained from the test with the WHO standard of the cytokine, the ED_{50} can be used to calculate the activity of the sample solution in international units (IU/mg) [94].

Chapter 3

Results and Discussion

3.1 96-Well PCR-Plates: Sublimation Tests

3.1.1 Determination of Effective Contact Area

Simple print tests conducted with 96-well PCR-plates without aluminium blocks revealed that the effective area of direct contact to a flat surface (i.e. the freeze dryer shelf) is extremely small. The middle section of the well plate itself is slightly warped upwards so that, regardless of fill volume, the tips of the wells in the middle rows are not in contact with the shelf surface at all. Tips at the two long edges of the well plates have very little contact. Therefore the total area of contact consists of only a few needle point sized spots. In addition to the small area of contact, the polypropylene wall is thicker at the tips of the well plates. Polypropylene, the material of the well plates, is a poor thermal conductor ($\lambda = 0.24$ $\mathrm{Wm^{-1}K^{-1}}$, [96]).

As a simplification for well plates placed directly on the freeze dryer shelf, the area of heat input by direct conduction can be assumed to be negligible. Thus, heat flow by direct conduction was not taken into account in the following calculations.

The contact area of 96-well PCR plates inserted into Al-blocks was very heterogeneous from one well to the next and ranged from almost no contact (0 %) to over 90 % of contact. A tendency to better contact for wells in edge rows was noted. Most wells showed partial contact to the block cavities (cf. Figure 3.1). The average ratio of contact area to outer well area immersed in the

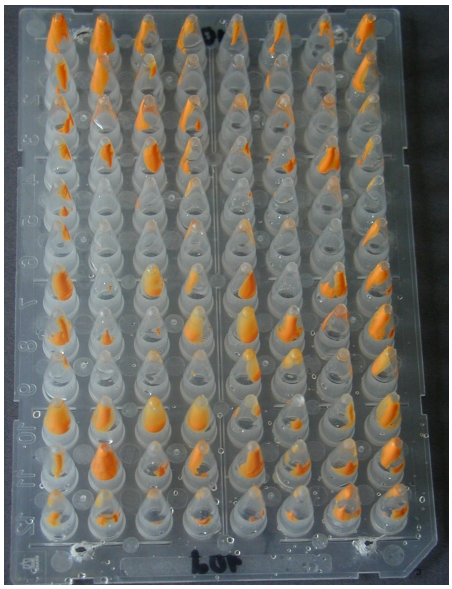

Figure 3.1: Example of print test with well plate inserted into Al-block.

Al-block cavity was estimated to be 25 %. The heterogeneous contact areas of well plates inserted into Al-blocks may originate in the bending or warping of the well plate base-plate itself, and in different amounts of pressure applied on the well plates when placed into the Al-block. If a well plate is carefully placed into the Al-block, without any application of additional pressure, the contact of the wells in the middle of the well plate (in the section warped upwards) to the bore holes in the Al-block is poor.

3.1.2 Theoretical Discussions on Heat Input into Well Plates

For a well plate placed directly on a freeze dryer shelf, it has been pointed out in section 3.1.1 that there is practically no heat transfer by direct conduction. However, heat input by conduction through the gas is an effective way of heat transfer as long as the separation distance between heat source and heat sink is in the order of magnitude of the mean free path or smaller. Even small differences in the separation distance have a large influence on the resulting heat transfer coefficient [83].

As for the slightly warped well plate on the freeze dryer shelf, the separation distance between shelf surface and well tip is likely to be within the range of heat transfer by conduction through the gas even though the separation distance of a few millimetres (approximately 1 to 5 mm, depending on the position of the considered well within the warped wellplate) may be larger than the mean free path, MFP. It has been pointed out in section 1.4.5 on page 35 that the "mean" free path is a statistical value and not all gas molecules collide with each other while overcoming the distance l_{MFP} [97]. The small number of molecules which have not yet collided with another molecule after the length of l_{MFP} will be able to transfer some of their energy upon collision with the well plate. The wall of the well plates is reinforced at the well tip to approximately twice the thickness of the wall of the rest of the well. Heat transferred to the well tip by collision of gas molecules has to overcome this additional barrier before it is transferred into the product. Considering this and the small area of the well tip, heat transfer by conduction through the gas may have little importance for heat transfer into the well plate at this position. All other sections of the well plate are even further removed from the heat source (shelf surface), so that heat transfer by conduction through the gas to the conic section of a well will also be limited and most pronounced for the part adjacent to the well tip.

The main contribution to heat flow into a 96-well PCR-plate placed on a freeze dryer shelf might originate from heat input by radiation. The radiation energy can enter into the well plate from three directions: top, bottom, and sides, corresponding to Q_1, Q_2, and Q_3, respectively, as stated in Equations 1.2 to 1.4 on page 32. Radiation from the top originates from the bottom side of the shelf above the shelf on which the well plate rests. The area for radiative heat flow from the top, $A_{PCR,top}$ was assumed to be equal to the cross sectional area of the well opening calculated from the inner top diameter of a well. Practically all emitted radiation that strikes this area will add to the heat flow to the product in the well, either by directly entering into the upper layer of the product via the product surface or by striking the well wall and reflection deeper into the well. A small part of this radiation might be absorbed by the well wall.

For vials, heat flow from the sides only has a notable impact on the sublimation rate if the considered vial is placed in direct view of a warmer surface, i.e., freeze dryer walls and / or door. For well plates, the shelf surface itself must also be considered as a source for transfer of radiative energy into the well walls: each well can be considered as an individual container that is not in direct contact with its neighbours. In addition to this radiation originating from the shelf surface, all wells on the outer edges and at the corners of an array of well plates on the shelf receive an extra amount of radiative heat transfer from the freeze dryer walls and door.

One fraction of radiation which effectively contributes to heat transfer into the product is radiation emitted from the shelf surface directly underneath the well. From here, radiation must be emitted perpendicularly to strike the well wall. The "effective" area of the container wall, $A_{PCR,bot,w/oAl}$, for this fraction of radiation corresponds roughly to the projection area of the outer well wall up to the filling level of the well (cf. Figure 3.2). Radiation that is emitted in more acute angles from the shelf surface succeeds in striking the well tip or lower part of a well. However, it would not be expected to impact the upper regions of the well.

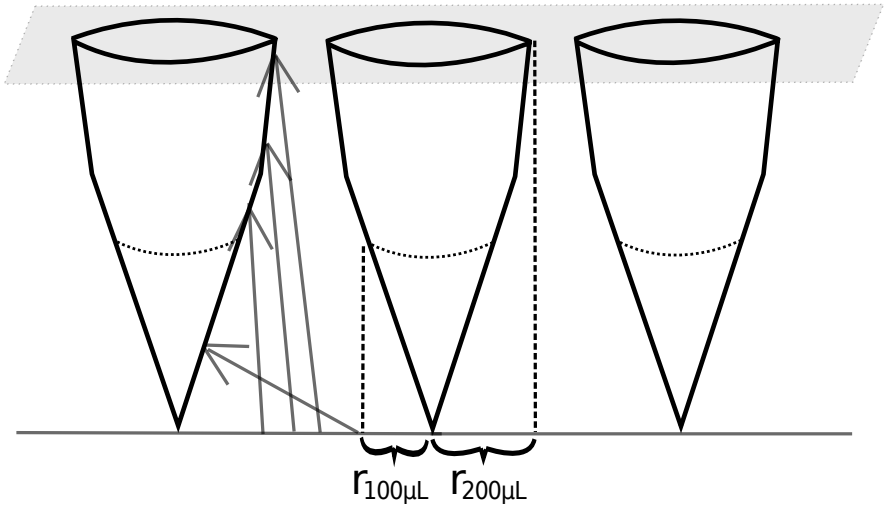

Figure 3.2: Schematic of well plate to illustrate calculation of projection area. $r_{100\mu L}$ and $r_{200\mu L}$ represent radii for calculation of projection area of 100 and 200 μL fill volume, respectively. Arrows on the left show that radiation must be emitted almost perpendicularly to strike the upper part of the well.

For a well plate inserted into an aluminium block heat transfer principles seem similar to those for a well plate without Al-block. The contribution to overall heat flow by radiative heat transfer from the top ($A_{PCR,top}$) may be assumed to be essentially the same for a well plate with and without Al-block. For heat transfer from the sides and from the bottom into a well plate inserted into an Al-block, the situation is clearly different. The lower portion of the conic part of the well (100 μL filling level) is inserted into the bore hole of the aluminium block. The well wall inserted into the drilling is partially in direct contact with the Al-block cavity (roughly 25 % of contact, as mentioned before), and partially separated from the wall of the bore hole by a small gap (width $<<$ 1 mm). This small gap limiting the area of direct contact between well wall and bore hole is caused by irregularities of the bore hole (alterations in material surface due to extensive use, oxidation, etc) and / or of the well wall. Even though the well plates are highly uniform with smooth surfaces, the manufacturing process cannot guarantee exactly the same wall thickness and contour in all areas of each of the cavities for all well plates.

Heat is transferred from the surface inside the drilling in the Al-block to the well wall by direct conduction in areas with direct contact, and by conduction through the gas (and radiation) in areas with a small separation distance. The area for heat flow into this part of the well, $A_{PCR,bot,Al}$, is equal to the outer surface area of the well portion immersed in the Al-block. If the filling level of the well is less than 100 μL, the product does not fill out the whole portion of the well that is inside the bore hole. In this case, the area for heat flow from the bottom is the outer surface of the well up to the filling level.

If the filling level of the well is more than 100 μL, then there is also radiative heat transfer from the sides into the portion of the well that protrudes from the Al-block. For this fraction of the container, heat input by radiation originates from the surface of the Al-block. The "effective" area for radiative heat transfer into this portion of the well, $A_{PCR,side,Al}$ is again approximated as the projection area of the protruding well part. A_{PCR} is the sum of $A_{PCR,top}$, $A_{PCR,side}$ (if applicable) and $A_{PCR,bot}$. Values used for calculation of A_{PCR} at different filling levels with and without Al-block are summarised in Table 3.1.

Since 96 wells are interconnected by the base plate of the PCR-plate, heat can be conducted within the well plate itself. As long as a temperature gradient exists within the well plate and as long as heat is constantly removed by sublimation of ice, heat may be transferred to the coldest spots (well wall in direct contact with product) by conduction through the polypropylene [23]. Polypropylene, the material of the well plates, is a poor thermal conductor. The heat

Table 3.1: Overview of areas relevant for heat flow into a single well for well plates without Al-block ($A_{PCR,w/oAl}$) and well plates with Al-block ($A_{PCR,Al}$).

Description	Area (mm^2) Fill Volume per Well		
	$200\mu L$	$100\mu L$	$20\mu L$
Lateral surface of truncated cone	(266)	127	47.9
Area of tip (truncated)	3.57	3.57	3.57
Area of well opening ($A_{PCR,top}$)	19.8	19.8	19.8
Projection area	32.8	23.7	9.33
Proj. area (200 μL) - Proj. area (100 μL)	9.04		
$A_{PCR,w/oAl}$	52.6	43.5	29.1
$A_{PCR,Al}$	159	150	71.3

transfer coefficient of polypropylene is in the order of 0.24 $Wm^{-1}K^{-1}$, [96], which corresponds to approximately $5 \cdot 10^{-4}$ $cals^{-1}cm^{-1}K^{-1}$ [28]. Therefore, the rate of heat transfer by direct conduction through the well plate will be low. The total amount of heat transferred by direct conduction is inversely proportional to the distance between the "hot" and the "cold" spot within the well plate. This further limits transfer of significant amounts of heat energy from warmer parts of a well plate to distant colder parts (i.e. from a relatively warm corner well to a colder centre well). Based on these considerations, it seems reasonable to argue that the wells of a 96-well plate can, in essence, be treated as individuals, although interconnected by a base plate.

$A_{PCR,bot,w/oAl}$ has been defined as the projection area of the well at the filling level. This assumption is justified as long as the well wall in direct contact with the product is the coldest part of the well: the heat supplied to this portion of the well is constantly removed through sublimation of ice. During the sublimation phase, ice in direct contact to the container will sublime and leave the matrix of dried product behind. This matrix contains many small pores (diameter $<<$ 1 mm) which are filled with a mixture of the inert gas of the freeze drying chamber and water vapour. As long as sublimation continues, the fraction of water vapour will be high [1].

Within this dried matrix, heat will be transferred by gas conduction and by direct conduction through the dried product matrix. The matrix consists of a porous structure with only thin connections of dried product between well wall and matrix as well as to different parts of the product matrix. Water vapour is constantly being produced by sublimation of ice and therefore present in abundance. It could be argued that, taking this into consideration, heat transfer by gas conduction is more pronounced than heat transfer by conduction through the dried product matrix. Nonetheless, the effective area for heat transfer from the container wall to the inside of the product is probably reduced by the continued removal of frozen water.

The upper parts of the well wall that are not in direct contact with the product may be substantially warmer, as the product serves as the "heat sink" with constant consumption of heat by sublimation. A temperature gradient might build up from the base plate of the well plate (warmest) to the well wall in contact with frozen product. Since polypropylene is a poor thermal conductor, the gradient will probably be high, with the base plate of the well plate having almost the same temperature as the shelf surface.

The ice-sublimation interface recedes further down into the well with proceeding ice sublimation, thereby changing A_{PCR}. Also, it has been observed that the sublimation interface gradually curbs downward at the sides (no near-horizontal movement of the sublimation front as typically assumed in steady state heat and mass transfer [72], [1]), thereby increasing the area

of the sublimation interface (cf. Figure 3.6). At the same time the contact area between ice or frozen solution and container wall is decreasing.

As has been mentioned before for well plates without Al-block, the well tip receives a higher amount of radiation than the upper portions of the well because radiation that is emitted in more acute angles from the shelf may still strike a well tip. Thus, the assumption that $A_{PCR,bot,w/oAl}$ is equal to the projection area of the well may be far from real conditions, in particular for low fill volumes. If all these changes in parameters have a large impact on K_{PCR}, the pseudo-steady state model can no longer be used.

Note that all presented results were calculated based on pseudo-steady state assumptions (constant temperature difference between ice temperature at sublimation interface and shelf surface, constant sublimation interface area, constant area for heat flow into the product, constant mass flow).

3.1.3 Sublimation Tests for Well Plates Without Al-Blocks

PCR-plate heat transfer coefficients $K_{PCR,w/oAl}$ calculated from sublimation rates of well plates without aluminium blocks during sublimation tests with 200 μL pure water per well are summarised in Table 3.2. Heat transfer coefficients were calculated using Equation 1.5.

When the well plates were taken out of the freeze dryer after the sublimation tests, frost formation was noted on the still cold walls of the well plates. This may have produced a weighing error and added to the overall error introduced into the calculations. In order to minimise this error, the offset runs described in section 2.2.1 were performed and the mass difference calculated from these offset runs was subtracted from the weight difference determined in between well plates prior to and just after the sublimation test. The area for heat input from the bottom for a well plate was calculated as the projection area of a well up to the 200 μL filling level multiplied by 96 (cf. Table 3.1). Values for $K_{PCR,w/oAl}$ range from approximately $2.17 * 10^{-4}$ cal s^{-1}cm^{-2}K^{-1} at 30 mTorr to $3.54 * 10^{-4}$ cal s^{-1}cm^{-2}K^{-1} at 500 mTorr.

Compared to reported vial heat transfer coefficients in the literature [83], [1], and to results obtained with well plates immersed into Al-blocks (see section 3.1.5), the increase of $K_{PCR,w/oAl}$ over the tested pressure range is rather low. Figure 3.3 shows a plot of $K_{PCR,w/oAl}$ and a fit of the data to Equation 1.7. Error bars in Figure 3.3 represent standard deviations of the mean value of $K_{PCR,w/oAl}$ calculated from each sublimation test. A comparison with data gathered for sublimation tests using Al-blocks (cf. Figure 3.7) clearly shows that heat input into well plates without Al-blocks is much less pressure dependent than heat input into vials or well plates used with Al-blocks.

As expected, heat input into well plates without Al-blocks was dominantly achieved by radiation. Radiative heat transfer is pressure independent so that no great change of $K_{PCR,w/oAl}$ with a change in chamber pressure was expected. During sublimation tests, no "lag time" in between reaching of the shelf temperature set point for the sublimation phase and reaching of the steady state "product"-temperature within the tips of the well plates has been observed. This is a difference to well plates inserted into Al-blocks which might lead to shorter primary drying times than the set-up of well plates with Al-blocks.

Results of the fitting parameters K_K, $l_{PCR,w/oAl}$, and K_P are $1.40 \cdot 10^{-4}$ cal s^{-1}cm^{-2}K^{-1}, 0.19 cm, and $33.2 \cdot 10^{-4}$ cal s^{-1}cm^{-2}K^{-1}Torr^{-1} (fixed), respectively. Table 3.3 gives an overview of the results of data fits. For well plates used without Al-blocks, K_K can be considered as roughly equal to heat input by radiation, K_r. The gap size l is derived from the fitting result of the expression $l * (K_P/\lambda_0)$. This number is large compared to the same parameter for vials and well plates used with Al-blocks. These findings are as expected as the mean size of the gap between heat source (shelf surface) and container wall is considerably larger for the set-up of well plates without Al-blocks than for the other two systems.

K_P has been set to $33.2 \cdot 10^{-4}$ cal s^{-1}cm^{-2}K^{-1}Torr^{-1}, the same value as has been determined for vials. This seems to be justified as K_P is a function of the accommodation coefficient a_c. Note that a_c depends on the nature (the roughness) of the surface and of the gas. In both cases (well plates and vials), the gas is the same, and the surface of polypropylene has some similarities to the glass surface as well: both materials have very smooth surfaces. One way to estimate the

Table 3.2: Results of sublimation tests with 96-well PCR-plates with and without use of Al-blocks, suspended well plates, and well plates with heat sink grease.

Set-Up	Pressure Setting ($mTorr$)	$10^4 * K_{PCR}$ ($cal\ s^{-1}cm^{-2}K^{-1}$)
Without Al-Block	30	2.17
	50	2.28
	100	2.69
	200	3.06
	500	3.54
Susp. Well Plates	100	2.10
With Al-Block	30	1.15
	50	1.70
	100	2.79
	200	4.17
	500	6.23
Heat Sink Grease	30	2.30
	100	3.88
	500	8.66

roughness of a surface is by determination of the coefficient of friction. The dynamic coefficient of friction for polypropylene on steel has been determined as 0.23 [98]. The static coefficient for glass on steel has been found to be within the range of 0.5 to 0.7 [28]. The dynamic coefficient of friction is always smaller than the static coefficient [23]. The measuring methodology influences the results, so that coefficients of friction for different materials are only comparable if the same set up has been used for their determination [99].

3.1.4 Suspended Well Plates Test

The mean value of $K_{PCR,suspWP}$ determined from sublimation tests at 100 mTorr is $2.1 \cdot 10^{-4}$ cal $s^{-1}cm^{-2}K^{-1}$. It is shown in Figure 3.3 with the results of sublimation tests for well plates placed on the shelf without Al-blocks. $K_{PCR,suspWP}$ is smaller than the corresponding value of $K_{PCR,w/oAl}$, yet at the same time larger than K_K calculated from the fit of $K_{PCR,w/oAl}$. The experiment with well plates suspended above the shelf was conducted to achieve heat input solely by radiation. Theoretically, the heat transfer coefficient calculated from this experiment would then be equal to K_K, the y-axis intercept of the fit of K_{PCR} data. The higher value of $K_{PCR,suspWP}$ may be due to residual heat input by conduction through the Plexiglas holder / foamed styrofoam, as well as to residual conduction through the gas, since the well plates were placed in between two shelves with a distance of approximately 5 cm between well tips / bottom shelf and base plate / top shelf, respectively. In previous experiments [26], this separation distance has been higher (11 cm). The heat transfer coefficients calculated from mass flow data of suspended well plates show a certain amount of scattering, but they are all grouped around the same value (cf. Figure 3.3).

In the experiments reported in the literature, no dependence of heat transfer coefficient on chamber pressure has been found for vials suspended above the shelf and within the pressure range

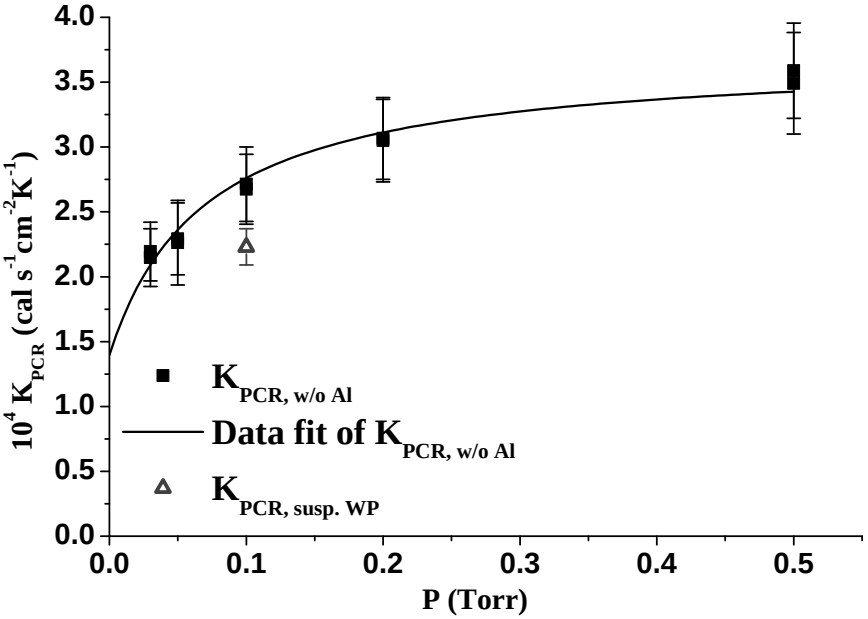

Figure 3.3: Fit of heat transfer coefficients calculated from sublimation test data of 96-well PCR-plates without Al-blocks. $K_{PCR,w/oAl}$ (black squares) increases only slightly with pressure. The black line shows the fit of the data to Equation 1.7. The grey open triangle shows K_{PCR} of suspended well plates (determined at 100 mTorr). Error bars show the standard deviation of the mean value of K_{PCR} for each sublimation test.

of 50 to 250 mTorr. However, in the present study, heat transfer coefficients of suspended well plates have only been determined for a single pressure set point. Heat input by direct conduction into suspended well plates has been reduced to a minimum as the well plate holders were made of plexiglas and the areas in contact with well plates were additionally insulated with foamed material. Both of these materials are poor thermal conductors with thermal conductivities in the same order as polypropylene (plexiglas) or less (foamed insulation material: 0.03 $\mathrm{Wm^{-1}K^{-1}}$) [28].

3.1.5 Sublimation Tests of Well-Plates With Al-Blocks

Prior to conduction of this set of experiments, the emissivity of the Al-blocks used with the well plates was determined using an infrared thermometer with a thermocouple port (cf. section 2.2.5). The emissivity setting of the infrared thermometer had to be adjusted in between 0.2 and 0.3 to achieve agreement of temperature readings of the infrared thermometer and the TC. The effective emissivity of Al-blocks was therefore assumed to be 0.25.

Heat transfer coefficients calculated from sublimation tests of 96-well PCR-plates with Al-blocks are also summarised in Table 3.2. The area of heat flow into well plates, $A_{PCR,Al}$ was calculated from the total outer surface area of a well inserted into the Al-block cavity, projection area of the well-part protruding form the Al-block, and inner cross sectional area of the well at the top (see Table 3.1), multiplied by 96. When the well plates inserted into Al-blocks were taken out of the freeze dryer after the sublimation tests, a strong tendency for frost formation was noted on the cold Al-blocks. Frost might also have formed on the well plates, as had been noted for sublimation tests without A-blocks (cf. section 3.1.3). This may have produced a weighing error and added to the overall error introduced into the calculations. In order to minimise this error, the offset runs described in section 2.2.1 were performed and the mass difference calculated from these offset runs was subtracted from the weight difference determined in between well plates prior to and just after the sublimation test.

A plot of calculated heat transfer coefficients $K_{PCR,Al}$ is shown in Figure 3.4. Mean values

for $K_{PCR,Al}$ range from $1.15 \cdot 10^{-4}$ cal s^{-1}cm^{-2}K^{-1} at 30 mTorr to $6.23 \cdot 10^{-4}$ cal s^{-1}cm^{-2}K^{-1} at 500 mTorr. Error bars shown in Figure 3.4 are standard deviations of the mean calculated from each individual sublimation test.

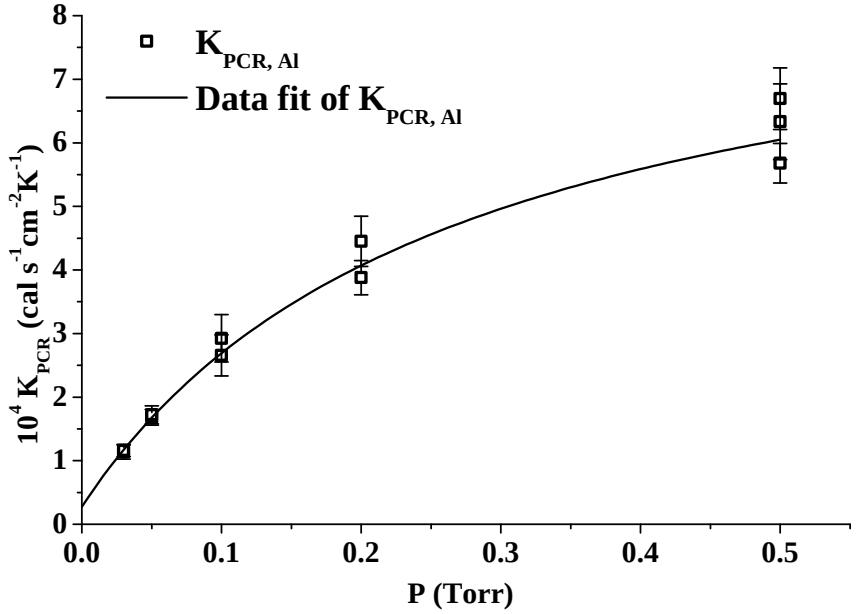

Figure 3.4: Fit of heat transfer coefficients calculated from sublimation test data of 96-well PCR-plates with Al-blocks. $K_{PCR,Al}$ (black open squares) increases notably with pressure. The black line shows fit of data to Equation 1.7. Error bars show standard deviation of mean value of $K_{PCR,Al}$ for each sublimation test.

The increase of heat transfer coefficients with pressure is more pronounced for this set up with Al-blocks than for well plates without blocks. Data were fitted to Equation 1.7. The shape of the fitted curve is found comparable to the course of the curve of fitted heat transfer coefficients of $2R$ vials (see section 3.4.2). This increase in heat transfer coefficients with pressure shows that heat input by conduction through the gas plays a major role in total heat transfer into the product.

K_K, the y-axis intercept, is much smaller for well plates with Al-blocks ($K_K = 0.28 \cdot 10^{-4}$ cal s^{-1}cm^{-2}K^{-1}, see Table 3.3) than for well plates used without Al-blocks ($K_K = 1.40 \cdot 10^{-4}$ cal s^{-1}cm^{-2}K^{-1}). The results suggest that there is little heat input by direct conduction and / or by radiation into well plates inserted into Al-blocks. It has been illustrated by print test experiments (see section 3.1.1) that the contact between the surface of a well plate inserted into the Aluminium block and the bore hole wall of the block is only about 25 %. Also, the Al-block greatly reduces heat transfer by radiation from the freeze dryer wall, door, and from the shelf surface, as it serves as an effective radiation shield. This well explains the smaller value of K_K found for well plates with Al-blocks.

The separation distance l was derived from the results of the data fit (see Table 3.3) to be approximately 0.05 cm. For well plates in Al-blocks, two small gaps exist: the first in between the shelf surface and the Al-block, the second in between bore hole wall and container wall. The gap in between shelf surface and Al-block will be largest for well plates equipped with TCs, as a TC was taped underneath the Al-block of well plates with temperature probes. This experimental design is not typical. One would not necessarily tape TCs underneath the Al-blocks during a freeze drying cycle. Typically, it can be expected that the separation distance between the inside of a drilling and the outer well wall is in the same order of magnitude or even bigger than the separation distance between Al-block and shelf surface. Although the used TCs were of extremely small wire diameter (smallest commercially available), the contact area in between

Table 3.3: Values of fitting parameters l (cm) and K_K (10^{-4} cal $s^{-1}cm^{-2}K^{-1}$) for 96-well PCR-plates tested with Al-blocks, without Al-blocks and with heat sink grease (hsg) applied to Al-blocks. Values in parenthesis are errors as calculated by Origin 7.5*G* software. K_P equals $33.2 * 10^{-4}$ $cals^{-1}cm^{-2}K^{-1}Torr^{-1}$, λ_0 equals $4.29 * 10^{-5}$ $cals^{-1}cm^{-1}K^{-1}$, see section 1.4.5 on page 35.

Parameter	$K_{PCR,Al}$		$K_{PCR,w/oAl}$		$K_{PCR,hsg}$	
l	0.05		0.19		0.03	
$l * (K_P/\lambda_0)$	3.751	(0.186)	14.350	(0.787)	2.521	(0.084)
K_K	0.276	(0.046)	1.396	(0.049)	1.309	(0.079)

shelf surface and Al-block was reduced and the gap in between shelf surface and Al-block was enlarged. The value determined for l must be considered as the sum of the widths of the two gaps in between shelf surface and Al-block as well as in between Al-block cavity and the outer surface of the well plate. This value is in the same range as separation distances l_v determined for vials [83].

K_P has again been fixed to the same value as has been determined for vials, for the same reasons as have been given in section 3.1.3 for well plates without Al-blocks. The value of the term, $l * (K_P/\lambda_0) = 3.75$ $Torr^{-1}$, for well plates inserted into Al-blocks is in the same range as the same value determined for $2R$ vials (2.48 $Torr^{-1}$, see section 3.4.2 on page 124). This also shows that the "average" width of the gap between heat source (shelf surface) and heat sink (container wall) is in the same range for well plates and glass vials.

However, heat transfer coefficients of well plates inserted in Al-blocks are smaller than corresponding heat transfer coefficients of vials with a similar separation distance [83]. The smaller heat transfer coefficients of well plates could be explained by the existence of the two barriers in between shelf surface and Al-block as well as in between Al-block and container. In addition to the second small gap which acts as a barrier to heat transfer, some of the energy provided by the shelf is solely consumed to heat up the Al-block: the heat capacity of aluminium reduces the efficiency of heat transfer to the product.

Product temperature curves measured in tips of well plates inserted in Al-blocks show a reproducible pattern (cf. Figure 3.5). At the beginning of the sublimation phase at very low pressures (30 and 50 mTorr) there is first a decrease in product temperature before it slowly rises with rising shelf temperature. This phenomenon might be explained with consumption of heat energy by rapid onset of sublimation. At the initial product temperature of −40 °C at the beginning of primary drying, the vapour pressure of ice is approximately 100 mTorr (see section 1.1.2).

The pressure difference between the two lowest tested chamber pressures, 30 and 50 mTorr, or, rather, the difference between the corresponding, even lower pressures in the condenser and the sublimation pressure at −40 °C appears to sustain the sublimation process. A certain "undershoot" of the chamber pressure at the initial evacuation phase might also contribute to this phase of extreme mass flow until the pressure valve securely controls the set point. Prior to evacuation of the freeze drying chamber, the condenser is pre-cooled to approximately −80 °C. The sublimation pressure of ice at this low temperature is less than 1 mTorr (see section 1.1.2), and all of the ice vapour created by sublimation is effectively removed from the gaseous phase. Therefore, the sublimation attains a high rate as soon as the chamber pressure drops below the sublimation saturation pressure at the product temperature, and the product temperature immediately decreases.

For pressure settings of 100 mTorr and higher, the sublimation rate is lower at the beginning of primary drying as long as the product temperature is still low, and considerably increases when the product has been warmed to a temperature above −40 °C with a corresponding ice

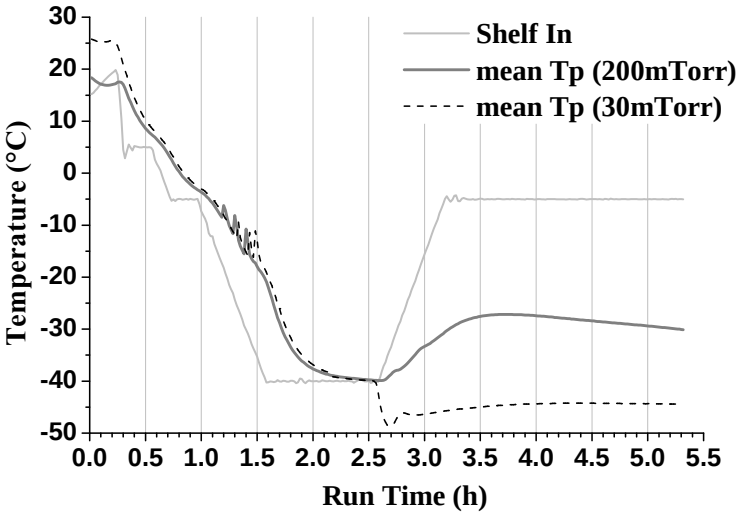

Figure 3.5: Plot of shelf fluid temperature (thin, light grey) during sublimation tests versus mean of ice temperature measured in tips of well plates inserted into Al-blocks at 200 mTorr (grey) and 30 mTorr (black dashed line).

sublimation pressure which is higher than the set chamber pressure. This well explains why the initial decrease of product temperature is not observed for these higher pressure settings.

When the shelf temperature set point (−5 °C) is attained, the product temperature still keeps on rising until it levels out in a plateau phase. This plateau is attained for all pressure settings approximately 25 min after the self temperature set point is reached. During this time, a fraction of the heat provided by the shelf surface is used to warm up the Al-block, thereby prolonging the non-steady state phase of sublimation in the product container. Temperature over time curves of thermocouples taped into bores of otherwise empty Al-blocks confirmed that the lag time for temperature equalisation between shelf surface and inside of Al-block hole may be as long as 2 h. The lag times were longer for higher ramp rates and larger temperature differences.

When the product temperature has completed its slow increase, it passes through a maximum. The subsequent decrease in product temperature is then very slight at low pressure settings (i.e. from −44.1 °C to −44.4 °C at 30 mTorr) and more pronounced for higher pressure settings (from −27.0 °C to −29.7 °C at 200 mTorr). This phenomenon could be ralated to a gradually decreasing efficiency of heat transfer to the sublimation front.

At very low pressure settings, there is only a small amount of heat transfer by gas conduction and the gap appearing between well wall and ice core widens slowly. Heat transfer to the sublimation interface by direct conduction through container wall and frozen water is kept up until a rather late stage of the sublimation process. At higher pressure settings, the higher amount of heat transfer by gas conduction between warm container wall and cold ice core leads to accelerated formation of the gap separating ice core and container wall. Percentage-wise, less heat is provided to the ice core by direct conduction. The ongoing sublimation consumes heat energy still contained in the frozen ice core, thereby decreasing the temperature of the frozen water.

This assumption is based on observations made during the sublimation tests: after conduction of a sublimation test at low pressure (30 or 50 mTorr), the remaining ice cores in the wells were still tightly fixed in their positions. A protruding keg or pillar had only formed in the upper portion of the well (the part receiving the highest portion of radiative heat transfer). After conduction of the test at a high pressure set point (200 or 500 mTorr), the ice cores had an almost cylindrical form and had lost all contact to the sides of the well. The pillar-shaped ice cores moved freely within the wells (cf. Figure 3.6)

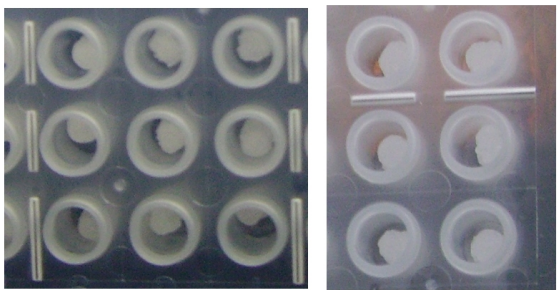

Figure 3.6: Photographs of well plates directly after the end of a sublimation test at 500 mTorr. Ice core has lost nearly all contact to the well wall.

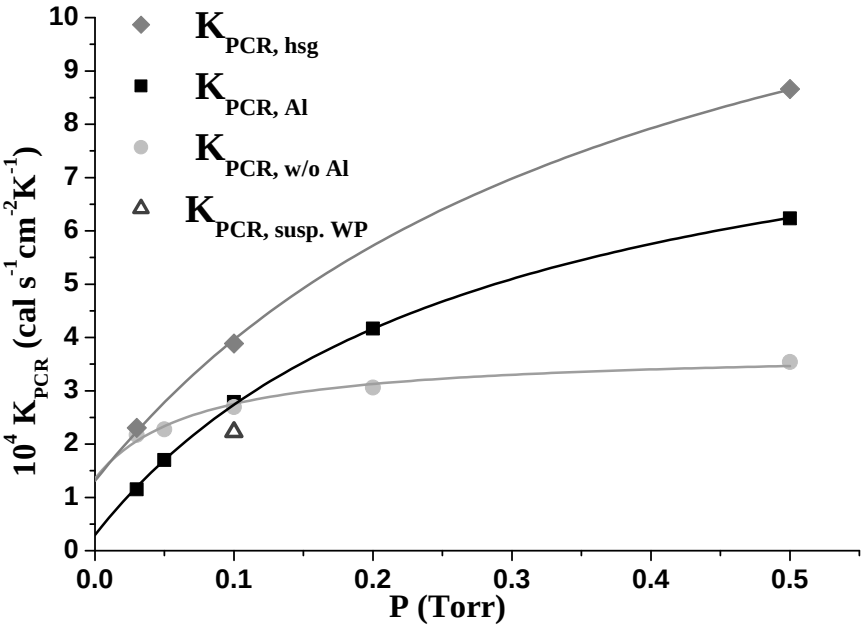

Figure 3.7: Comparison of heat transfer coefficients calculated from sublimation test data of 96-well PCR-plates with Al-blocks ($K_{PCR,Al}$; black squares), without Al-blocks ($K_{PCR,w/oAl}$; light grey circles), with suspended well plates ($K_{PCR,susp.WP}$; grey open triangle), and of well plates with heat sink grease ($K_{PCR,hsg}$; grey diamonds).

3.1.6 Sublimation Tests with Heat Sink Grease

Heat transfer coefficients calculated from sublimation tests with well plates inserted in Al-blocks lined with heat sink grease, $K_{PCR,hsg}$, are given in Table 3.2. The area of heat input $A_{PCR,hsg}$ for this experimental set-up was assumed to be equal to the area of well plates used with Al-blocks without heat sink grease, $A_{PCR,Al}$. Sublimation rates (and therefore heat transfer coefficients) in well plates inserted into these blocks are found considerably higher than for well plates with Al-blocks without heat sink grease. Figure 3.7 shows a direct comparison of heat transfer coefficients of 96-well PCR-plates, PCR-plates inserted into Al-blocks, suspended well plates, and well plates inserted into Al-blocks with heat sink grease applied to the cavities. Note that the experiments with heat sink grease were only performed for three pressure settings.

Data of these tests was also fitted to Equation 1.7. This data fit might not be as representative as a fit with more pressure set points. It is, however, obvious that the y-axis intercept, K_K is larger for this set-up than for well plates used with Al-blocks without heat sink grease (see Table 3.3). The increase in K_K can be explained by two influencing factors: very good heat transfer from the Al-block to the container, and the increase in contact area in between well

plate and Al-block due to the grease. The curve is not exactly parallel to the curve of PCR-plates used with Al-blocks, but found higher at all tested pressure set points. For higher pressures (exceeding approximately 200 mTorr), the large standard deviation in calculated heat transfer coefficients must be taken into account. This scattering of data which is regularly observed at higher pressures might be responsible for the non-parallel increase of the curve in comparison to data found for well plates with Al-blocks (without the grease).

This nearly parallel increase in heat transfer coefficients for the two different designs might suggest that the contact area in between shelf surface and Al-block has not changed and that the contact area in between Al-block and individual wells of the well plate might still be less than 100 %. However, the total gap width in between shelf surface and container wall might be reduced. The term $l*(K_P/\lambda_0)$ is smaller for the set up with heat sink grease than without it and in the same order of magnitude as it is for $2R$ vials (see section 3.4.2). This indicates the smaller separation distance l_{PCR}. The value of l_{PCR} calculated from the fitting result is approximately 0.03 cm, almost exactly the same as it is for $2R$ vials.

The temperature difference in between the underside of the Al-block (T_s) and the ice at the tip of the well (T_b) is smaller than for well plates with Al-blocks without heat sink grease. The "lag time" in reaching steady state temperature in the product after reaching the shelf temperature set point for the sublimation phase (approximately 25 min for well plates in Al-blocks without heat sink grease) seems to be a few minutes shorter for Al-blocks plus heat sink grease. The absolute difference, however, is less than 10 min. This time span is only slightly higher than the error in determination of the (average) time point when the steady state temperature in the product is reached. A 20 % to 40 % gain in efficiency for swiftness of temperature equalisation is only a rough estimation.

3.1.7 Summary: Heat Transfer into Well Plates

Heat input by direct conduction does not contribute significantly to total heat transfer into PCR-plates used without Al-blocks. For well plates used with Al-blocks, heat transfer by direct conduction plays a minor role due to the limited area of full contact between well plate and Al-block bore holes. Higher precision in production of Al-blocks and well plates might elevate heat transfer by direct conduction. The contact area can also be increased by application of heat sink grease to the bore holes. However, for well plates used with Al-block, additional time and energy are necessary for heating up the Al-block to the primary drying temperature after completion of the freezing step. This effect consumes part of the advantage in efficiency of heat transfer compared to well plates without Al-block.

The contribution to heat transfer by radiation is very high for well plates used without Al-blocks and very limited for Al-blocks used with Al-blocks. For the latter set-up, the Al-blocks used for enhancement of heat transfer by direct conduction also serve as radiation shields, blocking out radiation from the sides as well as from the bottom shelf.

At pressure settings of approximately 100 mTorr and higher, heat transfer by conduction through the gas becomes a significant contribution to total heat transfer. The impact of this heat transfer mechanism is only slight for well plates used without Al-blocks as the separation distance between "hot" shelf surface and "cold" well plate is large in comparison to well plates inserted into Al-blocks. For the small gap sizes between shelf surface and bottom of Al-block as well as between Al-block bore hole wall and well plate, heat transfer by conduction through the gas is very efficient. It can be increased by application of heat sink grease to the bore hole walls, as the layer of grease further reduces the gap size in areas with no perfect contact between Al-block cavities and the inserted well plate. The use of heat sink grease in this study was only explorative (i.e. to show the difference in effect). It was not considered as an option for a GMP environment, or even sterile production and clean room conditions.

Under low pressure conditions, heat transfer by direct conduction (which is inefficient for either set-up, with or without Al-block) and by radiation (higher contribution for well plates without Al-blocks) are the predominant heat transfer mechanisms. Therefore, for freeze drying cycles which need very low pressure settings of less than approximately 100 mTorr during primary drying (usually in combination with very low shelf temperatures), it could be advantageous to

use well plates without Al-blocks.

However, for this set-up, effects of atypical radiation leading to heterogeneous drying rates might be more pronounced as edge and corner wells are not shielded from additional radiation from freeze dryer door / walls. In addition to drying inhomogeneity caused by the position on the freeze dryer shelf, the curvature of the base plate of this type of well plate leads to a slightly elevated position of wells in the centre compared to wells along the two long edge rows. This difference in separation distance from the shelf surface may also be a cause for differences in product temperature profiles and hence for drying heterogeneity. Using a different type of well plate with a more level base plate may be a way to circumvent this problem. Based on the observations made during experiments with excipient solutions (cf. section 3.2), the influence of the position on the shelf seems to have a strong impact on primary drying time.

At intermediate to higher pressure settings, the increased efficiency of heat transfer by conduction through the gas in the set-up with Al-blocks might outweigh the disadvantage of a prolonged warming phase at the beginning of primary drying. Heat transfer can be expected to be more homogeneous throughout the whole batch if Al-blocks are used.

3.2 96-well PCR-Plates: Product Runs

3.2.1 Applicability of Heat Transfer Coefficients

Relevance and applicability of heat transfer coefficients determined from sublimation tests with distilled water to model product solutions were tested. In principle, Equation 1.5 should also be applicable to a product solution with a constant temperature difference $T_s - T_b$ during primary drying. This temperature difference will remain constant or relatively constant as long as the product resistance and hence the mass flow rate do not change significantly.

$$\frac{\mathrm{d}m \cdot q_{s,ice}}{A_v \cdot K_v \cdot (T_s - T_b)} = \mathrm{d}t. \tag{3.1}$$

The product resistance has been found to increase during primary drying with increasing thickness of the dried product layer [100]. For amorphous products with low fill depths (i.e. not more than 1 cm), the increase of the initial product resistance is only slight to moderate with progress of primary drying [69].

The mass flow rate may also vary if the efficiency of heat transfer into the product undergoes changes, i.e. due to a change of the area which is relevant for heat transfer. However, as long as the premises for pseudo-steady state conditions apply, the heat transfer coefficients calculated from sublimation tests with distilled water could be used in combination with the temperature difference $T_s - T_b$ obtained from TC data during the freeze drying run to estimate the remaining primary drying time.

This applicability of heat transfer coefficients to a freeze drying run with product solution was tested for crystalline and amorphous model products. In addition, average heat transfer coefficients were also calculated from these product runs and compared to the heat transfer coefficients obtained from sublimation tests. Results of these comparisons were evaluated to determine useful rules for cycle optimisation with well plates.

3.2.2 Calculation of Primary Drying Time from Initial Temperature Differences

The applicability of heat transfer coefficients for 96-well PCR-plates determined from sublimation tests for prediction of primary drying times when using an actual product was first tested with 50 mg/g trehalose solution. In order to estimate the remaining primary drying time from the temperature difference between shelf surface and frozen product solution, the total amount of ice which needed to be sublimed had to be calculated.

The fill volume per well was 100 μL. Assuming a density of 1 g/cm^3 for the solution, the mass of water per well can be calculated as 95 mg, and the mass of water per well plate is $96 \cdot 0.095\mathrm{g} = 9.12\mathrm{g}$. The actual mass of water per well differs slightly, because the density is slightly higher than 1 g/cm^3. An example for calculation of the actual mass from experimental data is given in the following:

- weigh in of trehalose: 7.50 g
- total weigh in of solution: 150.01 g
- reweighing after all cavities in well plates to be used for the freeze drying run have been filled: 32.67 g
- mass distributed into well plates (total weigh in minus residual mass in beaker): 117.34 g
- amount of trehalose evenly distributed in wells: $\frac{7.50\mathrm{g} \cdot 117.34\mathrm{g}}{150.01\mathrm{g}} = 5.87\mathrm{g}$
- amount of water evenly distributed in wells: $117.34\mathrm{g} - 5.87\mathrm{g} = 111.47\mathrm{g}$
- number of filled well plates: 12
- mass of water per well plate: $\frac{111.47\mathrm{g}}{12} = 9.29\mathrm{g}$

The difference between the estimated mass of water per well plate (9.12 g) and the caculataed mass of water per well (approximately 9.29 g) is less than 2 %. For the value calculated from the difference of absolute weight of solution and weight of the residual solution after filling of all cavities, the error introduced due to evaporation of water during the filling process must be considered. The solution was filled into the well plates directly after preparation. During the filling process, care was taken to prevent evaporation of the solvent, i.e. by covering the beaker containing the solution with a water tight foil. The weight loss caused by evaporation of water was still noticeable, and some of the deviation between the calculated mass of water and the estimate of 9.12 g may be caused by this effect.

For the estimation of the remaining primary drying time, the average value of 9.22 g of water per well was used. For a fill volume of only 20 μL per cavity, a similar calculation was performed. For this set-up with the lower fill volume, the average mass of water per well plate was calculated to be 1.85 g.

To calculate the temperature difference $T_s - T_b$, the average value determined of all thermocouple readings of TCs placed in wells 30 min after first reaching the shelf temperature set point was used for T_b. The delay of 30 min was used to assure that steady state conditions were attained in the product. The value for T_s was calculated as the average of the TC readings of thermocouples placed beneath well plates / Al-blocks at the time point chosen for calculation of T_b. Table 3.4 gives an overview of $T_s - T_b$ data, estimated primary drying times, and actually observed primary drying times for several exemplary freeze drying cycles with trehalose solution.

Table 3.4: Comparison of primary drying time duration calculated from temperature data at the beginning of primary drying, and of actually observed primary drying times for trehalose solution freeze dried using different set-ups.

SET-UP	SET POINT $^\circ C$	$T_s - T_b$ K	PRIMARY DRYING TIME (h) CALCULATED	OBSERVED
100 μL without Al	−20	10.6	14.4	14.3
	−10	16.9	9.0	9.1
	0	23.9	6.4	6.5
20 μL without Al	−20	9.7	4.7	4.0
	−10	15.2	3.0	2.6
	0	22.4	2.0	2.0
100 μL with Al	−20	9.1	4.4	9.4
	−10	13.6	3.0	5.7
	0	18.0	2.2	4.2
20 μL with Al	−20	8.6	2.1	3.8
	−10	13.4	1.3	2.5
	0	19.8	0.9	2.1

The calculated primary drying times are in very good agreement with the observed primary drying times for all freeze drying runs with trehalose solution using the well plates without Al-blocks. This agreement is nearly perfect for the higher fill volume of 100 μL. For the lower fill volume, 20 μL per well, the difference between predicted and actual primary drying time is less than 1 h in all cases. For the low fill volume, there appears to be a tendency for a shorter actual primary drying time than the predicted primary drying time. However, this set of data is too small to confirm this tendency.

The case is clearly different for trehalose solution freeze dried in well plates when using Al-blocks. For this set-up, the predicted primary drying time is always shorter than the observed

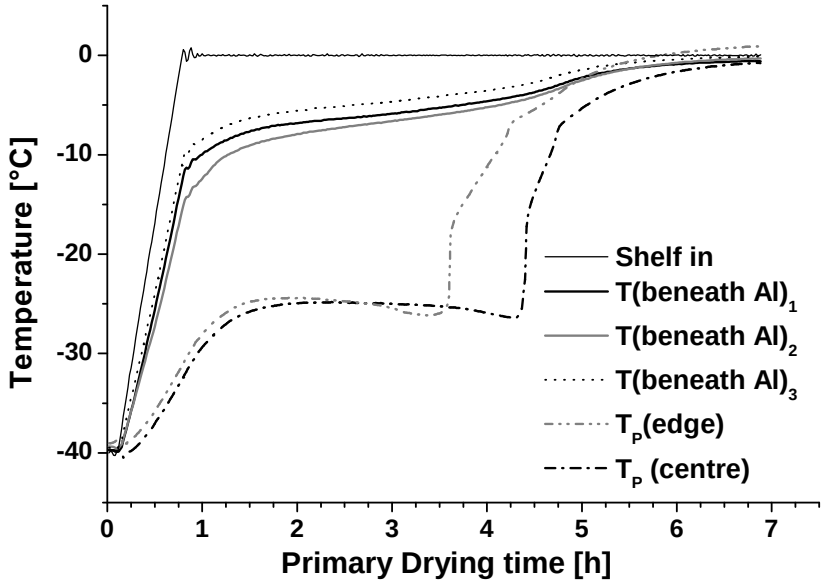

Figure 3.8: The diagram shows temperature over time curves measured during the primary drying phase of a freeze drying run with 96-well PCR plates in Al-blocks at 0 °C shelf temperature. The thin black line represents the shelf fluid inlet temperature. The dash-dotted, black line and the dash-dot-dotted grey line are exemplary product temperature profiles measured in a centre and an edge well, respectively. The grey line, the black line, and the black dotted line show data of TCs placed underneath the Al-blocks. These temperatures steadily increase from approximately −10 °C at the beginning of the "steady state" phase of primary drying to approximately −5 °C at the end of primary drying.

primary drying time. The difference between the prediction and the actual value is roughly a factor of 2. It is assumed that this disagreement between prediction and actual value is caused by the prolonged warming phase for the Al-blocks and by a constantly changing (diminishing) area for heat input.

The temperature measured beneath the Al-blocks constantly rises and never reaches a constant value until the primary drying phase is completed (cf. Figure 3.8, also see Figure 3.13). This indicates that the steady state assumption is not valid for the freeze drying cycles using Al-blocks. In addition, it is assumed that the major portion of heat is transferred into the product by conduction through the gas over a small separation distance between frozen product and Al-block bore hole. In sublimation tests with water, it was observed that the ice core retreats towards the centre of a well (cf. Figure 3.6). It is furthermore assumed that this behaviour also occurs when freeze drying a product solution. The remaining, gas-filled pores in primary dried product might act as an insulation to heat conduction (increasing separation distance), and therefore the effective area for heat transfer into the product decreases. This phenomenon is of lesser importance for heat transfer by radiation, the main mechanism of heat transfer for well plates without Al-blocks, as heat transfer by radiation is independent of the separation distance (cf. section 1.4.3). The combination of these effects may be the reason why calculation of a primary drying time estimate using Equation 3.1 does not yield valid results when using Al-blocks.

The estimation of the primary drying time for a product run with a crystalline product (i.e. mannitol solution) is more difficult. In this case, the product resistance constantly increases as the dry layer thickness increases with progression of the primary drying phase [69]. This, in turn, decreases the mass flow rate, and the steady state condition for applicability of Equation 3.1 is

not fulfilled. However, the calculation of primary drying time was performed using thermocouple data from freeze drying runs with mannitol solution in the same way as has been described for trehalose solution. The results for calculation of the primary drying time (based on the steady state assumption) of mannitol solution freeze dried in well plates are shown in Table 3.5.

Table 3.5: Comparison of primary drying time duration calculated from temperature data at the beginning of primary drying, and of actually observed primary drying times for mannitol solution freeze dried using different set-ups.

SET-UP	SET POINT $^{\circ}C$	$T_s - T_b$ K	PRIMARY DRYING TIME (h) CALCULATED	OBSERVED
100 μL without Al	−20	10.3	14.8	20.7
	−10	15.7	9.7	13.3
	0	22.4	6.8	9.2
20 μL without Al	−20	8.7	5.2	6.2
	−10	12.5	3.7	3.6
	0	16.4	2.8	2.7
100 μL with Al	−20	9.1	4.7	20.8
	−10	13.9	3.1	11.4
	0	17.1	2.5	7.2
20 μL with Al	−20	8.4	2.2	6.4
	−10	11.9	1.5	4.0
	0	15.0	1.2	3.1

The difference in congruity of predicted and observed primary drying times between the two experimental designs of well plates with Al-blocks versus well plates without Al-blocks is also found for freeze drying of mannitol solution. For mannitol solution freeze dried using Al-blocks, the factor for the difference between estimated and observed primary drying time is in the order of 3 to 4. The probable reasons for this large deviation, in addition to the increasing product resistance, have been explained above for trehalose solution (changing area of "effective" heat transfer, non-steady state conditions).

For the other experimental design, well plates without Al-blocks, the agreement between primary drying time estimate and the actual value is better. For the high fill volume of 100 μL, the actual primary drying time is approximately 35 % longer than the estimated duration of primary drying. As has been explained above, the product resistance of a crystalline product has been found to increase almost linearly with increasing dry layer thickness [69], that is, with progression of primary drying. The 35 % deviation between estimated and observed primary drying time for 100 μL mannitol solution per well might be explained by the continually reduced mass flow rate due to the increased product resistance.

For the low fill volume (20 μL) of mannitol solution per well in well plates without Al-blocks, the agreement between the estimated and the observed duration of the primary drying phase is very good. The effect of decrease of mass flow rate with increasing dry layer thickness might be of lesser impact for this very low fill volume / fill height in the well.

As a conclusion from these experiments, it can be stated that the heat transfer coefficients determined from sublimation tests with distilled water for the design of well plates used without Al-blocks may be a useful help in estimation of the total primary drying time for a previously untested formulation. The applicability of the heat transfer coefficients appears to be best for amorphous formulations. For crystalline formulations, the degree of accuracy for the primary drying time estimate seems to decrease with increasing fill volume / fill depth of the solution in

the well.

The heat transfer coefficients determined from sublimation tests performed with well plates using Al-blocks have shown limited value for estimation of the primary drying time. It is assumed that the heat transfer rate and hence the mass flow rate decrease significantly with progression of primary drying time for this set-up. Another possible reason for the mismatch of predicted versus actually observed primary drying times could be that the area for heat input into the well plate, $A_{PCR,Al}$, has not been correctly estimated, and is actually larger. Therefore, the values of the heat transfer coefficients $K_{PCR,Al}$ at different chamber pressure set-points might have been assumed to be slightly higher than they actually are.

3.2.3 Estimation of Average Mass Flow from Product Run Results

Pure mannitol and trehalose solutions were freeze dried in 96-well PCR-plates at different shelf temperatures and with different fill volumes. All freeze drying runs were performed at a chamber pressure of 100 mTorr. This pressure setting was chosen as representing the intermediate range of pressure settings usually applied in freeze drying. Amorphous product solutions with very low critical temperatures may ideally be primary dried at low shelf temperatures (at or below −20 °C) and chamber pressure settings in between approximately 50 and 100 mTorr. Crystalline or partially crystalline formulations are often freeze dried at higher shelf temperatures (0 °C or even higher) and intermediate to higher pressure settings.

The chosen combinations of shelf temperatures with the pressure setting of 100 mTorr represent a range of well suited to manageable, if not ideal freeze drying conditions for both model products, amorphous trehalose solution and crystallising mannitol solution. The same conditions were applied to both model formulations to ensure comparability of primary drying behaviour. Most freeze drying runs were performed in duplicate. Each run was performed at least once with and once without Al-blocks.

To determine the average mass flow rates, dm/dt, during the primary drying phase of these product runs, the residual moisture content at the end of primary drying was determined and subtracted from the amount of water initially filled into the well plates (calculation of dm). The time interval of the primary drying phase (dt) was used to calculate the water vapour mass flow rate.

Primary Drying Endpoint Determination

The primary drying endpoint was determined by comparative pressure measurement, using the pressure readings of a capacitance manometer and a Pirani gauge calibrated for nitrogen. The endpoint of primary drying was considered to have been reached when the difference between Pirani and capacitance pressure reading was within a 5 mTorr range and had not changed for at least 20 min. These conditions were chosen for the definition of the primary drying endpoint because they seem suited to describe the transfer phase from ending of sublimation of ice (the pressure difference remains nearly constant, and does not decrease rapidly any more) to a low level of water vapour mass flow by desorption.

Errors may be introduced into the data set when the pressure readings of Pirani gauge and capacitance manometer showed identical or nearly identical values for a longer period of time (more than approximately 1 h). The secondary drying phase starts as soon as all ice has been removed from the product section under consideration. The desorption process is more efficient at higher shelf temperatures with temperature set points above room temperature. However, the residual moisture content of samples which have been left at −20 °C shelf temperature and 100 mTorr chamber pressure for more than 1 h will probably already have lost a significant portion of their initial residual moisture content.

Residual Moisture at the End of Primary Drying

When the endpoint of primary drying was reached, the shelf temperature was lowered and the chamber was vented to take out samples and determine the residual moisture of these. This procedure of removing samples at the beginning or prior to completion of the secondary

drying phase has been used to assess the optimal duration for secondary drying, as well as for determination of water vapour sorption isotherms [2], [20].

The calculation of average mass flow based on the residual moisture content at the end of primary drying is certainly prone to error due to the start of secondary drying in the late stage of primary drying, when little ice remains in the product containers, as has been pointed out above [2]. Also, the residual moisture content may differ from one container to the next [20], [101].

The error introduced into the calculation due to the difference between the residual moisture content determined from measurements in a few samples and the "true" average residual moisture content of the whole batch at the end of primary drying will be relatively small, as the total difference between those two values should not exceed a few percentage points (less than 5 %) in relation to the total mass of the primary dried product. The error introduced into the calculation of average mass flow during primary drying by including a portion of secondary drying (desorption of "unfrozen" water) in the late stage of primary drying is expected to be of the same order of magnitude. The main portion of the water initially contained in the solution (approximately 90 % of the initial content of 950 mg/g of the product solution) will have been removed by sublimation of ice.

Table 3.6 gives an overview of residual moistures of the samples as determined by Karl-Fischer titration. Typical residual moisture results were found in between 2 and 4 %, based on the weigh-in value of the primary dried sample. Mannitol freeze dried with Al-blocks at a shelf temperature of 0 °C contains even less than 2 % of residual water at the end of primary drying. There seems to be a trend for less residual moisture content in product freeze dried with Al-blocks and for the low fill volume (20 μL), respectively. These differences, however, are small (in most cases the absolute difference in percent residual moisture values is less than 1 %) and the trend was not found consistent for all cases (cf. mannitol with Al-blocks at −20 °C, 100 μL vs. 20 μL and trehalose 100 μL with / without Al-blocks also at −20 °C).

Table 3.6: Residual moisture (%) at the end of primary drying of mannitol and trehalose as determined by Karl Fischer titration. Values given in the Table are averages calculated from 3 to 5 individual measurements per run.

	Shelf Temp. °C	Fill Vol. 100 μL w. Al	Fill Vol. 100 μL w/o Al	Fill Vol. 20 μL w. Al	Fill Vol. 20 μL w/o Al
Mannitol	0	1.64	3.40	1.66	2.20
	−10	2.24	3.52	2.22	2.48
	−20	2.09	3.71	2.50	3.58
Trehalose	0	2.80	3.40	1.99	2.95
	−10	2.93	3.82	2.62	2.54
	−20	3.19	2.81	2.28	3.07

It is probable that a considerable amount of unfrozen water is removed from the product in the well plates during the late stage of primary drying even though the shelf temperature remains low. Typically, a residual moisture content of approximately 10 % is found in a sucrose solution freeze dried in vials at the end of the primary drying phase [2]. In this study it was observed that especially for trehalose, the residual moisture results were much lower than has been reported for other amorphous products. The secondary drying effect during primary drying seems to be more pronounced for product freeze dried in 96-well PCR-plates.

A possible explanation for this observation might be the limited volume of product solution per well. Freeze drying small aliquots of product solution signifies that the surface area per millilitre of solution is higher than for freeze drying a similar (total) volume in vials with a comparable fill depth. The efficiency of desorption increases with increasing temperature of the

product and with an increase in (total) surface area [33].

These low residual moisture contents found at the end point of primary drying defined for this study led to the assumption that not the equalisation of pressure readings of Pirani and capacitance manometer should be considered as the end of the sublimation phase, but an earlier time point within the phase of decreasing pressure readings for the Pirani gauge. It is suggested here to further analyse this critical phase for freeze drying cycles when using 96-well PCR-plates, and to test if, i.e. the average value between Pirani pressure reading during the steady state phase of primary drying and the capacitance manometer reading may be used to identify the endpoint of primary drying.

Primary Drying Times: Mannitol Solution

Primary drying times of excipient solutions freeze dried with and without Al-blocks were compared. All primary drying intervals were determined from the starting point of the initial ramping phase (−40 °C to the designated shelf temperature) until the end of the decline in the Pirani pressure reading (Pirani gauge reading was within 5 mTorr range of capacitance manometer reading). Primary drying times of mannitol solution, which have first been reported in Table 3.5 in section 3.2.2 are again summarised in Table 3.7.

Table 3.7: Primary drying times (hours) of mannitol solution in 96-well PCR-plates with different experimental designs (with Al-blocks, without Al-blocks, different fill volumes, single shelf, and full load runs) and at different shelf temperatures. All runs were performed at 100 mTorr chamber pressure.

No. of Shelves	shelf Temp. °C	Mannitol 100 µL w. Al	Mannitol 100 µL w/o Al	Mannitol 20 µL w. Al	Mannitol 20 µL w/o Al
1	0	7.2	9.2	3.1	2.7
1	0	7.6			
3	0	7.7	9.5		
1	−10	11.4	13.3	4.0	3.6
1	−10	11.6			
3	−10	12.4	14.1		
1	−20	20.8	20.7	5.8	6.2
1	−20			6.4	

For mannitol at the 100 µL fill volume, the total primary drying time is found in between 7.2 h at 0 °C and 20.8 h at −20 °C. With the exception of freeze drying runs performed at −20 °C shelf temperature, primary drying times for 100 µL of mannitol solution in well plates inserted in Al-blocks are shorter than the same fill volume of mannitol solution in well plates without Al-blocks. The use of the Al-blocks shortened primary drying times by approximately 2 h. This corresponds to a decrease of primary drying time of approximately 15 to 25 %, depending on the shelf temperature chosen for primary drying. The percentage shortening of cycle time was highest for the highest shelf temperature setting of 0 °C. For −20 °C shelf temperature, primary drying times were nearly identical for the two different experimental designs.

At least for mannitol-based formulations, the superior heat transfer characteristics of the Al-block over well plates placed directly on the shelf seem to be most relevant not only at sufficiently high chamber pressure (>100 mTorr), but also at higher shelf temperature settings. At low shelf temperature settings during primary drying (−20 °C), the gain in efficiency of heat transfer by

the use of Al-blocks with subsequent shortening of primary drying time seems to be balanced by the extra time needed to warm up the Al-block at the beginning of primary drying.

Four runs (two with and two without Al-blocks) with 100 μL mannitol solution per well were repeated as full load runs with all three shelves of the freeze dryer fully loaded. Primary drying times determined from these runs were slightly longer than the corresponding average primary drying time of single shelf experiments. The difference in the time interval corresponds to approximately 7 % and 5 % lengthening of primary drying time at a shelf temperature setting of -10 °C and 0 °C, respectively.

The exact determination of the primary drying endpoint is prone to error, since the slope of the decreasing Pirani gauge readings flattens out towards the end of primary drying, and the Pirani reading may remain constant for more than 15 min before further decreasing. The error is estimated to be within ± 10 min for shelf temperature set points of 0 °C and -10 °C, and ± 30 min for a shelf temperature of -20 °C. A criterion that helps in defining the endpoint of primary drying more precisely would be helpful, i.e. the time point when the Pirani reading first comes within 10 mTorr of the capacitance manometer reading, or the Pirani reading comes within 1.1 (or even 1.3) times the capacitance manometer reading.

The approximately 5 % longer primary drying times for the full load runs might be explained by the higher accuracy of the Pirani measurements at full load conditions and / or by the higher heat transfer rate from the shelf fluid / shelf surface (due to higher demand of heat to sustain sublimation on three shelves) into the product under full load conditions. This may lead to a slightly lower average shelf fluid temperature during primary drying. It was also noted that the average product temperature determined from TC data is slightly (less than 1 K) lower for full load runs at corresponding time points during primary drying (i.e. two hours after reaching the shelf temperature set point for primary drying). This small difference in product temperature is still less than the known range of accuracy of ± 1 K of the TCs. At a lower product temperature, mass flow would be slightly lower for full load runs, leading to a longer primary drying phase.

As for the low fill volume of 20 μL, primary drying times for the two set-ups with and without aluminium blocks are almost identical. For mannitol solution, they range from 2.7 h at 0 °C to 6.4 h at -20 °C. A tendency for shorter primary drying times for mannitol solution without Al-blocks might be noticeable from the data (see Table 3.7). Here, the more efficient heat supply by the use of Al-blocks seems to be completely compensated by the additional heat consumption due to heat accumulation in the Al-block. It will be shown later in the text that heat transfer by radiation into well plates with low fill volume also seems (by comparison) more efficient than radiative heat transfer into well plates with higher fill volumes.

Primary Drying Times: Trehalose Solution

Table 3.8 gives an overview of primary drying times of trehalose solution freeze dried at different fill volumes (100 μL per well, 20 μL per well) and at different shelf temperatures (0 °C, -10 °C,-20 °C) in PCR-plates with and without Al-blocks. A similar summary of the primary drying times has also been provided in Table 3.4 in section 3.2.2. For the high fill volume, primary drying times range from 4.2 h at 0 °C to 14.3 h at -20 °C. Primary drying times of trehalose solution were found to be shorter than corresponding primary drying times of mannitol solution. Also, primary drying for the set-up with Al-blocks is considerably shorter than primary drying without Al-blocks in all of the cases tested with trehalose: the use of Al-blocks shortens the primary drying phase for 100 μL trehalose solution by more than 2 h or approximately 35 % for a shelf temperature of 0 °C and by more than 4 h (also 35 %) for a shelf temperature of -20 °C. The results illustrate that for trehalose heat transfer is enhanced when using Al-blocks.

The question arises why primary drying times are shorter for trehalose than for mannitol. The answer lies in the difference between mannitol as a crystalline and trehalose as an amorphous product. As has been noted before, it has been reported that the product resistance for crystalline products continually rises during the primary drying phase [100]. The increasing product resistance reduces mass flow rates if heat supply remains stable (cf. Equation 1.1). Heat which is not consumed in the same amount for sublimation of ice instead leads to warming of the product. This also explains why the product temperature of mannitol solution continually rises during primary drying in well plates (cf. Figure 3.9, also Figures 3.16 and 3.17 in section

Table 3.8: Primary drying times (hours) of trehalose solution in 96-well PCR-plates with different set-ups (different fill volumes, with Al-blocks, without Al-blocks, single shelf, and full load runs) and at different shelf temperatures. Chamber pressure was 100 mTorr for all runs.

No. of Shelves	shelf Temp. $°C$	Trehalose 100 μL w. Al	Trehalose 100 μL w/o Al	Trehalose 20 μL w. Al	Trehalose 20 μL w/o Al
1	0	4.2	6.5	2.1	2.0
3	0		7.3		
1	−10	5.7	9.1	2.5	2.6
3	−10	6.0	9.8		
3	−10	6.2			
1	−20	9.4	14.3	3.8	4.00
3	−20	10.3			

3.2.7) whereas trehalose product temperature nearly reaches a plateau phase (cf. Figures 3.9, 3.16,3.17). The efficiency of ice sublimation seems to be lower in mannitol solution than in trehalose solution freeze dried under the same conditions.

Amorphous products may undergo the phenomenon of micro collapse: if the product temperature at the sublimation interface is close to or even exceeds the critical formulation temperature, pore-walls start to "flow". The pores change their forms, thereby increasing the pore diameter in the primary dried matrix adjacent to the sublimation interface. These bigger pores generate less hindrance for the water vapour flow created through sublimation. The gain in product resistance by increase of the dried layer may therefore be balanced by the relative "reduction" of product resistance due to the formation of these larger passage ways. In addition to that, the "flow" of the pore walls is macroscopically discernible as a certain, small amount of shrinkage of the lyophilisate cake. When shrinkage occurs, the primary dried product matrix may lose contact to the well wall, causing the appearance of a small gap. This gap may also contribute to the relative decrease of the product resistance.

Four full load runs (three shelves) were performed with trehalose solution at 100 μL fill volume, two with Al-blocks (−10 °C, −20 °C) and two without Al-blocks (0 °C, −10 °C). Again, the primary drying phase of full load runs was slightly longer than for corresponding single shelf runs. The differences in primary drying time are in the same order of magnitude as stated for mannitol experiments (5 % to 10 % elongation of primary drying time under full load conditions). The probable explanations for this difference in primary drying time are similar to what has been stated for mannitol solutions (difference in accuracy of Pirani measurements of single shelf versus full load conditions, small differences in shelf fluid / shelf surface temperatures due to different amounts of heat consumption for single shelf versus full load conditions).

Primary drying times for freeze drying of 20 μL trehalose solution range from approximately 2 h at a shelf temperature of 0 °C to 4 h at −20 °C. They are nearly identical for well plates placed directly on the shelf and for well plates with Al-blocks. It is probable that for such short total primary drying times the increase in heat transfer efficiency by the Al-block is compensated by heat accumulation in the Al-block.

Calculation of Average Mass Flow Rates in Well Plates

The average mass flow during the sublimation phase was calculated from the mass of water removed by sublimation (taking into account the residual moisture of the product at the end

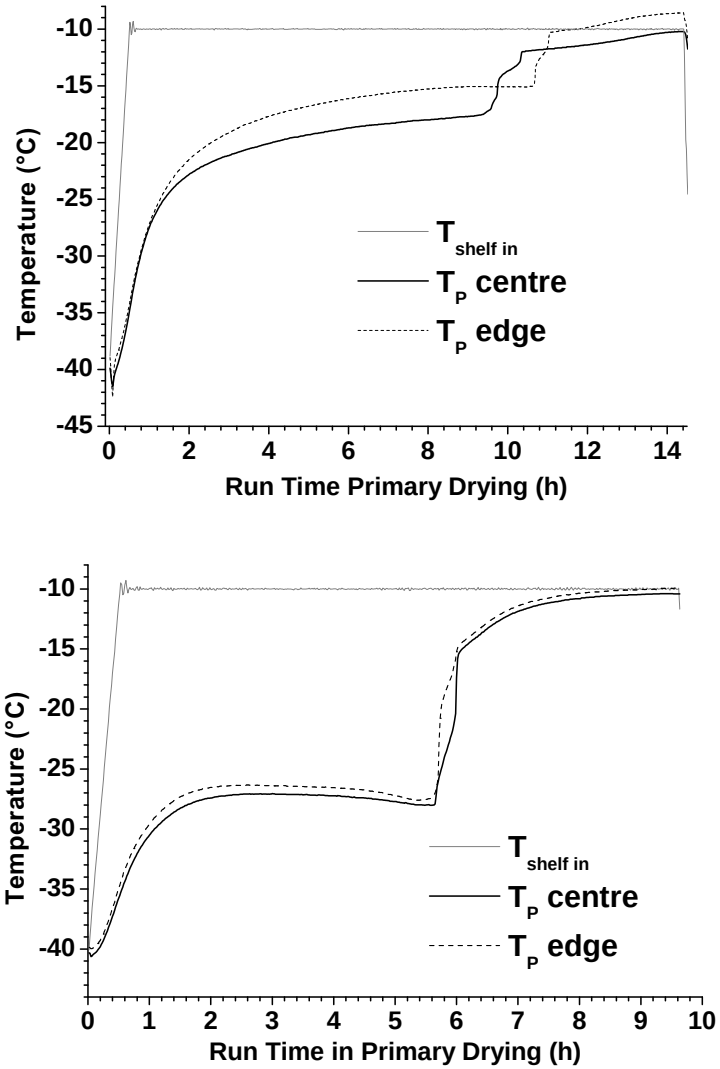

Figure 3.9: Plots of product temperature (T_P) over time profiles during primary drying of 100 μL mannitol (upper panel) and trehalose (lower panel) solutions freeze dried in well plates with Al-blocks at -10 °C shelf temperature. Temperature data from centre wells is given as straight black line, temperature data from edge wells as dashed black line. Shelf temperature inlet data are shown as grey lines.

of primary drying), and from the primary drying times determined from comparative pressure measurement data. Tables 3.9 and 3.10 give an overview of these average mass flow rates for mannitol solution and trehalose solution.

The data shows that the mass flow rates of corresponding experimental designs are always smaller for mannitol solution than for trehalose solution. The probable reason for this has already been explained above with the higher product resistance of mannitol versus the amorphous treahalose matrix.

For both products, the enhancement of mass flow by the use of Al-blocks is clearly shown for the higher fill volume of 100 μL. At -20 °C shelf temperature, the mass flow rates for mannitol solution are very low for either set-up. At these low mass flow rates ($0.122 \cdot 10^{-3}$ gs^{-1} or less), the advantage of the Al-block for heat transfer appears to be insignificant.

For both products freeze dried using the low fill volume of 20 μL, the average mass flow rates

Table 3.9: Summary of average mass flow rates calculated from mass of water removed by sublimation and primary drying times for mannitol solution freeze dried in well plates using different experimental designs. Average mass flow rates are given in 10^{-3} gs^{-1}.

No. of Shelves	shelf Temp. $°C$	Mannitol 100 μL w. Al	Mannitol 100 μL w/o Al	Mannitol 20 μL w. Al	Mannitol 20 μL w/o Al
1	0	0.351	0.279	0.166	0.190
3	0	0.327	0.265		
1	−10	0.223	0.192	0.0128	0.142
3	−10	0.212	0.179		
1	−20	0.122	0.123	0.080	0.083

Table 3.10: Summary of average mass flow rates calculated from mass of water removed by sublimation and primary drying time for trehalose solution freeze dried in well plates using different experimental designs. Average mass flow rates are given in 10^{-3} gs^{-1}.

No. of Shelves	shelf Temp. $°C$	Trehalose 100 μL w. Al	Trehalose 100 μL w/o Al	Trehalose 20 μL w. Al	Trehalose 20 μL w/o Al
1	0	0.602	0.397	0.248	0.261
3	0		0.348		
1	−10	0.447	0.280	0.206	0.201
3	−10	0.414	0.260		
1	−20	0.270	0.177	0.130	0.130
3	−20	0.246			

during primary drying appear to be in the same order of magnitude regardless of the use (or non-use) of the Al-blocks. This might be an indication for less efficient heat transfer into the lower portion of a well when using Al-blocks, in comparison to heat transfer into upper portions of a well for this experimental design.

However, only the average mass flow can be determined using this method. The average mass flow value is not representative for the initial phase of primary drying (the mass flow rate will be higher than the average value, because the product resistance is still low) and for the end of primary drying (the mass flow rate will be lower than the average value due to higher product resistance). The increase of the product resistance over primary drying time may be linear for crystalline products, yet in many cases (i.e. for formulations with amorphous components) it is not [69]. The deviation of average mass flow to maximum and minimum mass flow values is very difficult to estimate without product resistance data of the tested formulation.

3.2.4 Online Determination of Mass Flow by TDLAS

Two freeze drying cycles (well plates used without Al-blocks) were performed using TDLAS technology as an additional tool allowing an instantaneous and real-time measurement of the water vapour mass flow rate. The diode laser was used to measure concentration and velocity of water molecules in the duct connecting the drying chamber and the condenser. Momentary mass flow can be calculated from these data. Figure 3.10 shows the mass flow measured during freeze drying of mannitol. The results are similar for trehalose (cf. Figure 3.11).

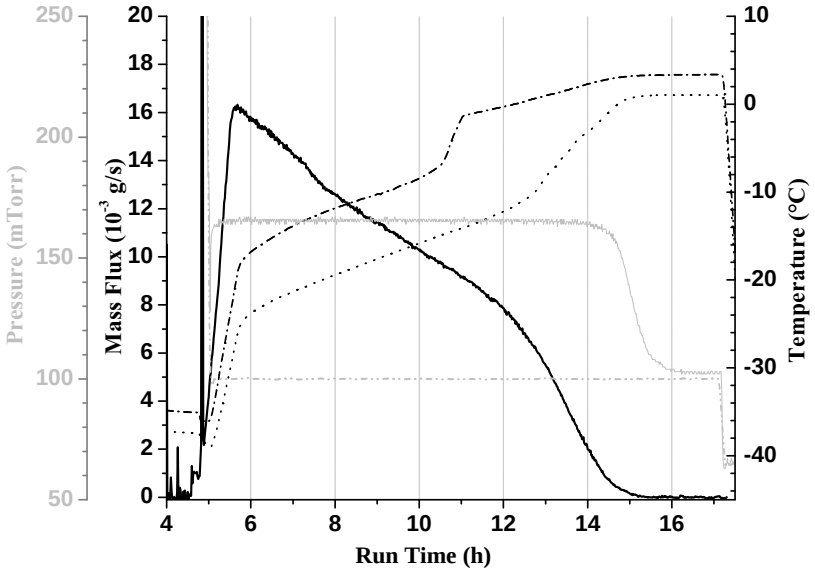

Figure 3.10: The diagram shows the primary drying phase of a freeze drying run (full load without Al-blocks) of 100 μL mannitol solution at 0 °C shelf temperature in 96-well PCR-plates. Product temperature is shown on the right axis (black dash-dotted line: TC corner placed, black dotted line: TC centre placed), pressure curves (grey straight line: Pirani, grey dash-dot-dotted line: capacitance manometer) on the outer left axis, and mass flux (black straight line) on the inner left axis.

It is obvious that water vapour mass flow reaches a maximum shortly after the beginning of primary drying and then quickly declines. When the Pirani gauge reading starts to decline, mass flow has already subsided to very low values (less than $2 * 10^{-3}$ g/s). However, the mass flow measurement by TDLAS is a function of the gas velocity. This, in turn, is less accurate towards the end of primary drying when the mass flow decrerases. The comparison of the mass flow rate and the pressure reading of the Pirani gauge in Figures 3.10 and 3.11 suggests that the inflection point of the slope of the Pirani readings towards the end of primary drying might be used to define the end point of the phase in which sublimation of ice still takes place. Table 3.11 summarizes maximum and average mass flow data determined by TDLAS during the two freeze drying runs.

The average mass flow of a single well plate with 100 μL mannitol solution per well for a full load run at 0 °C shelf temperature (without Al-blocks) was calculated as $0.265 \cdot 10^{-3}$ g/s, using the weighing procedure (cf. Table 3.9). Multiplied with 36, the number of well plates in the fully loaded freeze dryer, total mass flow equals $9.54 \cdot 10^{-3}$ g/s. This value is close (within ± 1 %) to the average mass flow calculated from TDLAS data (approximately $9.52 \cdot 10^{-3}$ g/s, cf. Table 3.11).

The comparison of average mass flow of trehalose data yields similar results: the total mass flow for a single shelf run calculated with the weighing procedure and residual moisture measurements is $14.3 \cdot 10^{-3}$ g/s. The total mass flow calculated from data of a (separate) full load run is $12.5 \cdot 10^{-3}$ g/s. The average mass flow calculated from TDLAS data (experimental design also

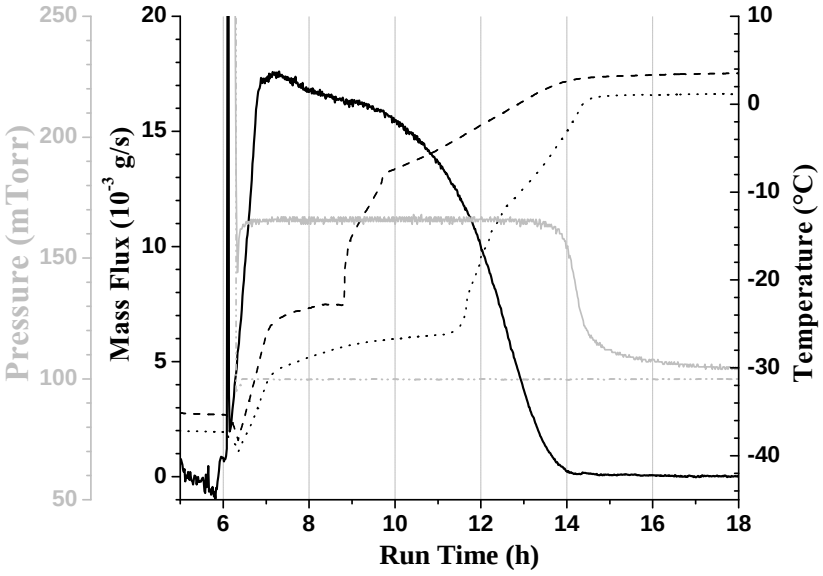

Figure 3.11: The diagram shows the primary drying phase of a freeze drying run (full load without Al-blocks) of 100 μL trehalose solution at 0 °C shelf temperature in 96-well PCR-plates. The product temperature is shown on the right axis (black dotted line: TC centre placed, black dashed line: TC corner placed), pressure curves (grey straight line: Pirani, grey dash-dot-dotted line: capacitance manometer) on the outer left axis, and mass flux (black straight line) on the inner left axis.

Table 3.11: The table summarises average mass flow and maximum mass flow data determined by TDLAS measurement during the primary drying phase of one full load run with mannitol solution in PCR-plates and one full load run with trehalose solution in PCR-plates. Both freeze drying runs were carried out at 0 °C shelf temperature.

Excipient	max. mass flow 10^{-2} gs^{-1}	average mass flow 10^{-2} gs^{-1}
Mannitol	3.72	0.95
Trehalose	4.03	1.22

as full load run) is $12.2 \cdot 10^{-3}$ g/s (cf. Table 3.11). Here, the difference between the average mass flow determined with the weighing procedure and average mass flow determined by TDLAS is less than ± 5 %.

In brief, the water vapour mass flow determined on-line by TDLAS is in very good agreement to the mass flow calculated from the gravimetric procedure in combination with residual moisture measurements. Since the TDLAS method directly measures the water vapour mass flow, it can be assumed that water vapour mass flow rates calculated from the excipient runs are fairly accurate.

3.2.5 Auto MTM with 96-Well PCR-Plates

The comparison of the product temperature at the bottom of the well determined by MTM ($T_{b,MTM}$) to the product temperature determined with TCs shows different patterns for the two tested excipient solutions. For mannitol, trends of TC recordings and $T_{b,MTM}$ are in good agreement until primary drying is approximately half complete. At the beginning of primary drying, the TC readings usually are roughly 1 to 2 °C higher than $T_{b,MTM}$. However, fluctuations in product temperature of approximately ±2 °C were observed in TC recordings while manometric temperature measurements were carried out (cf. Figure 3.12). $T_{b,MTM}$-values roughly correspond to the low points of the temperature fluctuations recorded with TCs. With progress of primary drying, MTM becomes less accurate, most probably due to the decreasing area of the total sublimation interface. When approximately half of the primary drying phase is over, $T_{b,MTM}$ and TC readings start to drift further apart (>3 °C) as MTM leads to decreasing results for $T_{b,MTM}$. Similar observations for freeze drying in vials have been reported in the literature [25].

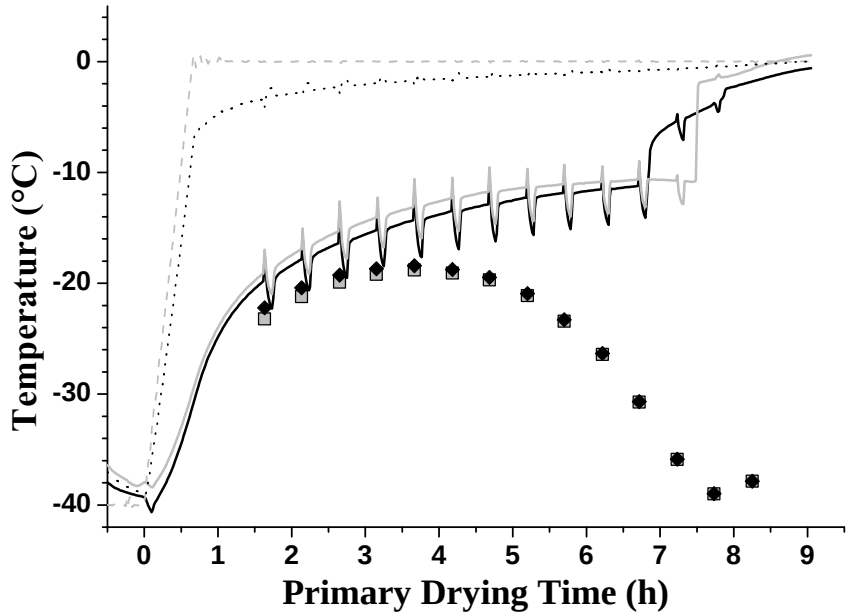

Figure 3.12: The diagram shows the primary drying phase of a freeze drying run (full load with Al-blocks, total sublimation interface approx. 660 cm^2) of 100 μL mannitol solution at 0 °C shelf temperature (light grey dashed line) in 96-well PCR-plates. Product temperature determined by TCs (grey straight line: corner well, black straight line: centre well) is plotted against $T_{b,MTM}$ (black diamonds) and $T_{p,MTM}$ (grey squares). The black dotted line represents the shelf temperature beneath the Al-block determined with a TC.

For MTM-full load runs with trehalose, TC data and MTM data are in fairly good agreement throughout all of primary drying (cf. Figure 3.13). During the phase of data collection for MTM data points, the same fluctuations in product temperature recorded by TCs as have been described for mannitol are also observed in trehalose solution. However, the difference between TC reading and $T_{b,MTM}$ is less than 1 °C at the beginning of primary drying (and also less than the low extreme of the product temperature fluctuation). The difference between the two values for product temperature at the bottom of the well increases to approximately 2 °C at the end of primary drying of trehalose solution.

The differences in agreement of MTM data points to TC data might be explained by the different heat transfer characteristics of well plates in comparison to glass vials. The software algorithm is pre-programmed based on the heat transfer characteristics of vials, and therefore might not be applicable to other container systems. In addition to that, it has been found and reported in the literature that a minimum sublimation interface of approximately 300 cm^2

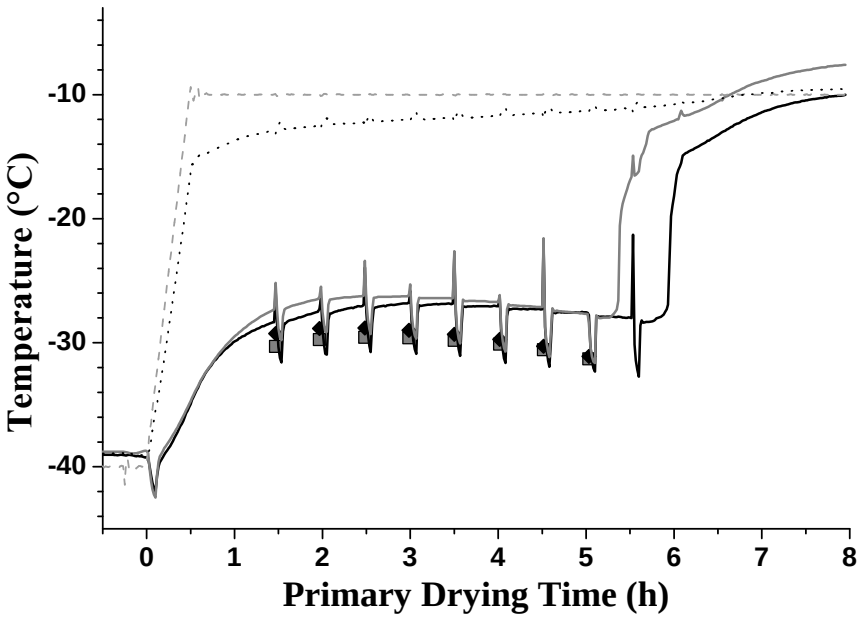

Figure 3.13: The diagram shows the primary drying phase of a freeze drying run (full load with Al-blocks, total sublimation interface approx. 660 cm^2) of 100 μL trehalose solution at -10 °C shelf temperature (light grey dashed line) in 96-well PCR-plates. The product temperature determined by TCs (grey straight line: corner well, black straight line: centre well) is plotted against $T_{b,MTM}$ (black diamonds) and $T_{p,MTM}$ (grey squares). The black dotted line represents the shelf temperature beneath the Al-block determined with a TC. For MTM carried out at approx. 5.7 h primary drying time, $T_{b,MTM}$ and $T_{p,MTM}$ could not be calculated by the software.

is required for an accurate MTM result with the Lyostar II freeze dryer [102]. The initial sublimation interface for a full load run with 96-well PCR-plates is only approximately 660 cm^2, and it might decrease at a faster rate than the sublimation interface during vial freeze drying, as the wells have a conic shape, and the inner diameter of a well decreases with progression of sublimation into deeper and narrower parts of the well.

MTM primarily determines the product temperature at the sublimation interface, $T_{p,MTM}$. For vial freeze drying, the value of $T_{p,MTM}$ is lower than $T_{b,MTM}$ as long as sublimation still continues. As the thickness of the remaining frozen layer decreases, the MTM results of these values become more similar until they are practically identical. The same is true for MTM measurements carried out during full load runs with well plates. The difference between $T_{b,MTM}$ and $T_{p,MTM}$ for the first MTM data point is approximately 1 °C for both tested excipient solutions.

3.2.6 Heat Transfer Coefficients Calculated from Excipient-Runs

Heat transfer coefficients were calculated from temperature data obtained during freeze drying of excipient solutions and average mass flow, dm/dt, determined from the initial water content and the residual moisture at the end of primary drying. Average mass flow rates per well plate determined from freeze drying runs with mannitol and trehalose have been summarised in Tables 3.9 and 3.10.

Mean heat transfer coefficients $K_{PCR,w/oAl}$ calculated from excipient runs with 100 μL fill volume (using well plates without Al-blocks) differ significantly from heat transfer coefficients calculated from runs with 20 μL fill volume (cf. Table 3.12). Heat transfer coefficients calculated from excipient runs with 100 μL fill volume are within the range of $2.69 \pm 0.45 * 10^{-4}$ cal $s^{-1}cm^{-2}K^{-1}$.

Table 3.12: Heat transfer coefficients calculated from excipient runs of 96-well PCR-plates without Al-blocks. Units of heat transfer coefficients $K_{PCR,w/oAl}$ are 10^{-4} cal $s^{-1}cm^{-2}K^{-1}$. Avg is the mean value of $K_{PCR,w/oAl}$ calculated from all runs with the same excipient and the same fill volume. The chamber pressure was set to 100 mTorr for all of the freeze drying runs with excipients.

No. of Shelves	shelf Temp. °C	Mannitol 100 µL	Mannitol 20 µL	Trehalose 100 µL	Trehalose 20 µL
1	0	2.24	3.09	2.81	3.33
3	0	2.51		2.38	
1	−10	2.64	3.44	2.79	3.39
3	−10	2.52		2.57	
1	−20	2.91	3.66	3.13	3.68
Avg		2.56	3.40	2.74	3.46

They are all in good agreement with the heat transfer coefficient calculated from sublimation tests at 100 mTorr ($2.69 * 10^{-4}$ cal $s^{-1}cm^{-2}K^{-1}$, see Table 3.2). Heat transfer coefficients calculated from freeze drying runs with trehalose seem to be slightly higher than coefficients calculated from mannitol runs. However, more experiments need to be performed to verify that this is a real trend rather than the standard deviation imposed by the experimental procedure. Heat transfer coefficients derived from excipient runs with a fill volume of 20 µL per well are higher, ranging from $3.09 * 10^{-4}$ cal $s^{-1}cm^{-2}K^{-1}$ to $3.68 * 10^{-4}$ cal $s^{-1}cm^{-2}K^{-1}$.

It has been stated in section 3.1.2 that the area for heat flow from the bottom into well plates placed directly on the shelf was approximated as the projection area. It has also been pointed out that this assumption might not be valid for the lower portion of the well, as there most probably is radiative heat transfer originating in acute angles from the shelf surface, striking the wall of the lower well part almost perpendicularly. If the area for heat input from the bottom shelf into wells is calculated including the outer surface area of the well tip up to a certain (low) filling level, then the total area for heat input $A_{PCR,w/oAl}$ would be higher and the resulting heat transfer coefficients would be smaller. The relative increase in the total area for heat input would be highest for low fill volumes. Note that it was beyond the scope of the present research to design and perform experiments for exact determination of $A_{PCR,w/oAl}$ at different fill volumes.

Instead, the ratio $\frac{dQ}{dt*dT}$ which is equal to the product $A_{PCR} * K_{PCR}$ was determined from the data of each excipient run. The results for the two different fill volumes of the runs with the same excipient were compared (see Table 3.13). The average ratio of these calculated values of higher fill volume to lower fill volume is approximately 1.15 for both excipients. If the heat transfer coefficient $K_{PCR,w/oAl}$ is not dependent on the fill volume (which can be expected, as the combination of shelf surface and well plate remains the same), then this ratio is equal to the ratio of the total area for heat input of higher to lower fill volume, $\frac{A_{PCR,w/oAl,100\mu L}}{A_{PCR,w/oAl,20\mu L}}$. This means that the total area for heat flow into well plates with a 100 µL fill per well is 1.15 times larger than the area for a 20 µL fill per well. The ratio of the areas of heat input used for calculation of heat transfers is 0.435 cm^2/0.291 cm^2 = 1.49. This is another indicator that $A_{PCR,w/oAl,bot}$ cannot be determined solely from the projection area of the well up to the filling level.

For a comparative overview, heat transfer coefficients determined for the set-up of well plates

without Al-blocks from sublimation tests with distilled water, from sublimation tests with water in suspended well plates, and from excipient runs with trehalose and mannitol solution with different fill volumes are plotted in Figure 3.14.

Table 3.13: Calculation of the ratio $\frac{\mathrm{d}Q}{\mathrm{d}t*\mathrm{d}T}$ from product runs in well plates without Al-blocks. Units are 10^{-3} cals^{-1}K^{-1}.

No. of Shelves	shelf Temp. $^{\circ}C$	Mannitol 100 μL	Mannitol 20 μL	Trehalose 100 μL	Trehalose 20 μL
1	0	9.35	8.64	11.76	9.31
3	0	10.48		9.40	
1	−10	11.02	9.63	11.66	9.48
3	−10	10.52		10.73	
1	−20	12.15	10.25	13.07	10.29
Avg		10.71	9.51	11.32	9.69

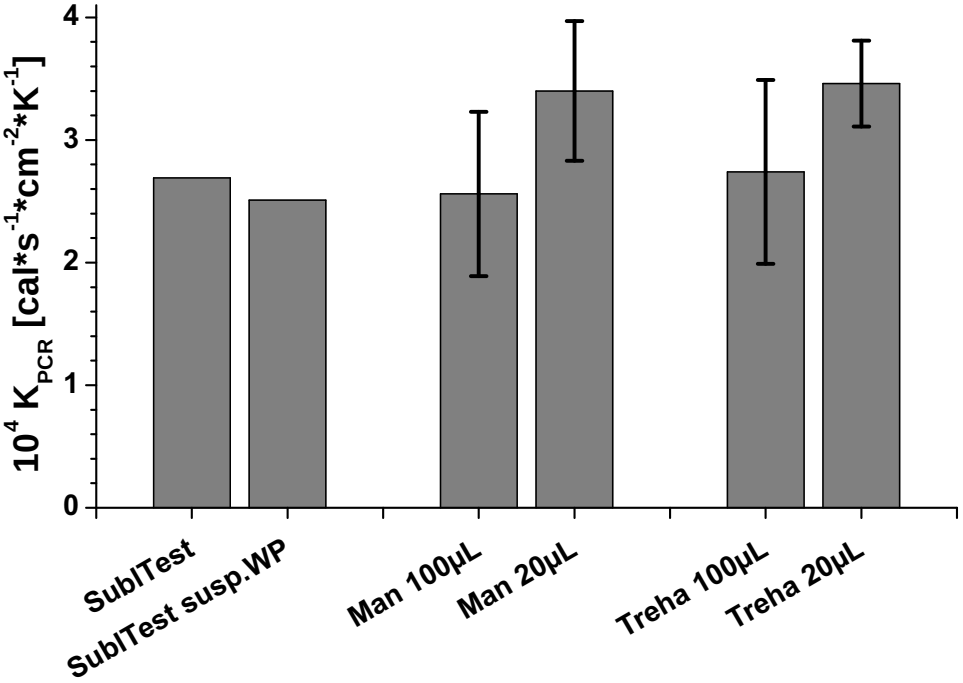

Figure 3.14: Average K_{PCR} values of well plates without Al-block determined from sublimation tests with pure water (SublTest) and from the set-up with suspended well plates (SublTest susp.WP) are compared to the heat transfer coefficients which were determined from product runs with mannitol (Man) and Trehalose (Treha) solution using different fill volumes.

As for excipient runs with Al-blocks, all values of heat transfer coefficients calculated from the data of excipient runs are within the range of $1.45 \pm 0.25 * 10^{-4}$ cal s^{-1}cm^{-2}K^{-1}, regardless

Table 3.14: Heat transfer coefficients calculated from excipient runs of 96-well PCR-plates inserted into Al-blocks. Units of heat transfer coefficients K_{PCR} are 10^{-4} cal $s^{-1}cm^{-2}K^{-1}$. Avg is the mean value of $K_{PCR,Al}$ calculated from all runs with the same excipient and the same fill volume. The chamber pressure was set to 100 mTorr for all of the freeze drying runs with excipients.

No. of Shelves	shelf Temp. $°C$	Mannitol 100 μL	Mannitol 20 μL	Trehalose 100 μL	Trehalose 20 μL
1		1.44	1.36	1.55	1.38
1	0	1.43			
3		1.26			
1		1.43	1.44	1.60	1.54
1	−10	1.23			
3		1.37		1.42	
1		1.63	1.46	1.68	1.65
1	−20		1.70		
3				1.41	
Avg		1.40	1.49	1.49	1.52

of excipient or fill volume (cf. Table 3.14). Heat transfer coefficients determined from full load runs seem to be smaller than heat transfer coefficients calculated from single shelf experiments.

The value of $K_{PCR,Al}$ calculated from sublimation tests of well plates used with Al-blocks at 100 mTorr is $2.79 * 10^{-4}$ cal $s^{-1}cm^{-2}K^{-1}$ (see Table 3.2). Compared to this value, the values calculated from excipient runs are roughly 50 % smaller. Similar observations were made for $2R$ vials as well (see sections 3.4.2, 3.4.3). For a comparative overview, heat transfer coefficients determined for the set-up of well plates with Al-blocks from sublimation tests with distilled water, from sublimation tests with water in well plates lined with heats sink grease, and from excipient runs with trehalose and mannitol solution with different fill volumes are plotted in Figure 3.15. Heat transfer coefficients determined from MTM-freeze drying runs are also shown in the same Figure.

At least for the well plates, a possible explanation for this difference between heat transfer coefficients determined from sublimation tests with pure water (with a fill volume of 200 μL) and heat transfer coefficients determined from product runs (with lower fill volumes) might again be found in the estimation of the area relevant for heat transfer into the product, $A_{PCR,Al}$.

For the high fill volume of 200 μL used for sublimation tests with pure water, the relevant area of the portion of the well wall protruding from the Al-block bore hole has also been approximated as the projection area. This might lead to an estimate of $A_{PCR,Al}$ which is too small. This assumption could be tested by conduction of a set of sublimation tests and product runs using different, but equivalent fill volumes per well to assure equivalent values for $A_{PCR,Al}$ in both cases, sublimation of pure water, and primary drying of product solution. Using a larger area for heat transfer for calculation of heat transfer coefficients from sublimation tests with 200 μL fill volume would result in smaller heat transfer coefficients for well plates with Al-block (cf. Equation 1.5). A smaller heat transfer coefficient would also imply that the estimated duration of primary drying time based on product temperature data would be longer and possibly in better agreement with actual primary drying times which have been summarised in Tables 3.4

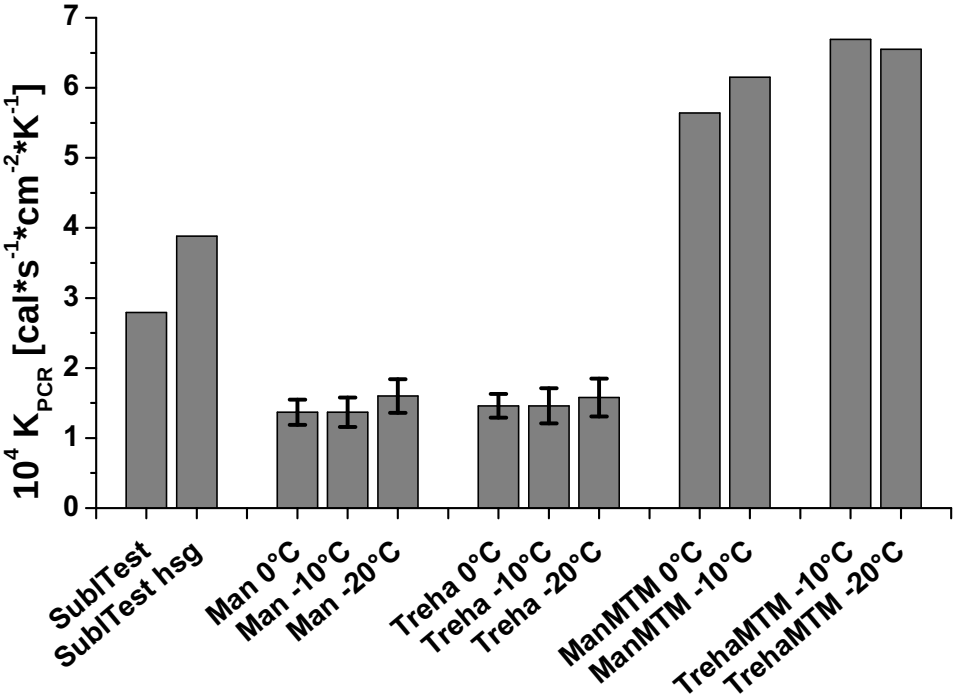

Figure 3.15: Average K_{PCR} values of well plates with Al-blocks determined from sublimation tests with pure water (SublTest) and from the set-up with well plates lined with heat sink grease (SublTest hsg) are compared to the heat transfer coefficients which were determined from product runs with mannitol (Man) and Trehalose (Treha) solution using different fill volumes. Heat transfer coefficients determined from MTM data (ManMTM / TrehaMTM) of freeze drying runs at different shelf temperatures during primary drying are also shown.

and 3.5.

As shown by TDLAS measurements (see Figures 3.10, 3.11), initial mass flow rates for excipient solutions in well plates are high and then rapidly decrease with increasing product resistance. These findings demonstrate that during a freeze drying run with product solution in well plates, there does not exist a "pseudo-steady state" interval during primary drying. All calculations of heat transfer coefficients in this work are based on the steady state assumption, so that it might be questionable if the Equation 1.5 which was used for calculation of the heat transfer coefficients is suitable to properly describe the situation in a product freeze drying run in well plates. However, similar observations of "non-steady state" conditions with regard to water vapour mass flow have been made for product runs using glass vials [89].

For glass vials, heat transfer coefficients determined from sublimation tests with pure water and from MTM measurements during product runs have been found to be in agreement, as long as it can be assured that the determination of the combined, normalised product and stopper resistance by MTM is accurate [68]. This pre-condition might not be fulfilled for the well plates, so that heat transfer coefficients determined from MTM data may be too high (cf. Figure 3.15).

Another reason for differences in heat transfer coefficients calculated from sublimation tests with pure water and from excipient runs might be differences in the progression of the sublimation interface (i.e. due to differences in heat conduction within primary dried excipient and frozen water). These differences may lead to differences in the area of the sublimation interface with progression of the sublimation phase.

3.2.7 Product Temperature Profiles

Due to the usually increasing resistance of a "real" product to water vapour flow, the product temperature at the bottom of the container T_b in excipient runs also increases with progression of primary drying [100]. In this way, T_b observed in excipient runs becomes higher than the ice temperature at the bottom of the container during sublimation tests with pure water. Figures 3.16 and 3.17 give comparative overviews of product temperature (T_b) - time profiles of excipient runs.

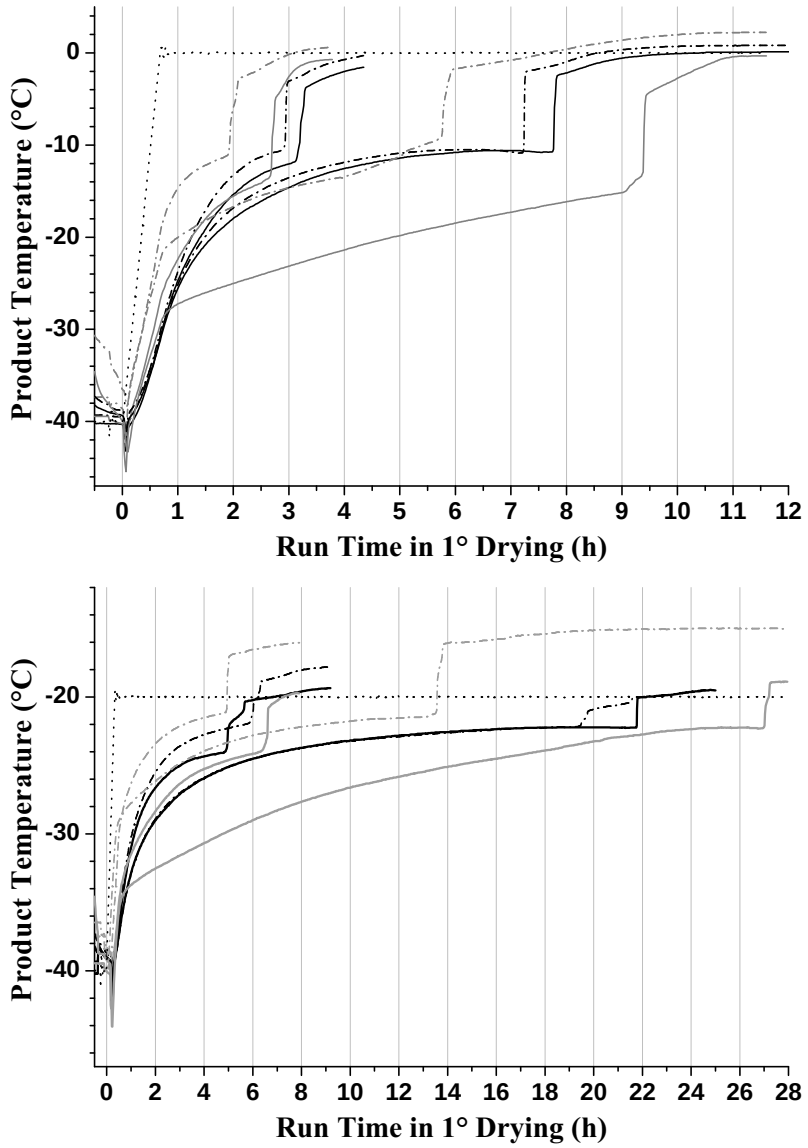

Figure 3.16: Plots of product temperature (T_P) over time profiles during primary drying of mannitol solutions. Each diagram shows data of four individual cycles. The primary drying phase of cycles with 20 μL fill volume is short and it is longer for cycles with 100 μL fill volume. Data from freeze drying cycles with Al-blocks is shown in black, data from cycles without Al-blocks in grey. Temperature data from centre wells is given as straight line, temperature data from corner wells as dash-dotted line. Upper panel: temperature data of freeze drying cycles with 0 °C shelf temperature, lower panel: temperature data of cycles with −20 °C shelf temperature. Exemplary shelf inlet data are shown as black dotted lines.

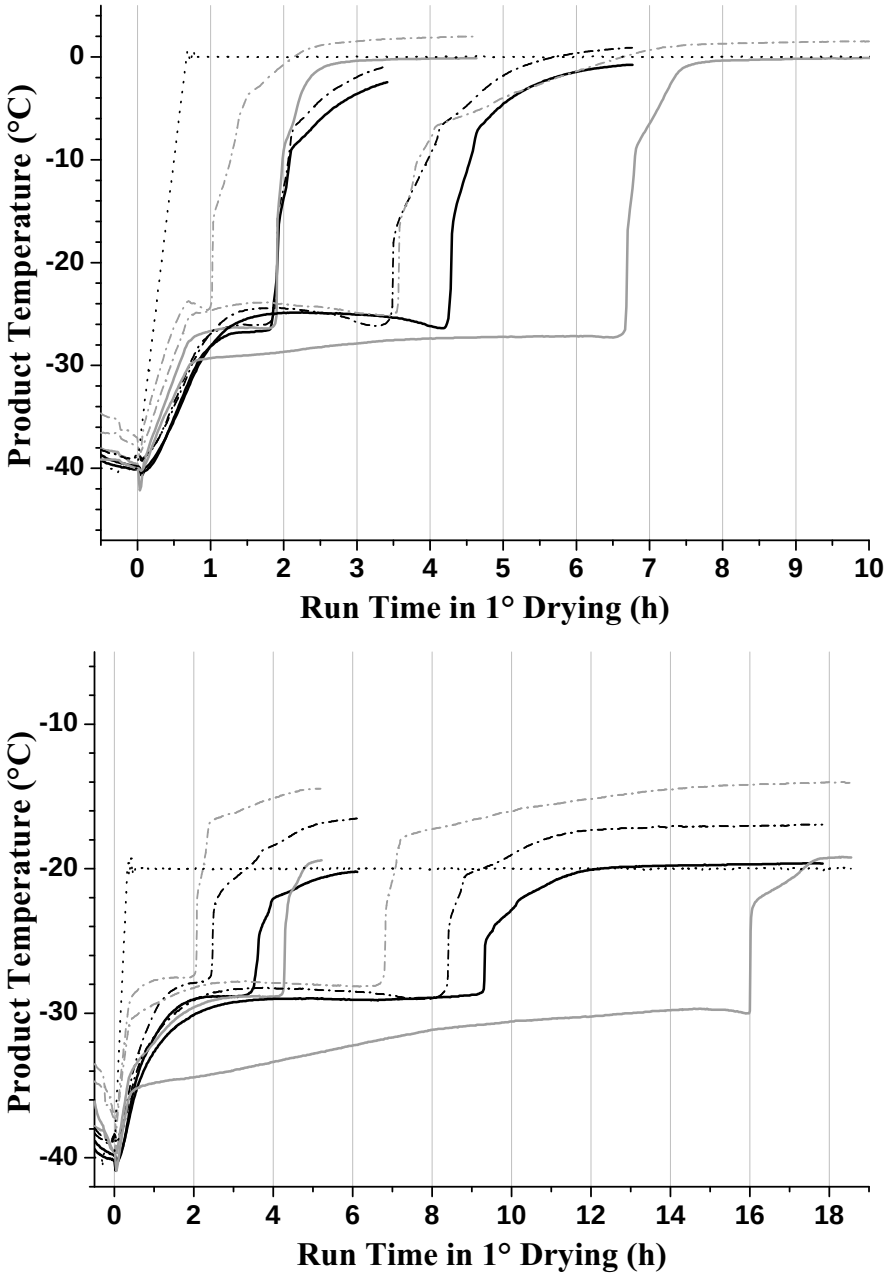

Figure 3.17: Plots of product temperature (T_P) over time profiles during primary drying of trehalose solutions. Each diagram shows data of four individual cycles. The primary drying phase of cycles with 20 μL fill volume is short and it is longer for cycles with 100 μL. Data from freeze drying cycles with Al-blocks is shown in black, data from cycles without Al-blocks in grey. Temperature data from centre wells is given as straight line, temperature data from corner wells as dash-dotted line. Upper panel: temperature data of freeze drying cycles with 0 °C shelf temperature, lower panel: temperature data of cycles with −20 °C shelf temperature. Exemplary shelf inlet data are shown as black dotted lines.

As examples, TC data of one centre-placed and one corner-placed thermocouple per freeze drying run are plotted. Each diagram is a summary of product temperatures of four individual runs. Data of procedures with the same excipient at the same shelf temperature but with two

different fill volumes (20 μL and 100 μL) and with the two different set-ups (with / without Al-blocks) are shown in the same diagram. The diagrams display data for two different shelf temperatures (0 °C and −20 °C) in two layers. All TC curves of product temperatures measured in the tips of wells follow the same pattern: increase of T_P at the beginning of primary drying with increasing shelf temperature, gradually lessened incline when the anticipated shelf temperature for primary drying is reached, sharp increase to approximately shelf temperature towards the end of primary drying.

For both excipients, freeze drying of 20 μL of solution per well leads to similar temperature profiles for both set-ups (with and without Al-blocks). The exception to this trend is the product temperature profile of corner wells: here, the product temperature is significantly higher and primary drying times are shorter than for centre wells. The temperature difference between corner and centre wells is visible for both set-ups and at all shelf temperatures. It is most pronounced for freeze drying runs without aluminium blocks at low shelf temperature (cf. Figures 3.16, 3.17). For the low fill volume of 20 μL, the product temperature in centre wells of well plates without Al-blocks is sometimes lower than for centre wells in well plates with Al-block and sometimes similar to the temperature measured in centre wells of well plates used with Al-block. When the product temperature in the centre well of the well plate without Al-block was found to be lower than the corresponding temperature for the set-up with Al-block, the primary drying time for the set-up without Al-block was found to be longer (cf. bottom panels in Figures 3.16, 3.17). This observation once more underlines the enhancement of heat transfer into the product which is achieved through the Al-blocks when using higher shelf temperatures during primary drying.

Temperature profiles of freeze drying cycles with the higher fill volume are also similar for both excipients. For the experimental design without Al-block, there are large differences in primary drying times for corner wells and centre wells (difference of 3 h for mannitol solution at 0 °C, more than 10 h for mannitol solution at −20 °C shelf temperature, see Figure 3.16). The product temperature in corner wells is also several degrees higher than the temperature in centre wells during the entire primary drying phase of freeze drying runs without the use of Al-blocks.

Again, the product temperature in centre wells of well plates used without Al-blocks is significantly lower than the corresponding temperature data obtained from freeze drying runs with Al-blocks. The higher product temperatures measured in centre wells of well plates with Al-block also correspond to shorter primary drying times in comparison to the primary drying times determined for centre wells when using well plates without Al-blocks. For the higher fill volume, the effect of enhanced heat transfer due to the Al-blocks leads to primary drying times which are at least 15 to 20 % shorter. For freeze drying of trehalose solution, the decrease in primary drying time is even higher (approximately 40 %, cf. Figure 3.17).

Especially in the runs with 100 μL of mannitol solution in well plates without Al-blocks, the product temperature rises steadily throughout primary drying. This gradual increase is also noticeable, if less pronounced, for the same cycles with Al-blocks. A rising product temperature with an unchanged shelf temperature setting signifies a continuous reduction of the sublimation rate. Reasons for this T_P-profile can be the reduced efficiency in heat transfer (loss of contact between ice core and container wall) and / or the increasing product resistance. As the temperature profiles of the same cycles with trehalose solution do not exhibit this considerable increase in product temperature with progression of primary drying, the reason for this temperature rise is probably caused by differences in the product resistance behaviour of the two excipients.

The area-normalized product resistance of 5 % mannitol solution has been found to increase linearly with increasing thickness of the dried product layer [50], [69]. The product resistance of amorphous formulations at similar concentrations, however, usually rises at the beginning of the primary drying stage but then levels out into a more or less distinct plateau phase [69]. This non-linear curve shape was explained with formation of larger pores due to microscopic collapse if the product temperature T_P came close to the collapse temperature T_c of the concerned excipient solution [69], [103]. Signs of micro-collapse can be determined by scanning electron microscopy (SEM).

MTM-measurements were performed during full load cycles with 100 μL of trehalose and mannitol solution per well in PCR-plates with Al-blocks. Amongst data provided by Auto-MTM measurements are data on product resistance [31]. The change of product resistance R_P over

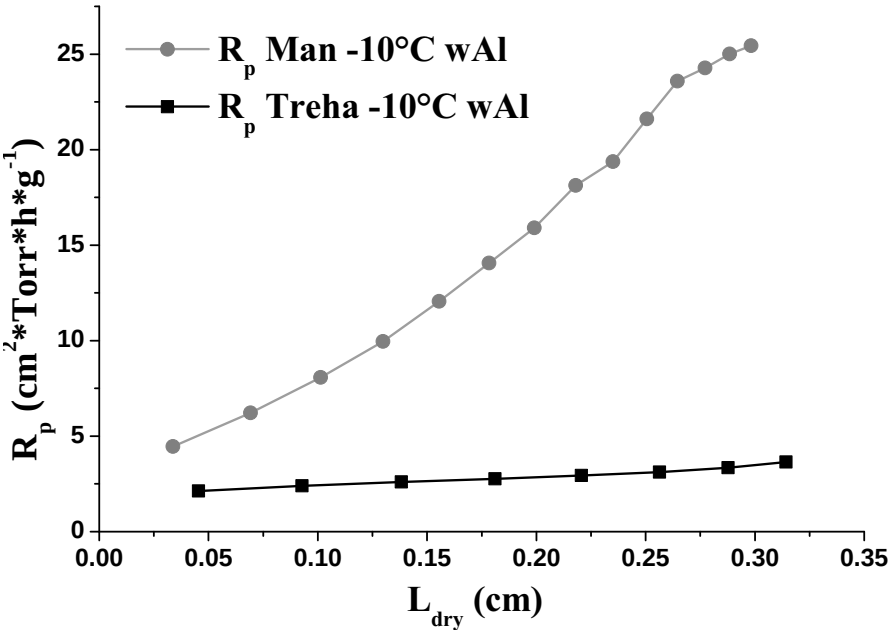

Figure 3.18: Product resistance R_P $(cm^2 * Torr * h * g^{-1})$ in dependence of dry layer thickness, l_{dry} (cm). Data was obtained during freeze drying cycles with Al-blocks at -10 °C shelf temperature during primary drying. Mannitol solution: grey dots, trehalose solution: black squares.

the increasing thickness of the dried layer is shown in Figure 3.18. Numerical values determined for R_P and dry layer thickness (l_{dry}) might not be entirely correct because the software used for data analysis is optimised for processes in vials. For example, the resistance of a dry layer of approximately 0.3 cm thickness of 5 % mannitol solution freeze dried in glass vials has been found to be approximately 5 $cm^2 Torr hg^{-1}$ [69]. The value determined for this thickness of dried product layer freeze dried in well plates is much higher (cf. Figure 3.18).

Thus, only the trends revealed in these examinations of the product resistance should be directly compared. It is obvious that the product resistance in the mannitol solution increases sharply with increasing thickness of the dry layer whereas the resistance of the dry trehalose layer only slightly increases during primary drying. These data also confirm that the pronounced rise of product temperature during primary drying of mannitol solution is primarily caused by the increased product resistance R_P. The T_P profiles of trehalose solution, roughly exhibiting plateau phases during primary drying (cf. Figure 3.17), suggest occurrence of small-scale collapse at least in some regions of the product matrix.

3.2.8 Product Analysis

Scanning Electron Microscopy

Scanning electron microscopy (SEM) pictures of trehalose solution freeze dried at different shelf temperatures without Al-blocks are shown in Figures 3.19, 3.20, and 3.21. The magnification of each picture is given in the caption of each Figure.

Pictures of lyophilisates freeze dried at -20 °C shelf temperature during primary drying can be seen in Figure 3.19. The pictures in the left panel at the top and in the middle are typical for all trehalose lyophilisates freeze dried in 96-well PCR-plates, regardless of shelf temperature.

The top picture in the left panel of Figure 3.19 shows an overview of the whole lyophilisate. The picture in the middle of the left panel in the same Figure shows the top surface of the lyophilisate. A smooth surface or "skin" is visible. Water vapour forcing its way through this rigid surface has formed channels as passage ways, visible as slit-like fissures and holes in the top surface.

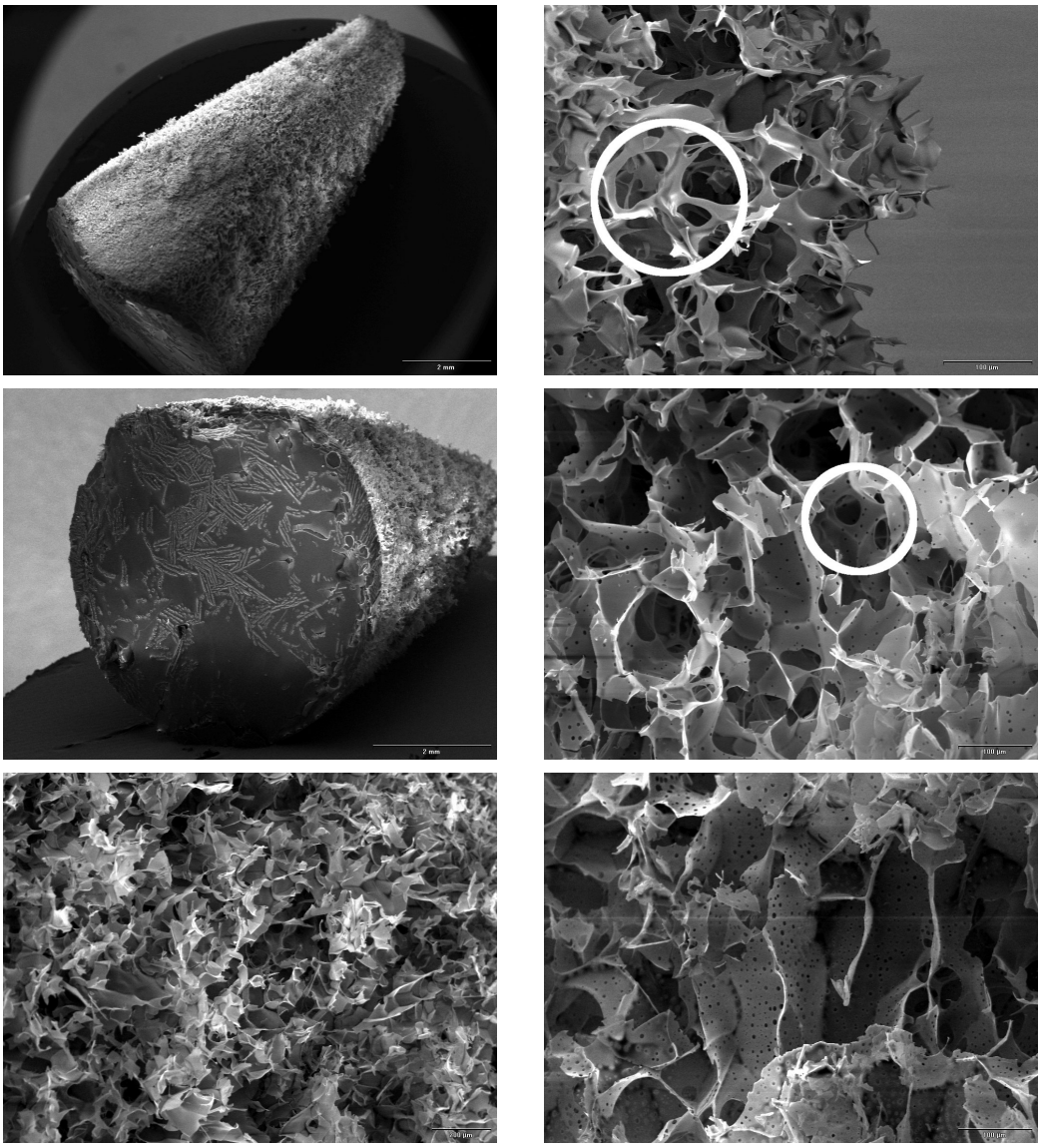

Figure 3.19: SEM pictures of 50 mg/g trehalose solution (100 μL) freeze dried in well plates without Al-blocks at -20 °C. Numbers in parenthesis give the magnification of the original picture. Left panel from top to bottom: overview (15x), view on top surface (20x), middle section of outer surface (100x). Right panel from top to bottom: outer surface of tip (300x), middle section of inner structures (250x), inner structure near the tip (250x). White circles indicate signs of microscopic collapse. More explanations are given in the text.

The bottom picture in the left panel shows a 100-fold smagnification of the middle section of the outer surface of the lyophilisate, about half way in between top surface and the tip of the lyophilisate. This is a typical SEM picture of an amorphous product [103]. The solid matrix consists of a foliaceous, in some places honeycomb-like pattern. Individual foil-like structures are extensively interconnected. These broad connections in between solid components make up the rigidity of the lyophilisate.

The topmost picture in the right panel shows the outer surface of the tip 300-fold magnified. Here, the foil-like pattern has undergone some changes due to elevated heat input. The white circle marks a spot where the broad "sheets" interconnecting different solid partitions have shrunk to mere narrow "bridges". These changes are typically observed when the amorphous solid reaches temperatures close to its collapse temperature: the material softens and viscous flow starts to develop. For trehalose, the temperature for onset of collapse has been reported as approximately −29 °C [101].

The pictures in the middle and at the bottom of the right panel have been taken after the sample lyophilisate has been cut in half from top surface to the tip. These pictures show structures in the inside of the sample in the middle section (picture in the middle) and near the tip (bottom picture). In the middle picture, the white circle marks a larger and several of many small round holes that have appeared in the amorphous foils. These small holes become more frequent moving towards the tip of the sample, as the bottom picture shows. The holes mark the beginning of micro-collapse that has no macroscopic effect on the lyophilisate. Yet these small pores increase the number of channels through which water vapour can escape from the solid matrix. As a consequence, the product resistance R_P decreases, the sublimation rate increases. As TC-data shows (Figure 3.17), the product temperature during primary drying at −20 °C already reaches −29 °C which is close to the critical temperature for macroscopic collapse of trehalose solution (−28.5 °C [30]).

Figure 3.20 shows SEM pictures of a trehalose solution freeze dried (without Al-blocks) at −10 °C shelf temperature in primary drying. The top picture is a 400-fold magnification of a section of the outer surface of the lyophilisate close to the top surface. Unlike the sample freeze dried at −20 °C, this picture reveals small holes even in this upper section. This part of the lyophilisate finishes primary drying early during the sublimation phase. If holes appear at this early stage, the product temperature has been close to the collapse temperature almost throughout all of primary drying. Product temperatures measured in centre wells of well plates during the freeze drying run at −10 °C reach temperatures in between −30.3 and −31.9 °C within 10 min after completion of the initial ramping phase of primary drying. These temperatures are close to the collapse temperature of the trehalose solution. Excepting corner wells (for which considerably higher T_P values were measured), the product temperature during the "plateau" phase of primary drying for trehalose solution at −10 °C shelf temperature without Al-blocks is within the range of −28 °C to −29 °C.

The middle picture in Figure 3.20 shows part of the outer surface at the tip of the lyophilisate. Shrunken sheet-like structures and other signs of viscous flow are more distinct than in the sample freeze dried at −20 °C. The bottom picture has been taken from a lyophilisate cut in half and shows inner structures in the top section of the sample. The holes are larger and more numerous than on the outer surface of the sample. The rigidity of the whole lyophilisate is still supported by the remaining parts of the amorphous matrix so that no macroscopic signs of collapse are visible.

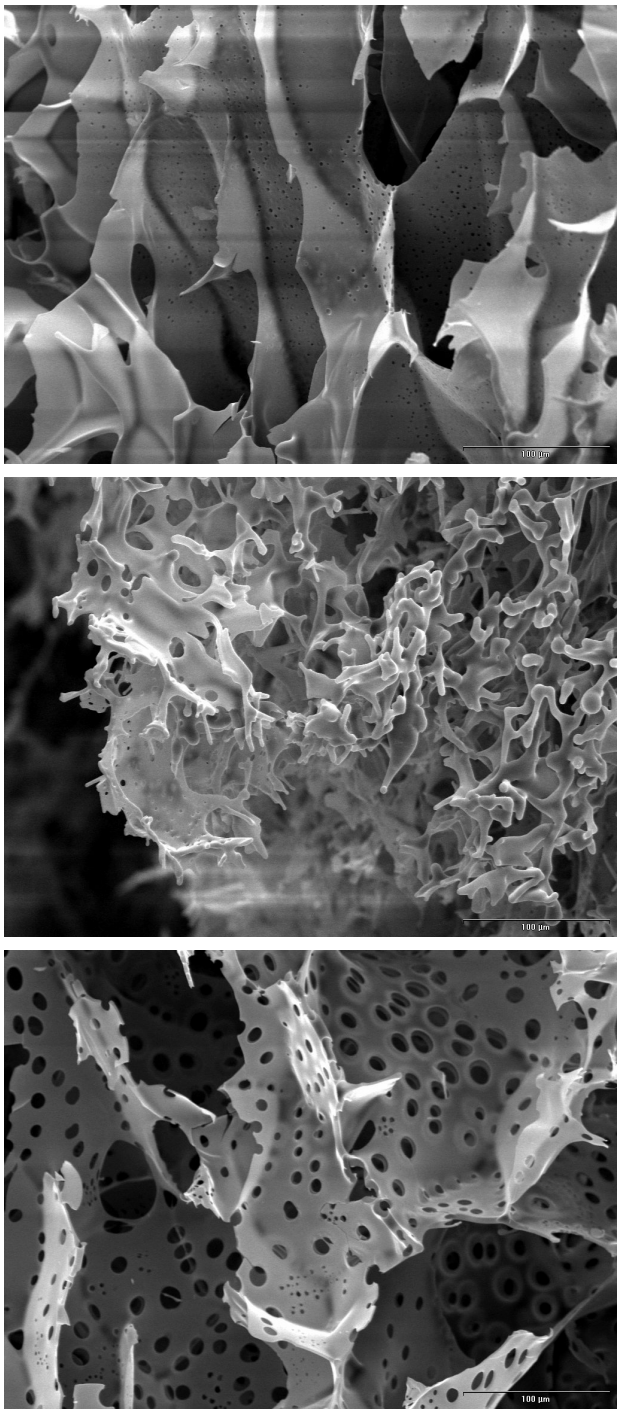

Figure 3.20: SEM pictures of trehalose solution freeze dried in well plates without Al-blocks at −10 °C. Numbers in parenthesis give the magnification of the the original picture. From top to bottom: upper section of outer surface (400x), outer surface at the tip (400x), upper section of inner structure (400x). Explanations are given in the text.

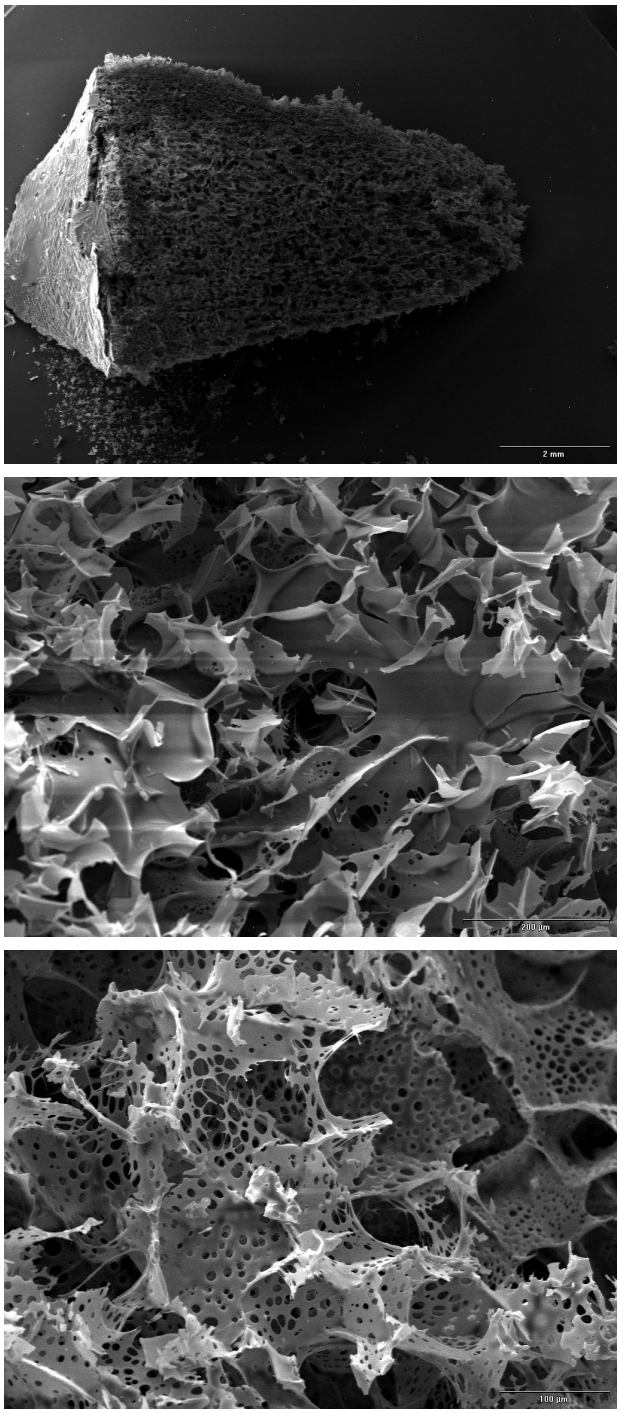

Figure 3.21: SEM pictures of trehalose solution freeze dried in well plates without Al-blocks at 0 °C. Numbers in parenthesis give the magnification of the original picture. From top to bottom: overview of lyophilisate cut in half (15x), upper section of outer surface (200x), middle section of inner structure (300x). Explanations are given in the text.

Pictures of trehalose solution freeze dried without Al-blocks at 0 °C during primary drying are shown in Figure 3.21. The topmost picture is an overview of the sample cut in half from top surface to tip. In this more macroscopic view, no significant structural differences are visible within the different sections of the lyophilisate.

The middle picture shows part of the upper portion of the outer surface of the lyophilisate

(close to the top surface). As expected from findings of samples freeze dried at −10 °C, pores are visible even in this section of the lyophilisate. The holes are larger than those observed in the same part of the trehalose lyophilisate freeze dried at the lower shelf temperature (observe difference in magnifications).

The bottom picture in Figure 3.21 shows part of the inner structures in the middle part of the lyophilisate. The holes are large, the original "sheet"-like structure of the amorphous network components starts to lose integrity. It is questionable whether the trehalose matrix would withstand even higher shelf temperatures during primary drying without macroscopic signs of collapse (shrinkage, loss of rigid structure).

The maximum product temperature observed during primary drying of trehalose solution freeze dried in well plates without Al-blocks at the different shelf temperatures (−20, −10, 0 °C) rises from approximately −29 °C at −20 °C primary drying temperature to approximately −26 °C at 0 °C shelf temperature. Even the high product temperature encountered during primary drying at 0 °C is supported remarkably well by the product, although signs of microscopic collapse could be forund in the product for all shelf temperature settings. It would be advantageous to use a high shelf temperature setting for a trehalose formulation containing an active ingredient in order to shorten primary drying times. If the ingredient withstands micro-collapse, then the primary drying phase for 100 μL of a trehalose-containing product solution freeze dried in well plates could be as short as 10 h. This is considerably shorter than common primary drying times for i.e. sucrose-based formulations in vials [37]. Such a formulation might be designed using a higher total solids content (i.e. more than 100 mg/g of trehalose), as this increases the collapse temperature of the formulation which will then be more resistant to collapse at the designated product temperature [52]. For freeze drying of small volumes per dosage of amorphous product solution, freeze drying in well plates could be a suitable alternative.

Figures 3.22, 3.23, and 3.24 show SEM pictures of trehalose freeze dried with Al-blocks at different shelf temperatures. SEM pictures of trehalose freeze dried at −20 °C are shown in Figure 3.22. The top picture shows a section of the outer surface close to the top in a 250-fold magnification. Small holes are visible, showing that the product temperature at −20 °C shelf temperature is higher in this part of the frozen product if Al-blocks are used. The temperature profiles shown in Figure 3.17 confirm this assumption.

The middle picture in the same Figure shows inner structures and part of the top surface. The top surface shows the fissures noticed for trehalose freeze dried without well plates as well. Holes are visible in the sheet-like structures of the amorphous matrix. The bottom picture shows structures of the amorphous matrix in the middle of the lyophilisate. This part of the lyophilisate looks very similar to the upper section of the same sample, the difference in number and size of holes is not significant. This observation confirms results of product temperature profiles showing that primary drying in well plates is more homogeneous if Al-blocks are used. The product temperature faster reaches a plateau temperature range and remains at this temperature range for a longer period of time.

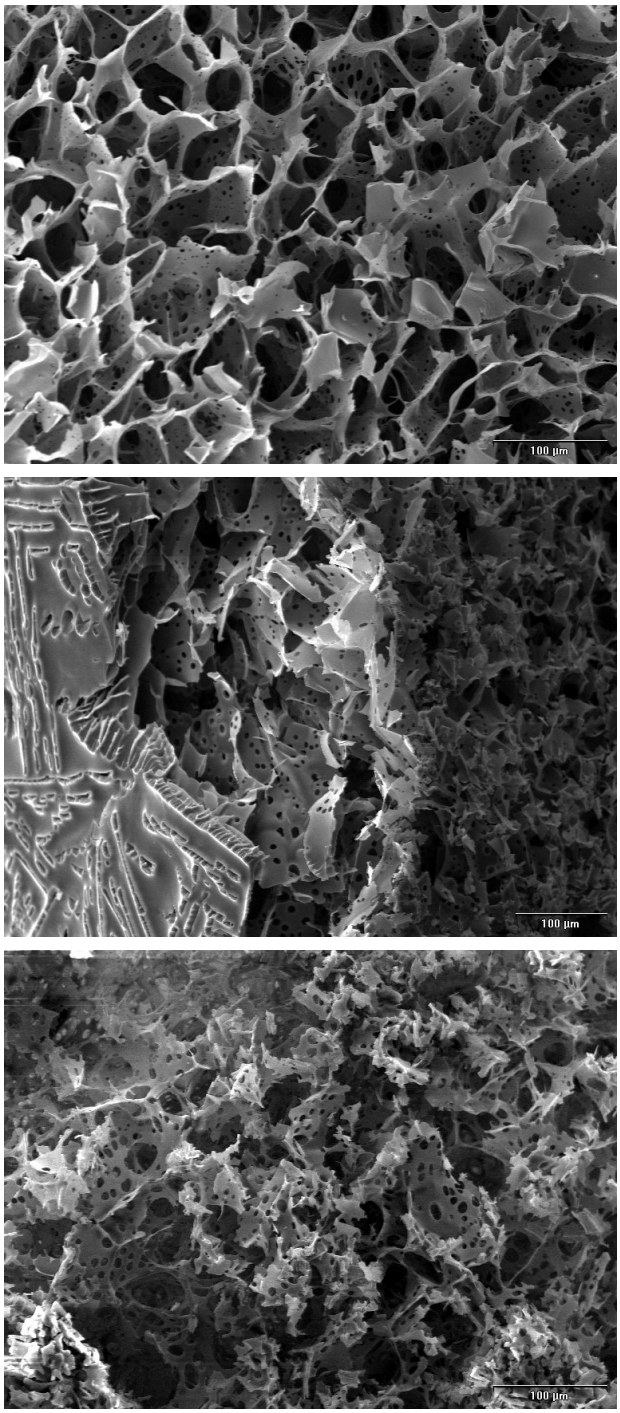

Figure 3.22: SEM pictures of trehalose solution freeze dried in well plates with Al-blocks at −20 °C. Numbers in parenthesis give the magnification of the original picture. From top to bottom: upper section of outer surface (250x), inner structure / upper surface at breaking edge (200x), middle section of inner structure (250x). Explanations are given in the text.

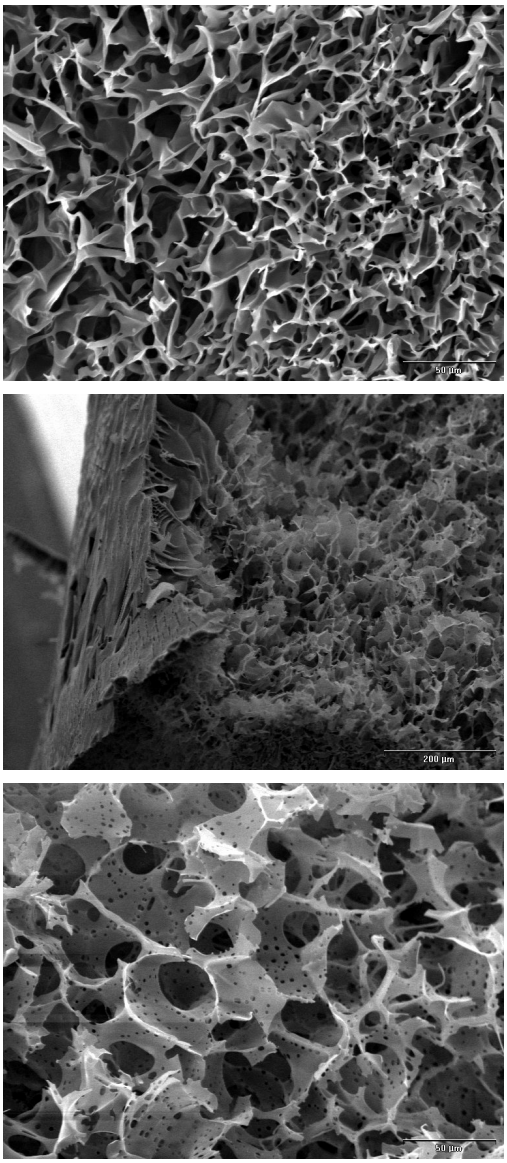

Figure 3.23: SEM pictures of trehalose solution freeze dried in well plates with Al-blocks at −10 °C. Numbers in parenthesis give the magnification of the original picture. From top to bottom: upper section of outer surface (500x), inner structure / upper surface at breaking edge (150x), inner structure near the tip (500x). Explanations are given in the text.

Figure 3.23 shows pictures of trehalose freeze dried at −10 °C with Al-blocks. The upper picture shows a section of the outer surface of the lyophilisate in 500-fold magnification. No holes are visible in the foil-like components of the matrix, yet signs for viscous flow can be noticed. The sheets are narrow, in some places only string-like connections remain between different parts. The structure in this part of the lyophlisate is very dense, as can be seen by comparison to the middle and bottom pictures. This reduction in open space might be an indication of small-scale shrinkage.

The middle picture in Figure 3.23 shows inner structures and the top surface at the breaking edge of the sample cut in half at 150-fold magnification. This part of the lyophilisate looks similar to trehalose freeze dried at −20 °C. The bottom picture displays inner structures close to the tip. Visible holes look similar in size and number to those in the sample freeze dried at the lower shelf temperature.

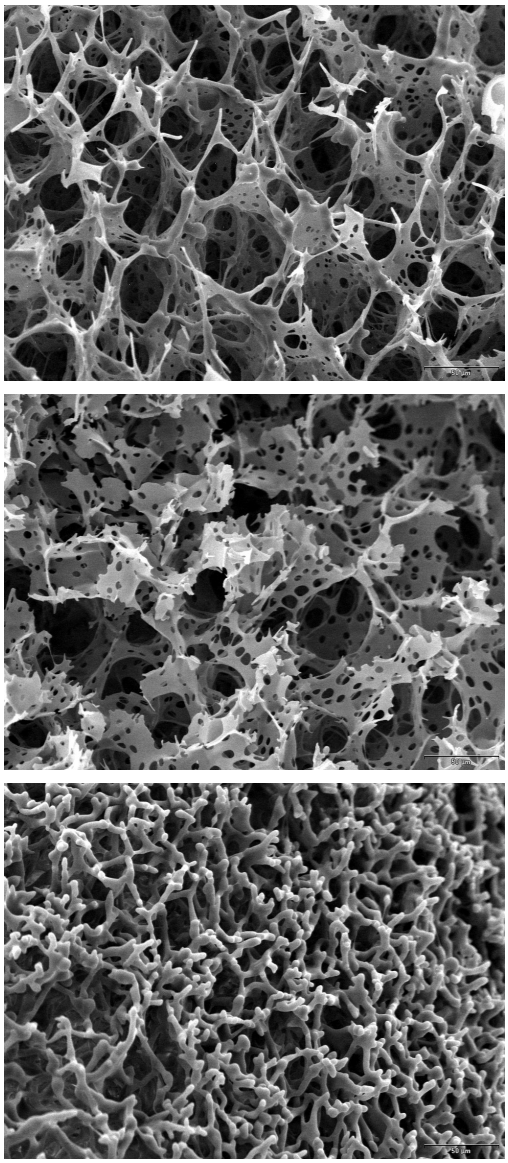

Figure 3.24: SEM pictures of trehalose solution freeze dried in well plates with Al-blocks at 0 °C. Numbers in parenthesis give the magnification of the original picture. From top to bottom: middle section of outer surface (500x), inner structure (sample cut open) (500x), inner structure near the tip (500x). Explanations are given in the text.

Pictures of trehalose freeze dried with Al-blocks at 0 °C shelf temperature during primary drying are shown in Figure 3.24. The top picture shows the outer surface of the sample. Signs for viscous flow are visible: holes have formed, the originally foil-like structures have lost their broad span. Thin bridge- or string-like connections remain in between different sections.

The middle picture shows inner structures, also displaying numerous holes in the foil-like frame. Integrity still remains. The lower picture displays inner structures of the trehalose sample close to the tip. The foil-like structures have disappeared, a network of thick string-like components remains.

As a summary of the above observations, freeze drying of amorphous (trehalose) solution in well plates using Al-blocks also leads to good or acceptable results, even when aggressive conditions with high shelf temperatures during primary drying are used. However, signs of microscopic collapse in the product are more pronounced for the experimental design with Al-block. As has been pointed out in section 3.2.7, the application of Al-blocks further shortens primary drying time for high fill volumes in well plates and reduces the drying heterogeneity. If micro-collapse is tolerable with regard to API stability and product appearance, then freeze drying of small volumes of amorphous formulations in well plates using Al-blocks could be an even better alternative than freeze drying in well plates without the Al-blocks. The SEM pictures are in agreement with the analysis of T_P data gathered during freeze drying cycles and confirm the assumptions concerning the decrease of the mass flow rate and increase of product resistance during primary drying which were given in sections 3.2.7 and 3.2.4 based on T_P over time profiles and TDLAS data.

The following Figure 3.25 shows SEM pictures of a 20 μL trehalose sample freeze dried at 0 °C shelf temperature without Al-blocks. The overview (top picture) reveals a low amount of shrinkage in the top part of the sample (notice reduction of girth beneath top surface). The other pictures, showing inner structures in the middle and towards the tip of the lyophilisate, reveal a large degree of micro-collapse, comparable to the results at the higher fill volume of 100 μL freeze dried at the same, high shelf temperature. The small fill volume of 20 μL is typical if the lyophilisate in the well plate is intended for a molecular biological application, and a biologic, i.e. DNA-containing, sample is added to the well.

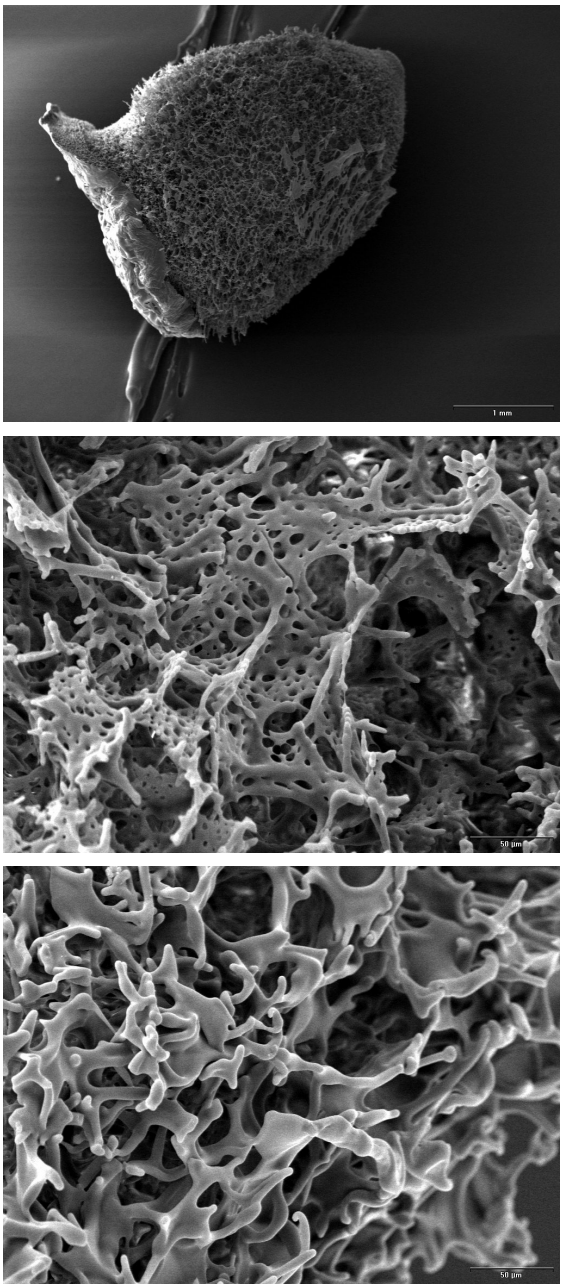

Figure 3.25: SEM pictures of 20 μL trehalose solution freeze dried in well plates without Al-blocks at 0 °C. Numbers in parenthesis give the magnification of the origianl picture. From top to bottom: Overview of lyophiliate (30x), middle section of inner structure (500x), inner structure near the tip (500x). Explanations are given in the text.

Figure 3.26 shows pictures of a mannitol solution freeze dried at 0 °C with Al-blocks. The structures in the mannitol sample look different, as this is, in contrast to trehalose, typically a crystallising excipient [92], [104]. The solid components also make up a sheet-like three-dimensional network. There are also holes visible in this scaffold, yet the form is different. The matrix does not show signs of softening and its integrity remains.

Mannitol solution freeze dried in well plates leads to elegant-looking lyophilisates in all cases. However, primary drying times at the tested pressure setting and the three shelf temperature settings were longer than for trehalose solution, at least for the 100 μL fill volume (see Figures 3.16, 3.17). The longer primary drying times of a crystallising excipient, such as mannitol, in comparison to an amorphous product, have been observed for freeze drying in vials, as well [101].

The advantages of (partially) crystalline formulations (stabilising effect of amorphous component in combination with well-looking lyophilisates, high shelf temperature during primary drying and comparatively short cycle times) reported for freeze drying in vials [60] may not be as significant for freeze drying in well plates. Here, the macroscopic appearance of amorphous and crystalline lyophilisates is comparable and primary drying times of amorphous trehalose solution are shorter than the corresponding primary drying times for mannitol solution in all of the tested cases.

The primary drying time required for the crystallising mannitol solution may be shortened if a higher mass flow rate during primary drying can be attained. The mass flow rate increases with the shelf temperature. If primary drying of a mannitol-containing formulation is carried out at shelf temperatures above 0 °C, the cycle time may become shorter than cycle times for purely amorphous trehalose formulations which may not withstand primary drying at such high shelf temperatures (i.e. shelf temperature during primary drying may not exceed 0 °C for these). Under such aggressive primary drying conditions, a crystalline matrix may indeed prove to be the better alternative as a formulation strategy. Based on SEM-data for trehalose-solution (Figures 3.21 and 3.24), shelf temperatures above 0 °C cannot be recommended for freeze drying of trehalose solution in well plates.

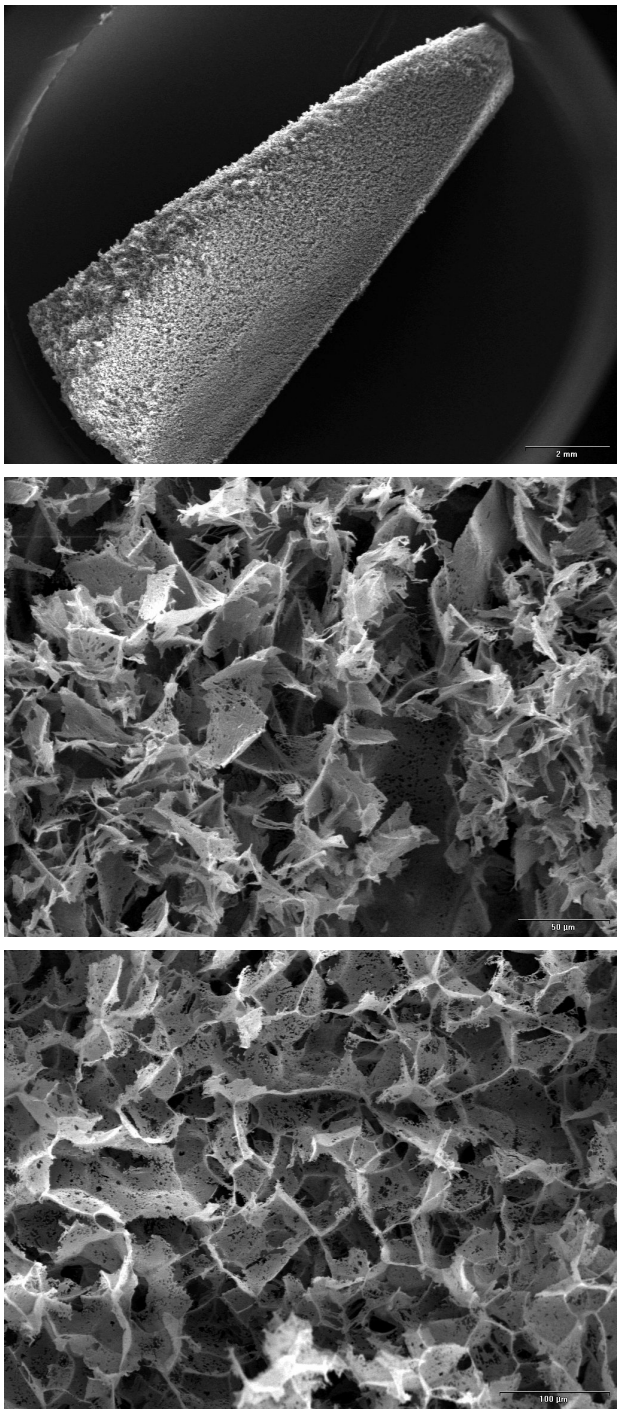

Figure 3.26: SEM pictures of mannitol solution freeze dried in well plates with Al-blocks at 0 °C. Numbers in parenthesis give the magnification of the original picture. From top to bottom: Overview of lyophiliate cut open (11.5x), middle section of outer surface (500x), middle section of inner structure (300x). Explanations are given in the text.

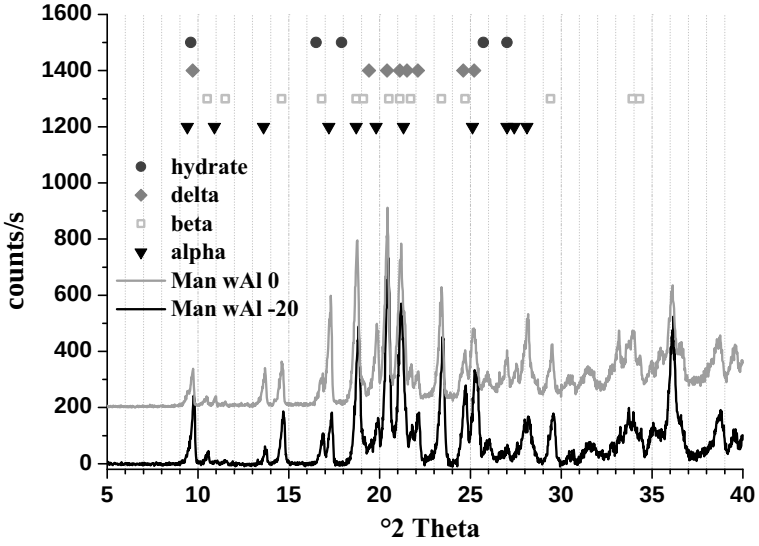

Figure 3.27: RD-spectopgraph of mannitol solution freeze dried in well plates with Al-blocks. Grey line: 0 °C, black line: −20 °C shelf temperature during primary drying. Symbols show position of peaks of different mannitol modifications and mannitol hydrate. The spectra of the two samples are very similar.

X-Ray Powder Diffraction

Secondary-dried mannitol samples were also analysed by X-ray powder diffraction. The method used for estimation of crystallinity (according to Ph.Eur. 2.9.33) does not yield absolute degree-of-crystallinity values. It was used for comparative purposes only.

Sample spectographs are shown in Figures 3.27 and 3.28. The spectra for each experimental design, with or without Al-blocks, are similar. At comparable, but not completely identical net weights, the intensities of the observed peaks are higher for samples freeze dried with Al-blocks. The freeze dried samples revealed a mixture of all mannitol polymorphs, the beta-polymorph being the most dominant for samples freeze dried with Al-blocks (i.e. $°2\theta = 14.6; 20.5; 23.4$, [92], cf. Figure 3.27).

These findings are consistent with results reported for freeze drying of 50 mg/mL mannitol solution in vials [92]. The spectograph of mannitol freeze dried at 0 °C shelf temperature with Al-blocks (cf. Figure 3.27) has higher intensities in typical peaks for the alpha-polymorph ($°2\theta = 13.6; 17.3; 19.8; 28.1$).

Some authors have reported formation of a mannitol (hemi-) hydrate which can be converted to an anhydrous form if secondary drying is carried out at sufficiently high temperatures [105], [60], [61]. In the secondary-dried samples analysed for this study, no hydrate could be observed (absence of typical peak in the XRD-spectograph at $°2\theta = 17.9$)

In samples freeze dried without Al-blocks (cf. Figure 3.28), the most dominant peaks belong to the delta polymorph ($°2\theta = 9.6; 19.5; 20.4; 22.1$, [92]), while the beta polymorph is only detectable in traces. These results hint at a faster freezing rate of mannitol solution freeze dried without Al-blocks in comparison to freeze drying with Al-blocks [92]. Nucleation occurs during the freezing step when the solution is cooled. In these studies, supercooling to at least −10 °C was observed in all cases prior to crystallisation. Upon nucleation, T_P rises to the (eutectic) melting temperature due to the latent heat of crystallisation which is given off into the remaining solution. The interval during which T_P breaks the pattern of the cooling curve for crystallisation after nucleation is longer for 100 μL mannitol solution freeze dried in well plates without Al-blocks (approximately 10 min) than for well plates freeze dried with Al-blocks (less than 5 min), cf. Figure 3.29.

Heat transfer into the mannitol solution using Al-blocks might be more homogeneous so that the temperature profile in the solution may also be more homogeneous upon freezing. These

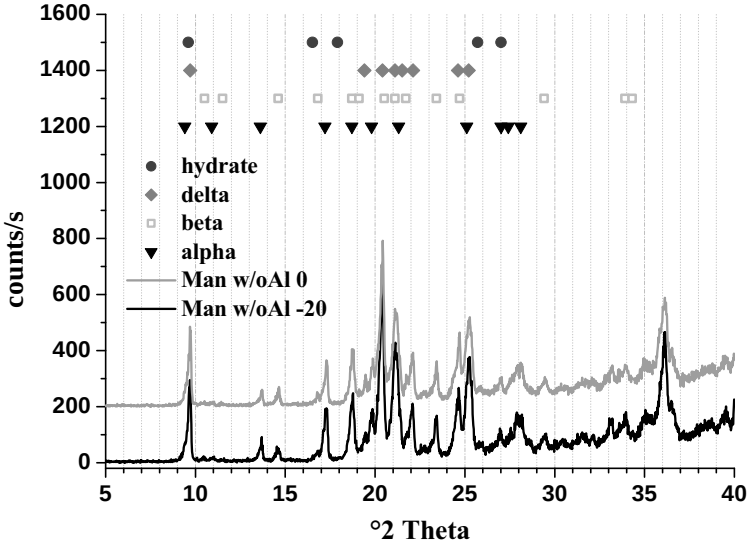

Figure 3.28: RD-spectopgraph of mannitol solution freeze dried in well plates without Al-blocks. Grey line: 0 °C, black line: −20 °C shelf temperature during primary drying. Symbols show position of peaks of different mannitol modifications and mannitol hydrate. Spectra of the two samples are very similar. Intensities are lower than for samples freeze dried with Al-blocks.

conditions may favour slow and continuous growth of ice crystals throughout the whole solution volume in the well.

For well plates without Al-blocks, heat transfer is probably less homogeneous, i.e. mainly the tip of the well and the corresponding, small volume of the solution in the well tip are cooled. It is pointed out that for both set-ups, well plates with and without Al-blocks, the T_P data generated during the freeze drying runs originates from the tip part of the well plates equipped with TCs. The temperature difference or temperature profile in between the tip of the well plate and the surface of the solution in the wells has not been evaluated during this study. Nucleation phenomena have not been studied extensively. SEM pictures of the freeze dried matrix of mannitol solution freeze dried in well plates with Al-blocks were compared to pictures of the matrix from freeze drying runs without Al-blocks. No significant differences in the appearance could be observed which might have been caused by different nucleation behaviour (cf. Figure 3.30).

For well plates without Al-blocks, ice crystallisation probably starts first in the tip-part of the well and then may extend to the remaining, warmer solution. These are clearly two different, plausible scenarios for freezing in well plates with and without Al-blocks. The longer "hump" during freezing of mannitol solution in well plates without Al-blocks as seen in Figure 3.29 may be an indication for heterogeneous nucleation occurring in several parts of the solution in the same well. The smaller, less pronounced peaks after the first high and broad nucleation peak, as observed especially for mannitol solution (without Al-block) in the corner well, further indicate that multiple nucleation sites may appear in well plates without Al-block. These additional peaks were not observed during freezing of mannitol solution in well plates using Al-blocks, but regularly in well plates without Al-blocks.

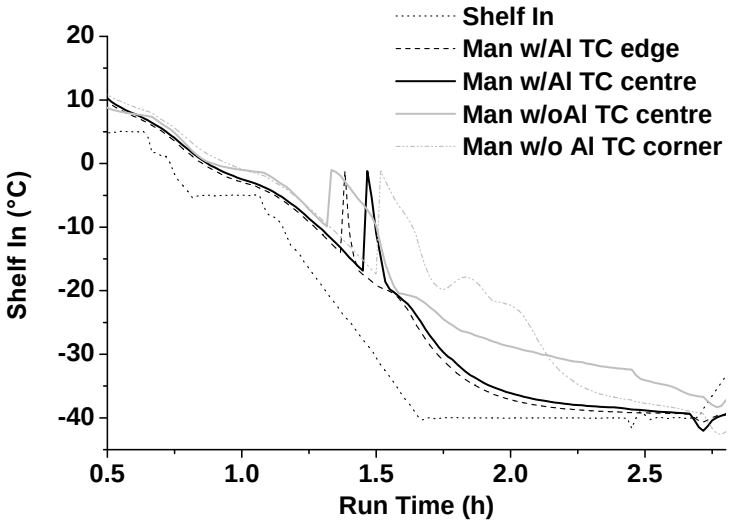

Figure 3.29: Freezing curves observed from TC-data during freezing of mannitol solution in well plates with (black) and without (grey) Al-blocks. The delay in the temperature drop during / right after crystallisation is longer for freezing without Al-blocks. In some cases, multiple

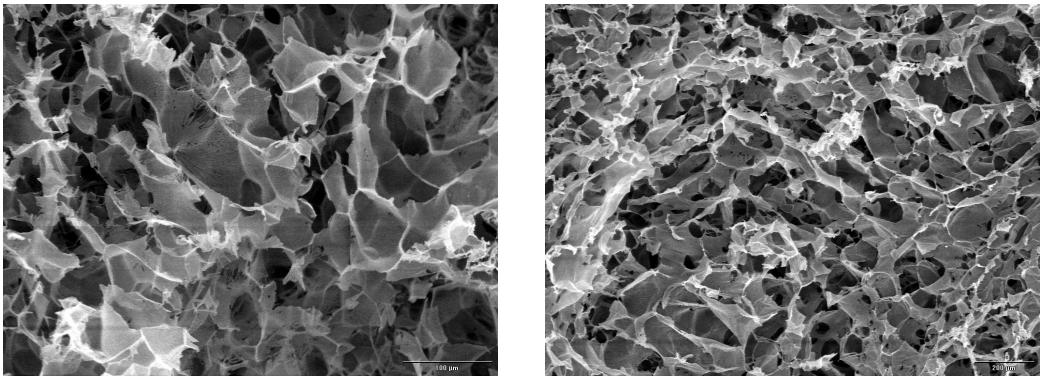

Figure 3.30: SEM pictures of 50 mg/g mannitol solution (100 μL) freeze dried in well plates with Al-blocks at -20 °C (left panel) and without Al-blocks at -20 °C (right panel). Numbers in parenthesis give the magnification of the original picture. Left: middle section of inner structures (300x),right: middle section of inner structures (100x). No significant differences in the structures can be observed.

3.2.9 Considerations for Cycle Design in 96-Well PCR-Plates

The heat transfer coefficients determined from sublimation tests with pure water for 96-well PCR-plates used without Al-blocks were successfully applied for estimation of the primary drying time based on product temperature data obtained during the initial (pseudo-steady state) phase of primary drying (cf. section 3.2.2, Table 3.4). The predicted primary drying duration was slightly shorter than actually observed when using higher fill volumes of mannitol solution (cf. Table 3.5).

The prediction of primary drying phase duration was however less accurate when using Al-blocks, possibly due to less accurate determination of the area relevant for heat transfer for different fill volumes. The heat transfer coefficients for well plates using Al-blocks might need to be recalculated using a more precise estimation of this area, then the applicability to prediction of primary drying times should be equivalent to the set-up without Al-blocks.

Another, major question when designing a freeze drying cycle for an untested product is the definition of the shelf temperature (and chamber pressure) appropriate for the pseudo-steady state primary drying phase. Here, product temperature profiles obtained from TC data can be used to adjust the shelf temperature needed to achieve a certain target product temperature for a new, untested formulation. This approach has been used for freeze drying in vials prior to availability of new technology for automatic cycle optimisation [50]. Data collected during this study confirms that it is also suitable to use the TC-data approach for freeze drying cycles using the rather atypical product container 96-well PCR plate.

For freeze drying cycle development in vials, the fill volume of the solution as well as the product resistance profile of the untested formulation will influence the required shelf temperature profile. For well plates, the fill volume and fill depth are small in all possible cases. Therefore, different fill volumes should only have a small influence on R_P over primary drying time-profiles and the resulting T_p over primary drying time curves.

For low fill volumes (approximately 20 μL per well), there is no significant difference in total primary drying time in between the two designs with or without Al-blocks at the tested chamber pressure of 100 mTorr. Shelf temperature over time profiles would therefore be interchangeable. However, radiation effects are much more pronounced for the set-up without Al-blocks. Additional heat input by atypical radiation plays a major role if heat input from the shelf is low, as is the case at low shelf temperatures (i.e. -20 °C) [26]. The amount of heat input by radiation cannot be controlled as it strongly depends on the material, geometry, and construction of the freeze dryer. A T_p over time profile observed in one freeze dryer (or for a container placed in a specific position on the freeze dryer shelf) may not be reproducible if the experiment is repeated using a different freeze dryer (or a different position in the array on the freeze dryer shelf). Primary drying times of well plates as well as microscopic product appearance in centre and edge positions can be expected to be more homogeneous for the set-up with Al-blocks.

For the estimation of the optimal shelf temperature for a freeze drying cycle with a higher fill volume per well (close to 100 μL) without use of Al-blocks, the following should be considered. At the beginning of primary drying, the product temperature steadily rises, even after the shelf temperature set point is reached. This can be explained with the varying efficiency of heat transfer with progressing sublimation and the continually changing effective area for heat transfer. To shorten primary drying time, it would be useful to first set the shelf temperature to a high set point (0 °C or even higher, depending on the critical formulation temperature) and lower the shelf temperature to the estimated shelf temperature set point when the product temperature comes close to the target product temperature.

A similar approach can be used for freeze drying higher fill volumes in well plates with Al-bocks. However, the product temperature for high fill volumes freeze dried with use of Al-blocks reaches a plateau or even passes through a maximum. Therefore, an optimised primary drying phase would also start with a high shelf temperature (in between 0 °C and -10 °C for the tested excipient solutions) to quickly heat up the Al-block. After a holding time of approximately one hour, the shelf temperature must be adjusted to the estimated shelf temperature for achievement of the target product temperature. The interval with the higher shelf temperature setting will most probably be shorter for the set-up with Al-blocks than for the set-up without Al-blocks as heat transfer is more efficient using the Al-blocks and the product temperature will more quickly come close to the anticipated primary drying temperature.

Care should be taken when estimating the shelf temperature needed to achieve the target product temperature during the pseudo-steady state phase of primary drying. The data generated during this study for amorphous trehalose solution shows that even at -20 °C shelf temperature during primary drying, the product temperature comes very close to the collapse temperature of trehalose (approx. -28 °C, [21]). During this study, signs of viscous flow and micro collapse were detected for trehalose freeze dried at this shelf temperature. To avoid changes in the amorphous product morphology, the shelf temperature set point after the initial warming phase during primary drying should be closer to the designated target product temperature. A temperature difference of 5 °C between shelf temperature and target product temperature would be a suggestion for an initial test.

In this study, it was found that even at product temperatures exceeding the collapse temper-

ature by approximately 2 °C, changes in the lyophilisate structure were not yet macroscopically detectable. If these changes are acceptable and do not decrease reconstitution times, activity, and stability of the active ingredient, a higher shelf temperature set point could be used during primary drying. This approach would be similar to using a partially crystalline formulation yet without the need to employ a large share of a crystallising bulking agent. As can be seen in the diagrams, raising the shelf temperature for freeze drying trehalose solution by 20 °C led to a change in "plateau" product temperature of only approximately 4 °C. Once collapse starts to develop, the pore size increases, the product resistance decreases and the sublimation rate also increases disproportionately. The increased sublimation rate requires more heat which is taken from the frozen product, producing a cooling effect.

The effect of a 20 °C rise in shelf temperature leads to a larger change in the resulting product temperature during primary drying of mannitol solution in well plates with Al-blocks. The highest average product temperature achieved during the run at 0 °C shelf temperature is approximately −11 °C, overall average product temperature is −15 °C. During the run at −20 °C shelf temperature, these product temperatures are −22 °C and −25 °C, respectively. The 20 °C change in shelf temperature led to a change in product temperature of approximately 10 °C. The conclusion from these observations is that a change in shelf temperature of 2 °C leads to a change in product temperature of 1 °C. Product temperatures recorded during the freeze drying cycle at −10 °C shelf temperature are in accordance with this rule. Similar observations have been made for freeze drying of mannitol solution in vials. However, for vials, an increase of shelf temperature by 5 °C is needed for increasing product temperature by 1 to 2 °C [50], [20].

Freeze drying high fill volumes in well plates without Al-blocks is not economic. If it cannot be avoided, the initial high shelf temperature approach should be used. For a formulation with intermediate product resistance and a critical formulation temperature of −25 °C, the following program could be used for a first attempt to optimise primary drying: at the beginning of primary drying, ramp the shelf temperature up to 0 °C and then immediately down to −23 °C. Hold at −23 °C for approximately 10 to 20 h.

The rule derived for well plates with Al-blocks of extent of change in product temperature for given change in shelf temperature might apply for well plates without Al-blocks as well, as data from the freeze drying runs with low fill volume suggest. For well plates without Al-blocks, no such rule can be derived from runs with high fill volume as the product temperature at −20 °C shelf temperature during primary drying of 100 μL mannitol solution never reached a plateau or maximum temperature before all ice had sublimed.

As can be seen from SEM pictures of trehalose, amorphous formulations withstand aggressive primary drying conditions surprisingly well. This additional temperature margin may be used for cycle optimisation when the critical product temperature is defined and the API also withstands these aggressive drying conditions, but stability tests must be conducted to confirm the feasibility of this drying recipe. Reconstitution times may be longer for a product that was primary dried at temperatures exceeding the collapse temperature of the formulation [106]. The safety margin between collapse temperature of the formulation and designated target product temperature may also be reduced as in comparison to the suggested safety margin for freeze drying processes in vials. For short primary drying phases (< 2 h) and intermediate primary drying phases (< 48 h) in vials, safety margins of approximately 3 to 5 °C are usually advisory. Duration of primary drying phases for freeze drying processes using 96-well PCR-plates can be expected to usually fall into these categories. However, since heat transfer into well plates is less efficient as compared to vials, and therefore changes in product temperature tend to be slight and slow, the safety margin may be reduced to approximately 2 °C.

Concerning a suggestion for optimisation of chamber pressure for freeze drying processes with 96-well PCR-plates, reference is made to an empirically derived equation for calculation of optimal chamber pressure for a product with given collapse temperature in a vial [20]. Basically, the same equation could be used for freeze drying in well plates. The influence of chamber pressure is similar for well plates with Al-blocks and for vials. Increased heat transfer into the product (expressed by higher product temperature) by increase of chamber pressure was demonstrated during sublimation tests with pure water (cf. 3.1.5). As heat transfer into well plates with Al-blocks is slightly less efficient than heat transfer into vials, the calculated result

of the Pikal-equation may lead to lower than optimum chamber pressures for well plates with Al-blocks. More data from freeze drying runs performed at different chamber pressures with well plates is needed to adjust the empiric equation for well plates.

The situation is different for freeze drying cycles using well plates without Al-blocks. Here, heat transfer by radiation is the major contribution to total heat transfer into the product (cf. 3.1.3). The optimisation of the chamber pressure may still be important to minimise drying heterogeneity between wells / well plates situated in exposed positions at the corners or at the edge of an array of well plates on the shelf and those product containers which are placed in the centre of the array. Therefore, extremely low chamber pressures (i.e. less than approximately 80 mTorr) as well as higher chamber pressures (i.e. over 200 mTorr) should be avoided [26].

At the same settings for shelf temperature and chamber pressure, the product temperature of a solution in a well plate will most probably be lower than in a vial. Increasing the shelf temperature for the freeze drying cycle with well plates would probably be the more efficient possibility to optimise heat transfer into the product. A substantial increase in chamber pressure (to more than 200 mTorr) would also increase the heterogeneity in the progression of primary drying in between individual wells. As a suggestion, chamber pressures not exceeding 100 mTorr could be used.

3.2.10 Testing the SMART™ Software with 96-Well PCR-Plates

A single freeze drying cycle with trehalose in well plates without Al-blocks was completed using the SMART™ software for automatic cycle optimisation. This test was performed to assess the suitability of the SMART™ freeze dryer software for cycle optimisation in a container system with characteristics differing significantly from characteristics of vials (i.e. differences in geometry, different distribution of contribution to total heat transfer between heat transfer by contact / radiation / conduction through the gas). All three shelves of the freeze dryer were loaded. Based on the input data (cf. Table 2.1 on page 42), the SMART™ software calculated an initial chamber pressure set point of 67 mTorr and an initial shelf temperature for primary drying of -33 °C.

After 60 min of primary drying, a manometric temperature measurement (MTM) was carried out to determine the product temperature at the sublimation interface and automatically adjust the shelf temperature. The results obtained for both, the product temperature at the bottom of the container and the product temperature at the sublimation interface as determined by the software are approximately 1 °C lower than average thermocuple readings from centre wells, as shown in Figure 3.31. The difference between T_b (product temperature at the container bottom) and T_P (product temperature at the sublimation interface) calculated from MTM data by the SMART™ software is in between 0.2 and 0.6 °C for the first four measurements. The largest difference for these two product temperatures was determined from data of the second measurement.

The bias between product temperature at the container bottom calculated by the SMART™ algorithm and measured with centre-placed thermocouples is consistent throughout the first four manometric temperature measurements. The temperature curve of the thermocouple and the temperature determined by the algorithm start to deviate by more than one degree from the fifth measurement on. The steep rise in product temperature of the TC placed in the corner well, indicating end of primary drying for this well, almost coincides with the sixth MTM. Nonetheless, product temperatures at the container bottom determined by the SMART™ algorithm for freeze drying trehalose solution in well plates is in far better agreement than could be expected, as the software has been designed to model freeze drying in vials.

The SMART™ algorithm yields accurate results for product temperature determination for vials as long as the total area of the sublimation interface is comparatively large and not more than two thirds of the vials in the whole batch have completed primary drying. This rule might also apply to well plates. A minimum ice interface area of at least 300 cm^2 is needed to get "accurate" results [25]. The total initial product surface of all well plates was approximately 680 cm^2 for this test, corresponding to the product surface of 36 well plates with all 96 wells filled with 100 μL of solution. It is possible that the different drying behaviour in well plates

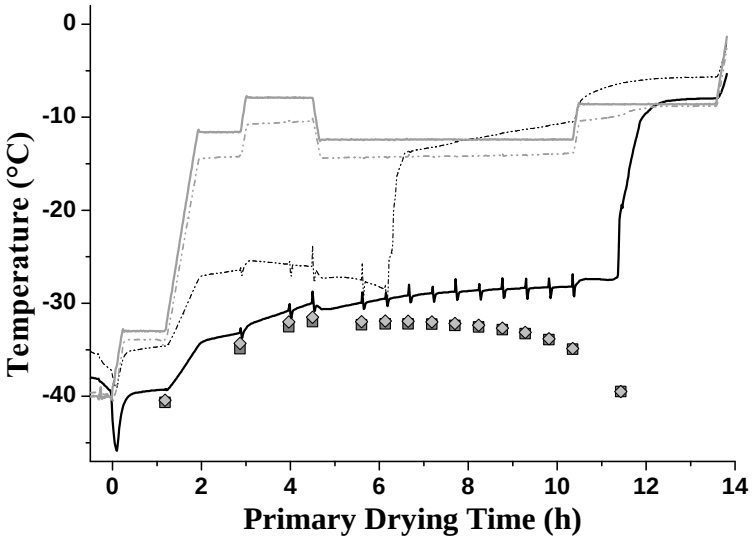

Figure 3.31: Diagram of freeze drying run with 100 μL trehalose solution in 96-well PCR-plates (without Al-blocks) using the SMART™ software for automatic cycle optimisation. Light grey line: temperature of shelf inlet, light grey dash-dotted line: temperature measured with TC on shelf surface beneath well plate, black dash-dotted line: product temperature measured with TC in corner well, black line: product temperature measured with TC in centre well. Dark grey squares: product temperature at sublimation interface (T_p) determined by MTM, grey diamonds: product temperature at the bottom of the container (T_b) determined by MTM.

(possibly more pronounced curvature of sublimation interface with proceeding of primary drying into the thinner part near the well tip) in comparison to vials (the SMART™-model assumes that the interface moves only downward in the vial) also contributes to the increase in the bias between MTM and TC readings with progress of the primary drying phase. A change of the product surface area with a receding sublimation interface could not be taken into account for the calculations carried out by the SMART™ software.

Another possible explanation for the drift in between TC data and the product temperature determined by SMART™ could be that, contrary to the assumption of a sublimation interface generally moving downward, ice sublimation in well plates might start along the well walls and then continue inwards. This would mean that the TCs placed in the tips of the wells might lose contact to the remaining ice in the frozen product at a rather early stage during primary drying. Loss of contact to the remaining ice core is accompanied by an increase in the temperature reading. Usually, this increase due to the lost contact to the ice is rather sharp (i.e. towards the end of primary drying). For the temperature readings of the corner-placed TC in Figure 3.31, this sharp increase is visible at approximately 6 h of primary drying time, which is considerably sooner than the similar temperature increase observed for the centre-placed TC (increasing temperature readings at approximately 12 h primary drying time). The fact that such a sharp increase of the product temperature seems to occur when no or little ice remains in the surroundings of the TC tip renders the explanation of the bias between TC data and MTM data as an early loss of contact of the TC tip to the ice core rather unlikely. This loss of contact should be visible in a similar, clearly discernible temperature change.

Another major difference in between freeze drying in well plates (without Al-blocks) and freeze drying in a closely arranged array of vials is the, by comparison, higher amount of radiative heat transfer into the wells. This shift in the contribution of radiative heat transfer to total heat transfer might also contribute to the bias in the product temperature determined by the software based on MTM-data.

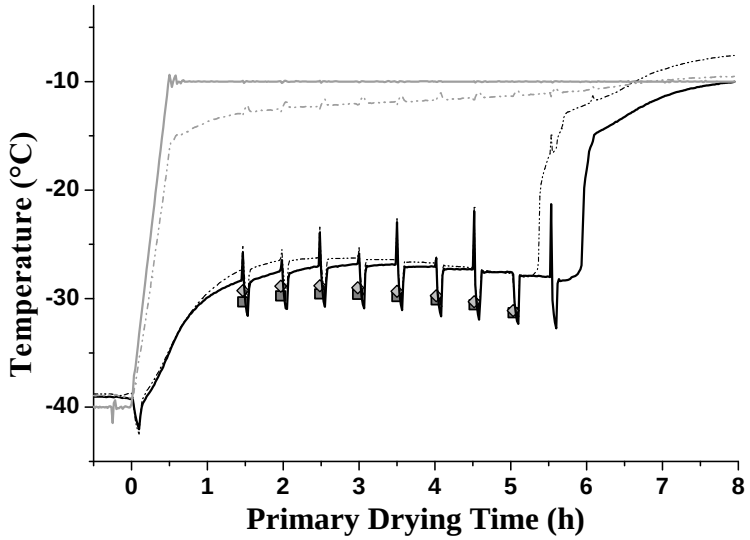

Figure 3.32: Diagram of freeze drying run with 100 μL trehalose solution in 96-well PCR plates (with Al-blocks) using the auto MTM technique. Light grey line: temperature of shelf inlet, light grey dash-dotted line: temperature measured with TC on shelf surface beneath Al-block, black dash-dotted line: product temperature measured with TC in corner well, black line: product temperature measured with TC in centre well. Grey squares: product temperature at sublimation interface (T_p) determined by MTM, light grey diamonds: product temperature at the bottom of the container (T_b) determined by MTM.

However, SMART™ provided an appropriate cycle recipe for freeze drying trehalose in 96-well PCR-plates. The cycle might yield a rather aggressive shelf temperature profile. Since data from single shelf product runs have shown that trehalose solution in well plates tolerates these temperatures without macroscopic signs of shrinkage or collapse, only the active component might be the critical factor in a partially collapsed state (i.e. stability could be compromised).

Further full load runs were performed with and without Al-blocks using the MTM technique without the cycle optimisation algorithm (Auto MTM runs, cf. section 2.1.3). Results of these runs are similar to the SMART™ results: there is a difference between thermocouple data and MTM product temperature data of approximately 1 °C (cf. Figure 3.32). This difference becomes increasingly larger starting from the third manometric temperature measurement (i.e. before two thirds of primary drying are over).

Manometric temperature measurements in the freeze drying cycle of trehalose solution with Al-blocks at −10 °C shelf temperature were accompanied by unusually large fluctuations in product temperatures (Figure 3.32). These fluctuations were caused by the pressure change during the measurement, when the valve connecting the drying chamber to the condenser was closed. The subsequent increase of chamber pressure led to a decrease of the sublimation rate. The amount of heat supplied by the shelves and the Al-blocks did not alter, therefore the change in sublimation rate resulted in a product temperature increase (cf. sections 1.3.1, 1.4.1). The initial increase in chamber pressure is not always captured in the data logs, as the measuring interval was one minute, the MTM itself, however, only takes 25 s.

When the manometric temperature measurement is finished, the valve connecting freeze drying chamber and condenser quickly reopens. That in itself might alter the pressure in the drying chamber. In addition, the chamber pressure control will readjust the chamber pressure to its set point as quickly as possible, initially lowering the chamber pressure even past the set point. During this short period in the MTM cycle, chamber pressure readings of the capacitance manometer which were lower than 40 mTorr were frequently observed in all MTM / SMART™ freeze drying cycles with well plates. This considerable "overshoot" might be associated with the

rather small sublimation interface area of a full load freeze drying cycle using well plates. Control of chamber pressure was always regained approximately 5 min after the end of each MTM.

During the interval with a chamber pressure which was lower than the designated set point, lower-than-steady-state product temperatures were observed, as a consequence of the substantial increase in the sublimation rate caused by the "overshoot" of chamber pressure control. The product temperature fluctuations observed during MTMs for the auto-MTM cycle described above ranged from −21 °C to −33 °C within the same incident.

The same temperature fluctuations were noted during the SMART™ cycle as well (cf. Figure 3.31), but were less pronounced. One possible explanation for the stronger fluctuations of the product temperature observed during the auto-MTM freeze drying cycles could be the use of Al-blocks. The two scenarios tested in this study, freeze drying in well plates and freeze drying in well plates using Al-blocks, would therefore not be identical, and considerations for cycle design are most probably not interchangeable for these scenarios. It might be that the better heat transfer into the product when using Al-blocks enhances the quick rising of the product temperature during a single MTM with a duration of only 25 s, as well as the subsequent rapid decrease of the product temperature during the few minutes when the chamber pressure is below the designated set point.

The amplitude of the product temperature fluctuations became larger with progress of primary drying. Towards the end of each MTM, the product temperature at the sublimation interface exceeded the collapse temperature of trehalose by 2 to 7 °C. This excess of the collapse temperature is critical. Coincidentally this temperature rise during MTM resulted in a freeze dried product marked by regions which suffered more serious collapse than directly adjacent regions in the lyophilisate. This gave a detailed view on the progression of the sublimation interface in a well plate lyophilisate (Figure 3.33).

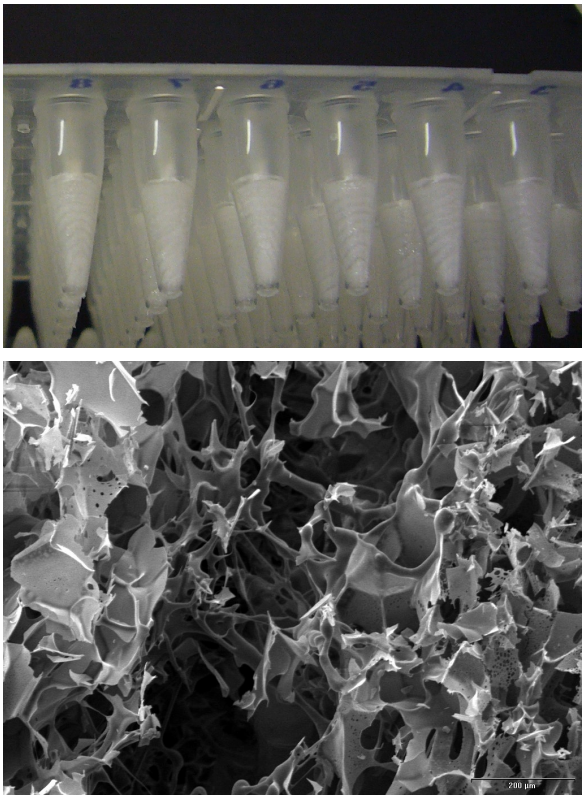

Figure 3.33: Top panel: photograph of trehalose solution freeze dried using the auto MTM technique. Marks of collapsed regions are visible in the wells. Lower panel: SEM picture of a sample from the same freeze drying run, sample cut in half. The magnification factor of the original picture is 150-fold.

The striped appearance of the product in the top panel of Figure 3.33 is not a result of the inner structure or surface of the well, but solely caused by the repeated increase of the product temperature above the critical formulation temperature during the manometric temperature measurements. The stripes mark the progression of the sublimation interface in between two individual MTMs. Apparently, the sublimation interface is not as extremely curved in product runs as has been observed for sublimation tests with pure water.

These large and recurring temperature fluctuations which have been observed when using the MTM technique for freeze drying runs with well plates might not only cause damage to the product matrix, but also severely diminish the stability or activity of an API. In order to regularly use this tool for non-invasive determination or estimation of the product temperature during primary drying in PCR-plates, this technology would need to be even more sensitive. If possible, the pressure rise interval should be shortened when MTM is applied to freeze drying runs in well plates, especially when the well plates are combined with Al-blocks.

3.3 96-Well Freeze Drying System™ (VirTis)

3.3.1 Contact Area to Flat Surface and to Al-Block Cavities

The contact area of the small tubes to a flat surface and to the Al-block cavities was investigated with simple print tests. The contact area of the tube bottom to a flat surface was determined in percent of effective cross sectional area of tube bottom and was found to be between 16 % to over 70 % with an error of approximately ±5 %. Note that a total of 30 tubes was tested. Most of the tested tubes (90 %) had a direct contact area to the flat surface of more than 30 %, half of the tested tubes had a contact area in between 60 % and 72 % (cf. Figure 3.34). Compared to 2R vials, this is a relatively large value for direct contact.

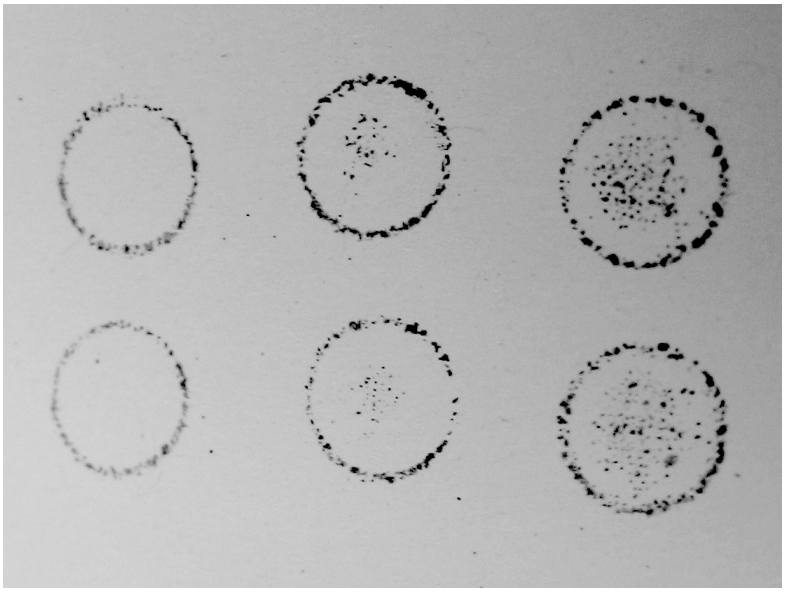

Figure 3.34: Example of results from print tests with the VirTis tubes. Tube bottoms were first placed on an ink-pad and then gently pressed on a sheet of paper on a flat surface. The picture shows two imprints each of three different tubes (prints of the same tube are placed on top of each other).

Evaluation of the contact area of VirTis tubes inserted into the Al-blocks designed for use with these tubes yielded different results to the print tests conducted by placing the tubes on a flat surface. For estimation of contact area of tubes inserted into the Al-blocks, a total of 90 of the small containers was used for the tests. The contact area was determined in percent of the total area of tube bottom and tube side. As the tubes used for this study (0.5 mL fill volume) were completely submersed into the Al-block cavities, the maximum theoretical contact area represents the total area of tube bottom and tube sides (100 %). However, the aluminium of the Al-block cavities did not surround the vials on all sides. Instead of circular bore holes, the Al-blocks of the FDS contained drillings which were set so close to each other that part of the bore hole walls had been cut away; only stumps of aluminium with a roughly diamond-shaped base remained in between neighbouring bores (cf. Figure 2.7). Therefore, the maximum area of the tube side in view of the Al-block was approximately 85 % to 90 % for corner tubes (here, three quarters of the bore hole wall were "intact", and there was one additional "stump"), 75 % for edge tubes, and only approximately 50 % for centre placed tubes.

Contact area values determined from the print tests range from approximately 10 % to 30 % of contact, considering the total outer surface of a tube as the reference of 100 %. It was noted that the points of contact were distributed between the tube bottom and the tube side. On average, the tube bottom had less contact to the Al-block than to a flat surface. This observation was explained with a certain roughness of the Al-block cavity. The aluminium-blocks were covered with a black paint or coating. This black coating extended into the cavities, but was visibly

Figure 3.35: Example of results from print tests with the VirTis tubes and the matching Al-blocks. The bore holes of the Al-block were lined with a water soluble, viscous paint. The tubes were inserted into the holes and removed again to estimate the amount of paint-covered tube surface.

incomplete and therefore non homogeneous in the flattened bottom area of the cavities. Tubes placed in the centre of the Al-block showed the widest range of contact area values: 11 % was the smallest and 34 % the highest value for these tubes. An example of the print test results with Al-block is given in Figure 3.35. The mean contact area of 59 tested tubes in centre position was determined as 22 %. Tubes placed in the edge rows of the Al-block had contact areas in the range of 18 % to 25 %. The average value was also 22 %. Only 9 tubes in corner positions were tested. For these, the range of contact area was determined as 27 % to 30 % with an average of 28 %.

Compared to 96-well PCR-plates, the small glass tubes inserted into Al-block cavities show a similar if slightly smaller average contact area of the outer container surface to the cavitiy walls of the respective aluminium block (22 % for VirTis tubes compared to approximately 25 % for 96-well PCR-plates). For the VirTis tubes, the contact between the outer surface of the container side and the cavity in the Al-block must be considerably less than complete, otherwise the glass tubes could not be removed from the Al-block. The glass tubes fit rather tightly into the Al-block cavities as it is. If the whole Al-block filled with tubes is tilted, however, the tubes slide out easily.

3.3.2 Results of Sublimation Tests

Prior to conduction of the sublimation tests, the emissivity of the black painted Al-blocks was determined using an infrared thermometer with a thermocouple port. For the black surface, the emissivity setting of the infrared thermometer had to be adjusted to a value of 0.9 to achieve identical readings for the temperature measured with the infrared thermometer and the temperature measured via TC.

The emissivity of the black painted Al-blocks was determined as approximately 0.9. The maximum value for the emissivity is 1, which describes the behaviour of a perfect black body that absorbs all radiation (the complete spectrum) which strikes the body. In reality, a body with a high coefficient of absorption, and a black, but smooth surface is no black body. A perfect black body does not reflect any radiation. The ability to reflect radiation of a smooth surface is dependent on the wavelength, and not zero [8]. The emissivity of 0.9 of the black Al-blocks signifies already a very high ability to absorb (and emit) radiation and is a good approximation of a black body. The higher the emissivity of a body, the higher is the output of radiation over the wavelength spectrum. This signifies that the radiative heat transfer (into the product) is

Table 3.15: Average mass flow data obtained from sublimation tests with the Freeze Drying System™ (FDS) and 96-well PCR-plates with (PCR w. Al) and without Al-blocks (PCR w/o Al). Data represent mass flow of a single tube for the Freeze Drying System™ and of a single well for the well plates.

Pressure Set Point	Mass Flow (10^{-6} g/s)		
mTorr	FDS	PCR w. Al	PCR w/o Al
30	13.45	8.44	5.84
50	12.85	10.45	5.90
100	15.78	14.12	5.75
200	18.74	15.53	5.26
500	19.71	14.31	4.23

enhanced when using a black surface (a surface with a high emissivity) as the surface of the heat source.

The emissivity determined for the black painted Al-blocks used with the FDS differs from the emissivity determined for the Al-blocks used with PCR-plates (0.25, cf. section 3.1.5), which clearly shows that the emissivity is a characteristic of the surface alone. The strongly reflecting surface of the polished Al-blocks used for the well plates has a low emissivity. The black paint on the Al-blocks used with the VirTis glass tubes significantly increases the emissivity to almost the maximum value of 1, maximising the amount of heat transferred into the product by radiation from the Al-block.

Sublimation tests with the freeze drying array were conducted to compare the efficiency of heat transfer into small tubes inserted into black-painted aluminium blocks with the efficiency of heat transfer into 96-well PCR-plates. Data of the average mass flow at different chamber pressures for the two systems is presented in Table 3.15. Mass flow is calculated for single tubes of the Freeze Drying System™, and, for reasons of comparability, for 1/96 of a well plate.

The mass flow is higher for the Freeze Drying System™ than for well plates and increases throughout the tested pressure range. The mass flow of well plates reaches a maximum at approximately 200 mTorr for well plates with Al-blocks and at approximately 50 mTorr for well plates without Al-blocks. The difference in mass flow data for well plates with and without Al-blocks is in agreement with the main mechanisms of heat input: partially by radiative heat transfer and partially by conduction through the gas over a large distance for well plates without Al-blocks and mostly by conduction through the gas for well plates with Al-blocks. Above a certain chamber pressure, heat transfer by conduction through the gas is hindered and the average mass flow decreases. Which chamber pressure enables maximum mass flow strongly depends on the gap width in between heat source and heat sink. If the separation distance is very small, heat flow by conduction through the gas reaches maximum efficiency at a higher pressure (shorter mean free path of gas molecules) than for a larger separation distance. Taking this into account, the average separation distance between heat source and heat sink seems to be smallest for the Freeze Drying System™.

Pure mass flow information is not an absolute indicator for efficiency of heat transfer, as the area for heat flow and the temperature difference between heat source and heat sink also play a major role. For a comparison of the Freeze Drying System™ to PCR-plates, heat transfer coefficients must be calculated. Just as has been done for well plates, the area for heat input into the product has first to be estimated from experimental set-up and geometrical data of the small tubes. Analogous to well plates, the contact area between the small tube and the Al-block plus product area would be considered as the effective area for heat flow into the product. However, results from sublimation tests revealed that the contact between ice and container system is lost at a very early stage during the sublimation process (see Figure 3.36). Since the shape of the small tubes is cylindrical and not conical as for the well plates, this means that apart from the

Figure 3.36: Ice core in a single tube of the Freeze Drying System™ photographed after conduction of a sublimation test. The ice has completely lost contact to the tube wall. The temperature of ice and tube at the time the photograph was taken was approximately 0 °C to minimise fogging of the glass. Note that at this temperature, some of the ice has already melted.

Table 3.16: Overview of geometric dimensions relevant for heat flow into a single tube of the Freeze Drying System™. A_{FDS} is the area used for calculation of K_{FDS}.

Description of Tube Part	Size
outer diameter (cm)	0.88
inner diameter (cm)	0.71
cross sectional area (outer diam., cm^2)	0.61
cross sectional area (inner diam., cm^2)	0.40
A_{FDS} (cm^2)	1.00

very beginning of the sublimation phase, no or little heat is transferred into the product by heat flow from the sides.

As a consequence, the area for heat flow into tubes of the Freeze Drying System™ was calculated from the area of the tube bottom (using the outer tube diameter) and the product area, using the inner tube diameter. Table 3.16 gives an overview of relevant dimensions of the tubes of the Freeze Drying System™. The calculated value for the area for heat flow into a tube of the Freeze Drying System™, A_{FDS}, is again an estimate since there was no means of calculating heat transfer coefficients using the actual and rapidly decreasing contact area for heat input into the product.

Heat transfer coefficients for the Freeze Drying System™, K_{FDS}, calculated from sublimation test data are summarised in Table 3.17 on the facing page. Average values range from $2.3 \cdot 10^{-4}$ cal $s^{-1}cm^{-2}K^{-1}$ at 30 mTorr to $11.1 \cdot 10^{-4}$ cal $s^{-1}cm^{-2}K^{-1}$ at 500 mTorr. They are higher than heat transfer coefficients found for well plates for both set-ups, with or without Al-blocks (cf. sections 3.1.3, 3.1.5, Table 3.2, and Figure 3.38 on page 123). The increase of K_{FDS} with pressure is again an indicator for a high amount of heat input by conduction through the gas.

Heat transfer coefficients calculated from sublimation tests with the Freeze Drying System™

Table 3.17: Heat transfer coefficients for the VirTis Freeze Drying System™, K_{FDS}, calculated from sublimation tests at different chamber pressure set-points. Values in the table represent the mean result of each sublimation test (n = number of tubes examined per test), ± the standard deviation. Initial mass flow data were corrected with an offset value taking into account the initial ramping phase prior to calculation of K_{FDS} values.

Pressure $mTorr$	K_{FDS} $10^4 cal\ s^{-1}cm^{-2}K^{-1}$	n
30	2.21 ± 0.54	72
30	2.40 ± 0.40	36
50	2.58 ± 0.48	72
50	3.25 ± 0.55	36
100	4.47 ± 0.76	72
100	4.50 ± 0.73	36
200	6.69 ± 0.99	72
200	6.72 ± 0.47	60
500	11.20 ± 1.26	72
500	10.93 ± 1.69	60

Table 3.18: Overview of separation distances l calculated from the data fit for each of the tested container systems. Results of K_K and the term $l \cdot (K_P/\lambda_0)$ from the data fit are also provided.

Container	$l(cm)$	$K_K(cal\ s^{-1}cm^{-2}K^{-1})$	$l \cdot (K_P/\lambda_0)(Torr^{-1})$
PCR w/o Al	0.19	1.40	14.35
PCR w. Al	0.05	0.28	3.75
PCR w.Al, hsg	0.03	1.31	2.52
FDS	0.02	1.40	1.36
$2R$ vials	0.03	1.98	2.48

were plotted and these data were fitted to Equation 1.7. Results of the data fit are shown in Figure 3.37. The fitting parameter K_P has been fixed to $33.2 \cdot 10^{-4}$ cal $s^{-1}cm^{-2}K^{-1}Torr^{-1}$. This is justifiable as this parameter mainly depends on the accommodation coefficient a_c, which in turn depends on the nature of the surfaces that are associated with heat transfer by conduction through the gas [1]. In case of the Freeze Drying System™, these surfaces are black painted aluminium and glass, which is a very similar constellation as for vials placed on a stainless steel freeze dryer shelf. Therefore the same value for the accommodation coefficient as for vials has been used ($a_c = 0.67$).

Results of the data fit for the parameters K_K and l_{FDS} are $1.40 \cdot 10^{-4}$ cal $s^{-1}cm^{-2}K^{-1}$ and 0.02 cm, respectively. The value of l_{FDS} is the smallest value determined for the separation distance between heat source and heat sink of the tested container systems (cf. Table 3.18). The term $l \cdot (K_P/\lambda_0)$ is equal to $1.36 \cdot 10^{-4}$ $Torr^{-1}$. This is also the smallest fitting result of all tested container systems and set ups. These data indicate that the contribution by conduction through the gas to total heat transfer into the product plays a major role for the Freeze Drying System™.

The value for K_K determined by the data fit is smaller than the value determined for vials ($1.98 \cdot 10^{-4}$ cal $s^{-1}cm^{-2}K^{-1}$, cf. Table 3.18, and section 3.4.2) and in the same order of magnitude as the values determined for well plates without Al-blocks and for well plates with Al-blocks

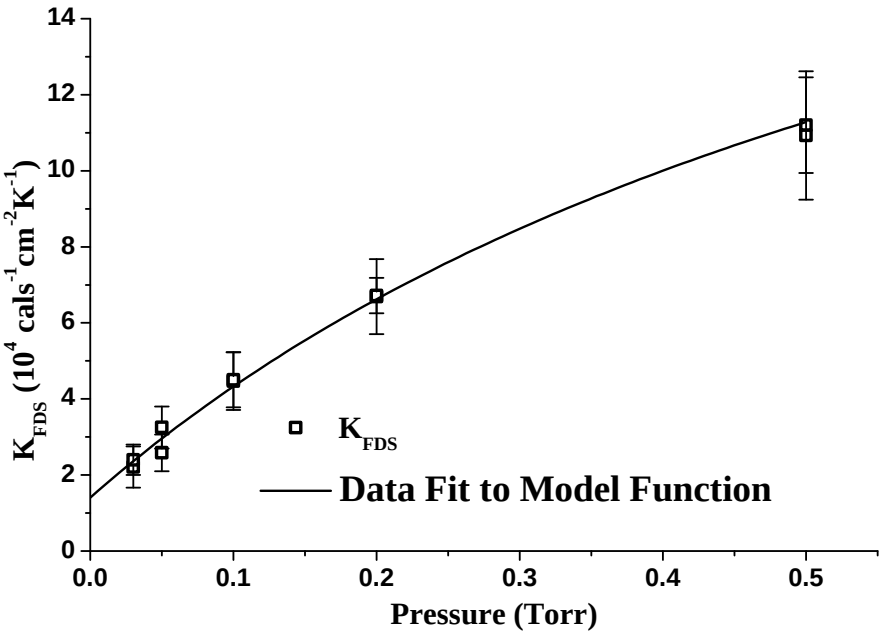

Figure 3.37: Plot of heat transfer coefficients calculated from sublimation tests with the Freeze Drying System™ (open squares). Error bars show the standard deviation of the mean calculated from each sublimation test. The black line represents the data fit to the model function, Equation 1.7.

with heat sink grease ($1.40 \cdot 10^{-4}$ cal s^{-1}cm^{-2}K^{-1}, $1.31 \cdot 10^{-4}$ cal s^{-1}cm^{-2}K^{-1}, respectively, see Table 3.18 as well as Table 3.3 and sections 3.1.3, 3.1.6). K_K of the Freeze Drying System™ is considerably larger than the value of K_K determined for the set-up of well plates inserted into Al-blocks ($0.28 \cdot 10^{-4}$ cal s^{-1}cm^{-2}K^{-1}, Table 3.18 and section 3.1.5).

As has been mentioned before (section 3.3.1), the percentage of area of direct contact to area of container inserted into the cavity of the Al-block is similar for the freeze drying array and for well plates with Al-blocks. The large difference in the values of K_K for the two similar set-ups (small tubes inserted into Al-blocks, well plates inserted into Al-blocks) even though percentage areas of direct contact are similar could be due to the approximation of the values of A_{PCR} and A_{FDS}, the effective areas relevant for heat flow. Another reason for the difference could be the higher emissivity ε of the black-painted Al-block ($\varepsilon \approx 0.90$) used with the freeze drying array compared to the emissivity of the non-coated Al-blocks ($\varepsilon \approx 0.25$) of the well plates.

Following the law of Stefan Boltzmann (Equation 3.2), a body or surface with a low emissivity radiates less energy towards its surroundings than a body or surface with a higher emissivity.

$$\mathrm{d}Q = \varepsilon \cdot \sigma \cdot A(T^4_{source} - T^4_{sink}) \tag{3.2}$$

In Equation 3.2 T^4_{source} is the temperature of the heat source in Kelvin to the fourth power. T^4_{sink} corresponds to the temperature of the heat sink to the fourth power. A is the area of "view" from the heat sink to the heat source. If the emissivity ε is high, the total heat flow is high. Therefore, radiative heat input from the black Al-block into the small glass tubes of the freeze drying array is higher than the radiative heat input from the non-painted Al-block into the well plates. This leads to a higher contribution of non-pressure dependent heat transfer into the small tubes of the freeze drying array as compared to well plates.

Figure 3.38 gives a comparative overview of heat transfer coefficients of 96-well PCR-plates with and without aluminium blocks and of the VirTis Freeze Drying System™.

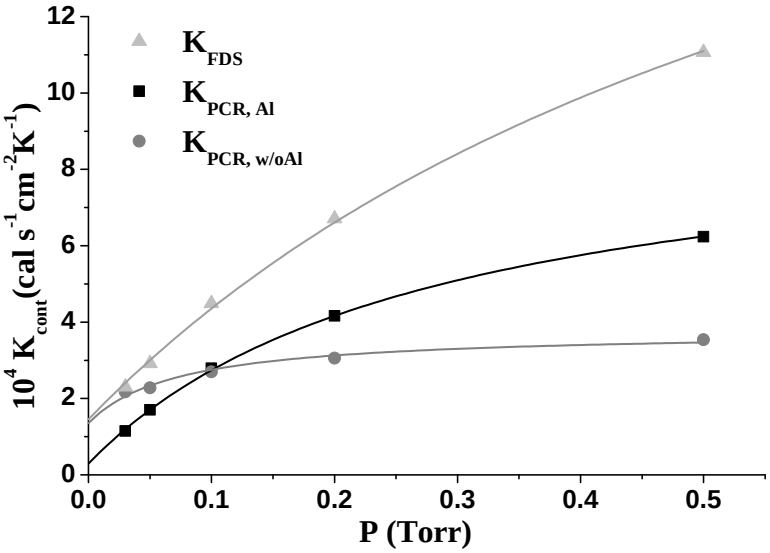

Figure 3.38: Plot of heat transfer coefficients of the Freeze Drying System™ (light grey triangles), PCR-plates with Al-blocks (black squares), and PCR-plates without Al-blocks (grey circles). Data used for the plot are average heat transfer coefficients calculated from all experiments performed for the particular pressure set point. Curves represent results of data fits to Equation 1.7.

3.4 2 R Serum Tubing Vials

3.4.1 Contact Area to Shelf Surface

Print tests conducted with 2R vials showed that the direct contact to a flat surface only exists in the form of a narrow ring near the circumference line of the vial bottom (cf. Figure 3.39). In some prints, the line of this circle was even broken. None of the prints of the vial bottoms on a piece of paper showed a contact area of more than approximately 10 % of the cross sectional area of the vial bottom. The average contact area was estimated to be 5 ± 3 % of the cross sectional area of the outer vial bottom.

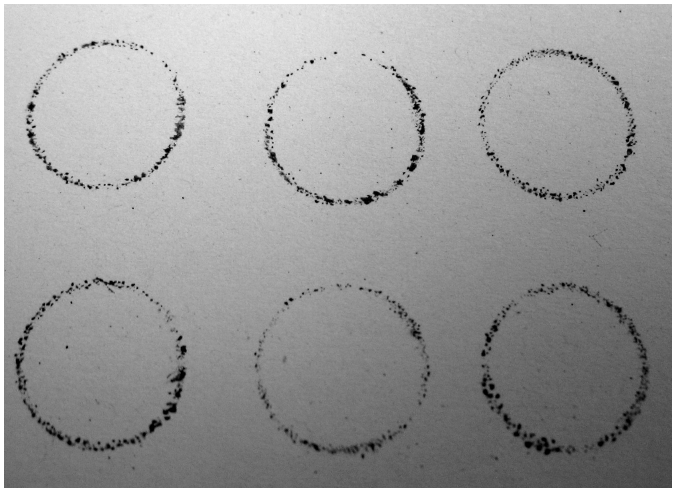

Figure 3.39: Imprints of the bottom of $2R$ vials. The vials were first pressed on an ink pad and then gently pressed on a sheet of paper on a flat surface.

Compared to 96-well PCR-plates and small tubes, both inserted into Al-blocks, heat input by direct conduction into 2R vials is of less importance. The main routes for heat supply to the product in 2R vials are by conduction through the gas and by radiation. At least for 2R vials placed in the centre of the array on a shelf, radiation into the product through the container side is almost completely blocked out by neighbouring vials. However, in places where the vial bottom is separated from the shelf surface by a small gap (i.e. no perfect contact to the shelf, separation distance), heat can not only be transferred by conduction through the gas, but also by radiation from the bottom shelf directly underneath the vial bottom. Top radiation originating from the underside of the shelf above the one on which the vials are placed (the radiation surface) also contributes to heat transfer into the vial. Some of the top radiation is absorbed by the stopper placed on the vial.

3.4.2 Results of Sublimation Tests

Results of sublimation tests with 2R vials are listed in Table 3.19. There is a significant difference in heat transfer coefficients calculated from sublimation rates in edge vials and from sublimation rates in centre vials (i.e. K_{2R} at 50 mTorr for centre vials equals approximately $3.3 \cdot 10^{-4}$ cal $s^{-1}cm^{-2}K^{-1}$ compared to $4.4 \cdot 10^{-4}$ cal $s^{-1}cm^{-2}K^{-1}$ for edge vials).

K_{2R} for edge vials is always higher than the corresponding value for centre vials [1], [26]. In this study, the values of $K_{2R,edge}$ for edge vials were approximately 30 % higher than the corresponding heat transfer coefficients for centre vials for all tested pressure settings. This is due to additional radiative heat input into the edge vials originating from drying chamber walls / the tray side and the door. Although stainless steel bands were used to shield the edge vials from this extra radiation, ice temperature data reveal that the metal bands only partially succeeded in reducing additional heat input into edge vials.

The stainless steel bands are also considerably warmer than the vials during primary drying,

Table 3.19: Results of sublimation tests with 2R vials for vials placed in centre and edge positions. One shelf of the freeze dryer was completely filled with vials (hexagonal packing). Vials were filled with distilled water, stoppers were placed in semi-stoppered position. Stainless steel bands were placed as radiation shields around the array. Values for K_{2R} are average values ± the standard deviation calculated from mass loss after subtraction of an offset value to take into account the non-steady state ramping phase at the beginning of the sublimation phase.

Pressure Setting $mTorr$	K_{2R} centre $10^{-4} cal\ s^{-1} cm^{-2} K^{-1}$	K_{2R} edge $10^{-4} cal\ s^{-1} cm^{-2} K^{-1}$
50	3.28 ± 0.524	4.40 ± 0.723
100	4.56 ± 0.288	6.02 ± 0.561
150	5.66 ± 0.400	7.55 ± 0.643
200	6.57 ± 0.762	8.24 ± 0.745
400	8.55 ± 0.589	10.92 ± 1.50

because the heat consumed in the vials by sublimation of ice results in a lower temperature in the frozen solution than the shelf temperature set point. The steel bands are not cooled by this effect and they are in direct contact with the shelf surface. The temperature of the tray sides will therefore be close to the temperature of the shelf surface. The material of the stainless steel bands is identical to the material of the freeze drying chamber walls. The surface finish of the stainless steel bands is not as highly polished as the freeze drying chamber walls, which slightly increases the emissivity of the stainless steel bands in comparison to the emissivity of the freeze drying chamber walls ($\varepsilon_{steelbands}$ is approximately 0.4, ε_{walls} is approximately 0.3). The stainless steel bands are also in direct contact with and in direct line of view of the outermost row of vials. The areas of direct contact are only small, because the vials have rounded walls. Still, this situation generates additional, mostly radiative, heat input into these edge vials and will account for at least part of the ice temperature and sublimation rate differences observed between edge and centre vials.

The temperature difference between edge and centre vials was highest for the lowest pressure setting (approximately 1.7 K at 50 mTorr and only 0.3 K at 400 mTorr). This confirms that heat input by radiation plays a large role at low pressures whereas heat input by gas conduction is most important at higher pressure settings [26] (see also Section1.4.5).

K_{2R} data were fitted to Equation 1.7 (cf. Figure 3.40). In addition to the two sets of data for edge and centre vials, a weighted average K_v has been calculated which takes into account the total number of edge and centre vials. A similar approach for determiniation of a weighted average of K_v has already been reported in the literature [106]. Such a procedure has not been considered for analysis of sublimation test data from well plates or the Freeze Drying System™ as the number of data points of true centre placed containers was limited for these container systems and experimental designs (i.e. only two centre placed well plates per shelf, not more than one half of a single shelf was used for the Freeze Drying System™). Moreover, for well plates used without Al-blocks, the difference in heat transfer into edge-placed and centre-placed containers is much less pronounced than for vials. The same may also be true for the glass containers placed in Al-blocks.

The weighted average values illustrate that even for a small batch size (one shelf in a laboratory freeze dryer) with a relative high percentage of edge vials the average heat transfer into a vial is comparable to heat transfer into centre vials. Note that heat transfer coefficients for edge vials are not representative for consideration of a whole batch of vials, as the majority of the vials are centre-placed vials.

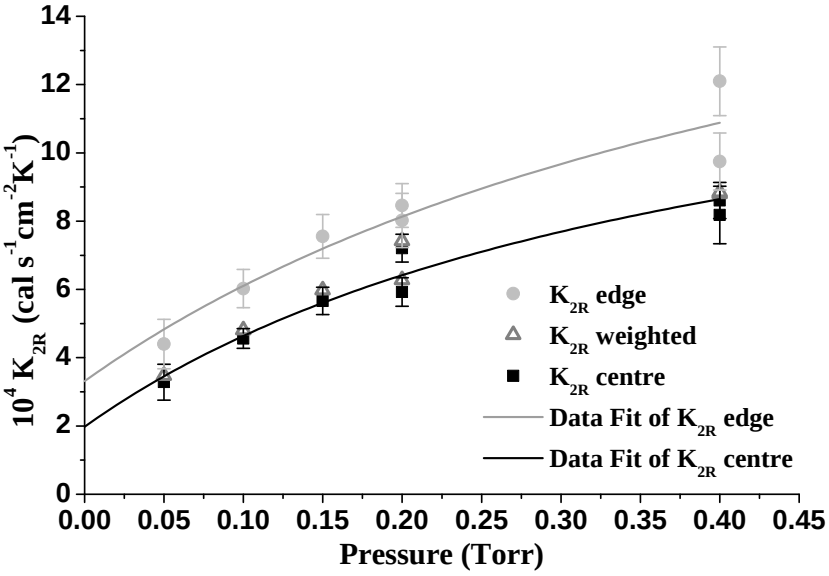

Figure 3.40: Fit of heat transfer coefficients calculated from sublimation test data of $2R$-vials. K_{2R} for edge vials is represented by light grey circles, calculated weighted average of K_{2R} by grey open triangles and K_{2R} for centre vials by black squares (top to bottom in diagram). Note that for the array used during the sublimation tests, approximately 80 % of the vials represent "centre" vials.

Table 3.20: Values of fitting parameters K_K and l for 2R vials in centre and edge positions of the vial array and weighted average of edge and centre vials. The unit of K_K is 10^{-4} cal $s^{-1}cm^{-2}K^{-1}$, given with errors as calculated by Origin 7.5G software. The unit of l is cm.

Parameter	K_{2R} centre		K_{2R} weighted		K_{2R} edge	
K_K	1.9771	$\pm$ 0.2846	2.2272	$\pm$ 0.2580	3.3122	$\pm$ 0.3837
l	0.033		0.030		0.025	

For all data fits, the value of the parameter K_P was fixed at $33.2{\cdot}10^{-4}$ cal $s^{-1}cm^{-2}K^{-1}Torr^{-1}$, the value which is commonly used in the literature [1], [83] (also see section 1.4.2 on page 31 and following pages). The values of the other fitting parameters, K_K and l, are shown in Table 3.20. The higher heat input by radiation into edge vials is also visible in Figure 3.40 as a larger value for K_K, the K_{2R}-axis intercept.

Heat transfer coefficients determined in these experiments for $2R$ vials are in the same range compared to heat transfer coefficients determined for tubing vials with different volumes (5 to 50 mL) [1], [83]. In the literature, the largest heat transfer coefficients were found for vials with the smallest separation distance l_v between shelf surface and vial bottom. These findings are consistent with the assumption that the main portion of heat input into vials is supplied by conduction through the gas.

Vials with similar heat transfer coefficients as the tested $2R$ vials have average separation distances l_v in the range of 0.02 to 0.05 cm [83]. l_{2R} of the tested $2R$ vials determined from the term $l \cdot (K_P/\lambda_0)$ of the data fit of centre vials is approximately 0.03 cm and therefore in very good agreement with the values found in the literature.

3.4.3 Verification of K_{2R} Data for Product Runs

The SMART™ Freeze Dryer technology can also be used to calculate heat transfer coefficients [68]. Product runs with excipient solution in 2R vials were conducted to verify the applicability of heat transfer coefficients determined from sublimation tests with pure water to product freeze drying. Trehalose solution (50 mg/g) was used as a model in two runs with 0.2 and 0.5 cm fill depth per vial, respectively. Table 3.21 summarizes product and container related input-data for the SMART™ Freeze Dryer software. For these experiments, one shelf of the freeze dryer was fully loaded with the vials. The outermost vials in the array were used as "dummy" vials which were left empty. These empty vials serve as an additional radiation shield.

Table 3.21: Summary of formulation related and container related input data used for the verification of vial heat transfer coefficients with the SMART™ Freeze Dryer software with 2R serum tubing vials.

Parameter	Fill Depth of Trehalose Solution	
	0.2 cm	0.5 cm
Physical Form	Amorphous	Amorphous
Nature of Drug Product	Small Molecule	Small Molecule
Type of Bulking Agent	Amorphous	Amorphous
Type of Vials	Tubing	Tubing
Number of Vials	493	493
Inner Area of Vials	1.52 cm^2	1.52 cm^2
Fill Volume	0.3 mL	0.7 mL
Fill Depth	0.2 cm	0.5 cm
Fill Weight	0.3 g	0.7 g
Collapse Temperature	−30 °C	−30 °C
Concentration of Solution	50 mg/g	50 mg/g

The software chose an initial pressure set point for primary drying of 68 mTorr for both runs. A summary of the "initial guess" data of the SMART™ software is given in Table 3.22.

The choice of initial shelf temperatures was based on input data of the collapse temperature (approximately −28 °C to −30 °C [49]) and included comparatively large safety margins as the total primary drying time for a total solids content of 50 mg/g and a fill depth of less than 1 cm was expected to be not more than approximately 24 h [31]. After the first manometric temperature measurement (MTM) the shelf temperature was adjusted to −13 °C for the run with 0.2 cm fill depth (cf. Figure 3.41) and first to −9 °C, after the second MTM to −5 °C for the run with 0.5 cm fill depth (cf. Figure 3.42). The lower shelf temperature setting for the run with the lower fill depth was accompanied by a slight lowering of the chamber pressure to 62 mTorr.

The product temperature at the sublimation interface determined from MTMs was lower or equal to −32.5 °C and in good agreement with thermocouple data of TCs placed in centre vials

Table 3.22: Summary of SMART™ software's "initial guess" data for freeze drying of trehalose solution in 2R serum tubing vials.

Parameter	Fill Depth of Trehalose Solution	
	0.2 cm	0.5 cm
Primary Drying Estimate (h)	5.6	11.5
Target Product Temperature (°C)	−35	−33
Chamber Pressure Set Point (mTorr)	68	68

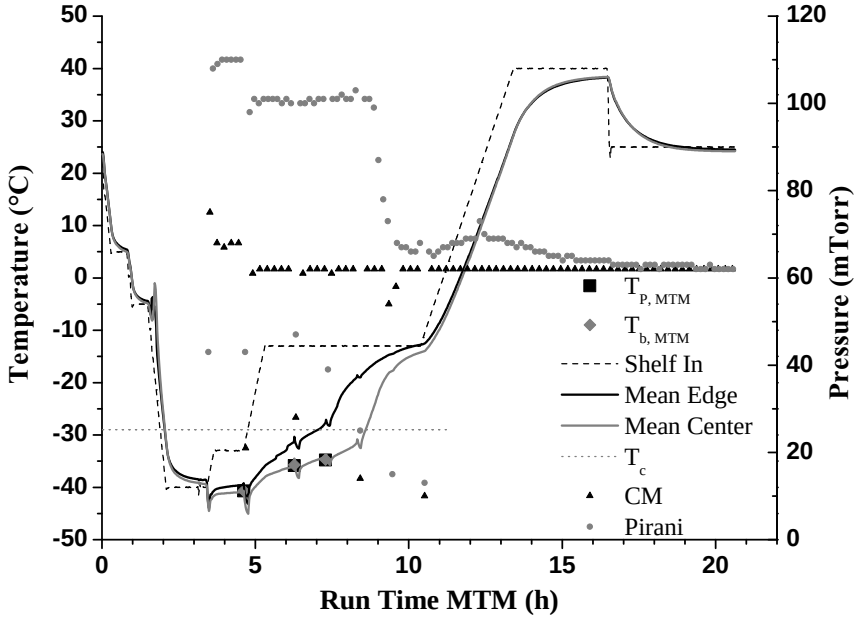

Figure 3.41: Data from the freeze drying run with trehalose solution (0.2 cm fill depth) in 2R vials. The shelf temperature is shown as a black dashed line. $T_{P,MTM}$ and $T_{b,MTM}$ are shown as black squares and grey diamonds, respectively. Thermocouple data are shown as straight lines in black (edge) and grey (centre placed TC). The collapse temperature T_c is shown as a grey dotted line. Pressure readings of CM and Pirani sensors are shown as black triangles and grey filled circles, respectively.

at all times. The product area for an array of vials on the freeze dryer shelf (approx. 750 cm^2) is much higher than the minimum required product area (300 cm^2, cf. 3.2.10) and does not change significantly until the major part of primary drying is over.

Other data acquired through MTMs include product resistance, mass flow rates, and estimation of container heat transfer coefficients. Table 3.23 gives a comparative overview of heat transfer coefficients, mass flow rates, and temperature differences between shelf surface and product for trehalose runs and sublimation tests.

Table 3.23: Comparison of K_{2R} calculated from data fit of sublimation test data and as determined from trehalose runs by the SMART^{TM} software.

Origin of Data		Pressure (mTorr)	$K_{2R} * 10^4$ (cal $s^{-1}cm^{-2}K^{-1}$)	Mass Flux (g/(h · vial))	$T_S - T_P$ (K)
T. 0.2 cm	first MTM	68	3.13	0.02	8.7
	intermed. MTM	62	2.69	0.06	22.3
	last MTM	62	2.2	0.05	21.6
T. 0.5 cm	first MTM	68	3.33	0.03	9.5
	intermed. MTM	68	2.85	0.08	27.8
	last MTM	68	2.19	0.06	27.9
H_2O	Data fit K_{2R}	68	3.91		
		62	3.76		
	Subl. Test	50	3.28	0.09	26.3
	Subl. Test	100	4.56	0.13	25.8

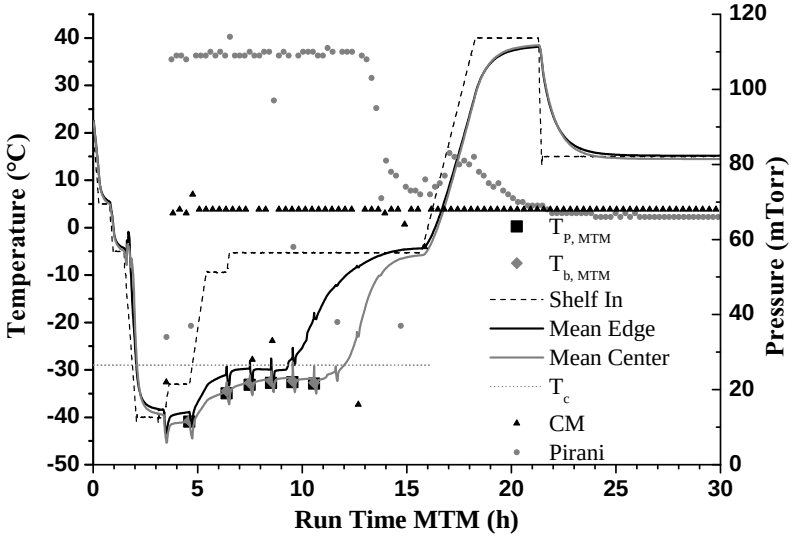

Figure 3.42: Data from freeze drying run with trehalose solution (0.5 cm fill depth) in 2R vials. The shelf temperature is shown as a black dashed line. $T_{P,MTM}$ and $T_{b,MTM}$ are shown as black squares and grey diamonds, respectively. Thermocouple data are shown as straight lines in black (edge) and grey (centre placed TC). The collapse temperature T_c is shown as a grey dotted line. Pressure readings of CM and Pirani sensors are shown as black triangles and grey filled circles, respectively.

In the table, mass flow data is given as calculated by the SMART™ software and as calculated from the sublimation tests at 50 mTorr and at 100 mTorr. The temperature difference ΔT was calculated from the shelf surface temperature above the fluid inlet T_S and from the product temperature at the sublimation interface $T_{P_{MTM}}$ for SMART™ runs. For the sublimation tests with distilled water, the temperature difference was calculated from the temperature of the shelf surface and from the product temperature at the bottom of the vial. T.0.2 cm and T.0.5 cm in Table 3.23 reflect trehalose runs with 0.2 cm and 0.5 cm fill depth, respectively.

It can be seen that K_{2R} determined from sublimation tests (or from the fit of sublimation test data to equation 1.7) are higher than heat transfer coefficients calculated by the SMART™ software for product runs. This is different from findings published in the literature [68]. Here, heat transfer coefficients calculated by the SMART™ software were usually higher than heat transfer coefficients which had been determined gravimetrically. In the literature, it could be demonstrated that the agreement between gravimetrically obtained heat transfer coefficients and SMART™ heat transfer coefficients improves when high chamber pressures, high shelf temperatures, and thermal shields are used [68]. In this study, thermal shields were used on the inside of the freeze dryer door to reflect radiation from the door.

It has also been pointed out that the accuracy of vial heat transfer coefficients (K_v) determined by MTM is depenent on the accuracy of P_{ice} and the value for the combined product and stopper resistance, R_{ps} [68]. P_{ice} has been shown to be usually accurate [102]. In the equation used by the SMART™ and MTM software, R_{ps} and K_v are inversely proportional [68]. By comparison of R_{ps} data determined for the trehalose solution freeze dried in $2R$ vials to trehalose R_{ps} data from the literature determined at several different freeze drying conditions [103], it might be possible that R_{ps} values determined in these trehalose SMART™ runs are slightly higher than expected (cf. Table 3.24). This would explain why K_{2R} values determined by SMART™ are lower than the gravimetrically determined values.

As primary drying proceeds, mass flow rates and heat transfer coefficients decrease while the product resistance increases (cf. Figure 3.43). The decrease of the mass flow rate is a direct

Table 3.24: Comparison of *Rps* values (combined product and stopper resistance values) calculated by the SMART™ software from trehalose runs in $2R$ vials and approximated values taken from the literature [103].

Origin of Data		Pressure (mTorr)	shelf temp. (°C)	R_{ps} ($\frac{cm^2 \cdot Torr \cdot h}{g}$)	l_{dry} (cm)
T. 0.2 cm	first MTM	68	−13	1.41	0.02
	intermed. MTM	62	−13	2.33	0.07
	last MTM	62	−13	3.57	0.11
T. 0.5 cm	first MTM	68	−31	1.22	0.02
	intermed. MTM	68	−5	2.71	0.14
	last MTM	68	−5	3.68	0.30
	Overcashier et al.	50	−30	2	0.1
		50	−30	3	0.2
		50	−30	4	0.3
		100	−20	0.5	0.1

consequence of the increasing product resistance / the increasing thickness of the dry layer, cf. Equation 1.1. The decrease of the K_{2R} values at later stages of primary drying may be caused by readsorption of water vapour into the primary dried product matrix during the MTM [107]. Therefore, the first few SMART™ K_{2R} values are the most representative (i.e. for the freeze drying run with the low fill depth of only 0.2 cm, only the first value), and the values determined at a later stage are biased.

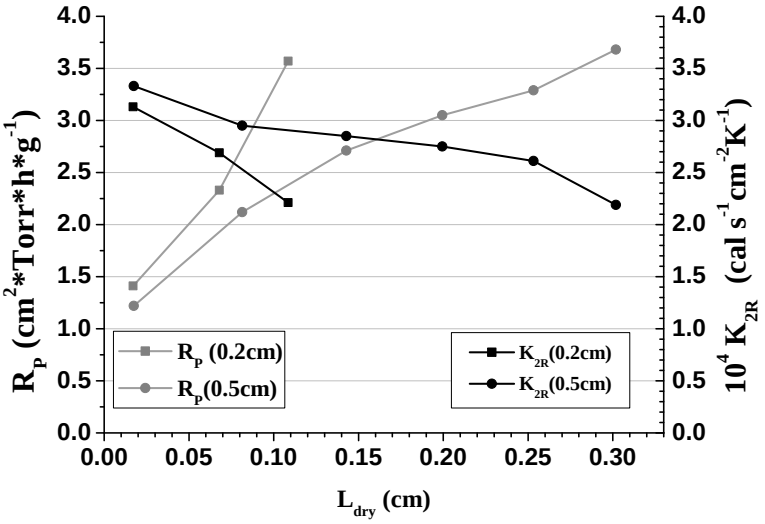

Figure 3.43: The product resistance R_P of trehalose (50 mg/g) increases as the thickness of dried product layer (L_{dry}) increases. Heat transfer coefficients K_{2R} determined by SMART™ software decrease with increasing product resistance.

3.5 Formulation Design for Small Volumes to be Freeze Dried: A Case Study with a Cytokine

3.5.1 General Introduction

In the previous sections, results of sublimation tests and heat transfer coefficients were presented for all of the tested container systems and experimental designs. For 96-well PCR-plates (with / without Al-blocks) and for 2R serum tubing vials, the applicability of these experimentally determined heat transfer characteristics to sample formulations was examined. Results from both of these approaches to container characterisation and conclusions for freeze drying cycle design were combined for the tests described in the following section.

Trehalose and mannitol, two excipients commonly applied for freeze drying formulation design have both been extensively studied already [44], [60], [61]. In the next section, the development of an entirely new and more complex model formulation containing an active ingredient is described. The active ingredient is a recombinant human cytokine with a molecular weight of 17,000 Da. In addition to numerous other reactions and stresses which may affect their stability, proteins are often sensitive to the ionic strength of the surrounding media as well as to its pH value [38]. For these reasons, buffering agents were included in the formulation design. The ideal pH for stabilisation of the cytokine used in the present study was not known. Therefore, two pH ranges were tested: one acidic (citrate buffer, approximately pH of 4), one basic (phosphate buffer and Tris buffer, pH in between 7.5 and 8). Sucrose, trehalose, and raffinose were tested as stabilising, lyoprotective agents. Mannitol was used as a bulking agent.

3.5.2 Optimisation of Amorphous Formulations

As described in Section 2.2.4, the anticipated concentration of cytokine in the formulation was 10 μg/mL. Formulation testing was carried out in 2R vials with a fill volume of 0.5 mL. For initial tests, all amorphous cytokine formulations contained 10 mg of lyoprotectant (sucrose, trehalose, or raffinose) per vial. This corresponds to a molar ratio of cytokine to lyoprotectant from approximately $1:5,000$ (for raffinose) to $1:10,000$ (for sucrose). It has been reported in the literature [48] that a molar ratio of proteinic API to lyoprotectant of $1:360$ may be needed for maximum stabilisation.

This corresponded to a solid content of approximately 20 mg/mL (see section 2.2.4 on page 52). DSC scans of all formulations containing Tris buffer showed extremely low glass transition temperatures (T_g'), some as low as -45 °C (cf. Table 3.25). Most likely the non-crystallising Tris buffer had formed a mixed glass with the stabiliser. The glass transition of two-component mixtures (lyoprotectant and buffer) was investigated and always found to be in between the very low glass transition of the pure Tris base (-78 °C according to own measurements, -79 °C according to [108]) and the glass transition of the concerned lyoprotectant. This behaviour can be expected from homogeneous mixtures of two (or more) glass-forming components.

According to the Gordon-Taylor equation, T_g of a homogeneous mixture of two (or more) amorphous components can be estimated from the T_g values of the individual components. The calculation takes into account the weight fraction and the true density of each individual component in the mixture [109]. Application of this equation on the two glass transition temperatures of Tris buffer and sucrose in the initial formulation composition (20 mg/mL sucrose, 50 mM Tris), taking into account the weight fraction of both excipients in the solution, yields an estimated T_g' value of the mixture of approximately -43 °C. This estimate is not taking into account the true densities of the individual components. The difference in the true densities of Tris, the lyoprotectant, and the solvent (water) was assumed to be small so that the bias in the calculation would be small. The obtained result from the estimation is close to the T_g' value which has been determined with DSC-measurements (cf. Table 3.25), indicating that the Tris buffer remains completely amorphous during freezing. The Gordon-Taylor equation is not suited for prediction of the glass transition temperature for more complex formulations showing, i.e., phase separation or partial crystallisation of one or more components during freezing.

As the T_g' values of all Tris buffer containing amorphous formulations in the initial composition

Table 3.25: List of amorphous mixtures with Tris buffer tested for formulation of the cytokine. Formulations with T_g' values of less than −36 °C were modified. Increasing the fraction of lyoprotectant and decreasing the fraction of buffering agent yielded desirable results. The concentration of Tris buffer is given in the description of the formulation composition.

Composition	Conc. of Lyoprotectant ((mg/mL) in Solution)	T_g' (°C)
Sucrose + Tris 50 mM	20	−45.5
	40	−41.1
	70	−37.5
	100	−36.5
Sucrose + Tris 25 mM	70	−35.8
	100	−35.3
Trehalose + Tris 50 mM	20	−45.6
	40	−36.5
	70	−35.3
	100	−33.9
Trehalose + Tris 25 mM	40	−36.3
	70	−33.7
Raffinose + Tris 50 mM	20	−44.1
	40	−38.5
	70	−34.2
	100	−32.3
Raffinose + Tris 25 mM	40	−34.8
	70	−31.4

were very low (cf. Table 3.25), the total amount of stabiliser was then raised in order to increase T_g' above −36 °C. This temperature was chosen as the lowest acceptable critical formulation temperature. Adding a safety margin of 2 to 3 °C to this critical temperature leads to a target product temperature for primary drying just barely above −40 °C. Controlling the product temperature below −40 °C during primary drying is extremely difficult, and freeze drying below −40 °C shelf temperature would need to be conducted at very low chamber pressures. At this low temperature, the primary drying phase would take very long (cf. Section 1.1.2). In short, designing a formulation with a critical formulation temperature of −40 °C or lower would not be reasonable. Especially for the formulation containing sucrose and Tris buffer, a 100 mg/mL content of lyoprotectant was not sufficient to attain a critical formulation temperature of −36 °C, cf. Figure 3.44. Therefore the Tris buffer content was reduced from initially 50 mmol/L to half of the original concentration (25 mmol/L) in all Tris containing formulations. This measure led to satisfactory T_g' values (cf. Table 3.25), while not noticeably altering the crystallisation behaviour of the components, Tris buffer and sucrose.

All other amorphous formulations, containing either phosphate or citrate buffer, also showed low glass transition temperatures of the maximally freeze concentrated solution (all below −30 °C), yet none was as low as the T_g' values of the initial Tris containing formulations (cf. Table 3.26).

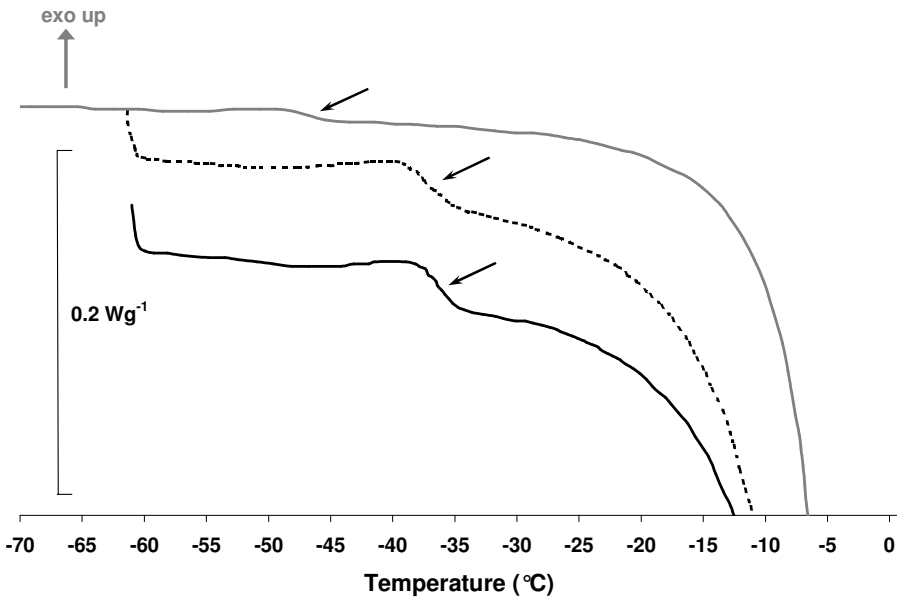

Figure 3.44: The diagram shows DSC scans of selected cytokine formulations with sucrose and Tris buffer. The upper, grey line represents the original formulation with 20 mg/mL sucrose and Tris in the concentration of 50 mmol/L. The dashed line represents the DSC scan of a formulation with the cytokine in addition to 100 mg/mL sucrose and Tris in the concentration of 50 mmol/L. Only the lowest DSC curve was found to have a T_g' value of more than -36 °C, cf. Table 3.25. Here, the amount of Tris was lowered to only 25 mmol/L, the sucrose concentration remained at 100 mg/mL. The arrows indicate the approximate position of each T_g'.

Table 3.26: List of amorphous mixtures with citrate and phosphate buffer tested for formulation of the cytokine. The concentration of each buffer is given in the formulation description.

Composition	Conc. of Stabiliser ((mg/mL) in Solution)	T_g' (°C)
Sucrose + Citrate 50 mM	20	−36.5
Sucrose + Citrate 25 mM	20	−36.5
Sucrose + Phosphate 19 mM	20	−36.2
Sucrose + Phosphate 9.5 mM	20	−36.2
Trehalose + Citrate 50 mM	20	−36.2
Trehalose + Phosphate 19 mM	20	−35.0
Raffinose + Citrate 50 mM	20	−32.8
Raffinose + Phosphate 19 mM	20	−31.5

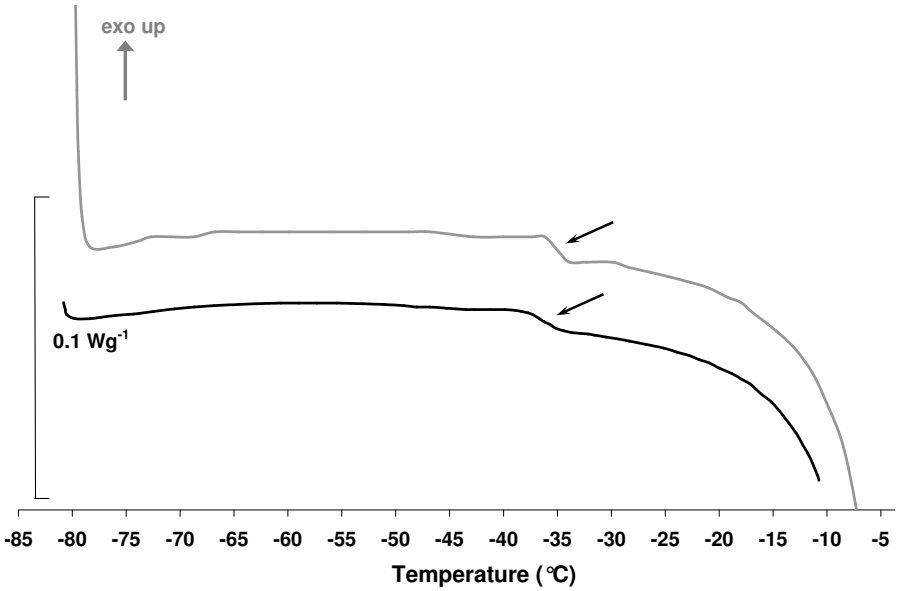

Figure 3.45: The diagram shows DSC scans of two cytokine formulations with sucrose and phosphate buffer. The upper, grey line represents the formulation with 20 mg/mL sucrose and 19 mmol/L phosphate buffer. The black line shows the DSC curve of the same formulation with only half of the amount of the phosphate buffer. The arrows indicate the approximate position of each T_g'.

T_g' values of pure buffer solutions were reported as approximately −55 °C for citric acid [110] and −45 °C for sodium phosphate [21]. The T_g' value of citrate buffer has been found to be dependent on the pH value of the solution [111]. The pH value of the citrate buffer solution used in this study has been adjusted to 4.0 with NaOH. T_g' of sodium citrate buffer at this pH value has been determined as approximately −35 °C [111]. This T_g' value is comparatively close to T_g' values of lyoprotectant solutions (the latter ranging from approximately −29 °C for trehalose to −32 °C for sucrose [46], [44]).

For citrate and phosphate buffer containing formulations, the initial concentration of buffering agent was approximately 19 mmol/L (2-fold) for the phosphate buffer (relating to the concentration of phosphate ions) and 50 mmol/L for the citrate buffer. A reduction of the amount of buffering agent to one half of the initial concentration had little effect on T_g' values for formulations with either citrate or phosphate buffer (cf Figure 3.45). For the phosphate containing formulations, the minimal change in glass transition temperature of the maximally freeze concentrated solution can be explained by the fact that phosphate buffers tend to crystallise during freezing [64]. If a fraction of the buffering agent remains amorphous, it can be assumed to be very small. Only this amorphous fraction of the buffering agent affects T_g' of the formulation.

For citrate buffer or citric acid, amorphous behaviour has been reported to occur during freezing [110]. According to the Gordon-Taylor equation, reducing the concentration of citrate buffer to one half (at a pH value of 4) will have little effect on the T_g' of the formulation, as the difference between T_g' values of the individual formulation components is small and the weight fraction of citrate buffer in comparison to the weight fraction of the lyoprotectant is also small. This explains the negligible change of T_g' of the solution for the decreased concentration of citrate buffer observed from DSC scans with sucrose and citrate buffer mixtures (cf. Table 3.26).

Glass transition temperatures of mannitol-containing formulations were determined. Mannitol containing formulations were annealed during the freezing step of the DSC programme in order to yield a high fraction of crystalline mannitol as these formulations were intended to be processed during freeze drying experiments as partially crystalline formulations. Therefore, as long as crystallisation of the major portion of mannitol was ensured, the critical formulation tem-

Table 3.27: List of mixtures intended for partially crystalline formulations with the cytokine. The concentration of each buffer is given for all the formulations with the description of the formulation composition. M: mannitol, S: sucrose, T: trehalose.

Composition	Conc. of Excipient (mg/mL) M	Lyoprotectant	T'_g (°C)
M + S + Tris 50 mM	20	4	−48.6
	20	2	−52.7
M + S + Phosphate 19 mM	20	2	−42.0
M + T + Tris 50 mM	20	4	−54.5

perature for design of the primary drying phase of mannitol containing solutions was considered to be the eutectic melting temperature of the mixture, and not the T'_g. Concerning the stability and activity of the incorporated API, it is more correct to still refer to T'_g as the relevant critical temperature as long as at least a small amorphous fraction is present.

In the mannitol containing formulations analysed by DSC, thermal events were detected at low temperatures (less than −40 °C, cf. Table 3.27). These were interpreted as the glass transition of the mixture of lyoprotectant, possibly a small amorphous fraction of mannitol, and the buffer component, signifying that citrate and even phosphate buffer remained partially amorphous in these mixtures. In the formulation containing mannitol and sucrose in a weight ratio of 5 : 1 as well as 50 mmol/L Tris buffer, T'_g was approximately −49 °C. For mannitol-sucrose mixtures with a similar weight ratio of mannitol to sucrose, T'_g values of approximately −41 to −43 °C have been reported [105]. In the formulation analysed for this study, the T'_g value is probably lowered further due to inhibition of crystallisation of the Tris buffer.

For mannitol solutions without stabilisers or other additives, two glass transition temperature have been reported, with $T'_{g,1}$ at −32 °C and $T'_{g,2}$ at −25 °C [112]. The authors also reported that $T'_{g,2}$ is difficult to observe. No second T'_g could be observed during DSC experiments performed for this study.

In the formulation containing mannitol and sucrose in a weight ratio of 10 : 1 as well as Tris buffer, a lower T'_g was observed (−53 °C) and explained with an even higher influence of the Tris buffer for this mixture of excipients, i.e. further suppression of mannitol crystallisation. In the formulation containing mannitol and trehalose in the weight ratio of 5 : 1 in combination with 50 mmol/L Tris buffer, the observed T'_g was also very low (−55 °C, cf. Figure 3.46). The formulation containing a mixture of mannitol and sucrose (again in the weight ratio of 5 : 1) with 19 mmol/L phosphate buffer was found to have a T'_g of −42 °C, corresponding to the T'_g value observed for mixtures of mannitol and sucrose with a comparable weight ratio of excipients. Therefore it can be assumed that phosphate buffer had fully crystallised in this formulation.

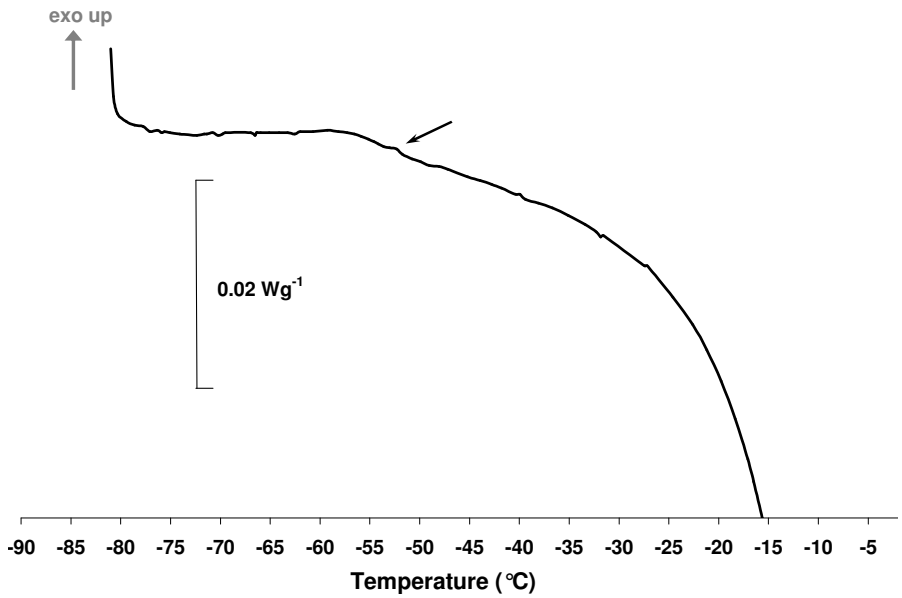

Figure 3.46: The diagram shows a DSC scan of the cytokine formulation with trehalose (4 mg/mL), mannitol (20 mg/mL), and Tris buffer (25 mg/mL). The arrow indicates the approximate position of the T_g'.

3.5.3 General Product Characteristics

The formulations were freeze dried in two individual runs. The first run was conducted with all purely amorphous formulations, the second with only mannitol containing formulations. Product temperatures were controlled by one TC per formulation and always remained below the corresponding critical formulation temperatures during primary drying. The residual moisture at the end of secondary drying was less than 1 % for all formulations. The overall average residual moisture as determined by Karl-Fischer titration was 0.5 $\pm$ 0.2 %.

The freeze dried formulations were re-dissolved in 1 mL of distilled water. Reconstitution times were recorded: partially crystalline formulations had the shortest reconstitution times (30 s at the longest), amorphous formulations with phosphate buffer had acceptable reconstitution times (less than 60 s), all other amorphous formulations needed more than 3 min for complete dissolution (cf. Table 3.28).

Cakes of sucrose-based amorphous formulations showed a visible amount of shrinkage but were otherwise smooth and without cracks. Shrinkage during freeze drying of sucrose-based formulations has been observed and reported even when the product temperature T_P remained below T_c during the whole freeze drying cycle [103]. Photographs of selected amorphous formulations are shown in Figure 3.47.

Table 3.28: Summary of product characteristics of cytokine formulations after freeze drying. Given concentrations are after reconstitution with 1 mL of water. S: sucrose, T: trehalose, R: raffinose, PB: phosphate buffer, Δt: reconstitution time. ±: acceptable appearance, −: appearance not acceptable, +: good appearance, ++: very good appearance.

Composition	appearance	Δt (s)	activity (IU/mg)	T_g (°C)
50 mg/mL S + Tris 12.5 mM	±	> 180	$9.36 \cdot 10^7$	65
10 mg/mL S + PB 9.5 mM	−	< 60	$1.08 \cdot 10^8$	8
10 mg/mL S + Citrate 25 mM	±	> 180	$4.53 \cdot 10^7$	68
35 mg/mL T + Tris 12.5 mM	±	> 180	$5.71 \cdot 10^7$	92
10 mg/mL T + PB 9.5 mM	−	< 60	$5.87 \cdot 10^7$	92
10 mg/mL T + Citrate 25 mM	−	> 180	$1.44 \cdot 10^8$	40/71
35 mg/mL R + Tris 12.5 mM	−	> 180	$9.93 \cdot 10^7$	92
10 mg/mL R + PB 9.5 mM	−	< 60	$1.67 \cdot 10^8$	97
10 mg/mL R + Citrate 25 mM	−	< 60	$3.32 \cdot 10^7$	75
10 mg/mL M + 2 mg/mL S + Tris 25 mM	++	30	$7.65 \cdot 10^7$	−
10 mg/mL M + 1 mg/mL S + Tris 25 mM	++	20	$1.43 \cdot 10^8$	−
10 mg/mL M + 1 mg/mL S + PB 9.5 mM	++	15	$5.69 \cdot 10^7$	−
10 mg/mL M + 2 mg/mL T + Tris 25 mM	+	25	$4.06 \cdot 10^7$	−
10 mg/mL M + Tris 25 mM	+	12	$6.06 \cdot 10^7$	−

Figure 3.47: Photographs of selected amorphous cytokine formulations after freeze drying. Left side: Sucrose / Tris (top) and trehalose /Tris (bottom). Note crack in lyophilisate of one of the trehalose vials. Right side: Trehalose / phosphate buffer (top) and raffinose / phosphate buffer (bottom). All formulations containing phosphate buffer showed white specks in cakes.

Amorphous trehalose formulations also showed cake shrinkage; the extent of shrinkage was comparable to that of the sucrose-based amorphous formulations. Lyophilisates in individual vials of amorphous trehalose formulations with Tris and citrate buffer revealed cracks, while the cake surfaces and sides still looked smooth. A possible explanation for formation of these cracks could be adherence of the lyophilisate to the vial wall during primary drying. When the shrinking process sets in, adhesion forces of the lyophilisate to the (non-siliconised) vial wall might be stronger than cohesive forces within the primary dried structure: parts of the lyophilisate are torn apart. A similar explanation for formation of cracks in lyophilisates can be found in the literature [35]. The cohesion forces within the lyophilisate might be increased by further increasing the total solids content. Adhesion forces to the vial wall might be decreased by using siliconised vials.

The amorphous formulation containing the excipients trehalose and phosphate buffer exhibited an uneven, cragged cake surface. Raffinose formulations looked similar to amorphous trehalose formulations: minor shrinkage, a small number of vials with cracked cakes and otherwise smooth looking cake surfaces. The cake surface of the phosphate buffer containing raffinose formulation looked smoother than the cake surface of the trehalose / phosphate buffer formulation. All formulations with phosphate buffer showed white specks in the central part of the lyophilisate surface. These might be an indication of phase separation during freezing. As expected, cakes of mannitol containing formulations had a smooth appearance without any cracks or signs of macroscopic collapse (cf. Figure 3.48).

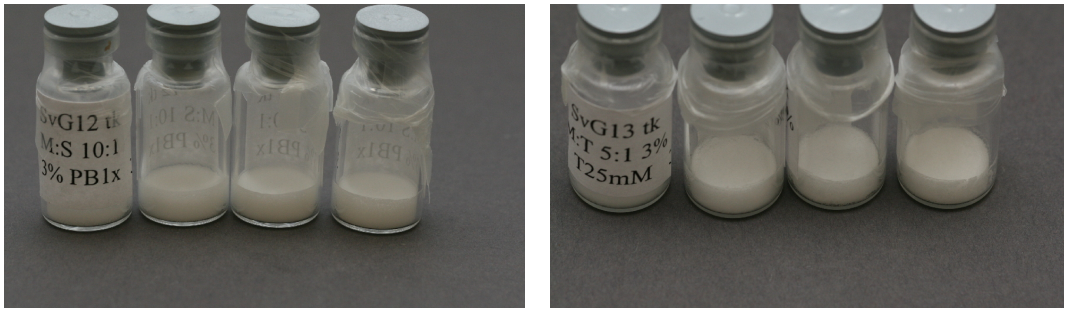

Figure 3.48: Photographs of two of the partially crystalline cytokine formulations. Left: mannitol / sucrose in the weight ratio 10 : 1 with phosphate buffer. Right: mannitol / trehalose in the weight ratio 5 : 1 with Tris buffer.

3.5.4 DSC Scans of Lyophilised Product

Glass transition temperatures of freeze dried formulations were determined by DSC. Table 3.29 gives an overview of glass transition temperatures, T_g, and other thermal events observed in the scans.

Glass transition temperatures for amorphous formulations were found to range from approximately 40 °C to 96 °C. Raffinose formulations exhibited the highest values for T_g. In some cases, especially in phosphate containing amorphous formulations, two glass transitions were observed. In these scans, the lower glass transition was always observed within the range of 39 °C to 46 °C.

In other studies, different T_g values have been observed for formulations containing buffer components. In a formulation consisting of 10 mg/mL sucrose, 40 mg/mL mannitol, 20 mg/mL glycine, and sodium phosphate buffer, a low T_g of only 26 °C has been found [113]. In a different study, a formulation consisting of sucrose and disodium phosphate / potassium dihydrogen phosphate buffer was found to have a T_g of 64 to 65 °C [114]. Furthermore, it has been shown that drastic changes in T_g may occur in sucrose-phosphate and trehalose-phosphate systems depending on pH and amount of counter ion in the initial solution [44], [115].

The tested amorphous cytokine formulations with phosphate buffer generally showed two distinctive glass transitions (cf. Table 3.29), yet the glass transition at the lower temperature was weaker. Considering that phosphate buffer was present in smaller (molar) quantities than

Table 3.29: Glass transition temperatures of freeze dried formulations. For the formulation description, excipients are abbreviated with their initial letter (S: sucrose, T: trehalose, R: raffinose, M: mannitol). Melting (MT) and / or crystallisation (CT) temperatures are given if they could be determined from the DSC scan. Some scans showed two glass transitions (especially phosphate containing formulations). Often, the first glass transition was weaker (ΔC_p in the order of magnitude of 10^{-2} $Jg^{-1}K^{-1}$) and is given in parentheses. ΔC_p of the stronger glass transitions was in the range of 0.3 to 0.9 $Jg^{-1}K^{-1}$. All scans of mannitol containing formulations exhibited melting endotherms starting at approximately 140 °C. Note that the melting peak could not be determined for all formulations.

Formulation	T_g (°C)	Melting / Cryst. Temp. (°C)	
50 mg/mL S + Tris 12.5 mM	65	147 (CT)	
10 mg/mL S + PB 9.5 mM	(41), 81		
10 mg/mL S + Citrate 25 mM	68		
35 mg/mL T + Tris 12.5 mM	92		
10 mg/mL T + PB 9.5 mM	(46), 92		
10 mg/mL T + Citrate 25 mM	39, 71		
35 mg/mL R + Tris 12.5 mM	92	111 (MT)	
10 mg/mL R + PB 9.5 mM	96	119 (MT)	
10 mg/mL R + Citrate 25 mM	74		
10 mg/mL M + 2 mg/mL S (5 : 1) + Tris 25 mM	–	98 (M)	
10 mg/mL M + 1 mg/mL S (10 : 1) + Tris 25 mM	(49)	100 (MT)	
10 mg/mL M + 1 mg/mL S (10 : 1) + PB 9.5 mM	44	81 (CT)	
10 mg/mL M + 2 mg/mL T (5 : 1) + Tris 25 mM	–	96 (MT)	145 (MT)
10 mg/mL M + Tris 25 mM	–	93, 108 (MT)	148 (MT)

the lyoprotectant, this weaker glass transition might be attributed to the phosphate buffer. The observed (low) T_g values observed in all of the tested phosphate buffer containing formulations are 41 °C (amorphous sucrose / phosphate combination), 46 °C (amorphous trehalose / phosphate combination), and 44 °C (partially crystalline sucrose / phosphate combination with mannitol). No low T_g value was observed in the DSC scan of the amorphous formulation with raffinose and phosphate buffer. Within the scope of this study, a portion of the phosphate buffer which has been used for the cytokine formulations has been freeze dried without any other additives. In DSC scans which were obtained from this freeze dried buffer, no glass transition could be determined.

Assuming complete crystallisation of the phosphate buffer components during freezing, their melting points as true ionic crystals are very high (>> 200 °C) and could not be detected during the DSC experiments performed in this study. It has been reported that the addition of solutes such as mannitol and sucrose may inhibit crystallisation of dibasic sodium phosphate [19]. The weak glass transition observed for three of the total of four phosphate buffer containing formulations could be an indicator for incomplete crystallisation of the phosphate buffer.

The glass transition of a substance may be followed by its crystallisation [114]. An exothermal event which might indicate crystallisation of the buffering agent was observed directly after the

first glass transition in the cytokine formulation additionally containing trehalose and phosphate buffer, cf. Figure 3.49. Similar exothermal events were observed at similar temperature ranges in scans of other formulations containing a different buffering agent (cf. Figure 3.50). Here, the exothermal events might also be explained as crystallisation of the buffering agent contained in the formulation, although no previous glass transition could be detected.

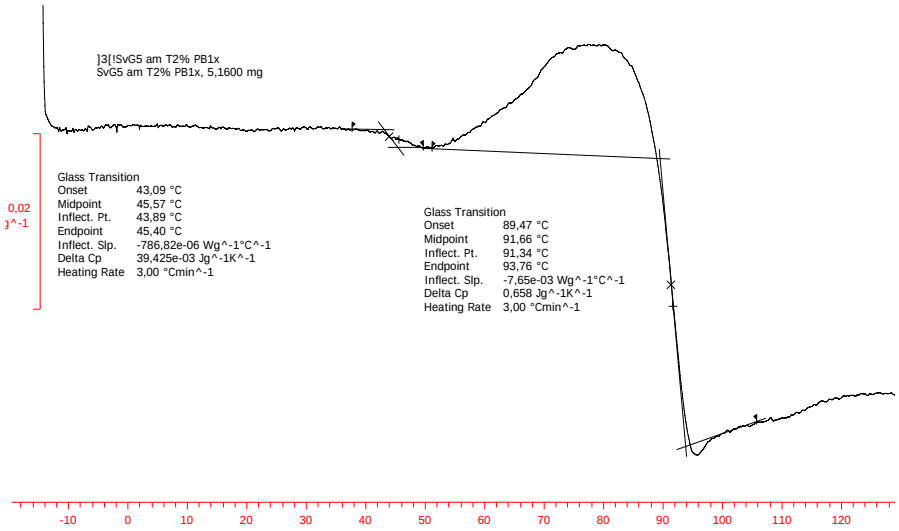

Figure 3.49: DSC scan of the formulation containing the cytokine with trehalose and phosphate buffer. Exotherm is upwards. The first, weak glass transition was observed at approximately 46 °C, the second, large glass transition at approximately 92 °C. The exotherm in between the two glass transitions might be explained as the crystallisation of an amorphous fraction of the buffer component. A small amount of enthalpy relaxation was also observed.

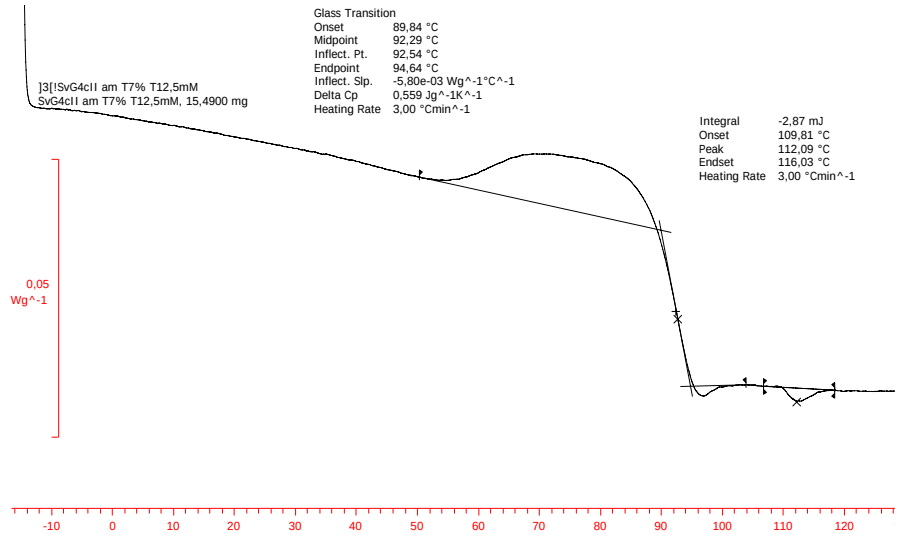

Figure 3.50: DSC scan of the formulation containing the cytokine with trehalose and Tris buffer. Exotherm is upwards. The glass transition was observed at approximately 92 °C. The exotherm just prior to the glass transition might be explained as the crystallisation of an amorphous portion of the buffer component.

Another possible explanation for the low, weak glass transition might be the influence of the cytokine included in the formulation. The cytokine was also present at a much lower molar

quantity than the lyoprotectant. However, proteins such as the cytokine used in this study usually behave as "strong" glasses and exhibit very broad glass transitions with small changes in the heat capacity [116]. These glass transitions of "strong" glasses are very difficult to determine from a DSC scan. For this reason, it seems unlikely that the observed weak, but distinctive glass transitions at the lower temperatures are caused by the cytokine. The exothermal event following the first glass transition could not be explained by the influence of the cytokine.

The partial loss of the remaining adsorbed water in the freeze dried formulation might also be attributed with a glass transition. Then the lyophilisate - or a part of it with a higher residual moisture, i.e. the exterior surface - would initially show a low glass transition, lose a small amount of water (exothermal event), and the "drier" formulation will show a subsequent, higher glass transition. Loss of adsorbed water at such low temperatures (below 100 °C) would mean that the water was only attached by weak bonds. A minor water uptake might have been caused during sample preparation, as the residual moisture in the used glove box could not be maintained at 0 % relative humidity during the whole time. Moisture values stepped up as high as approximately 5 % for short intervals during the sample preparation. However, even though the adsorbed water may only exhibit weak bonds to the lyophilised matrix, the temperature at which water desorption occurs is usually higher, above 100 °C [114].

The higher T_g values are in agreement with glass transition temperatures reported for sucrose (65 °C according to [19], also reported as 80 °C at 0 % RH, [117]), trehalose (117 °C at about 0 % RH, [118]), and raffinose (116 °C at 0 % RH, [119]), all with low residual moisture contents, in the literature. It has also been reported that even small amounts of water in the sample decrease T_g significantly [119], [44]. This susceptibility to slight changes in residual moisture accounts for the span of T_g values reported in the literature for amorphous excipients (and especially for sucrose). The residual moisture content in the samples of approximately 0.5 % could be an explanation for the depression of T_g in amorphous samples in comparison to some of the literature values. Applying the Gordon-Taylor equation to an amorphous trehalose formulation with a residual moisture of 0.5 % yields a T_g of the mixture of 111 °C, based on a T_g value of water of −138 °C [120], [109]. This calculated value is only an approximation, because the true density of amorphous trehalose in the lyophilisate is not known, but assumed to be not more than the density of crystalline trehalose (1.54 g/cm^3, [121]).

The T_g of anhydrous citric acid has been determined to be approximately 11 °C [109]. The approximate result of the Gordon-Taylor equation for the three-component mixture of Trehalose (10 mg), Citrate (4.8 mg), and a residual moisture of 0.5 % is 44 °C. This value is close to the temperature of the lower glass transition which has been found for the amorphous cytokine formulation with trehalose and citrate buffer (cf. Table 3.29). In this formulation, a low glass transition temperature of 39 °C (possibily caused by the mixture of amorphous citrate buffer, trehalose, and residual moisture) and a higher glass transition of 71 °C, attributable to trehalose and residual moisture, are observed.

For pure Tris buffer, no glass transition temperature could be determined. The melting point of freeze dried Tris buffer was found to be approximately 102 °C. The melting temperatures of partially crystalline and the purely crystalline formulations are lower than reported in the literature. Melting temperatures for the different mannitol polymorphs have been reported as 155 °C (δ-polymorph) and approximately 165 °C (α-, β-polymorphs) [104]. It is possible that mannitol forms eutectic mixtures with other crystalline components, i.e. crystalline buffer. The eutectic melting temperature of the mixture of two components is usually lower than the melting temperatures of the individual components [3], [122]. In the formulation containing mannitol and (presumably crystalline) phosphate buffer, however, no melting temperature could be determined.

3.5.5 Gel Electrophoresis and Activity Tests

A sample of each formulation was analysed by gel electrophoresis to study the extent of aggregation / formation of oligomers of the cytokine during the freeze drying process. The gels of all formulations showed a thick band at approximately 17 kDa, corresponding to the cytokine monomer (cf. Figure 3.51 and Table 3.30).

Table 3.30: Position of samples in the lanes of the electrophoresis gel shown in Figure 3.51. Numbering is from left to right.

Lane No.	Sample Descritption
1	0.25 μL Prestained Marker
2	0.5 μg bulk cytokine (reference, stored at -70 °C)
3	0.5 μg Form. 1: Sucrose 50 mg/mL, Tris 12.5 mM
4	0.5 μg Form. 2: Sucrose 10 mg/mL, Phosphate 1-fold
5	0.5 μg Form. 3: Sucrose 10 mg/mL, Citrate 25 mM
6	0.5 μg Form. 4: Trehalose 35 mg/mL, Tris 12.5 mM
7	0.5 μg Form. 5: Trehalose 10 mg/mL, Phosphate 1-fold
8	0.5 μg Form. 6: Trehalose 10 mg/mL, Citrate 25 mM
9	0.5 μg Form. 7: Raffinose 35 mg/mL, Tris 12.5 mM
10	0.25 μL Mark12 standard

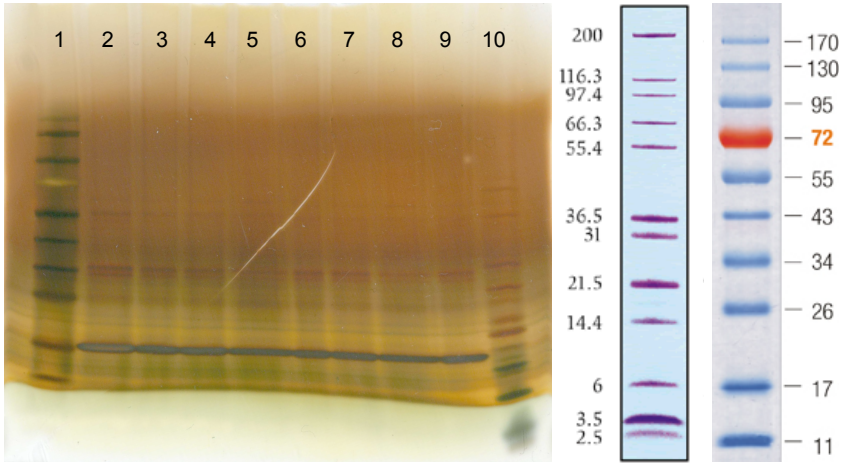

Figure 3.51: Electrophoresis gel of bulk cytokine and formulations 1 through 7. For the positioning of the samples see Table 3.30. Samples are non reduced. Thick bands of cytokine are visible at approximately 17 kDa in all of the tested samples. Thinner bands are visible at approximately 34 kDa, a third band is just perceptible in between 50 and 60 kDa. Pictures of the standard 2.5 to 200 kDa and of the prestained marker are shown to the right of the gel.

A thinner band was visible at approximately 34 kDa and traces of a third band showed at 50 to 60 kDa. The pattern of bands was similar to the pattern of the original bulk cytokine stored at -70 °C which was used as a reference.

The bands at 34 kDa and 50 kDa were probably caused by aggregation of two or more monomers. These bands at higher molecular weight disappeared almost completely after treatment of the samples with dithiothreitol (DTT) as a reducing agent prior to gel electrophoresis, as Figure 3.52 shows. Size exclusion chromatography performed at a later stage confirmed the existence of oligomers in the freeze dried samples.

The formulation containing mannitol, trehalose, and Tris buffer was also tested after one week of storage at 37 °C and at a high relative humidity (> 95 %). 40 °C and 75 % relative humidtiy are considered as the standard conditions for accelerated storage. The non-standard conditions described above were chosen partly to simulate a "worst case" scenario, and partly for practical

Table 3.31: Positioning of the samples on the lanes of the electrophoresis gel shown in Figure 3.52. Samples were tested after storage for one week at 37 °C.

Lane No.	Sample Descritption
1	0.25 μL Prestained Marker
2	1 μg bulk cytokine (stored at −70 °C)
3	1 μg cytokine / mannitol 10 mg/mL / trehalose 2 mg/mL, Tris 25 mM
4	0.25 μL Mark12 standard
5	0.25 μL Prestained Marker
6	1 μg bulk cytokine, reduced
7	1 μg cytokine / mannitol 10 mg/mL / trehalose 2 mg/mL, Tris 25 mM, reduced
8	0.25 μL Mark12 standard

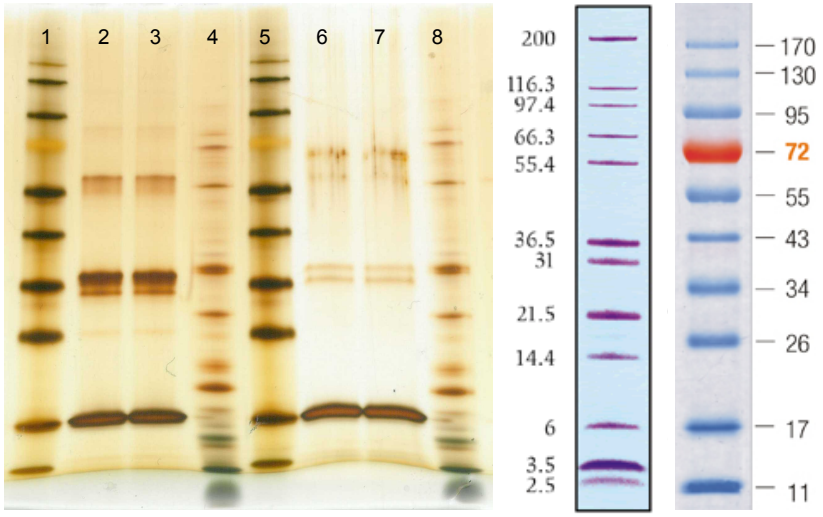

Figure 3.52: Electrophoresis gel of the bulk cytokine and the partially crystalline formulation containing the cytokine with mannitol, trehalose, and Tris buffer after storage at 37 °C for one week. Samples were tested non-reduced (left) and reduced (right). For positioning of the samples see Table 3.31. Thick bands of cytokine are visible in both samples at approximately 17 kDa. Thinner bands are visible at approximately 34 kDa, a third band is just perceptible in between 50 and 60 kDa. The bands at higher molecular weight disappeared almost completely after treatment with a reducing agent. Pictures of the standard 2.5 to 200 kDa and of the prestained marker are shown to the right of the gel.

reasons: As there were no climate chambers available, the samples were stored in incubators used for proliferation of cell cultures. The temperature and humidity in these incubators are subject to tight control. It was expected that such a short storage time at this temperature would already have a strong influence on the activity of the cytokine contained in the formulation. The temperature of 37 °C was considered close enough to 40 °C to be representative for the temperature condition of accelerated storage. The higher humidity in the incubator, however, might impose a considerably higher stress on the formulation than the standard relative humidity for short term storage.

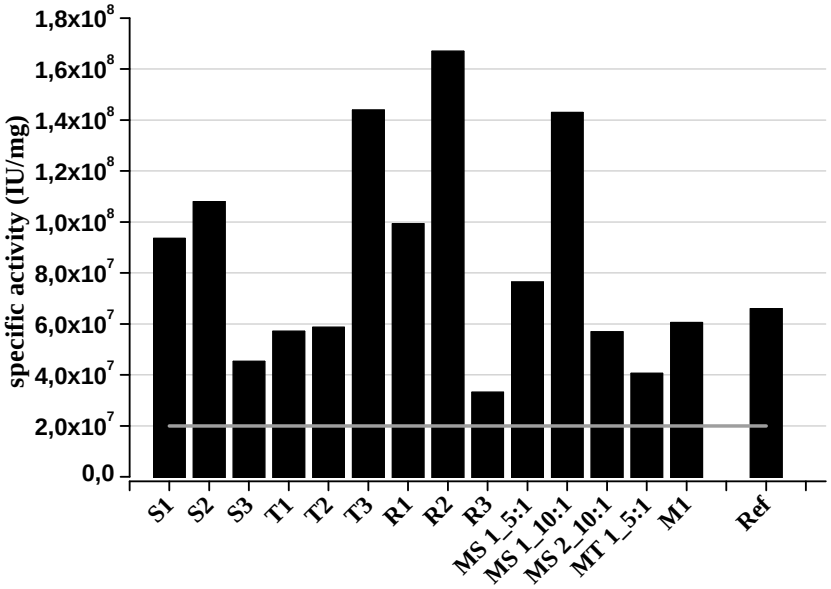

Figure 3.53: Cytokine activities as determined with a specific proliferation assay directly after freeze drying. S: amorphous sucrose formulations, T: amorphous trehalose formulations, R: amorphous raffinose formulations. MS / MT: partially crystalline formulations with sucrose or trehalose, respectively (mass ratio of mannitol to stabiliser is provided with the label). 1: formulation contains Tris buffer, 2: formulation contains phosphate buffer, 3: formulation contains citrate buffer. Ref: bulk cytokine stored at −70 °C was used as a reference. Grey line: required minimal activity of formulations ($2{\cdot}10^7$ IU/mg).

The results of the gel electrophoresis performed on the sample which had been stored under these aggressive conditions for the short period of one week are shown in Figure 3.52 and Table 3.31. The pattern of the bands on the gel had not changed in comparison to the reference stored at −70 °C, no increase in non-reducible aggregates could be detected.

These data suggest that the cytokine chosen for this study resists the stresses imposed during mixing of the formulation, freezing, freeze drying, and subsequent (short term) storage under aggressive conditions surprisingly well. Although this behaviour is not generally expected for proteins, other studies have already shown that well-formulated proteins may be very robust even at temperatures exceeding room temperature [36]. For example, the protein albumin has been frequently used as a lyoprotectant for another protein [19].

In addition to the verification of the cytokine concentration after freeze drying, the cytokine activity was tested for all formulations and, as a reference, for the bulk cytokine, with a specific proliferation assay. The aim was to create a formulation with a minimum activity of $2{\cdot}10^7$ IU/mg. This dosage strength is considered most convenient for the planned purpose of the cytokine formulation. A certain loss of the initial activity due to the stresses attributed to freeze drying was expected, and the initial amount of cytokine in each formulation contained a surplus (an overage). All formulations were tested directly after freeze drying and all formulations fulfilled the minimum activity condition with individual activities ranging from $3.3 \cdot 10^7$ IU/mg (raffinose + citrate buffer) to $1.7 \cdot 10^8$ IU/mg (raffinose + phosphate buffer), see Figure 3.53.

The activity assay was performed only once for each formulation and the bulk cytokine. As this is a biological assay, the variability is considerably high even though all the results were compared to an international standard. Multiple repetitions would be necessary to verify and ascertain the apparent activity differences from one formulation to the next and from each formulation to the reference (the bulk cytokine). The amount of sampling solution was chosen such that the theoretically expected activity for each formulation was equal to the activity of the reference. In this way, none of the tested formulations should have a cytokine activity

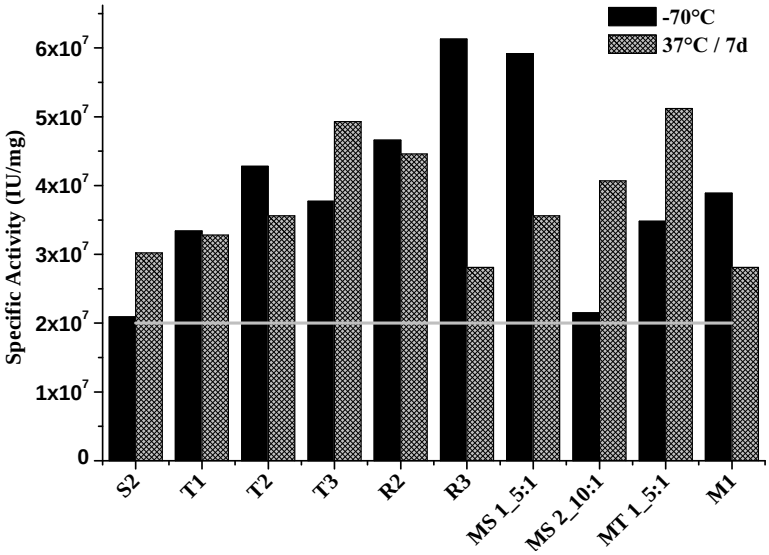

Figure 3.54: Cytokine activities after one week of storage at −70 °C versus one week of storage at 37 °C. S, T, R, M: sucrose, trehalose, raffinose, mannitol, respectively (mass ratio of mannitol to stabiliser for partially crystalline formulations is provided with the label). 1: formulation contains Tris buffer, 2: formulation contains phosphate buffer, 3: formulation contains citrate buffer. Grey line: required minimal activity of formulations ($2 \cdot 10^7$ IU/mg).

exceeding the activity of the tested sample of the bulk cytokine. The degree of variability in the assay can be roughly estimated from the range of the highest activity results to the activity of the reference, i.e. the variability is approximately a factor of 2. Taking this into account, the apparent activity differences which have been determined with the biological assay in between the individual formulations are insignificant.

Selected formulations were tested after one week of storage in the incubator used for cell proliferation (37 °C, high relative humidity of > 95 %). The reasons for choosing these storage conditions have been described earlier in this section. The activities of the samples of stressed formulations were compared to the activity of another sample of the same formulation stored at −70 °C for the same period of time. It was expected that no significant change of activity would occur during storage at this low temperature.

Differences in between the "reference formulations" stored at −70 °C and the stressed samples of less than approximately ± 80 % can be attributed to the inherent variability of results. Therefore, even though the results presented in Figure 3.54 might at first glance suggest a loss of activity in some formulations after storage, no significant change in activity can be postulated from the data obtained.

The formulation of cytokine with raffinose and citrate buffer (R3) exhibited an activity of $3.3 \cdot 10^7$ IU/mg directly after freeze drying, which was the lowest activity found in the initial activity test performed directly after freeze drying for all formulations (cf. Figure 3.53). After one week of storage at 37 °C, the value has not changed significantly ($2.81 \cdot 10^7$ IU/mg, Figure 3.54). The sample of this formulation which had been stored at −70 °C for one week and which was used as a reference in Figure 3.54 shows the highest activity of all formulations in the test performed after short term storage ($6.13 \cdot 10^7$ IU/mg). This value is almost twice as high as the activity which had been determined prior to storage. A similar variance is found for the comparison of initial activity to activity after storage at −70 °C for one week for the other formulations which have been tested after short term storage (i.e. S2).

The data obtained after the short storage time of one week are not discriminatory. Testing after longer storage times would be needed to reveal differences in the storage stability of the different formulations.

3.5.6 Conclusions from Cytokine Formulation Experiments

The most important factor for choosing a formulation should be the retention of activity of the active ingredient. In the present study, there was no significant difference in activities of cytokine formulations as determined directly after freeze drying because the API was, surprisingly, very robust. The storage stability of the freeze dried formulation is also a major concern for formulation development. Data for long term storage stability of the tested cytokine formulations are not yet available as this formulation development was not the main scope of this work. Glass transition temperatures T_g were found to be predictive for the expected storage stability: the glass transition temperature should be significantly higher than the storage temperature [113], [114]. Under this aspect, the partially crystalline as well as the trehalose and raffinose containing amorphous formulations are the most promising ones. Unfortunately, the amorphous raffinose formulations did not form smooth cakes during lyophilisation but showed cracks. The same is true, to a lesser extent, for amorphous trehalose formulations. An easy-to-use lyophilised product should also have a short reconstitution time. This characteristic is best fulfilled for the partially crystalline formulations.

Considering all aspects, the mannitol containing formulations best fulfil the requirements. The mannitol-trehalose-Tris formulation was the first choice for this particular cytokine. If an amorphous formulation must be selected, i.e in order to reduce the number of formulation components which might interfere with the intended use of the cytokine, the sucrose containing formulations seem to yield best-looking lyophilisates. Still, the decision should best be based on long term storage stability data of the active ingredient freeze dried in the individual formulations. At least in these studies, raffinose showed no significant advantages to the well established stabilisers sucrose and trehalose.

It is recommendable to include an annealing step at -20 °C for several $(4-6)$ hours in the freeze drying cycle for the selected partially crystalline cytokine formulation (mannitol-trehalose-Tris) to ensure the complete crystallisation of mannitol. The product temperature during primary drying may be as high as -15 to -20 °C. The shelf temperature required for this product temperature will be high, at least -5 °C. Depending on the fill volume / fill depth of the solution and the gradually increasing product resistance with advancement of primary drying, the shelf temperature might need to be lowered (i.e. to -10 °C) during the last third of primary drying to avoid excessive warming of the product.

3.6 Case Study with a Cytokine: Testing of "First Guess" Freeze Drying Cycles for FDS and Well Plates

In the scope of this research, the information gained from freeze drying experiments with cytokine formulations in 2R vials were used as a basis for "first guess" freeze drying cycles using the two non-vial container systems (96-well PCR-plates and FDS). The information gathered from vial experiments consisted of a single product temperature over time profile for each formulation, collected during one of two non-optimised freeze drying runs. For this part of the research, the amorphous cytokine formulation containing sucrose and Tris buffer was chosen. (For the apparently best suited, partially crystalline formulation containing mannitol, trehalose, and Tris buffer, a suggestion for a "first guess" freeze drying cycle was given in the previous section 3.5.6.)

The amorphous cytokine formulation containing 100 mg/mL sucrose as a stabilising excipient and Tris buffer (12.5 mmol/L) was freeze dried in 96-well PCR-plates with Al-blocks and in the VirTis Freeze Drying System™ using two individual freeze drying cycles. The initial shelf temperature for primary drying was estimated from sublimation test data and from product temperature data of the freeze drying runs in $2R$ vials. At first, a target product temperature was defined for the chosen formulation. As the critical formulation temperature of the sucrose-Tris-formulation was low (approximately −35 °C), but the anticipated fill depth in well plates and FDS was not more than approximately 1 cm, an intermediate duration of the primary drying phase was expected. The safety margin in between critical formulation temperature and target product temperature was therefore set to 2 °C, with a resulting target product temperature of approximately −37 °C.

The product temperature profile during freeze drying of this formulation in 2R vials showed a slow, but steady increase of the product temperature at a shelf temperature set point of −34 °C, until the product temperature came very close to the target product temperature. After approximately two thirds of the total primary drying time for this formulation, the shelf temperature in the freeze drying run with 2R vials was lowered to −36 °C to avoid excessive warming of the formulation prior to completion of primary drying. A similar product temperature profile as observed for 2R vials was expected for the VirTis Freeze Drying System™. For freeze drying this formulation in well plates with Al-blocks, a more pronounced plateau phase was expected when using this container system.

The "initial guess" for freeze drying cycles for both container systems also incorporated the "initial high shelf temperature approach" suggested in section 3.2.9 for 96-well PCR-plates. The initially higher shelf temperature was intended to provide additional heat to compensate the amount of heat needed for warming up the Al-blocks used with each of the container systems. However, the initial high shelf temperature was set with prudence for the cycle using well plates to only −34 °C, a few degrees higher than the anticipated target product temperature. For the second freeze drying run performed with the FDS, the initial high shelf temperature was set to −30 °C with already more confidence.

The chamber pressure set point was calculated based on the critical formulation temperature / target product temperature and using an empirical equation proposed by Pikal et al. [20]. Applying the equation to the tested formulation yielded a chamber pressure set point of 55 mTorr.

After the initial shelf temperature was reached, the product temperature was closely monitored. The shelf temperature was readjusted during primary drying. The settings used for the freeze drying cycles are summarised in Table 3.32. In both runs, the volume of formulation per cavitty was 100 μL. Due to the narrow tips of the wells, this volume corresponds to a fill depth of approximately 1 cm in PCR-plates. The same volume in the small tubes of the freeze drying system equals a fill depth of roughly 0.3 cm. This difference in fill depth explains the large differences in total primary drying times of approximately 58 h for 96-well PCR-plates and only approximately 22 h for the Freeze Drying System™.

As the target product temperature was low (−37 °C), the initial shelf temperature set point was also very low in both cases. For the cycle performed with the Freeze Drying System™, the initial shelf temperature of −30 °C was subsequently adjusted to the required shelf temperature of −34 °C after about 40 min. For the freeze drying run performed with well plates, −34 °C was chosen as the initial shelf temperature. It was adjusted after approximately 3 h to −36 °C.

Table 3.32: Overview of lyophilisation parameters for freeze drying the chosen amorphous cytokine formulation in the Freeze Drying System™ and PCR-plates. Ramping rates were 1 °C/min except for ramping from end of primary drying to the secondary drying shelf temperature. Here, the ramp rate was 0.2 °C/min. Holding times for each step are given in the right column for each container system.

Parameter	96-Well PCR-Plates		Freeze Drying System	
freezing programme	5 °C	0.3 h	5 °C	0.3 h
	−5 °C	0.3 h	−5 °C	0.3 h
	−50 °C	1 h	−50 °C	1 h
chamber pressure	55 mTorr		55 mTorr	
initial shelf temp. prim. drying	−34 °C	3 h	−30 °C	0.7 h
shelf temp. adjustments	−36 °C	54.3 h	−34 °C	4.2 h
			−36 °C	16.6 h
total prim. drying time		57.9 h		22.2 h
shelf temp. second. drying	40 °C	4 h	40 °C	4 h

The need for lowering the shelf temperature to almost target product temperature was explained with an increase of product resistance of the dried layer in both freeze drying runs.

Figure 3.55 shows the product temperature over time profiles of both cycles. It can be seen that the product temperature was very close to, even slightly higher than the target product temperature throughout primary drying of the cytokine formulation in PCR-plates. The product temperature of the formulation freeze dried in the Freeze Drying System™ exceeded the designated product target temperature by approximately 1 °C for a long interval during primary drying. At one point close to the beginning of primary drying it also came very near to the critical formulation temperature of −35.3 °C. Figure 3.56 shows photographs of samples taken after completion of the respective freeze drying cycle. For both container systems, the lyophilisates show a small degree of shrinkage. No other signs of macroscopic collapse are visible.

Glass transition temperatures of the lyophilisates were determined as well. The mid points of the glass transitions were determined as 63 °C for the cytokine formulation in the Freeze Drying System™ and as 61 °C for the same formulation freeze dried in PCR-plates. These temperatures are very close to T_g determined for this formulation freeze dried in $2R$ vials (65 °C, Table 3.29). The temperature of the sucrose crystallisation peak of this formulation was approximately 147 °C for lyophilisates from all container systems.

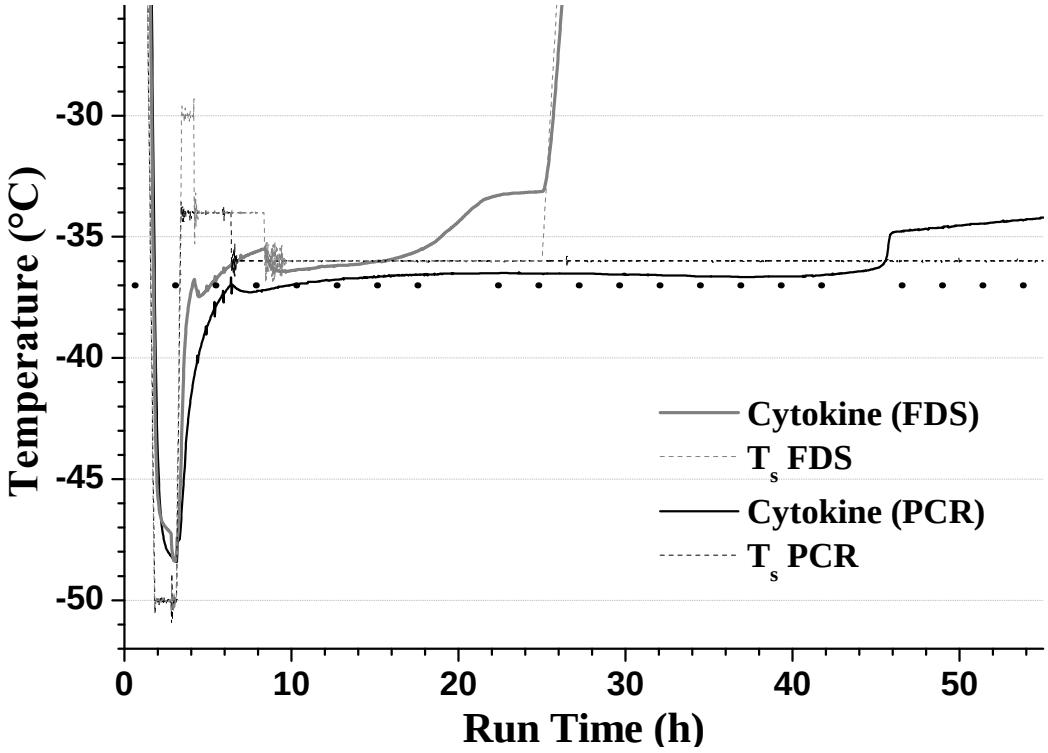

Figure 3.55: Product temperature over time profiles for the formulation with cytokine, sucrose, and Tris buffer freeze dried in PCR-plates (black line) and in the Freeze Drying Sytem™ (FDS, grey line). The black and grey short dashed lines show the shelf temperature over time profiles for the cycle with PCR plates and for the cycle with FDS, respectively. The black dotted line shows the designated target product temperature. The critical formulation temperature was −35.3 °C.

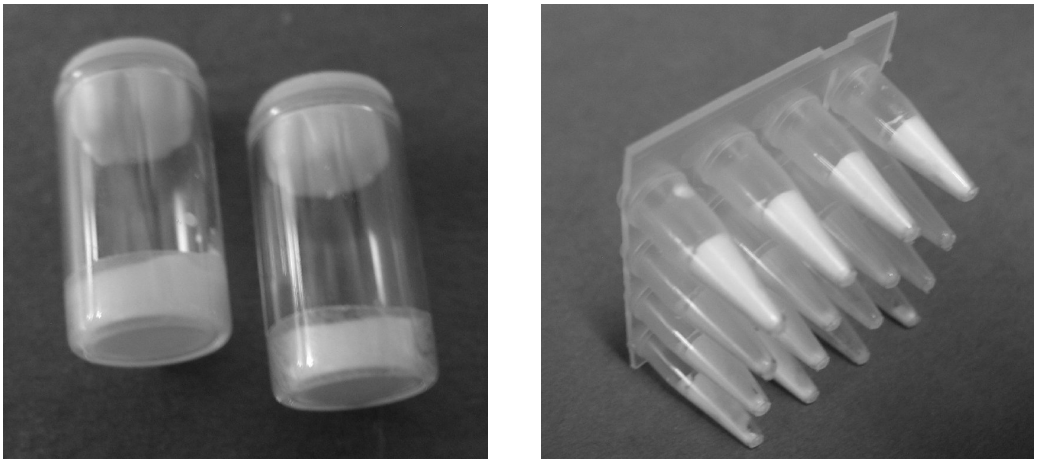

Figure 3.56: Photographs of the cytokine formulation containing sucrose and Tris buffer freeze dried in the Freeze Drying System™ (left panel) and in PCR-plates (right panel). A small amount of shrinkage is visible for both lyophilisates.

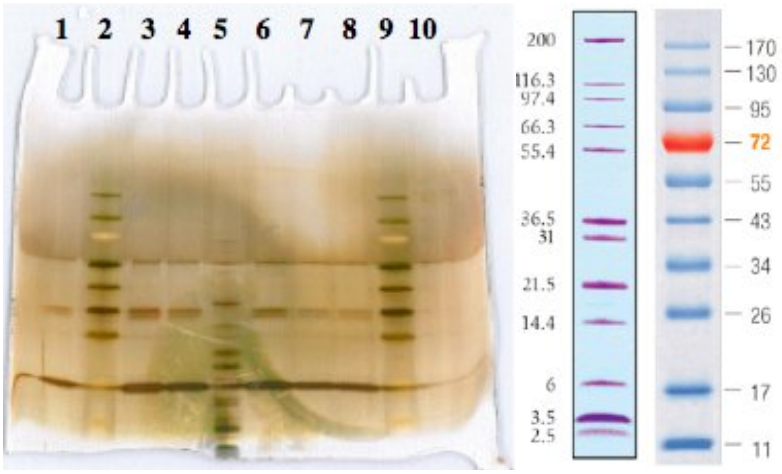

Figure 3.57: Electrophoresis gel of bulk cytokine and the cytokine in the amorphous sucrose-Tris formulation after freeze drying with subsequent storage at −70 °C and after storage at 37 °C for one week. Samples were tested non-reduced. For the positioning of the samples see Table 3.33. Further descriptions in the text.

Table 3.33: Positions of samples of the electrophoresis gel shown in Figure 3.57. Apart from the cytokine, the tested formulation contained 10 % sucrose (Sucr) and 12.5 mM Tris buffer.

Lane No.	Sample Descritption
1	0.25 μg bulk cytokine
2	0.25 μL Prestained Marker
3	0.25 μg cytokine / sucr / Tris processed in FDS, stored at −70 °C
4	0.25 μg cytokine / sucr / Tris processed in FDS, stored at 37 °C
5	0.25 μL Mark12 standard
6	0.25 μg bulk cytokine
7	0.25 μg cytokine / sucr / Tris processed in PCR-plate, stored at −70 °C
8	0.25 μg cytokine / sucr / Tris processed in PCR-plate, stored at 37 °C
9	0.25 μL Prestained Marker

The integrity and activity of the cytokine was tested directly after freeze drying and after storage at 37 °C for one week. The same conditions and methods as used for the formulation development in $2R$ vials were applied. The bands in the SDS-PAGE of bulk cytokine and freeze dried formulations were identical in position and thickness. The bands of all samples looked similar, regardless of the origin of the sample (PCR-plate or a tube of the Freeze Drying System™) or storage condition (−70 °C or 37 °C for one week). Figure 3.57 shows a photograph of the gel. The bands at 55 kDa are artefacts. The positioning of the samples on the lanes of the gel is given in Table 3.33.

Results of the specific cell-proliferation assay are shown in Figure 3.58. Storage stress tests (one week, 37 °C) were carried out with samples of the cytokine formulation processed in PCR-plates and in the tubes of the Freeze Drying System™. The relative humidity during the storage tests was high (> 95 %), as the incubators for cell proliferation were again used instead of climate chambers. The small tubes were only capped with matching stoppers which provided no air tight sealing. A temporary seal in the form of a self adhesive foil (designated for the use with samples for ELISA testing) was applied to the well plates. This foil did not supply a permanent barrier to gases and hmidity. Due to the low glass transition temperature of the formulation and additional

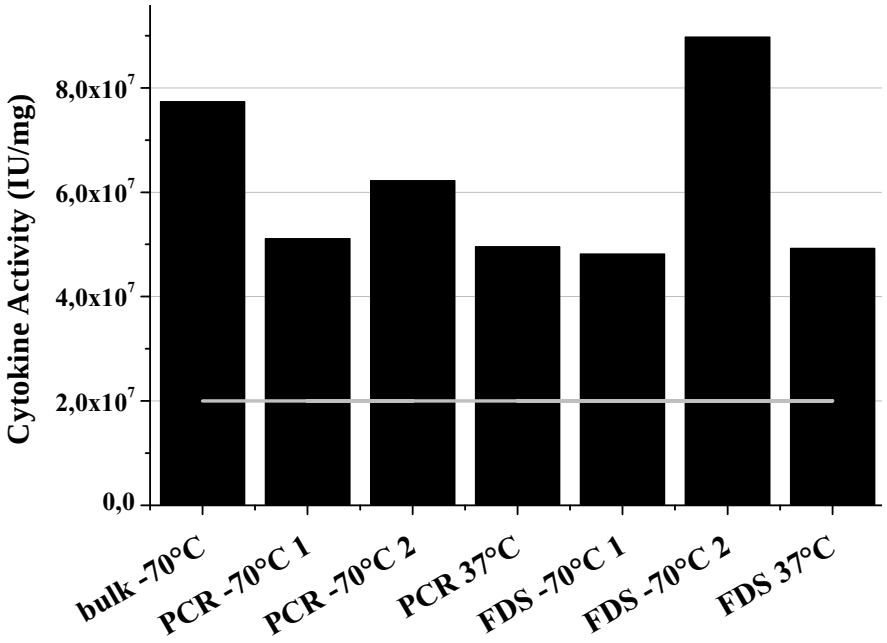

Figure 3.58: Activities of cytokine freeze dried in 96-well PCR-plates and in freeze drying system determined by specific cell proliferation assay. Second value determined for formulation in FDS stored at −70 °C is higher than value for bulk cytokine used as reference. This shows that results are liable to a rather high variability.

moisture uptake during storage, the lyophilisates shrank during the storage stress test.

Nonetheless, the activity of the cytokine after stress testing was still high enough to fulfil the minimum requirement of $2 \cdot 10^6$ IU/mg. The individual results ranged from $4.8 \cdot 10^6$ IU/mg for the cytokine freeze dried in the FDS, tested directly after the freeze drying run, to $9.0 \cdot 10^6$ IU/mg for the same formulation in the same container after one week of storage at −70 °C. The reference which was tested at the same theoretical concentration (purified bulk cytokine which had been stored at −70 °C, as well) was found to have an activity of only $7.7 \cdot 10^6$ IU/mg, so the range of values for the different cytokine preparations stored at −70 °C for one week again illustrates the variability of the results. The activities found for the cytokine formulation freeze dried in the two different small container systems were within the same range as the activities which had been determined not only for this, but for all tested formulations freeze dried in vials (cf. section 3.5.5).

It could be shown that 96-well PCR-plates and the Freeze Drying System™ are suitable containers for freeze drying. These containers are preferable if only small aliquots of a formulation are needed per application. These small quantities may be needed, for example, for pharmaceutical active ingredients of high potency or potent agents used in molecular biology. Well plates with their cone-shaped tips are suitable containers for volumes as small as 20 µL. If even smaller quantities need to be freeze dried, there may be a risk of product blow-out. The Freeze Drying System™ yields good results and short primary drying times for slightly higher fill volumes up to approximately 200 µL.

The cytokine used as a model API proved to be very stable, even in the one formulation which had been tested with 2R vials without addition of any lyoprotectant. Other APIs may be more delicate, causing significant stability problems that need to be addressed more profoundly during formulation development.

Product temperature over time profiles are similar to the data obtained from vial freeze drying. Minor adaptations need to be considered in order to optimise the freeze drying process. The most effective way of shortening primary drying times of formulations freeze dried in small containers with the additional use of aluminium blocks is ramping the shelf temperature up to

a temperature above the designated primary drying shelf temperature at the very beginning of the primary drying phase. This procedure shortens the time interval required until the product reaches the desired target product temperature in primary drying. Care must be taken not to exceed the target product temperature and to readjust the shelf temperature set point at the appropriate time.

As data suggests (Figures 3.55, 3.56), there exist excipients / formulations which tolerate a higher target product temperature than would be assumed from T_c values, exhibiting only tolerable signs of shrinkage. If this additional margin for processing conditions is used, the primary drying phase could also be shortened. However, formulations containing amorphous ingredients (lyoprotectants) which have been processed during freeze drying at temperatures exceeding the critical formulation temperature may exhibit longer reconstitution times due to a decrease in the total product surface / the porosity of the lyophilisate.

Chapter 4

Summary and Conclusion

For the first time, heat transfer coefficients have been determined for three different container systems designed for small fill volumes: 96-well PCR-plates, the VirTis Freeze Drying Array™, and $2R$ serum tubing vials (cf. Tables 3.2, 3.17, and 3.19). For all three container systems, a thorough qualitative analysis of the contribution to heat transfer by radiation, conduction through the gas, and by direct conduction has been performed as a help for freeze drying cycle optimisation when using these container systems.

For 96-well PCR-plates placed directly on a freeze dryer shelf, the heat transfer coefficients determined from sublimation tests with pure water were a good help in predicting the primary drying times of product runs (cf. Section 3.2.2, i.e. Table 3.4). For this set-up, radiative heat transfer plays a major role in total heat transfer into the product (cf. Section 3.1.3, Figure 3.3 on page 65). This leads to heterogeneous drying as atypical radiation strongly impacts the drying process in wells in edge positions (cf. Figures 3.16, 3.17). An optimised freeze drying cycle using well plates in this set-up needs comparably high settings of the shelf temperature in combination with an intermediate chamber pressure (not less than approximately 80 mTorr) to minimise the time needed for the primary drying phase and minimise drying heterogeneity (cf. section 3.2.9).

For well plates inserted into aluminium blocks, heat transfer by conduction through the gas significantly contributes to the overall heat transfer into the product, whereas heat transfer by radiation is reduced (cf. Section 3.1.5 on page 65, and Figure 3.7 on page 69). The better heat transfer achieved by conduction though the gas due to the small separation distance between shelf surface and A-block as well as between Al-block cavity and PCR-plate is, to a certain extent, balanced by the high heat capacity of the Al-block which needs a significant amount of energy (and time) to warm up to approximately the shelf temperature set point (see Section 3.1.5). This increase in primary drying time caused by the Al-block warming phase can be partially circumvented by initially using a high setting for the shelf temperature in primary drying and then lowering the shelf temperature to its appropriate set point when the product temperature comes close to the targeted product temperature.

The prediction of primary drying times based on the heat transfer coefficients which had been determined from sublimation tests with pure water was less accurate for the set-ups of well plates with Al-block (cf. Section 3.2.2). This difference between actual and predicted primary drying time durations could probably be explained with the difficulty in determining the correct area for heat transfer. In this study, all calculations of heat transfer coefficients were based on the assumption of steady state conditions. Freeze drying of a product in a well plate with Al-block seems to differ significantly from a (pseudo-) steady state (i.e. varying area for heat input), so that a different approach taking into account the constant changes in area for heat transfer, product temperature, and sublimation interface should lead to better results.

Heat transfer coefficients of well plates were not only determiend from sublimation tests with water (fill volume 200 μL), but also from product runs with excipient solutions (trehalose / mannitol solution, fill volume 100 μL or 20 μL, cf. Section 3.2.6 on page 86). For excipient runs with Al-block, these heat transfer coefficients were invariably smaller than the heat transfer coefficients determined previously from sublimation tests with pure water. It is assumed that the area for heat transfer needs to be determined more precisely for each of these fill volumes in

order to achieve better congruency between heat transfer coefficients determined from different fill volumes.

The heat transfer coefficients of the Freeze Drying System™ (FDS) were among the highest of all container systems evaluated in the scope of this research (cf. Table 3.17). The determined gap width of the combined separation distances (shelf surface to Al-block plus Al-block cavity to glass tube wall or bottom) was the smallest in this study (refer to Section 3.3.2, Table 3.18 on page 121). This small gap width results at least partially out of the remarkably flat and even bottom of the tubes with good contact to a flat surface (cf. Section 3.3.1, Figure 3.34 on page 117). In addition to a high amount of heat transfer due to gas conduction which increases with the chamber pressure, the black paint of the Al-block with its high emissivity may also significantly increase the amount of heat input by radiation (cf. Section 3.3.2). For freeze drying cycle optimisation in this container system, similar rules apply as for well plates used with Al-blocks.

The heat transfer coefficients determined for the $2R$ vials are in good agreement with heat transfer coefficients for other tubing vials found in the literature [83]. They are in the same order of magnitude as the heat transfer coefficients determined for the FDS (see Tables 3.17 and 3.19). Atypical radiation strongly impacts heat transfer into edge vials, resulting in approximately 30 % higher heat transfer coefficients for the tested 2R vials in these extreme positions (also Table 3.19). For best drying homogeneity, the array of product filled vials should be surrounded by dummy vials filled with a placebo solution which effectively blocks out this extra radiation.

The rules for freeze drying cycle optimisation described for the two non-vial container systems (well plates and FDS) were successfully tested in a single freeze drying run per container system with a new formulation developed for this purpose. These rules were integrated into a guideline for formulation and freeze drying cycle development which is included in the appendix to this work.

The SMART Freeze Dryer™ cycle optimisation software was tested for applicability to freeze drying in 96-well PCR-plates (cf. section 3.2.10). The SMART™ optimisation mechanism yielded a rather aggressive cycle recipe. The manometric temperature measurements were in agreement with thermocouple data for the beginning of the primary drying phase, when the sublimation interface was still high. Adaptations of the MTM algorithm are needed, taking into account i.e. the constantly changing area of the sublimation interface, to better fit MTM data to freeze drying in well plates.

It could be shown that all of the tested container systems are suitable for freeze drying. Well plates (preferably with Al-blocks) are best suited for very small volumes (less than 100 μL). The VirTis Freeze Drying System™ is a good alternative for volumes in between 100 μL and 400 μL. They seem to be a good alternative as a primary packaging material for very potent drugs that need to be administered in small volumes. Increasing research over the past two decades for biotechnological products may create a strong demand for such an alternative [123], [9]. For fill volumes exceeding approximately 400 μL, tubing vials can still be considered as the "gold" standard for freeze drying.

Chapter 5

German Summary (Deutsche Zusammenfassung)

Zum ersten Mal wurden Wärmeübergangskoeffizienten von drei Behälterarten bestimmt, die für kleine Füllvolumina ausgelegt sind: von 96-Well PCR-Platten, dem VirTis Freeze Drying System™, und von 2*R* "tubing" Vials mit flachem Boden (s. Tabellen 3.2, 3.17, und 3.19). Für alle drei Behälterarten wurde eine umfangreiche qualitative Analyse des Beitrags von Strahlung, Gaskonvektion und Wärmeleitung zum gesamten Wärmeeintrag durchgeführt, die als Hilfe zur Optimierung von Gefriertrocknungszyklen mit diesen Behältern verwendet werden kann.

Kern der hier vorliegenden Arbeit sind Sublimationstests mit destilliertem Wasser, die mit allen drei Behältersystemen auf ähnliche Art bei verschiedenen Kammerdrücken ausgeführt wurden. Dafür wird eine definierte Masse destilliertes Wasser in eine Anzahl der betreffenden Behälter eingefüllt. Die Behälter werden in die Produkt-Kammer des Gefriertrockners gestellt und abgekühlt, bis das Wasser zu Eis gefroren ist. Dann wird der Druck im Gefriertrockner auf einen vorher eingestellten Wert abgesenkt. Sobald der Sättitungs-Sublimationsdruck von Eis bei der Produkttemperatur unterschritten wird, setzt die Sublimation mit der unter diesen Bedingungen maximalen Flussrate ein.

Sublimation ist ein energieaufwändiger Prozess. Je Gramm Eis wird ein bestimmter Energiebetrag für die Sublimation benötigt (Sublimationsenthalpie, weitere Erläuterungen in Abschnitt 1.4.2). Um die Wasserdampfflussrate im Gefriertrockner hoch zu halten, wird über die Stellflächen in der Gefriertrocknungskammer Energie in Form von Wärme zugeführt. Wird die Produkttemperatur konstant gehalten, stellt sich ein Fließgleichgewicht zwischen Energieeintrag in das Produkt (durch die Wärme aus dem Wärmeträgerfluid in den Stellflächen) und Energieaustrag durch Sublimation des Eises ein. Für den Sublimationstest wird dieser Prozess unterbrochen, bevor mehr als ca. 50 % des Eises sublimiert sind. Der Druck im Gefriertrockner wird wieder auf den Luftdruck angehoben, so dass die Kammer geöffnet werden kann. Die Produktbehälter werden entnommen und die verbleibende Masse an Eis / Wasser in den Produktbehältern wird bestimmt.

Aus der Massendifferenz zwischen Einwaage an Wasser vor dem Versuch und der Restmenge nach dem Versuch sowie der Versuchsdauer kann der durchschnittliche Massenfluss (dm/dt) bestimmt werden. Zusammen mit der Temperaturdifferenz zwischen der Stellflächenoberfläche unter dem Produktbehälter und der Produkttemperatur am Boden des Behälters kann mit Hilfe der Gleichung 1.5 der Wärmeüberkangskoeffizient $K_{container}$ bestimmt werden. Je größer dieser Wärmeübergangskoeffizient, desto effizienter ist der Energieeintrag in die betreffende Behälterart.

Die Wärmeübergangskoeffizienten, die für direkt auf die Stellfläche platzierte 96-Well PCR-Platten bestimmt wurden, ermöglichten eine gute Vorhersage der Primärtrocknungszeit (s. Abschnitt 3.2.2, z. B. Tabelle 3.4). Bei dieser Anordnung wird der Wärmeeintrag in das Produkt hauptsächlich durch Strahlungseintrag erzielt (s. Abschnitt 3.1.3, Abbildung 3.3). Dies führt zu einem inhomogenen Trocknungsverhalten innerhalb der Behälter auf einer Stellfläche, da atypische Strahlung einen starken Einfluss auf den Trocknungsprozess von Behältern / Wells in Randpositionen nimmt (s. Temperaturverläufe in "edge" und "centre" Positionen in den Ab-

bildungen 3.16, 3.17). Ein für diese Anordnung optimierter Gefriertrocknungszyklus benötigt eine verhältnismäßig hohe Stellflächentemperatur in Kombination mit einem mittleren Kammerdruck (nicht weniger als ca. 80 mTorr), um die Primärtrocknungszeit und Inhomogenität der Produkttemperaturen / der Trocknungsverläufe zu minimieren (s.a. Abschnitt 3.2.9).

Werden die 96-Wellplatten in Aluminium- (Al-) Blöcke eingesetzt, so trägt der Wärmeeintrag durch Gaskonvektion erheblich zur gesamten Wärmeübertragung in das Produkt bei, während der Wärmeeintrag durch Strahlung deutlich reduziert wird (s. Abschnitt 3.1.5 und Abbildung 3.7). Die effizientere Wärmeübertragung, hervorgerufen durch den verringerten Abstand zwischen Stellfächenoberfläche und Al-Block einerseits sowie zwischen Al-Block Bohrung und PCR-Platte andererseits, wird teilweise kompensiert durch die hohe Wärmekapazität des Al-Blocks. Dieser benötigt einen erheblichen Energiebetrag (und erhebliche Zeit) um sich auf etwa Stellflächentemperatur zu erwärmen (siehe Abschnitt 3.1.5). Diese durch die Anwärmzeit für den Aluminium-Block verursachte Verlängerung der Primärtrocknungsphase kann teilweise vermieden werden, wenn am Anfang der Primärtrocknung eine besonders hohe Stellflächentemperatur verwendet wird, die erst auf eine passende Temperatur gesenkt wird, wenn die Produkttemperatur der Ziel-Produkttemperatur nahe kommt.

Für die Versuchsanordnung von Wellplatten in Aluminiumblöcken war die Vorhersage der Primärtrocknungszeit unter Berücksichtigung der aus den Sublimationstests ermittelten Wärmeübergangskoeffizienten weniger genau (siehe Abschnitt 3.2.2). Dieser Unterschied zwischen berechneter und tatsächlicher Primärtrocknungszeit kann wahrscheinlich durch die Schwierigkeit erklärt werden, die Fläche für den Wärmeeintrag korrekt zu bestimmen. In der hier vorliegenden Studie basieren alle Berechnungen auf der Annahme, dass während des größten Teils der Primärtrocknung ein Fließgleichgewicht besteht (keine wesentliche Änderung der Produkttemperatur, konstante Fläche für den Wärmeeintrag). Die Gefriertrocknung eines Produktes in Wellplatten mit Al-Blöcken scheint von diesen Bedingungen erheblich abzuweichen, so dass möglicherweise eine andere Herangehensweise, die die kontinuierlichen Veränderungen der Fläche für den Wärmeeintrag, der Produkttemperatur, und der Sublimationsgrenzfläche berücksichtigt, zu genaueren Ergebnissen führt.

Für 96-Well PCR-Platten wurden Wärmeübergangskoeffizienten nicht nur aus Sublimationstests mit Wasser (mit einem Füllvolumen von 200 μL je Well), sondern auch aus Produktläufen mit Trehalose- und Mannitollösung (mit Füllvolumina von 20 μL und 100 μL) bestimmt, s. Abschnitt 3.2.6 on page 86. Die Wärmeübergangskoeffizienten, die von Hilfsstoff-Läufen mit Al-Block bestimmt wurden, waren ausnahmslos kleiner als die Koeffizienten, die zuvor mit Sublimationstests ermittelt worden waren. Es wird vermutet, dass die Fläche für den Wärmeeintrag für diese verschiedenen Füllvolumina noch genauer bestimmt werden muss, um zu einer besseren Übereinstimmung der von diesen unterschiedlichen Volumina ermittelten Wärmeübergangskoeffizienten zu gelangen.

Die für das Freeze Drying System™ (FDS) ermittelten Wärmeübergangskoeffizienten gehören zu den höchsten in dieser Studie (s. Tabelle 3.17). Die Summe der für dieses Behältersystem bestimmten Abstände zwischen Stellfächenoberfläche und Al-Block einerseits, sowie zwischen der Kavität im Al-Block und der Wand bzw. dem Boden des Gläschens andererseits, war am kleinsten in dieser Untersuchung (s. Abschnitt 3.3.2, Tabelle 3.18 on page 121). Dieser geringe Abstand resultiert zumindest zu einem Teil aus dem bemerkenswert flachen und ebenen Boden der Gläschen, der einen guten Kontakt zu ebenen Flächen ermöglicht (s. Abschnitt 3.3.1, Abbildung 3.34 on page 117). Außer einem hohen Anteil zum gesamten Wärmeeintrag durch Gaskonvektion, der mit dem Kammerdruck ansteigt, begünstigt die aus der schwarzen Farbe resultierende hohe Emissivität des Al-Blocks einen hohen Wärmeeintrag durch Strahlung (s. Abschnitt 3.3.2). Für die Optimierung von Gefriertrocknungszyklen für dieses Behältersystem gelten ähnliche Regeln wie für Wellplatten mit Aluminium-Blöcken.

Die für 2R Glasvials bestimmten Wärmeübergangskoeffizienten stimmen gut mit Daten aus der Literatur für andere Glasvials vergleichbarer Geometrie überein [83]. Sie sind größenordnungsmäßig vergleichbar mit den Wärmeübergangskoeffizienten des FDS (s. Tabellen 3.17 und 3.19). "Atypische" Strahlung leistet einen hohen Beitrag zum Wärmeeintrag in Vials in Randpositionen, wodurch die Wärmeübergangskoeffizienten für Vials in diesen Extrempositionen bis zu 30 % höher ausfallen (s. a. Tabelle 3.19). Um eine hohe Homogenität des Trocknungsvorgangs

innerhalb einer Charge zu erzielen, sollten die mit Produktlösung gefüllten Vials von einer Reihe Vials mit Placebolösung ("Dummy"-Vials) umgeben werden, die diese zusätzliche Strahlung effektiv abschirmen.

Die hier beschriebenen Regeln zur Zyklusoptimierung für die zwei Nicht-Vial Behältersysteme (Wellplatten und FDS) wurden anhand je eines Gefriertrocknungslaufes mit einer neuen, für diesen Zweck entwickelten Formulierung erfolgreich getestet. Diese Regeln wurden dann in eine Leitlinie zur Entwicklung von Formulierungen und Gefriertrocknungszyklen integriert. Diese Leitlinie ist im Anhang zu dieser Arbeit enthalten.

Das SMART Freeze Dryer™ Programm zur Gefriertrocknungszyklusoptimierung wurde auf die Anwendbarkeit für Gefriertrocknung in 96-Wellplatten untersucht. Der SMART™ Optimierungsalgorithmus ermittelte ein recht aggressives Gefriertrocknungsprogramm. Am Beginn der Primärtrocknungsphase, mit noch ausreichend hoher Gesamt-Sublimationsoberfläche, stimmten die Ergebnisse der manometrischen Temperatur-Messungen (MTM) mit Daten aus Temperaturmessungen mit Thermoelementen überein. Für eine genauere Abbildung des Gefriertrocknungsprozesses in Wellplatten durch MTM sind Anpassungen des MTM-Algorithmus nötig, die beispielsweise die sich ändernde Sublimationsoberfläche berücksichtigen.

Es wurde gezeigt, dass alle getesteten Behälter für die Gefriertrocknung geeignet sind. Wellplatten (vorzugsweise unter Verwendung von Al-Blöcken) sind am besten für die Gefriertrocknung sehr geringer Volumina (weniger als 100 μL geeignet. Das Freeze Drying System™ ist eine gute Alternative als Produktbehälter für Volumina zwischen ca. 100 μL und 400 μL. Diese beiden für die Gefriertrocknung neuartigen Behältersysteme könnten ein gutes Primärpackmittel für sehr stark wirksame Arzneimittel darstellen, die nur in kleinen Dosen appliziert werden. Der über die letzten Jahrzehnte angestiegene Forschungsumfang auf dem Feld der Biotechnologie könnte für diese Art von Behälter einen Bedarf kreieren [123], [9]. Für Füllvolumina, die 400 μL übersteigen, können Vials noch immer als "Goldstandard" betrachtet werden.

References

[1] M. J. Pikal, M. L. Roy, and S. Shah. Mass and Heat Transfer in Vial Freeze-Drying of Pharmaceuticals: Role of the Vial. *Journal of Pharmaceutical Sciences*, 73(9):1224–1237, 1984.

[2] M. J. Pikal, S. Cardon, C. Bhugra, F. Jameel, S. Rambhatla, W. J. Mascarenhas, and H. U. Akay. The Nonsteady State Modeling of Freeze Drying: In-Process Product Temperature and Moisture Content Mapping and Pharmaceutical Product Quality Applications. *Pharmaceutical Development and Technology*, 10(1):17–32, 2005.

[3] Robert G. Mortimer. *Physical Chemistry*. Elsevier Academic Press, Burlington (MA), USA, third edition, 2008.

[4] C.Y. Ho, R. W. Powell, and P.E. Lidley. *Thermal Conductivity of the Elements: A Comprehensive Review*. Journal of Physical and Chemical Referene Data Supplements. AIP Press, January 1974.

[5] M. Bauccio, editor. *ASM Metals Reference Book*. ASM International, Materials Park, OH, 3rd edition, 1993.

[6] Chau V. Vo and Andrew N. Paquet. An Evaluation of the Thermal Conductivity of Extruded Polystyrene Foam Blown with HFC-134a or HCFC-142b. *Journal of Cellular Plastics*, 40(3):205–228, 2004.

[7] Saul Dushman. *Scientific Foundations of Vacuum Technique.* Wiley, New York, 1962.

[8] Wolfgang Demtröder. *Experimentalphysik 2:Elektrizität und Optik*, volume 2. Springer-Verlag, Heidelberg, 1995.

[9] J. Miller. Capacity Worries Fade for Biomanufacturing. *Pharmaceutical Technology*, 27(7):82–83, 2003.

[10] M. J. Pikal. Freeze drying. In James Swarbrick, editor, *Encyclopedia of Pharmaceutical Technology*, volume 3, chapter Freeze Drying, pages 1299–1326. Informa Healthcare, New York, third edition, 2007.

[11] M. R. DeFelippis. Overcoming the Challenges of Noninvasive Protein and Peptide Delivery. *American Pharmaceutical Review*, 6(4):21–30, 2003.

[12] R. Hwang, P. Noolandi, and D. B. Amgen. From Vial to Autoinjector. *American Pharmaceutical Review*, 10(2), 2007.

[13] H. J. H. B. Hirschberg, G. G. P. van de Wijdeven, A. B. Kelder, G. P. J. M. van den Dobbelsteen, and G. F. A. Kersten. Bioneedles^{TM} as vaccine carriers. *Vaccine*, 26(19):2389–2397, 2008.

[14] S. A. Yehia, O. N. El-Gazayerly, and E. B. Basalious. Design and In Vitro/In Vivo Evaluation of Novel Mucoadhesive Buccal Discs of an Antifungal Drug: Relationship Between Swelling, Erosion, and Drug Release. *AAPS PharmSciTech*, pages 1–11, 2008.

[15] Louis Rey and Joan Christine May, editors. *Freeze-Drying/Lyophilization of Pharmaceutical and Biological Products*. Informa Healthcare, New York (NY), USA, second edition, February 2004.

[16] James A. Searles, John F. Carpenter, and Theordore W. Randolph. Annealing to Optimize the Primary Drying Rate, Reduce Freezing-Induced Drying Rate Heterogeneity, and Determine Tg' in Pharmaceutical Lyophilization. *Journal of Pharmaceutical Sciences*, 90(7):872–887, 2001.

[17] Kyuya Nakagawa, Aurélie Hottot, Séverine Vessot, and Julien Andrieu. Influence of controlled nucleation by ultrasounds on ice morphology of frozen formulations for pharmaceutical proteins freeze-drying. *Chemical Engineering and Processing*, 45:783–791, 2006.

[18] J. E. K. Schawe. A quantitative DSC analysis of the metastable phase behavior of the sucrose-water system. *Thermochimica Acta*, 451(1-2):115–125, 2006.

[19] J. J. Schwegman, L. M. Hardwick, and M. J. Akers. Practical Formulation and Process Development of Freeze-Dried Products. *Pharmaceutical Development and Technology*, 10(2):151–173, 2005.

[20] X. Tang and M. J. Pikal. Design of Freeze-Drying Processes for Pharmaceuticals: Practical Advice. *Pharmaceutical Research*, 21(2):191–200, 2004.

[21] W. Wang. Lyophilization and development of solid protein pharmaceuticals. *International Journal of Pharmaceutics*, 203(1-2):1–60, 2000.

[22] R. Feistel and W. Wagner. Sublimation pressure and sublimation enthalpy of H_2O ice Ih between 0 and 273.16 K. *Geochimica et Cosmochimica Acta*, 71(1):36–45, 2007.

[23] Wolfgang Demtröder. *Experimentalphysik 1:Mechanik und Wärme*, volume 1. Springer-Verlag, Heidelberg, 1994.

[24] Gerlinde Schelenz, J. Engel, and H. Rupprecht. Sublimation during lyophilization detected by temperature profile and X-ray technique. *International Journal of Pharmaceutics*, 113(2):133–140, 1995.

[25] Henning Gieseler, Tony Kramer, and Michael J. Pikal. Use of Manometric Temperature Measurement (MTM) and SMART^{TM} Freeze Dryer Technology for Development of an Optimized Freeze-Drying Cycle. *Journal of Pharmaceutical Sciences*, 2007.

[26] S. Rambhatla and M. J. Pikal. Heat and Mass Transfer Scale-up Issues During Freeze-Drying, I: Atypical Radiation and the Edge Vial Effect. *AAPS PharmSciTech*, 4(2), 2003.

[27] Sajal M. Patel, Takayuki Doen, and Michael J. Pikal. Determination of End Point of Primary Drying in Freeze-Drying Process Control. *AAPS PharmSciTech*, 11(1):73–84, March 2010.

[28] Thermal conductivity of some common materials [online]. 2005. Available from: `http://www.engineeringtoolbox.com/thermal-conductivity-d_429.html` [cited August 29, 2009].

[29] Kh. I. Amirkhanov, A. P. Adamov, and U. B. Magomedov. Measurement of the thermal conductivity of water vapor at 375-600 °c and pressures up to 250mPa. *Journal of Engineering Physics and Thermophysics*, 34(2):141–143, February 1978.

[30] G. D. J. Adams and J. R. Ramsay. Optimizing the Lyophilization Cycle and the Consequences of Collapse on the Pharmaceutical Acceptability of Erwinia L-Asparaginase. *Journal of Pharmaceutical Sciences*, 85(12):1301–1305, 1996.

[31] X. Tang, S. L. Nail, and M. J. Pikal. Freeze-Drying Process Design by Manometric Temperature Measurement: Design of a Smart Freeze-Dryer. *Pharmaceutical Research*, 22(4):685–700, 2005.

[32] Y. H. Roos. FROZEN STATE TRANSITIONS IN RELATION TO FREEZE DRYING. *Journal of Thermal Analysis*, 48(3):535–544, 1997.

[33] M. J. Pikal, S. Shah, M. L. Roy, and R. Putman. The secondary drying stage of freeze drying: drying kinetics as a function of temperature and chamber pressure. *International Journal of Pharmaceutics*, 60(3):203–217, 1990.

[34] W. Q. Sun. Water Sorption and Glass Transition Behavior of Polyalditol (PD30), a New Nonreactive Malto-Oligosaccharide Cryo- and Drying-Protectant. *Cell Preservation Technology*, 5(2):77–84, 2007.

[35] S. Rambhatla, J. P. Obert, S. Luthra, C. Bhugra, and M. J. Pikal. Cake Shrinkage During Freeze Drying: A Combined Experimental and Theoretical Study. *Pharmaceutical Development and Technology*, 10(1):33–40, 2005.

[36] A. M. Abdul-Fattah, D. Lechuga-Ballesteros, D. S. Kalonia, and M. J. Pikal. The Impact of Drying Method and Formulation on the Physical Properties and Stability of Methionyl Human Growth Hormone in the Amorphous Solid State. *Journal of Pharmaceutical Sciences*, 97(1):163–184, 2008.

[37] J. D. Colandene, L. M. Maldonado, A. T. Creagh, J. S. Vrettos, K. G. Goad, and T. M. Spitznagel. Lyophilization Cycle Development for a High-Concentration Monoclonal Antibody Formulation Lacking a Crystalline Bulking Agent. *Journal of Pharmaceutical Sciences*, 96(6):1598–1608, 2007.

[38] B. S. Chang, G. Reeder, and J. F. Carpenter. Development of a Stable Freeze-dried Formulation of Recombinant Human Interleukin-1 Receptor Antagonist. *Pharmaceutical Research*, 13(2):243–249, 1996.

[39] A. M. Abdul-Fattah, K. M. Dellerman, R. H. Bogner, and M. J. Pikal. The Effect of Annealing on the Stability of Amorphous Solids: Chemical Stability of Freeze-Dried Moxalactam. *Journal of Pharmaceutical Sciences*, 96(5):1237–1250, 2007.

[40] E. B. Seligmann Jr. and J. F. Farber. FREEZE DRYING AND RESIDUAL MOISTURE. *Cryobiology*, 8(2):138–144, 1971.

[41] A. M. Abdul-Fattah, D. S. Kalonia, and M. J. Pikal. The Challenge of Drying Method Selection for Protein Pharmaceuticals: Product Quality Implications. *Journal of Pharmaceutical Sciences*, 96(8):1886–1916, 2007.

[42] B. S. Bhatnagar, R. H. Bogner, and M. J. Pikal. Protein Stability During Freezing: Separation of Stresses and Mechanisms of Protein Stabilization. *Pharmaceutical Development and Technology*, 12(5):505–523, 2007.

[43] L. Chang, D. Shepherd, J. Sun, D. Ouellette, K. L. Grant, X. Tang, and M. J. Pikal. Mechanism of Protein Stabilization by Sugars During Freeze-Drying and Storage: Native Structure Preservation, Specific Interaction, and/or Immobilization in a Glassy Matrix? *Journal of Pharmaceutical Sciences*, 94(7):1427–1444, 2005.

[44] K. Kawai and T. Suzuki. Stabilizing Effect of Four Types of Disaccharide on the Enzymatic Activity of Freeze-dried Lactate Dehydrogenase: Step by Step Evaluation from Freezing to Storage. *Pharmaceutical Research*, 24(10):1883–1890, 2007.

[45] Jürgen Falbe, Manfred Regitz, and Dr. Elisabeth Hillen, editors. *Römpp Chemie Lexikon*, volume 5. Georg Thieme Verlag, Stuttgart, 9 edition, 1992.

[46] K. Chatterjee, E. Y. Shalaev, and R. Suryanarayanan. Raffinose Crystallization During Freeze-Drying and Its Impact on Recovery of Protein Activity. *Pharmaceutical Research*, 22(2):303–309, 2005.

[47] P. Davidson and W. Q. Sun. Effect of Sucrose/Raffinose Mass Ratios on the Stability of Co-Lyophilized Protein During Storage Above the T_g. *Pharmaceutical Research*, 18(4):474–479, 2001.

[48] Jeffrey L. Cleland, Xanthe Lam, Brent Kendrick, Janet Yang, Tzung Horng Yang, David Overcashier, Dennis Brooks, Chung Hsu, and John F. Carpenter. A Specific Molar Ratio of Stabilizer to Protein is Required for Storage Stability of a Lyophilized Monoclonal Antibody. *Journal of Pharmaceutical Sciences*, 90(3):310–321, March 2001.

[49] K. Chatterjee, E. Y. Shalaev, and R. Suryanarayanan. Partially Crystalline Systems in Lyophilization: II. Withstanding Collapse at High Primary Drying Temperatures and Impact on Protein Activity Recovery. *Journal of Pharmaceutical Sciences*, 94(4):809–820, 2005.

[50] M. J. Pikal. Use of Laboratory Data in Freeze Drying Process Design: Heat and Mass Transfer Coefficients and the Computer Simulation of Freeze Drying. *Journal of Parenteral Science and Technology*, 39(3):115–139, 1985.

[51] F. Fonseca, S. Passot, O. Cunin, and M. Marin. Collapse Temperature of Freeze-Dried L*actobacillus bulgaricus* Suspensions and Protective Media. *Biotechnology Progress*, 20(1):229–238, 2004.

[52] Eva Meister. Methodology, Data Interpretation and Practical Transfer of Freeze-Dry Microscopy. Master's thesis, Naturwissenschaftliche Fakultät der Friedrich-Alexander-Univerisät Erlangen-Nürnberg, Erlangen, March 2009.

[53] Ronald D. Archer. *Inorganic and Organometallic Polymers*. Wiley-VCH, New York (NY), USA, 2001.

[54] M. P. Sepe. *Thermal analysis of polymers*. Rapra Technology Ltd., Shawbury, Shrewsbury, 1997.

[55] G.W.H. Höhne, W.F. Hemminger, and H-J. Flammersheim. *Differential Scanning Calorimetry*. Springer-Verlag, Berlin, second edition, 2003.

[56] Ludwik Szczesniak, Adam Rachocki, and Jadwiga Tritt-Goc. Glass transition temperature and thermal decomposition of cellulose powder. *Cellulose*, 15(3):445–451, June 2008.

[57] X. Lu and M. J. Pikal. Freeze-Drying of Mannitol-Trehalose-Sodium Chloride-Based Formulations: The Impact of Annealing on Dry Layer Resistance to Mass Transfer and Cake Structure. *Pharmaceutical Development and Technology*, 9(1):85–95, 2004.

[58] D. B. Varshney, S. Kumar, E. Y. Shalaev, P. Sundaramurthi, S. W. Kang, L. A. Gatlin, and R. Suryanarayanan. Glycine Crystallization in Frozen and Freeze-dried Systems: Effect of pH and Buffer Concentration. *Pharmaceutical Research*, 24(3):593–604, 2007.

[59] N. Milton, G. Gopalrathnam, G. D. Craig, D. S. Mishra, M. L. Roy, and L. Yu. Vial Breakage during Freeze-Drying: Crystallization of Sodium Chloride in Sodium Chloride-Sucrose Frozen Aqueous Solutions. *Journal of Pharmaceutical Sciences*, 96(7):1848–1853, 2007.

[60] R. E. Johnson, C. F. Kirchhoff, and H. T. Gaud. Mannitol-Sucrose Mixtures - Versatile Formulations for Protein Lyophilization. *Journal of Pharmaceutical Sciences*, 91(4):914–922, 2002.

[61] X. Liao, R. Krishnamurthy, and R. Suryanarayanan. Influence of Processing Conditions on the Physical State of Mannitol - Implications in Freeze-Drying. *Pharmaceutical Research*, 24(2):370–376, 2007.

[62] S. Rambhatla, S. Tchessalov, and M. J. Pikal. Heat and Mass Transfer Scale-Up Issues During Freeze-Drying, III: Control and Characterization of Dryer Differences via Operational Qualification Tests. *AAPS PharmSciTech*, 7(2), 2006.

[63] S. Passot, F. Fonseca, N. Barbouche, M. Marin, M. Alarcon-Lorca, D. Rolland, and M. Rapaud. Effect of Product Temperature During Primary Drying on the Long-Term Stability of Lyophilized Proteins. *Pharmaceutical Development and Technology*, 12(6):543–553, 2007.

[64] G. Gómez, M. J. Pikal, and N. Rodríguez-Hornedo. Effect of Initial Buffer Composition on pH Changes During Far-From-Equilibrium freezing of Sodium Phosphate Buffer Solutions. *Pharmaceutical Research*, 18(1):90–97, 2001.

[65] Wei-Youh Kuu, James McShane, and Joseph Wong. Determination of mass transfer coefficients during freeze drying using modeling and parameter estimation techniques. *International Journal of Pharmaceutics*, 124(2):241–252, 1995.

[66] A. I. Liapis and R. Bruttini. Freeze-Drying of Pharmaceutical Crystalline and Amorphous Solutes in Vials: Dynamic Multi-Dimensional Models of the Primary and Secondary Drying Stages and Qualitative Features of the Moving Interface. *Drying Technology*, 13(1):43 – 72, 1995.

[67] P. Sheehan and A. I. Liapis. Modeling of the Primary and Secondary Drying Stages of the Freeze Drying of Pharmaceutical Products in Vials: Numerical Results Obtained from the Solution of a Dynamic and Spatially Multi-Dimensional Lyophilization Model for Different Operational Policies. *Biotechnology and Bioengineering*, 60(6):712–728, 1998.

[68] X. C. Tang, S. L. Nail, and M. J. Pikal. Evaluation of Manometric Temperature Measurement (MTM), a Process Analytical Technology Tool in Freeze Drying, Part III: Heat and Mass Transfer Measurement. *AAPS PharmSciTech*, 7(4), 2006.

[69] X. C. Tang, S. L. Nail, and M. J. Pikal. Evaluation of Manometric Temperature Measurement, a Process Analytical Technology Tool for Freeze-drying: Part II Measurement of Dry-layer Resistance. *AAPS PharmSciTech*, 7(4), 2006.

[70] P. Chouvenc, S. Vessot, J. Andrieu, and P. Vacus. Optimization of the Freeze-Drying Cycle: Adaptation of the Pressure Rise Analysis Model to Non-Instantaneous Isolation Valves. *PDA Journal of Pharmaceutical Science and Technology*, 59(5):298–309, 2005.

[71] S. L. Nail, S. Jiang, S. Chongprasert, and S. A. Knopp. Fundamentals of Freeze-Drying. In Steven L. Nail and Michael J. Akers, editors, *Development and Manufacture of Protein Pharmaceuticals*, volume 14 of *Pharmaceutical Biotechnology*, chapter 6, pages 281–360. Kluwer Academics / Plenum Publishers, New York (NY), USA, 2002.

[72] M. J. Pikal, S. Shah, D. Senior, and J. E. Lang. Physical Chemistry of Freeze-Drying: Measurement of Sublimation Rates for Frozen Aqueous Solutions by a Microbalance Technique. *Journal of Pharmaceutical Sciences*, 72(6), 1983.

[73] Ansgar Petersen, Hendrik Schneider, Guenter Rau, and Birgit Glasmacher. A new approach for freezing of aqueous solutions under active control of the nucleation temperature. *Cryobiology*, 53:248–257, 2006.

[74] Adrian Riesbeck. H. Riesbeck Gummiwaren für Labor [online]. Available from: `http://www.riesbeck.com/` [cited 18.03.2009].

[75] F. Rene, E. Wolff, and F. Rodolphe. Vacuum freeze-drying of a liquid in a vial: determination of heat and mass-transfer coefficients and optimisation of operating pressure. *Chemical Engineering and Processing*, 32(4):245–251, 1993.

[76] R. Baethge, J. Del Boca, H. J. Weissgraeber, and P. A. Schroder. Quality and stability of Lyo-Ject dual-chamber syringes. *Pharmazeutische Industrie*, 52(5):635–641, 1990.

[77] Annette W. Ford and Peter J. Dawson. Effect of Type of Container, Storage Temperature and Humidity on the Biological Activity of Freeze-dried Alkaline Phosphatase. *Biologicals*, 22(2):191–197, 1994.

[78] S. v. Graberg and H. Gieseler. Freeze Drying in Non-Vial Container Systems: Evaluation of Heat Transfer Coefficients of PCR-Plates and Correlation to Freeze-Drying Cycle Design. *Proc. CPPR Freeze-Drying of Pharmaceuticals and Biologicals*, Garmisch-Partenkirchen, Germany, October 3-6 2006.

[79] S. v. Graberg and H. Gieseler. Freeze Drying from 96-Well PCR-Plates: Transferability of Heat Transfer Coefficients Obtained from Sublimation Tests to Product Runs and Considerations for Cycle Design. *Proc. AAPS Annual Meeting and Exposition*, San Diegeo (CA), USA, November 11-15 2007.

[80] S. v. Graberg, W. Hyla, and H. Gieseler. Freeze Drying from Small Product Containers and its Implication on Freeze Drying Process Design: Evaluation of Heat Transfer Coefficients of a New 96-Well Freeze Drying System in Comparison to 2R Tubing Vials and Polypropylene 96-Well PCR-Plates. *Proc. CPPR Freeze-Drying of Pharmaceuticals and Biologicals*, Breckenridge (CO), USA, August 6-9 2008.

[81] A. Hottot, J. Andrieu, S. Vessot, E. Shalaev, L. A. Gatlin, and S. Ricketts. Experimental Study and Modeling of Freeze-Drying in Syringe Configuration. Part I: Freezing Step. *Drying Technology*, 27(1):40–48, 2009.

[82] A. Hottot, J. Andrieu, V. Hoang, E. Y. Shalaev, L. A. Gatlin, and S. Ricketts. Experimental study and modeling of freeze-drying in syringe configuration. Part II: Mass and heat transfer parameters and sublimation end-points. *Drying Technology*, 27(1):49–58, 2009.

[83] Wei Y. Kuu, Steven L. Nail, and Gregory Sacha. Rapid Determination of Vial Heat Transfer Parameters Using Tunable Diode Laser Absorption Spectroscopy (TDLAS) in Response to Step-Changes in Pressure Set-Point During Freeze-Drying. *Journal of Pharmaceutical Sciences*, DOI 10.1002/jps:n/a, 2008.

[84] Suling Zhai, Haiyun Su, Richard Taylor, and Nigel K. H. Slater. Pure ice sublimation within vials in a laboratory lyophiliser; comparison of theory with experiment. *Chemical Engineering Science*, 60(4):1167–1176, 2005.

[85] Youngmin Sohn, Seung Wook Baek, and Takashi Kashiwagi. Transient Modeling of Thermal Degradation in Non-Charring Solids. *Combustion Science and Technology*, 145(1):83–108, September 1999.

[86] A. Hottot, S. Vessot, and J. Andrieu. Determination of mass and heat transfer parameters during freeze-drying cycles of pharmaceutical products. *PDA Journal of Pharmaceutical Science and Technology*, 59(2):138–153, 2005.

[87] Horst Stöcker, editor. *Taschenbuch der Physik*. Verlag Harri Deutsch, Frankfurt am Main, 3rd edition, 1998.

[88] Hirschfelder, Curtiss, and Bird. *Molecular Theory of Gases and Liquids*. Wiley, New York, 1954.

[89] H. Gieseler, W. J. Kessler, M. Finson, S. J. Davis, P. A. Mulhall, V. Bons, D. J. Debo, and M. J. Pikal. Evaluation of Tunable Diode Laser Absorption Spectroscopy for In-Process Water Vapor Mass Flux Measurements During Freeze Drying. *Journal of Pharmaceutical Sciences*, 96(7):1776–1793, 2007.

[90] S. D. Patel, B. Gupta, and S. H. Yalkowsky. Acceleration of heat transfer in vial freeze-drying of pharmaceuticals. I: Corrugated aluminium quilt. *Journal of Parenteral Science and Technology*, 43(1):8–14, 1989.

[91] S. H. Yalkowsky and S. D. Patel. Acceleration of heat transfer in vial freeze-drying of pharmaceuticals. II. A fluid cushion device. *Pharmaceutical Research*, 9(6):753–758, 1992.

[92] Alexander I. Kim, Michael J. Akers, and Steven L. Nail. The Physical State of Mannitol after Freeze-Drying: Effects of Mannitol Concentration, Freezing Rate, and a Noncrystallizing Cosolute. *Journal of Pharmaceutical Sciences*, 87(8):931–935, August 1998.

[93] Characterisation of Christalline and Partially Crystalline Solids by X-Ray Powder Diffraction (XRPD). In European Directorate of the Quality of Medicines and HealthCare of the Council of Europe (EDQM), editors, *European Pharmacopoeia - 7^{th} Edition*, chapter 2.9.33. C. H. Beck, Strasburg, 7 edition, 2010.

[94] Anthony Meager. Measurement of cytokines by bioassays: Theory and application. *Methods*, 38(4):237–252, 2006.

[95] Promega Corporation. CellTiter 96® AQ_{ueous} One Solution Cell Proliferation Assay. printed in USA, 2800 Woods Hollow Road - Madison, WI, 53711-5399 USA, July 2007.

[96] Abderrahim Boudenne, Laurent Ibos, Magali Fois, Evelyne Gehin, and Jean-Charles Majeste. Thermophysical Properties of Polypropylene/Aluminium Composites. *Journal of Polymer Science Part B: Polymer Physics*, 42(4):722–732, 2004.

[97] James Hopwood Jeans. *An Introduction to the Kinetic Theory of Gases*. Cambridge University Press, Cambridge, Great Britain, 1982.

[98] Clive Maier and Teresa Calafut. *Polypropylen - The Definitive User's Guide and Databook*. William Andrew, 1998.

[99] engineershandbook.com. Coefficient of friction [online]. Available from: `http://www.engineershandbook.com/Tables/frictioncoefficients.htm` [cited August 30, 2009].

[100] W. Y. Kuu, L. M. Hardwick, and M. J. Akers. Rapid determination of dry layer mass transfer resistance for various pharmaceutical formulations during primary drying using product temperature profiles. *International Journal of Pharmaceutics*, 313(1-2):99–113, 2006.

[101] Henning Gieseler. Product Morphology and Drying Behavior delineated by a new Freeze-Drying Microbalance. Master's thesis, University of Erlangen, Department of Pharmaceutics, July 2004.

[102] X. C. Tang, S. L. Nail, and M. J. Pikal. Evaluation of Manometric Temperature Measurement, a Process Analytical Technology Tool for Freeze-drying: Part I, Product Temperature Measurement. *AAPS PharmSciTech*, 7(1), 2006.

[103] D. E. Overcashier, T. W. Patapoff, and C. C. Hsu. Lyophilization of Protein Formulations in Vials: Investigation of the Relationship between Resistance to Vapor Flow during Primary Drying and Small-Scale Product Collapse. *Journal of Pharmaceutical Sciences*, 88(7):688–695, 1999.

[104] C. Telang, R. Suryanarayanan, and L. Yu. Crystallization of D-Mannitol in Binary Mixtures with NaCl: Phase Diagram and Polymorphism. *Pharmaceutical Research*, 20(12):1939–1945, 2003.

[105] A. Hawe and W. Friess. Impact of freezing procedure and annealing on the physico-chemical properties and the formation of mannitol hydrate in mannitol-sucrose-NaCl formulations. *European Journal of Pharmaceutics and Biopharmaceutics*, 64:316–325, 2006.

[106] Stefan C. Schneid, Henning Gieseler, William J. Kessler, and Michael J. Pikal. Non-Invasive Product Temperature Determination during Primary Drying using Tunable Diode Laser Absorption Spectroscopy. *Journal of Pharmaceutical Sciences*, 98(9):3406–3418, 2009.

[107] H. Gieseler, L. Mather, and M. J. Pikal. $SMART^{TM}$ Freeze Dryer Technology: Impact of Water Re-Adsorption of Polyvinylpyrrolidone (PVP) on Manometric Temperature Measurements (MTM) During Primary Drying. *Proc. 5th World Meeting on Pharmaceutics and Pharmaceutical Technology*, Geneva, Switzerland, March 27-30 2006.

[108] J. H. C. Eriksson, W. L. J. Hinrichs, G. J. De Jong, G. W. Somsen, and H. W. Frijlink. Investigations into the Stabilization of Drugs by Sugar Glasses: III. The Influence of Various High-pH Buffers. *Pharmaceutical Research*, 20(9):1437–1443, 2003.

[109] Q. Lu and G. Zografi. Properties of Citric Acid at the Glass Transition. *Journal of Pharmaceutical Sciences*, 86(12):1374–1378, 1997.

[110] Saori Kadoya, Ken itchi Izutsu, Etsuo Yonemochi, Katsuhide Terada, Chikako Yomota, and Toru Kawanishi. Glass-State Amorphous Salt Solids Formed by Freeze-Drying of Amines and Hydroxy Carboxylic Acids: Effect of Hydrogen-Bonding and Electrostatic Interactions. *Chem. Pharm. Bull*, 56(6):821–826, June 2008.

[111] E. Y. Shalaev, T. D. Johnson-Elton, L. Chang, and M. J. Pikal. Thermophysical Properties of Pharmaceutically Compatible Buffers at Sub-Zero Temperatures: Implications for Freeze-Drying. *Pharmaceutical Research*, 19(2):195–201, 2002.

[112] Andrea Hawe and Wolfgang Friess. Physicochemical Characterization of the Freezing Behavior of Mannitol-Human Serum Albumin Formulations. *AAPS PharmSciTech*, 7(4):E2–E9, December 2006.

[113] Byeong S. Chang, Robert M. Beauvais, Aichung Dong, and John F. Carpenter. Physical Factors Affecting the Storage Stability of Freeze-Dried Interleukin-1 Receptor Antagonist: Glass Transition and Protein Conformation. *Archives of Biochemistry and Biophysics*, 331(2):249–258, July 1996.

[114] Marcel P. W. M. te Booy, Rien A. de Ruiter, and André L. J. de Meere. Evaluation of the Physical Stability of Freeze-Dried Sucrose Containing Formulations by Differential Scanning Calorimetry. *Pharmaceutical Research*, 9(1):109–114, 1992.

[115] Satoshi Ohtake, Carolina Schebor, Sean P. Palecek, and Juan J. de Pablo. Effect of pH, Counter Ion, and Phosphate Concentration on the Glass Transition Temperature of Freeze-Dried Sugar-Phosphate Mixtures. *Pharmaceutical Research*, 21(9):1615–1621, 09 2004/09/01/.

[116] M. J. Pikal, D. Rigsbee, and M. L. Roy. Solid state chemistry of proteins: I. glass transition behaviour in freeze dried disaccharide formulations of human growth hormone (hGH). *Journal of Pharmaceutical Sciences*, 96(10):2765–76, October 2007.

[117] M. J. Pikal, D. Rigsbee, M. L. Roy, D. Galreath, K. J. Kovach, B. Wang, J. F. Carpenter, and M. T. Cicerone. Solid State Chemistry of Proteins: II. The Correlation of Storage Stability of Freeze-Dried Human Growth Hormone (hGH) with Structure and Dynamics in the Glassy Solid. *Journal of Pharmaceutical Sciences*, 97(12):5106–5121, 2008.

[118] Rahul Surana, Abira Pyne, and Raj Suryanarayanan. Effect of Aging on the Physical Properties of Amorphous Trehaloe. *Pharmaceutical Research*, 21(5):867–874, May 2004.

[119] D. P. Miller and D. Lechuga-Ballesteros. Rapid assessment of the structural relaxation behavior of amorphous pharmaceutical solids: effect of residual water on molecular mobility. *Pharmaceutical Research*, 23(10):2291–2305, 2006.

[120] Felix Franks. Storage Stabilization of Proteins. In Felix Franks, editor, *Protein Biotechnology*, chapter 14, pages 489–531. The Humana Press Inc., 1993.

[121] Juan Cheng and Nicholas Winograd. Depth Profiling of Peptide Films with TOF-SIMS and a C_{50} Probe. *Anal. Chem.*, 77:3651–3659, 2005.

[122] Erich Meister. *Grundpraktikum physikalische Chemie: Theorie und Experimente*. vdf Hochschulverlag AG, Zurich, 2006.

[123] Biotechnology: Pharmaceutical Aspects. In Henry R. Costantino and Michael J. Pikal, editors, *Lyophilization of Biopharmaceuticals*. American Association of Pharmaceutical Scientists, Arlington (VA), USA, 2004.